REGULATION OF TERNARY COMPLEX BY ELONGATION FACTOR TS

A Dissertation

Presented to the Faculty of the Weill Cornell Graduate School

of Medical Sciences

in Partial Fulfillment of the Requirements for the Degree of

Doctor of Philosophy

By

Benjamin Jay Burnett

May 2016

REGULATION OF TERNARY COMPLEX BY
ELONGATION FACTOR TS

Benjamin Jay Burnett, PhD
Cornell University, 2016

ABSTRACT

Elongation factor Tu (EF-Tu), bound to GTP, delivers aminoacyl-tRNA (aa-tRNA) as a ternary complex (TC) to the translating ribosome for the purpose of decoding messenger-RNA (mRNA). As such, TC is fundamentally important to the speed and fidelity of mRNA decoding. Here, a quantitative, kinetic framework for the formation and stability of ternary complex is presented. This framework includes novel features of Elongation Factor Ts (EF-Ts), a guanosine nucleotide exchange factor for EF-Tu. Specifically, EF-Ts accelerates both the formation and dissociation of TC by directly loading EF-Tu·GTP onto aa-tRNA as an EF-Tu/Ts·GTP·aa-tRNA quaternary complex. This newly described intermediate species quickly resolves into the canonical TC, which is then competent to participate in the decoding process. A major impact of this interaction is that, under cellular conditions, EF-Ts accelerates the formation of TC to a rate that is above the rate of tRNA selection and above the rate of protein synthesis in general. Leveraging these insights, a new model is proposed predicting that EF-Ts facilitates the dissociation of the deactivated EF-Tu·GDP species from the ribosome at the conclusion of the tRNA selection process. These results suggest a broader role for GEFs arguing in favor of a model wherein GEFs catalyze the formation of activated G-protien·effector complexes.

BIOGRAPHICAL SKETCH

Benjamin J. Burnett began his career in research in the laboratory of Dr. Gulamabas Sivjee at Embry-Riddle Aeronautical University, FL, where he earned a B.S. in Engineering Physics. Here, Ben learned the basics of the scientific method studying dynamic processes in the upper atmosphere and ionosphere. Ben then joined the lab of Dr. Samuel Durrance at the Florida Institute of Technology where he earned a M.S. in Physics. Ben played a lead role in assembling a biophysical research lab within the Department of Physics in an effort to initialize biophysical research at FIT. Ben aided in testing a hypothesis, put forth by Dr. Shaohua Xu from the Department of Biochemistry, which predicted the mechanism of amyloid fiber formation in Alzheimer's disease patients. His master's thesis investigated the dielectric properties of lysozyme amyloid fibers formed *in vitro* and identified the physical parameters necessary for protein misfolding.

Having developed a passion for biology and biotechnology, Ben then moved into the lab of Dr. Scott Blanchard at Weill Cornell Medical College, NY, in pursuit of a PhD in biophysics. Here, Ben investigated the fundamental properties of TRAFAC G-proteins and their involvement in bacterial protein synthesis. Under Dr. Blanchard's mentorship, Ben learned rigorous hypothesis testing, data-driven analysis, and, perhaps most importantly, an appreciation for detail in developing biological models. In addition to research, Ben gained exposure to the biotechnology industry by developing a business concept centered around diagnosing organ rejection in kidney transplant patients. Ben has published two peer reviewed research publications as a lead author and has presented at multiple conferences including posters at three scientific conferences. Ben was also an invited speaker at a biopharmaceutical industry conference.

DEDICATION

I dedicate this work to Lisa. Twice now she has seen me through to graduation. She is a constant source of strength and inspiration and I am sure that my achievements would not have been possible without her.

ACKNOWLEDGEMENTS

First, and foremost, I would like to acknowledge the support and mentorship of Dr. Scott Blanchard. His enthusiasm for science is unparalleled, perhaps only matched by the devotion he shows for his students. Dr. Blanchard molded me into a critical thinker, a strong communicator, and most importantly, a scientist. I will always be grateful for his tutelage.

I also owe a great deal to Drs. Steve Gross, Dan Heller, and Olaf Andersen. Their critical insights and support was instrumental to my scientific progress.

I am forever appreciative of the members of Dr. Blanchard's lab. Thank you Jose Alejo, Manuel Juette, and Angelica Ferguson for your enthusiasm for deep discussions on tRNA selection. Thank you Dan Terry and Mike Wasserman for guiding me through single molecule experimentation. Thank you Glenn Gregorio for entertaining my radical ideas about G-proteins. Thank you Randall Dass and Chad Kurylo for broadening my scope of biochemistry. Thank you Zhou Zhou and Hong Zhao for keeping me well supplied with fluorophores. Thank you Justin Morse for taking the baton and seeing this project through to the next milestone. Thank you Roger Altman for shepherding me though many difficult experiments, oftentimes trouble shooting worst-case scenarios.

TABLE OF CONTENTS

BIOGRAPHICAL SKETCH iii

LIST OF FIGURES xii

LIST OF TABLES xvi

LIST OF ABBREVIATIONS xvii

CHAPTER 1. Regulation of ternary complex by EF-Ts 1

1.1 OVERVIEW 1

1.2 THE SWITCHING CYCLE OF G-PROTEINS 2

1.3 TRAFAC G-PROTEINS ARE CRITICAL TO PROTEIN SYNTHESIS 5

1.4 THE ARCHITECTURE OF THE RIBOSOME 9

1.5 THE DECODING MECHANISM 11

1.7 GTP ENABLES EF-TU TO RECOGNIZE THE AMINOACYL MOIETY OF tRNA 13

1.8 EF-TS IS THE GUANOSINE NUCLEOTIDE EXCHANGE FACTOR FOR EF-TU 15

1.9 CURRENT MODELS OF tRNA SELECTION ARE TOO SLOW 17

CHAPTER 2. Methods 18

2.1 OVERVIEW 18

2.1 INSTRUMENTATION 18

2.1.1 PTI-QM4 Fluorometer 18

2.1.2 SX20 Stopped-flow Spectrometer 28

2.1.4 Single Molecule TIRF Microscopy 35

2.2 REAGENT EXPRESSION AND PURIFICATION 35

2.2.1 Bacterial Elongation Factor Tu Purification 35

2.2.2 Bacterial Elongation Factor Tu-ACP Purification 41

2.2.5 Bacterial Elongation Factor Ts Purification 43

2.2.6 Bacterial Elongation Factor Ts-A106C Purification 43

2.2.7 Phenylalanyl-tRNA Synthetase Purification 45

2.2.8 Arginyl-tRNA Synthetase Purification 47

2.2.9 TEV Protease Purification 47

2.2.9 Bacterial Phosphate Binding Protein Purification 49

2.2.10 Bacterial Phenylalanyl-tRNA Purification 50

2.1.11 Tight Coupled 70S Ribosome Purification 58

2.2.12 Nucleotide Purification 61

2.3 FLUORESCENT LABELING OF BIOMOLECULES 61

2.3.1 Cy5Q EF-Tu_{ACP} 61

2.3.2 Cyanine Dye Labeling Of EF-Ts^{A106C} (Cy3 and Cy5) 63

2.3.4 MDCC Labeling Of PBP 63

2.3.6 NHS-Cyanine Dye Labeling of tRNA 63

2.4 EXPERIMENTAL PROCEDURES 64

2.4.1 Acylation of $tRNA^{Met}$, $tRNA^{Arg}$, and $tRNA^{Phe}$ 65

2.4.2 Acylation and formylation of $tRNA^{fMet}$ 65

2.4.3 Formation of Ribosome Initiation Complex 65

2.4.4. Ternary Complex Isolation by Gel Filtration Chromatography 66

2.4.5 Relative Fluorescence Ternary Complex Assay 66

2.4.6 Quench-fluorescence Ternary Complex Assay 67

2.4.7 Ternary Complex Activity Assay 67

2.4.8 Rapid Stopped-flow Experiments Monitoring Relative Fluorescence 68

2.4.9 Rapid Stopped-flow Experiments Monitoring FRET 68

2.4.10 GTP Exchange Assay 69

2.4.11 Ternary Complex GTP Exchange Assay 69

2.4.12 Initiation Complex Activity Assay 69

2.4.13 tRNA Selection Dequench Assay 70

2.4.14 tRNA Selection GTP Hydrolysis Assay 70

2.4.15 smFRET tRNA Selection – tRNA Reaction Coordinate 71

2.4.16 smFRET tRNA Selection – EF-Tu Reaction Coordinate 71

2.4.17 smFRET tRNA Selection – EF-Tu & tRNA Reaction Coordinate 72

2.4.18 Simulation Of Ternary Complex Formation 72

CHAPTER 3. Dynamic properties of EF-Tu·GTP·Aminoacyl-tRNA ternary complex 74

3.1 OVERVIEW 74

3.2 SUMMARY 75

3.3 INTRODUCTION 75

3.4 RESULTS 79

3.4.1. Kinetics of Ternary Complex Formation 79

3.4.2 Steady State Measurements of Ternary Complex Formation 80

3.4.3 Pre-Steady State Measurements of Ternary Complex Formation 83

3.4.4. Physical Isolation of the Dynamic Ternary Complex 89

3.4.5. Direct Evidence That EF-Ts Facilitates Ternary Complex Dynamics 91

3.5 DISCUSSION 92

CHAPTER 4. Direct evidence of EF-Tu/Ts·GTP·aa-tRNA quaternary complex 100

4.1 OVERVIEW 100

4.2 SUMMARY 100

4.3 INTRODUCTION 101

4.4 RESULTS 105

4.4.1 EF-Tu Binds Distinct aa-tRNAs with High Affinity 105

4.4.2 EF-Ts Accelerates the Rate of Ternary Complex Formation 108

4.4.3 EF-Ts Facilitates Ternary Complex Dissociation in the Presence of GDP 109

4.4.4 EF-Ts Increases the Rate of Ternary Complex Turnover under Steady State Conditions 111

4.4.5 EF-Tu/Ts·GTP Is an Abundant Species under Cellular Conditions..... 114

4.4.6 Quaternary Complex Is Transient by Nature 116

4.5 DISCUSSION..... 118

CHAPTER 5. The reaction coordinate of EF-Tu 122

5. THE REACTION COORDINATE OF EF-TU..... 122

5.1 SUMMARY..... 122

5.2 INTRODUCTION 123

5.3 RESULTS 127

5.3.1 EF-Tu Hydrolyzes GTP In A Timeframe Consistent With aa-tRNA Accommodation 127

5.3.2 EF-Tu·GDP_{mant} Release Is Slow In The Absence Of EF-Ts 129

5.3.3 EF-Tu Releases aa-tRNA In A Timeframe Consistent With aa-tRNA Accommodation 133

5.3.4 Direct Measurements of EF-Tu Reveal A Short Residence Time With The Small Subunit 138

5.3.5 EF-Tu, aa-tRNA, and the ribosome are tracked simultaneously 141

5.4 DISCUSSION..... 143

CHAPTER 6. Impact and future implications 145

6.1 SUMMARY 145

6.2 INTRODUCTION 146

6.3 QUATERNARY COMPLEX 147

6.3.1 EF-Ts catalyzed Ternary complex formation is not rate-limiting 147

6.3.2 EF-Ts may tune global protein synthesis rates to GTP prevalence 148

6.3.3. Quaternary complex may represent a general mechanism of G-protein activation 150

6.4 DEACTIVATION OF G-PROTEINS 151

6.4.1 Do GEFs facilitate the removal of inactive G-proteins from their effectors? 151

6.5 FUTURE DIRECTIONS 152

6.5.1 Measuring the residence time of EF-Tu 152

6.6 CONCLUSION 153

APPENDIX: BUFFERS AND SOLUTIONS 154

BIBLIOGRAPHY 159

LIST OF FIGURES

FIGURE 1.1 The G-domain adopts distinct conformations that correlate with nucleotide binding..... 3
FIGURE 1.2 Life cycle of G-proteins..... 4
FIGURE 1.3 G-proteins play key roles in each of the three phases of protein synthesis..... 5
FIGURE 1.4 Structural elements of the bacterial ribosome..... 9
FIGURE 1.5 tRNA selection occurs in two phases..... 10
FIGURE 1.6 The fidelity of tRNA selection stems from proper codon-anticodon interactions..... 11
FIGURE 1.7 Structural elements of phenylalanyl ternary complex..... 13
FIGURE 1.8 Inactive EF-Tu adopts a unique switch conformation..... 14
FIGURE 1.9 Activation of EF-Tu requires the GEF EF-Ts..... 15
FIGURE 1.10 EF-Ts stabilizes the nucleotide binding transition state of EF-Tu... 16

FIGURE 2.1 PTI-QM4 Fluorometer..... 19
FIGURE 2.2 Light path of PTI-QM4 fluorometer..... 20
FIGURE 2.3 Manual aperture knob..... 21
FIGURE 2.4 Importing data into OriginLab..... 27
FIGURE 2.5 Data processing..... 27
FIGURE 2.6 Normalize data by percent change..... 27
FIGURE 2.7 Schematic of T-mixer flow cell..... 28
FIGURE 2.8 Applied Photophysics SX20 Stopped-flow spectrometer..... 29
FIGURE 2.9 Air tank and water bath for the SX20..... 30
FIGURE 2.10 Filter assembly..... 31
FIGURE 2.11 LED assembly. 31

FIGURE 2.12 Sample chamber valves..... 32
FIGURE 2.13 Extracting contaminating gas..... 33
FIGURE 2.14 Pro-Data SX20 software interface..... 34
FIGURE 2.15 Map of His6-EF-Tu expression vector..... 36
FIGURE 2.16 SDS-PAGE of EF-Tu purification..... 40
FIGURE 2.17 Chromatograph of EF-Tu purification..... 41
FIGURE 2.18 Map of His_6-EF-Tu_{ACP} construct..... 42
FIGURE 2.19 Site directed mutagenesis thermocycler protocol..... 44
FIGURE 2.20 Map of His_6-PheRS construct..... 46
FIGURE 2.21 Map of $tRNA^{Phe}$ construct..... 50
FIGURE 2.22 Isopropanol precipitation of $tRNA^{Phe}$..... 54
FIGURE 2.23 Hydrophobic separation of bulk tRNAs..... 56
FIGURE 2.24 Hydrophobic separation of Phe-$tRNA^{Phe}$..... 57
FIGURE 2.25 Hydrophobic separation of Phe-$tRNA^{Phe}$..... 58
FIGURE 2.26 Fractionation of TC70 preparation..... 60
FIGURE 2.27 Purification of Cy3 labeled $tRNA^{Phe}$..... 64

FIGURE 3.1 Ternary complex structure and steady state measurements of ternary complex formation..... 76
FIGURE 3.2 EF-Tu is highly active in both the absence and presence of EF-Ts... 81
FIGURE 3.3 Pre-steady state measurements of ternary complex formation and dissociation: dependence on factor concentration..... 85
FIGURE 3.4 EF-Ts accelerates the rate-determining step in EF-Tu binding to aa-tRNA..... 87
FIGURE 3.5 Physical isolation of ternary complex..... 88
FIGURE 3.6 EF-Ts directly facilitates ternary complex turnover..... 90

FIGURE 3.7 Ternary complex formation and disassembly can occur via two distinct pathways..... 94
FIGURE 3.8 Hypothetical EF-Tu·GTP·EF-Ts·Phe-tRNA^{Phe}..... 96

FIGURE 4.1 EF-Tu binds ternary complex with nanomolar affinity..... 106
FIGURE 4.2 EF-Ts directly facilitates ternary complex formation..... 107
FIGURE 4.3 EF-Ts accelerates ternary complex decay in response to GDP..... 108
FIGURE 4.4 Measuring ternary complex formation and dissociation via FRET..... 110
FIGURE 4.5 Significant amounts of EF-Tu/Ts remain bound to GTP under physiological nucleotide concentrations..... 113
FIGURE 4.6 Direct evidence of the transient intermediate, quaternary complex..... 117
FIGURE 4.7 EF-Ts regulates ternary complex abundance..... 118

FIGURE 5.1 EF-Tu delivers aa-tRNA to the leading edge of the ribosome..... 124
FIGURE 5.2 Kinetic model of tRNA selection..... 125
FIGURE 5.3 PBP binds P_i with a fast on-rate..... 127
FIGURE 5.4 GTP Hydrolysis during tRNA selection..... 128
FIGURE 5.5 EF-Tu binds mant nucleotides with high affinity..... 130
FIGURE 5.6 EF-Ts accelerates nucleotide release from EF-Tu..... 131
FIGURE 5.7 tRNA selection monitored using mant labeled EF-Tu..... 132
FIGURE 5.8 Schematic of quenched TC formation and tRNA selection..... 134
FIGURE 5.9 Initiation complexes are active in translation..... 135
FIGURE 5.10 tRNA selection occurs in multiple steps..... 136
FIGURE 5.11 EF-Ts does not accelerate EF-Tu dissociation for Phe-tRNA^{Phe}..... 137

FIGURE 5.12 Schematic for smFRET tRNA selection assay..... 138
FIGURE 5.13 EF-Tu engages the ribosome in close proximity to protein S12..... 139
FIGURE 5.14 EF-Tu interacts transiently with the ribosome..... 140
FIGURE 5.15 EF-Tu and Phe-tRNAPhe can be tracked simultaneously..... 142
FIGURE 5.16 Measurements of tRNA selection..... 144

FIGURE 6.1 EF-Ts couples TC stability with local nucleotide abundance..... 149
FIGURE 6.2 General mechanism for GEF mediated signal transduction..... 151

LIST OF TABLES

Table 1.1 Relative nucleotide affinities predict the need for GEFs..... 8

Table 3.1 Equilibrium dissociation constant of ternary complex..... 83

Table 3.2 Summary of kinetic parameters of ternary complex..... 89

Table 4.1 Kinetic parameters measured in the presence and absence of EF-Ts..... 109

Table 4.2 Apparent rates of ternary complex dissociation..... 111

Table 4.3 Apparent rates of EF-Tu and EF-Ts interactions..... 112

Table 4.4 Apparent rates of quaternary complex formation and decay..... 114

LIST OF ABBREVIATIONS

aa-tRNA	Aminoacyl-transfer ribonucleic acid
Acp^3U	3-(3-amino-3-carboxypropyl)uridine
ADP	Adenosine diphosphate
ArgRS	Arginyl-tRNA synthetase
ATP	Adenosine triphosphate
BME	β-mercaptoethanol
CoA	Coenzyme A
COT	Cyclooctatetraene
CTerm	Carboxy terminus
EDTA	Ethylenediaminetetraacetic Acid
EF-Ts	Elongation Factor Ts (T-factor, temperature stable
EF-Tu	Elongation Factor Tu (T-factor, temperature unstable)
EF-Tu/Ts	Heterodimer of EF-Tu and EF-Ts
FRET	Fluorescence resonance energy transfer
GAP	GTPase activating factor
GDI	GDP dissociation inhibitor
GDP	Guanosine diphosphate
GDPCP	β,γ-methyleneguanosine 5′-triphosphate
GDP_{mant}	2′-/3′-O-(*N*′-methylanthraniloyl)guanosine-5′-O-diphosphate
GDPNP	Guanosine 5′-(β,γ-imido) triphosphate
GEF	Guanosine nucleotide exchange factor
GTP	Guanosine nucleotide triphosphate
GTP_{mant}	2′-/3′-O-(*N*′-methylanthraniloyl)guanosine-5′-O-triphosphate
GTPγS	Guanosine 5′-(γ-thio) triphosphate

HEPES	4-(2-hydroxyethyl)piperazine-1-ethanesulfonic acid
His6	Hexahistidine
IC	Ribosome initiation complex
IPTG	Isopropyl β-D-thiogalactopyranoside
k_{app}	Apparent rate constant
K_D	Dissociation constant
Kirr	Kirromycin
MetRS	Methionyl-tRNA synthetase
mRNA	messenger ribonucleic acid
MWCO	Molecular weight cut-off
NBA	Nitrobenzylalcohol
NHS	*N*-hydroxysuccinimide
NTerm	Amino terminus
PheRS	Phenylalanyl-tRNA synthetase
Ppant	4′-phosphopantetheinyl
QC	Quaternary complex (EF-Tu/Ts·GTP·aa-tRNA)
RGS	Regulator of G-protein signaling
s^4U	4-thiouridine
TC70S	Tight-coupled 70S
TIRF	Total internal reflection fluorescence
Tris	Tris(hydoxymethyl)aminomethane
$tRNA^{Arg}$	Arginyl-transfer ribonucleic acid
$tRNA^{Met}$	Methionyl-transfer ribonucleic acid
$tRNA^{Phe}$	Phenylalanyl-transfer ribonucleic acid

CHAPTER 1

REGULATION OF TERNARY COMPLEX BY ELONGATION FACTOR TS

1.1 OVERVIEW

This chapter provides a foundation for the work discussed in subsequent chapters. First, a plenary overview of G-protein biology is discussed, with a focus on the subclass of G-proteins involved in protein synthesis. The current model of protein synthesis and tRNA accommodation is then presented. This chapter ends by highlighting some of the major shortcomings with the generally accepted, canonical models of protein synthesis.

In **Chapter 2**, the preparation of reagents and experimental procedures is discussed in detail. Experimental results demonstrating the kinetics underpinning the formation of critical components of the protein synthesis machinery will be discussed in **Chapter 3** and in **Chapter 4**. **Chapter 5** will summarize new insights and ongoing efforts to leverage these data towards a more complete and comprehensive model of protein synthesis. The indications of these findings will be summarized in **Chapter 6**.

1.2 THE SWITCHING CYCLE OF G-PROTEINS

G-proteins are a superfamily of regulatory guanosine triphosphate (GTP) hydrolases that are ubiquitous throughout all phylogeny of life having been found in every living organism studied to date[5,6]. Even within a single cell, G-proteins are found in high abundance and are involved in a diverse assortment of cellular processes including cell motility, signal transduction across cell membranes, cellular growth and differentiation, and gene expression[7,8]. G-proteins likely evolved into such a diverse set of roles because of their ability to cycle between two distinct states, thus making them ideally suited for decision making in biological processes[9].

The distinct states of G-proteins are achieved by the binding of guanosine nucleotides to a conserved three dimensional protein domain, termed the G-domain (Figure 1.1)[10]. Activation requires binding to GTP, which enables the G-protein to adopt an active conformation (Figure 1.1*A*)[7,10]. Deactivation of G-proteins occurs through the intrinsic hydrolysis of GTP to guanosine diphosphate (GDP), an irreversible process that leads to an inactive conformation (Figure 1.1*B*)[7,10]. Comparison of the active and inactive conformations reveals a dramatic repositioning of an alpha helix, termed the "switch" helix. Positioning of this helix occurs through allosteric coordination by either the GTP or the GDP, thus coupling the distinct conformations of the G-protein to guanosine nucleotide binding.

Many G-proteins require additional proteins to facilitate switching between the active- and inactive-states (Figure 1.2)[7,11,12]. Guanosine nucleotide Exchange Factors (GEFs) are a class of proteins that catalyze both the removal of GDP and the subsequent binding of GTP, thereby positively regulating G-protein function[7,13]. Once GTP bound, the activated G-protein is released from the GEF and is then competent to interact with secondary molecules to propagate a downstream signal or process. In the G-protein vernacular, these secondary molecules are referred to as Effectors, as their

function is modulated by activated, GTP-bound G-proteins for the purpose of eliciting a downstream effect.

Although G-proteins have intrinsic GTP hydrolysis capabilities, they rarely perform this function on their own. *In vitro*, the rate of GTP hydrolysis is measured to be very slow with respect to biological timescales (minutes to hours)[14]. In the cellular context, GTPase Activating Proteins (GAPs) are required to accelerate the rate of GTP hydrolysis, thereby negatively regulating G-protein function (Figure 1.2)[13]. GAPs, also known as Regulators of G-protein Signaling (RGS), interact directly with the effector-bound G-proteins and accelerate the hydrolysis reaction, often by many orders of magnitude. Catalogued rates of GTP hydrolysis range from ca. 10 s^{-1} to as much as 500 s^{-1} [11]. As a result of the hydrolysis reaction, the gamma phosphate (terminal

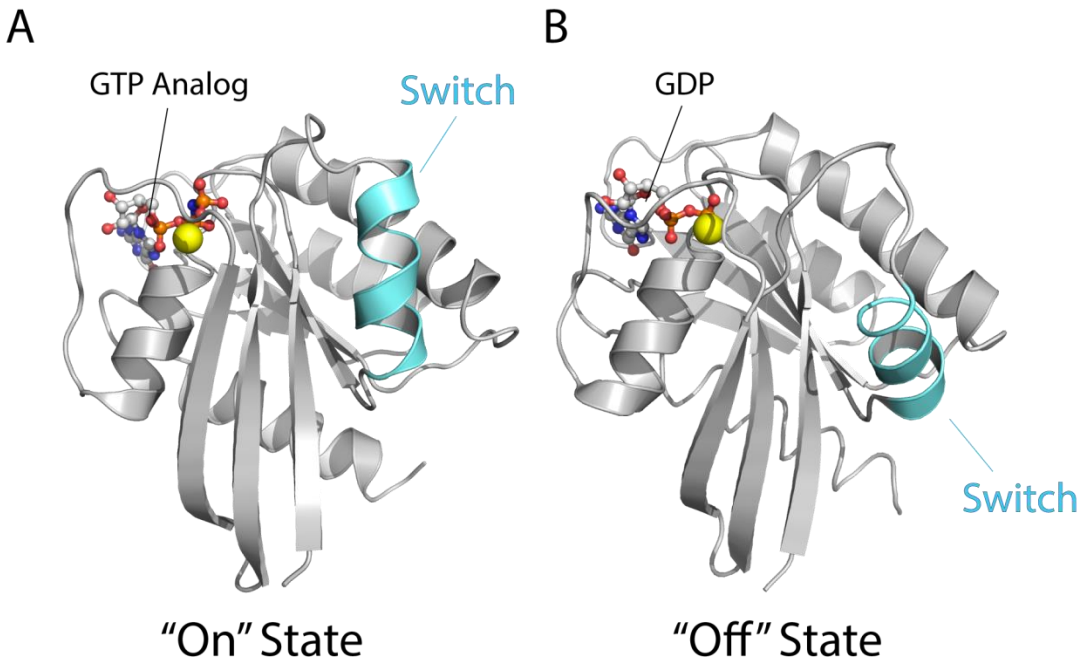

FIGURE 1.1 ***The G-domain adopts distinct conformations that correlate with nucleotide binding*****.** The The G-domain consists of a central β-sheet surrounded by a group of 5 α-helices. Shown here is the Ras G-domain bound to either a GTP analog, **A** (PDB accession code 5P21), or GDP, **B** (PDB accession code 4Q21). Nucleotide binding has a dramatic impact on one α-helix in particular, referred to as the switch helix (*blue*). The γ-phosphate of GTP positions the switch helix in close proximity and parallel to the β-sheet backbone. When GDP bound, the switch helix assumes a more distal, orthogonal position.

phosphate) is released and the G-protein adopts an inactive, GDP-bound conformation.

In some G-protein systems, Guanosine nucleotide Dissociation Inhibitors (GDIs) serve an important role in regulating G-protein function by binding to, and sequestering the inactive form of G-proteins (Figure 1.2)[12]. In doing so, they inhibit the dissociation of GDP and therefore compete with GEFs to negatively regulate G-protein function.

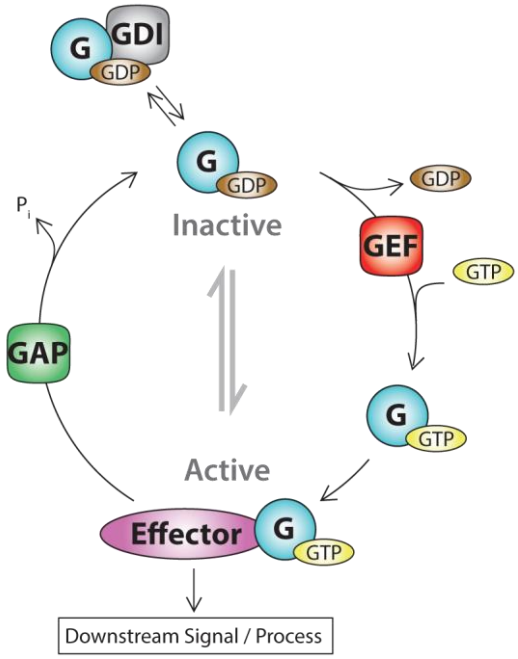

FIGURE 1.2 ***Life cycle of G-proteins.*** The general mechanism for G-protein activation and inactivation is a cyclical process that is unidirectional. The G-protein (*blue*) is inactive when bound to GDP (*brown*). Many G-proteins require a GEF (*red*) to facilitate the exchange of GDP for GTP (*yellow*). The GTP-bound G-protein is then released in an active state that is competent to bind to effector molecules (*purple*) which leads to further downstream processes. The inactivation of G-proteins occurs through the interaction of GAPs (*green*) which accelerate the GTPase mechanism intrinsic to all G-proteins. GTP hydrolysis results in an inactive GDP-bound form of the G-protein which, in some cases, can be sequestered by GDIs (*grey*) to compete with GEF interactions and thus maintain the G-protein in an inactive state. Adapted from Wittinghoffer et al.{Wittinghofer, 2011 #560}

1.3 TRAFAC G-PROTEINS ARE CRITICAL TO PROTEIN SYNTHESIS

G-proteins have been found in a myriad of processes within the cell, especially in the context of decision making. A subclass of G-proteins known as TRAFAC (translation factor)[7,15] G-proteins are critical to the fidelity of gene expression at the messenger RNA (mRNA) level[16,17]. Translation of mRNA occurs in three broad stages: initiation, elongation, and termination/recycling[18-21]. During initiation, the ribosome, a large megadalton ribonuclear protein complex, assembles on an mRNA at the start codon. This process is facilitated by a host of translation factors, including the G-protein Initiation Factor-2 (IF-2) in bacteria (eIF2 in humans). In the GTP bound state, IF2 delivers the initiator tRNA to the mRNA assembled 30S subunit of the ribosome. Upon correct 50S assembly, GTP is hydrolyzed and IF2 releases the initiator tRNA, leaving it positioned in the peptidyl site of the fully assembled ribosome. Owing to its relative affinity for GDP (K_D = 4.5 μM) and GTP (K_D = 10.6

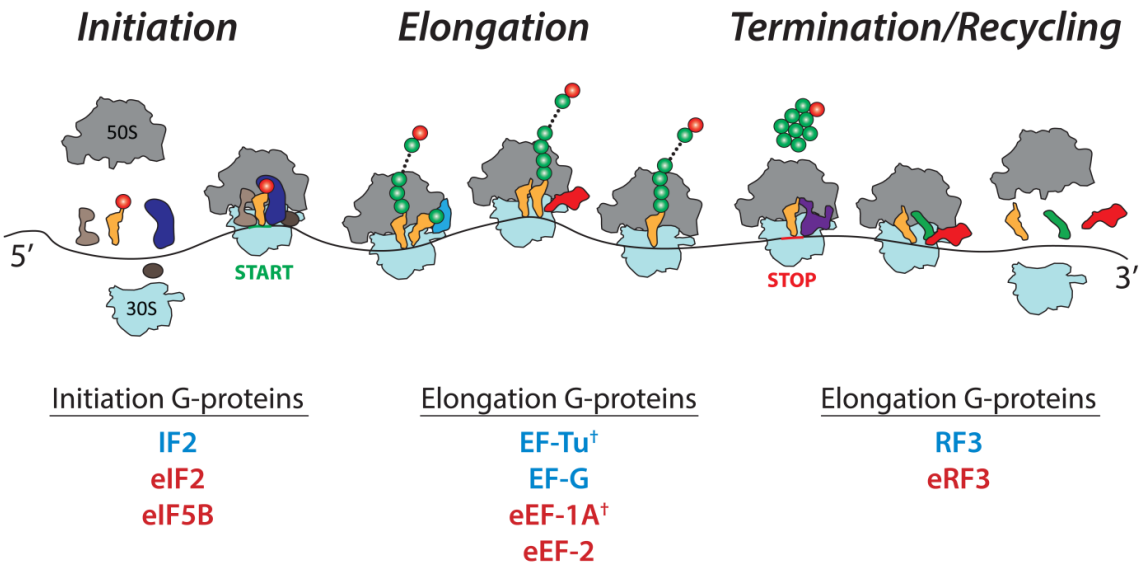

FIGURE 1.3 ***G-proteins play key roles in each of the three phases of protein synthesis.*** Translation occurs in three general steps. During *Initiation*, the translational machinery assembles onto the mRNA transcript, a process that requires the G-protein IF2 in bacteria, or eIF2 and eIF5B in eukaryotes. *Elongation* then proceeds with the cyclical action of EF-Tu delivering aa-tRNAs to the ribosome and EF-G translocating it to the next triplet codon in bacteria, or by the action of eEF-1A and eEF-2 in eukaryotes respectively). *Termination* requires an additional G-protein, RF3 in bacteria and eRF3 in eukaryotes.

μM), and given the relative abundance of these nucleotides in bacterial cells (100uM and 900uM respectively)[22], IF2 readily exchanges GTP for GDP without the need of a GEF[23].

During the elongation phase of protein synthesis, the initiated ribosome translates the mRNA open reading frame by decoding each triplet codon and catalyzing the polymerization of the ciphered amino acid to the nascent polypeptide chain. Each decoding step minimally requires the action of two G-proteins, Elongation Factor-Tu (EF-Tu) and Elongation Factor G (EF-G)[17]. EF-Tu plays a pivotal role in the decoding mechanism by delivering aminoacyl-tRNA (aa-tRNA) to the elongating ribosome in a process called tRNA selection[17,24-26]. Specifically, EF-Tu facilitates the binding of the tRNA anticodon with the mRNA codon. Upon correct pairing, EF-Tu hydrolyzes GTP and releases the aa-tRNA, allowing it to fully accommodate into the aminoacyl (A)-site of the ribosome[27,28]. The functional importance of EF-Tu in the decoding mechanism is highlighted by the fact that small molecule antibiotics that target EF-Tu and disrupt aa-tRNA binding have been shown to kill cells by inhibiting protein synthesis[29,30].

Unlike IF2, EF-Tu requires a GEF to achieve an active, GTP-bound state. EF-Tu's affinity for GDP ($K_{D(EF\text{-}Tu\bullet GDP)}$ = 1 nM) is 60 fold higher than is its affinity for GTP ($K_{D(EF\text{-}Tu\bullet GTP)}$ = 60 nM)[31]. Given that there is only about a 9 fold excess of GTP over GDP in the cell, EF-Tu would preferentially remain in an inactive, GDP-bound state in the absence of a GEF. In bacteria, the GEF for EF-Tu is Elongation Factor-Ts (EF-Ts) and it serves to increase the pool of active EF-Tu in the cell by catalyzing the formation of the GTP-bound form. Interestingly, EF-Ts does not increase EF-Tu's affinity for GTP, but, in a seemingly paradoxical way, reduces EF-Tu's affinity for both guanosine nucleotides. EF-Tu's affinity for GDP in the presence of EF-Ts is ~9 μM, roughly 1.5 fold higher than its affinity for GTP, ~14 μM. However, given the 9

fold excess of GTP in the cell, EF-Tu will be driven towards an active, GTP-bound state. The precise role of EF-Tu and EF-Ts in protein synthesis is the subject of this body of work and will be discussed in greater detail in subsequent sections.

Once aa-tRNA is fully accommodated, EF-G catalyzes the translocation of the ribosome by one codon along the mRNA open reading frame[32]. In doing so, the occupied tRNAs are shifted by one position within the ribosome, thus clearing the A-site and preparing the ribosomes for the next round of tRNA selection. When EF-G engages the ribosome, its affinity for GTP increases roughly 150 fold from ca. ~22 μM to ca. ~150 nM[33]. Given that EF-G's affinity for GDP is ca. 10 μM, EF-G is driven towards an active, GTP-bound state without the need of a GEF.

Protein synthesis concludes *via* the termination and recycling processes. Upon reaching a stop codon, a release factor (RF1 or RF2 depending on the stop codon) catalyzes the liberation of the nascent polypeptide chain. Release factor 3 (RF3) then binds to the A-site of the large subunit and facilitates the removal of the bound release factor (RF1 or RF2) in a GTP dependent manner. RF3 has a roughly 4.5 fold higher affinity for GDP than GTP (23 nM vs 108 nM)[34]. As such, RF3 is naturally driven towards the active, GTP-bound state under normal cellular conditions of guanosine nucleotides without the aid of a GEF. The disassembly of the post-termination complex is carried out in tandem with ribosome release factor (RRF) and EF-G, a process that requires the hydrolysis of GTP.

Protein synthesis is an energy intensive process, with the elongation phase requiring the lions share. The decoding of each codon minimally requires the hydrolysis of 2 GTP molecules per amino acid (the first by EF-Tu upon aa-tRNA delivery and the second by EF-G upon translocation)[14,33]. The rate at which a cell hydrolyzes GTP is directly proportional to both the rate of protein synthesis and to the

TABLE 1.1. ***Relative nucleotide affinities predict the need for GEFs.*** G-proteins typically have differing affinities for GDP and GTP. GEFs are needed when a G-protein's affinity for GDP is greater than ~9-fold higher than is its affinity for GTP as a result of the relative abundance of guanine nucleotides in the cell.

Factor	$K_D(GTP)$	$K_D(GDP)$	$K_D(GTP)/K_D(GDP)$	*Refs*
IF2	10.6 uM	4.5 uM	2.4	Hauryliuk V (2009)
eIF2*	1.7 (0.2♠)	0.02	85 (10♠)	Kapp LD (2004)
eIF5B$^{\Delta}$	16	2.3	7	Pisareva VP (2007)
EF-Tu	0.06	0.001	60	Gromadski KB (2002)
EF-Tu/Ts	14	9	1.6	Gromadski KB (2002)
EF-G	0.15	10	0.015	Wilden B (2006)
eEF-1A*	1.1	0.4	2.8	Gromadski KB (2007)
eEF-1A/1B*	25	9.3	2.7	Gromadski KB (2007)
eEF-2†	4.4	2	2.2	Gonzalo P (2000)
RF3	0.1	0.023	4.3	Koutmou KS (2014)
eRF3	200 (0.7♯)	1.3 (1.9♯)	150 (0.4♯)	Hauryliuk V (2006)

* yeast ♠ when bound to Met-tRNA$_i$
† rat ♯ in the presence of eRF1
Δ rabbit

number of ribosomes actively engaged in protein synthesis. During fast growth conditions, protein synthesis occurs at a rate of ~20 amino acids per second per ribosome[35]. Under these conditions, ribosome concentrations can reach as high as 100 μM[36,37]. With the assumption that at *least* 10% of these ribosomes are actively engaged in protein synthesis, it becomes apparent that roughly half of a cell's GTP reserve must be devoted to the production of new proteins every second.

$$Energy/_{Time} = \left(20\,\frac{amino\ acids}{Ribosome \cdot s^{-1}}\right)(10\ \mu M\ Ribosomes)\left(2\,\frac{GTP}{amino\ acid}\right)$$

$$= 400\ \mu M\ GTP/_{s}$$

EQUATION 1.1

Indeed, measurements of energy consumption suggest that up to two-thirds of the total energy produced by rapidly growing *Escherichia* coli (*E.* coli) cells is devoted to protein synthesis[38]. TRAFAC G-proteins are thus incredibly expensive tools to implement. Thus, their prevalent use underscores the importance of G-proteins to the translation phase of gene expression.

1.4 THE ARCHITECTURE OF THE RIBOSOME

Proteins synthesis requires the orchestration of an immense arsenal of proteins and RNA molecules, but at the forefront of this process is the 2.5 MDa ribonuclear particle called the ribosome (Figure 1.4). In *E. coli*, ribosomes consist of two subunits: a small

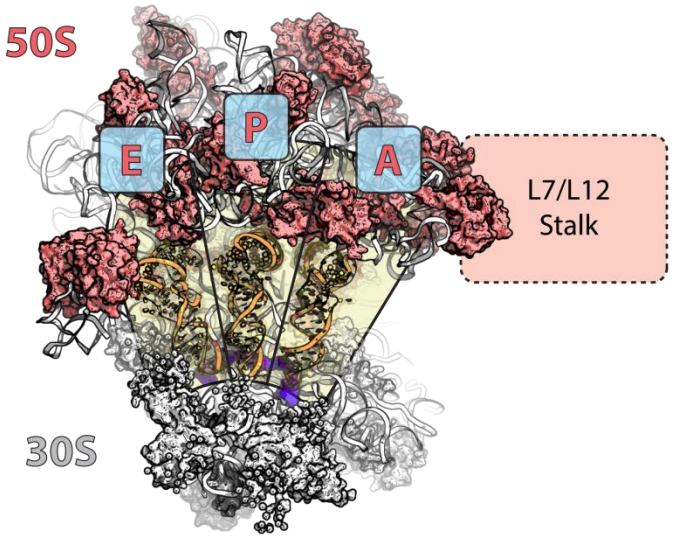

FIGURE 1.4 ***Structural elements of the bacterial ribosome*.** In bacteria, the 70S ribosome consists of two subunits. A small subunit, comprised of a 16S rRNA (*white*) and 21 proteins (*grey*), binds to the mRNA transcript (*purple*) and provides a platform for the anticodon loop of the tRNA substrates (*orange*). The large subunit consists of a 23S and a 5S rRNA (*white*) as well as 31 proteins (*red*). The leading edge of the ribosome (*right-hand side*) accepts aa-tRNA into the A-site. The nascent polypeptide (not shown) stemming from the peptidyl-tRNA in the P-site is then transferred to the A-site tRNA. The mRNA, along with the tRNAs, is then translocated through the ribosome by one position such that the leading edge tRNA is now positioned in the P-site, and the central tRNA is now positioned in the E-site. The E-site tRNA is ejected, setting up the ribosome to accept a new tRNA at the leading edge. Note that three tRNAs are shown here to clarify the three classical positions within the tRNA tunnel though, in actuality, under normal circumstances there are only two tRNA substrates in the ribosome at a time. Components of the leading edge of the large subunit are not shown (*L7/L12 stalk*). Adapted from PDB accession code 4V5L.

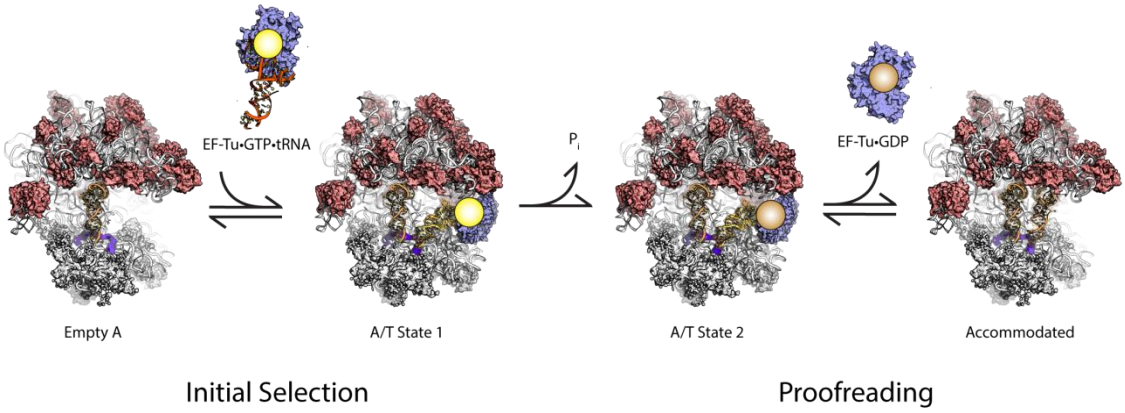

FIGURE 1.5 ***tRNA selection occurs in two phases.*** aa-tRNAs are delivered to the empty A-site ribosome as a ternary complex with EF-Tu·GTP. This leads to a testing of the codon-anticodon residues in a multistep process globally referred to as *Initial Selection*. If not rejected, GTP is hydrolyzed and a second testing of the codon-anticodon ensues through a process termed *Proofreading*. Upon correct pairing, the aa-tRNA fully accommodates into the ribosome and the tRNA selection process then concludes with the formation of a peptide bond.

and large subunit referred to by their sedimentation coefficient 30S and 50S respectively. The 30S subunit is constructed from 21 proteins and a 16S rRNA that is 1,540 nucleotides in length. The 50S subunit is comprised of 31 proteins, a 5S rRNA that is 120 nucleotides in length, and a much larger 23S rRNA that stretches 2,900 nucleotides. Together, these subunits associate on an mRNA transcript to form a 70S particle[39].

During elongation, tRNAs transit through the interior tRNA-tunnel of ribosome occupying distinct positions[40,41]. First, EF-Tu delivers aa-tRNA to the A-site of the ribosome on the leading edge of the tRNA tunnel. After the nascent polypeptide is transferred to the A-site tRNA, EF-G translocates the ribosome and bound substrates by one codon, shifting the A-site tRNA towards the interior of the ribosome to the peptidyl-site (P-site). Another round of tRNA selection and translocation further moves the tRNA towards the exit-site (E-site) of the tunnel where it is ultimately ejected from the ribosome

The translational machinery ultimately exists to decode mRNA. Biochemical and structural data have provided key insights to the decoding mechanism and indicate that it is a multistep process dependent on the GTPase function of EF-Tu.

1.5 THE DECODING MECHANISM

The primary function of the ribosome is to decode an mRNA transcript so that a polypeptide can be faithfully synthesized. This process requires testing the interaction between the mRNA codon with an anticodon of an adaptor tRNA molecule. The

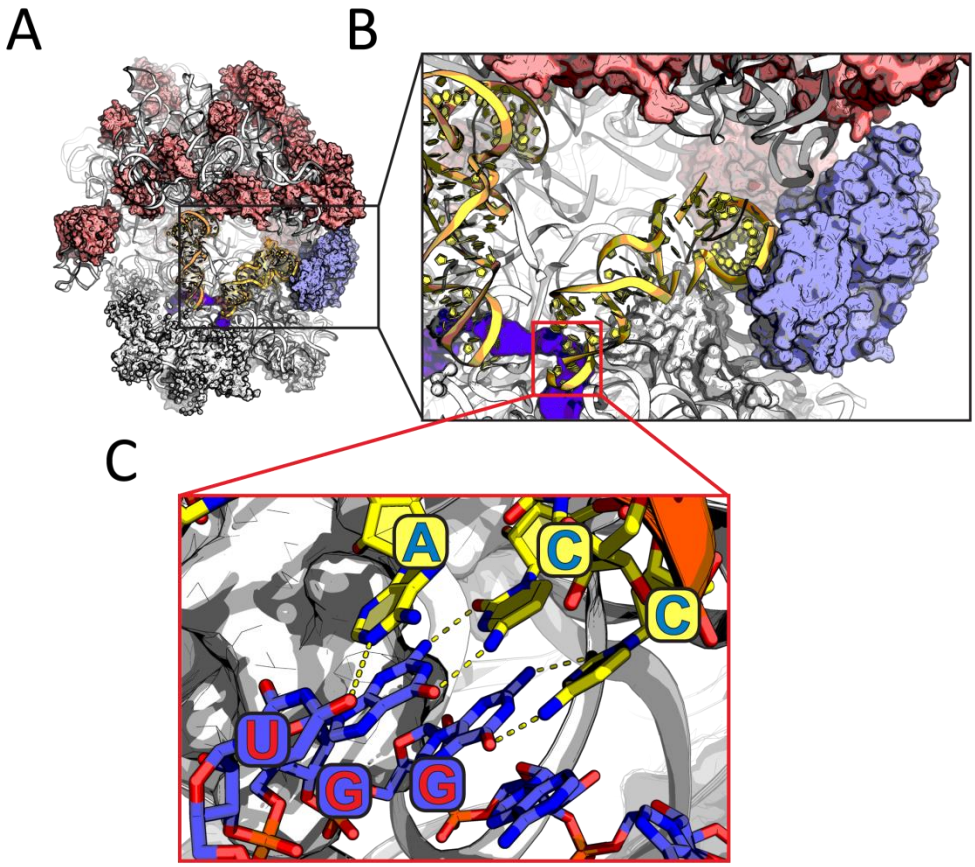

FIGURE 1.6 ***The fidelity of tRNA selection stems from proper codon-anticodon interactions.*** **A**, full view of the A/T-state ribosome (PDB accession code 4V5L). Large subunit proteins are colored *red*, small subunit proteins are colored *grey*, rRNA is colored *white*, tRNAs are *yellow*, mRNA is *purple*, EF-Tu is *blue*. **B**, closer view of the A/T-tRNA bound to EF-Tu. **C**, detailed view of the tryptophan codon (*blue*)-anticodon (*yellow*) interaction.

fidelity of protein synthesis is approximately five orders of magnitude less accurate than DNA replication, with error rates of about one incorrect amino acid incorporated per ten thousand (ca. $5x10^{-3} – 6x10^{-4}$)[42-44]. Under the gross assumption that the average protein contains roughly 400 amino acids, one out of twenty five proteins will contain an error at the amino acid level as a result of translational infidelity. Functional studies of the decoding process have revealed that the translational machinery can be driven to even higher levels of fidelity[45,46]. However, this has been speculated to occur at the expense of speed such that the rate of protein synthesis is inversely proportional to the accuracy of protein synthesis[42,47-50].

Specifically, this model postulates two distinct interactions that lead to either tRNA accommodation or tRNA rejection termed *initial selection* and *proofreading* (Figure 1.5). First, ternary complex interacts with an empty A-site ribosome in a bimolecular manner. Pre-steady state data of this process demonstrate that ternary complex binds to the ribosome with a very fast on-rate of 140 $\mu M^{-1}s^{-1}$ [1]. The anticodon of the aa-tRNA is first tested with the codon of the mRNA through a process termed codon recognition (Figure 1.6). The anticodon loop of the aa-tRNA is situated in the A-site of the small subunit, while the t-stem remains bound to EF-Tu in a bent conformation termed the A/T State. The codon-anticodon interaction is, in part, coordinated by key residues in the small subunit 16S rRNA. Improper placement leads to rapid ternary complex rejection[1,24]. If the tRNA is not rejected, the t-stem of the aa-tRNA begins to sample the A-site of the large subunit during the proofreading phase. The selection process completes when either the tRNA is rejected, or the CCA- end is fully accommodated into the A-site of the large subunit. If accommodated, a peptide bond is rapidly catalyzed by the peptidyl transferase center of the ribosome which leads to the transfer of the nascent polypeptide from the P-site tRNA to the A-site

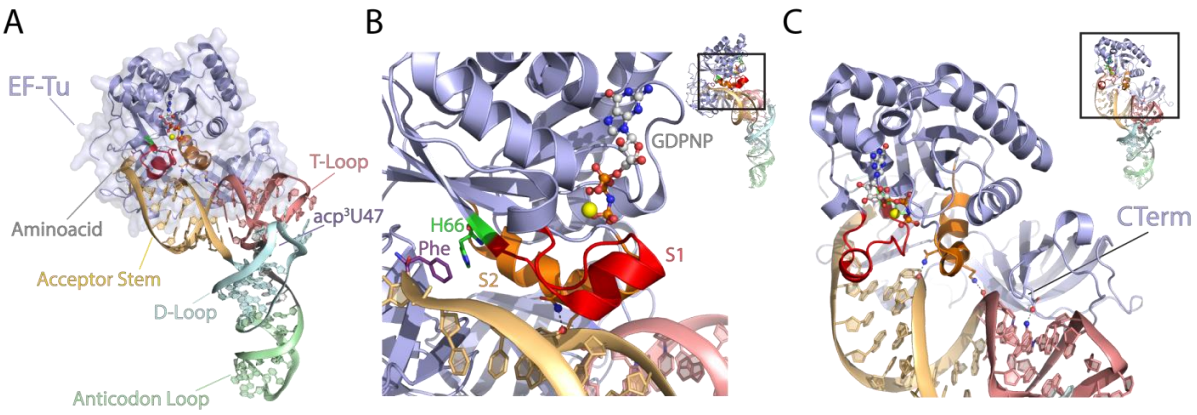

FIGURE 1.7 ***Structural elements of phenylalanyl ternary complex*****. A**, EF-Tu (*blue*) bound to the GTP analog GDPNP (carbon atoms are *grey*, nitrogen are *blue*, oxygen are *red*, and phosphorus are *orange*, Mg^{2+} is *yellow*) and Phe-$tRNA^{Phe}$. Elements of the tRNA are colored for clarity (acceptor stem is *yellow*, T-loop is *pink*, D-loop is *cyan*, anticodon loop is *green*) along with the site of fluorophore conjugation (acp^3U47, *purple*). **B**, detailed view of the allosteric pathway linking nucleotide binding to the formation of an amino acid binding pocket. The terminal phosphate of the nucleotide, along with the Mg^{2+} ion coordinate the switch regions (switch 1, S1, in *red*; switch 2, S2, in *orange*) which in turn orient the critical residue His66. **C**, detailed view of EF-Tu interactions with the T-stem of the tRNA (which collectively refers to the acceptor stem and the T-loop). The caroxy terminus (CTerm) of EF-Tu is highlighted.

tRNA. This final step is irreversible in this context and thus commits the ribosome to the selection of the A-site tRNA. Although this process has been studied extensively from the perspective of the incorporating tRNA[1,24,26,40,51-55], little is known about the precise contribution of EF-Tu during this process.

1.7 GTP ENABLES EF-TU TO RECOGNIZE THE AMINOACYL MOIETY OF tRNA

Ternary complex is the primary substrate for the ribosome during the decoding process. As such, errors in the construction of ternary complex could potentially result in the addition of an incorrect amino acid to the polypeptide chain being synthesized. Interestingly, EF-Tu·GTP exhibits extremely low affinity for non-acylated tRNAs (ca. $K_D > 1$ M) prohibiting the delivery of a tRNA without an amino acid. Structural and biochemical data has shed significant light on precisely how the aminoacylated state

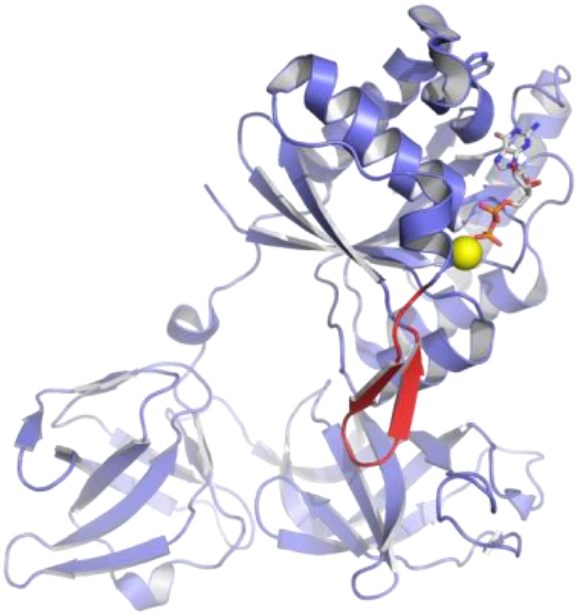

FIGURE 1.8 ***Inactive EF-Tu adopts a unique switch conformation.*** EF-Tu (blue) bound to GDP (carbon atoms are grey, nitrogen are blue, oxygen are red, phosphorous are orange, Mg^{2+} is yellow) adopts an extended conformation with the G-domain positioned distal from domain II. This is state is characterized by the switch 1 (red) which adopts a helix-loop-helix secondary structure, a dramatic change from the α-helix structure that it assumes in the GTP-bound state.

of tRNAs are recognized. EF-Tu·GTP binds to aa-tRNA along the acceptor stem and T-loop, collectively referred as the T-stem[56]. Domains I and II of EF-Tu are observed to fold around the aminoacyl-moiety of aa-tRNA, forming the amino acid binding pocket[57]. In the case of phenylalanyl-ternary complex (Phe-TC), the imidazole moiety of residue His66 of EF-Tu is oriented in a planar stacking configuration with the phenol element of the aminoacyl moiety of $Phe\text{-}tRNA^{Phe}$ (Figure 1.7). His66 is accordingly positioned by the neighboring switch 1 region consisting of EF-Tu residues 40-62. The switch 1 region derives its name because it adopts vastly different conformations depending on whether EF-Tu is bound to either GTP or GDP (Figures 1.7, 1.8). When EF-Tu binds GTP, it does so in conjunction with a Mg^{2+} ion that is coordinated by the β and γ phosphates. The Mg^{2+} ion in turn plays a role in coordinating the switch 1 helix thus allosterically coupling GTP binding with aa-tRNA binding.

In contrast, when EF-Tu is bound to GDP, the Mg^{2+} ion is coordinated by the α and β the phosphates of the nucleotide and is therefore not positioned appropriately to stabilize the switch 1 motif as a helix. Rather, the switch 1 motif adopts a beta hairpin structure (Figure 1.8). As such, EF-Tu·GDP does not form an amino acid binding pocket and exhibits no biological affinity for aa-tRNA. tRNA delivery to the ribosome is thus restricted by two conditions: EF-Tu must be bound to GTP and the tRNA must be aminoacylated.

1.8 EF-TS IS THE GUANOSINE NUCLEOTIDE EXCHANGE FACTOR FOR EF-TU

Owing to EF-Tu's relatively high affinity for GDP over GTP, EF-Tu requires the auxiliary protein EF-Ts to facilitate the formation of EF-Tu·GTP. This is a critical step since each round of tRNA selection has the ultimate effect of converting EF-Tu·GTP into its inactive form, EF-Tu·GDP (Figure 1.9). Mutagenesis studies have revealed

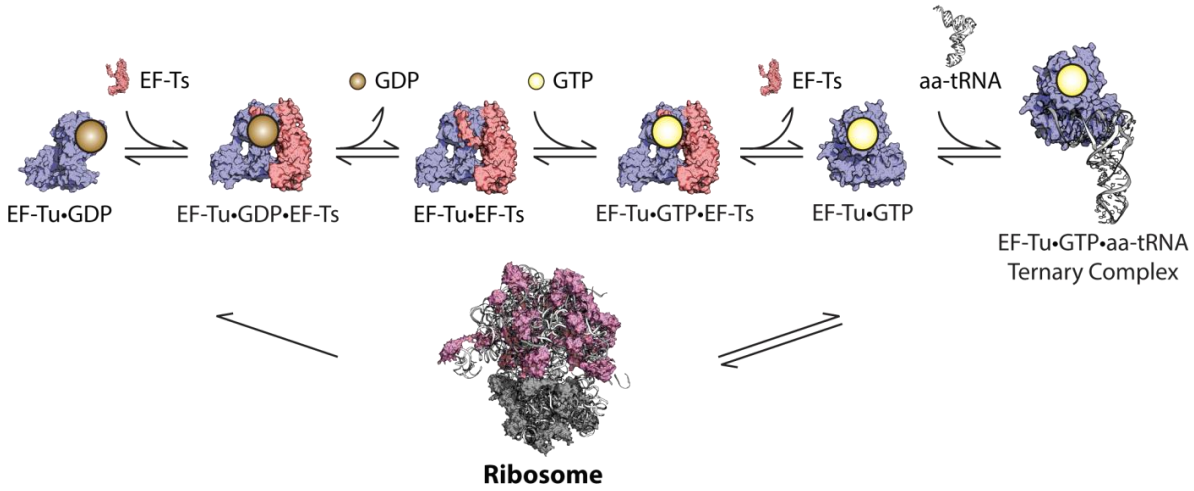

FIGURE 1.9 ***Activation of EF-Tu requires the GEF EF-Ts.*** EF-Tu (*blue*) disembarks from the ribosome (*pink/grey*) in an inactive state bound to GDP (*brown*). EF-Ts binds to this complex with high affinity and catalyzes the exchange of GDP for GTP (*yellow*). The canonical model then predicts that EF-Tu·GTP is released from EF-Ts in an active form that is then competent to bind aa-tRNA (*white*) and participate in tRNA selection with the ribosome.

that EF-Ts is critical to cell survival[58]. Indeed, efforts to recapitulate protein synthesis *in vitro* have revealed that the process is severely compromised without the inclusion of EF-Ts[59]. Current models predict that when EF-Tu·GDP disembarks from the ribosome, EF-Ts binds to this complex with high affinity[31]. This interaction leads to the removal of GDP and to the binding of GTP. Activated EF-Tu is then released and competent to bind to an aa-tRNA so as to engage in another round of tRNA selection.

EF-Ts facilitates nucleotide exchange by stabilizing the transition state of nucleotide binding (Figure 1.10)[60]. Crystallographic data show that when bound to EF-Ts, EF-Tu can adopt a conformation that is globally similar to its GDP-bound conformation. EF-Ts largely interacts with domains I and III of EF-Tu with the addition of a protruding C-terminal alpha helix, termed the C-domain, which interacts with helix D of EF-Tu. This causes a rearrangement of Lys136 and Leu175 which are normally involve the stabilization of the ribose and guanosine base[60]. A conserved residue of EF-Ts, Phe81, inserts between EF-Tu residues His118 in helix C and His84 in helix B of the switch 2 region. The repositioning of these residues are believed to lead to a rearrangement of the P-loop negatively impacting the stabilization of the

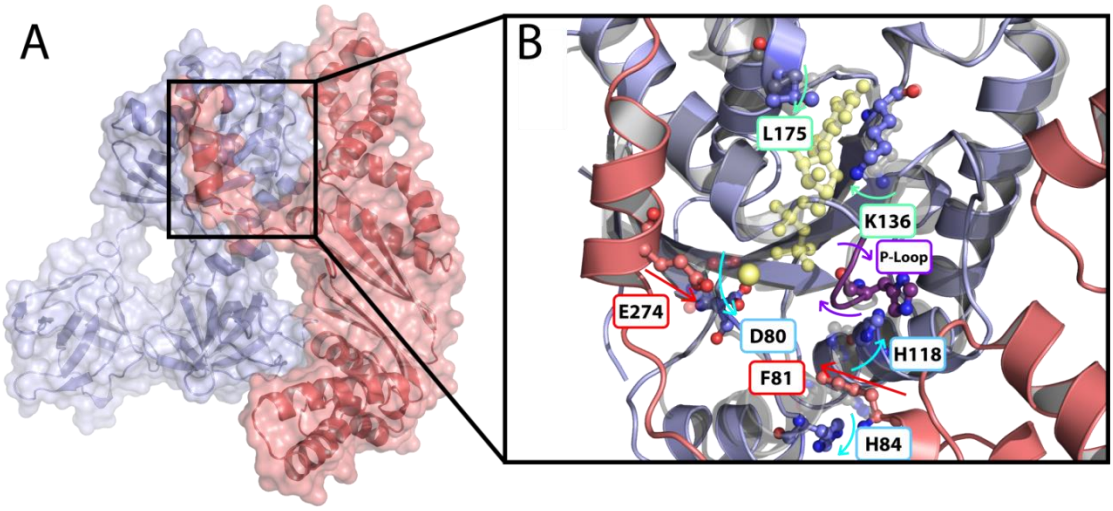

FIGURE 1.10 ***EF-Ts stabilizes the nucleotide binding transition state of EF-Tu***. Critical EF-Ts residues E274 and F81 destabilize the guanosine binding surface (EF-Tu residues L175 and K136) and the Mg^{2+} ion (EF-Tu residues D80, H118, and H84).

nucleotide's β-phosphate. The intrusion of EF-Ts residue Glu274 of the C-domain abolishes the coordination of the Mg^{2+} ion by altering the configuration of EF-Tu residues Asp80, Cys81, and Pro82[60]. The net effect of this interaction is that the nucleotide binding site is highly destabilized. Both the on-rate, and the off-rate of GDP and GTP are increased substantially[31] consistent with a lowering of the activation energy between the bound and unbound states.

1.9 CURRENT MODELS OF tRNA SELECTION ARE TOO SLOW

Protein synthesis has been studied from both *in vivo* and *in vitro* perspectives. Pulse-chase experiments conducted *in vivo* with a variety of bacterial species measure the rate of protein synthesis to be between 2 and 20 amino acids polymerized per ribosome per second depending on growth conditions[35,61,62]. Importantly, these measurements place an upper and lower limit to the molecular processes which lead to protein synthesis. As models are developed, they must ultimately operate within these limits. However, current models predict an upper limit to the rate of amino acid polymerization of $7\ s^{-1}$, about 3-fold too slow. These models stem from bulk measurements of peptide bond formation[2] and EF-Tu release from the ribosome after GTP hydrolysis[4,24]. Rectification of these short comings requires a more complete understanding of how TC is formed and decoded by the ribosome.

To advance our understanding of protein synthesis, and to reconcile the rate of protein synthesis with *in vivo* measurements, we examined the both the formation and stability of TC and the process of tRNA selection from multiple perspectives. The data presented in subsequent chapters highlights new assays designed to directly examine the molecular processes that lead to aa-tRNA accommodation. These data focus on the precise role of EF-Tu in this process and how EF-Tu activation is regulated.

CHAPTER 2

METHODS

2. OVERVIEW

Section 2.1 describes general operating procedures for the instrumentation used to acquire the data presented in subsequent chapters. Section 2.2 provides detailed reagent purification methods followed by fluorophore conjugation methods in section 2.3. This chapter concludes with a description of experimental procedures in section 2.4.

2.1 INSTRUMENTATION

This section describes the instruments used to perform the assays discussed in later sections and chapters. Specifically, a detailed description of the PTI-QM4 fluorometer and the Applied Photophysics SX20 are presented.

2.1.1 PTI-QM4 Fluorometer

A fluorometer (also referred to as a spectrofluorometer or a florimeter) is an instrument capable of measuring parameters of fluorescence. The experiments discussed in this document used a Photon Technology International QuantaMaster 4 fluorometer (Figure 2.1) to monitor time-dependent changes in fluorescence and, to a

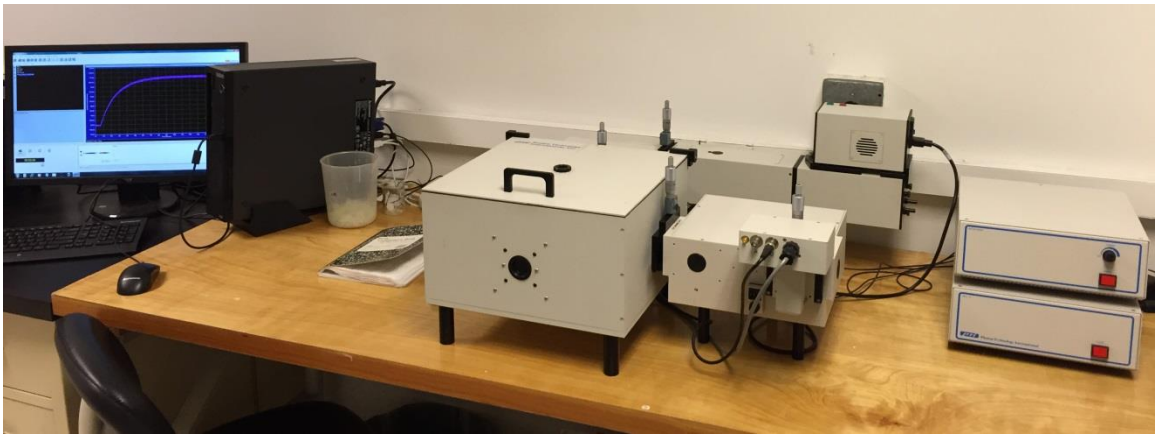

FIGURE 2.1 ***PTI-QM4 Fluorometer*****.** Photon Technology International QuantaMaster 4 spectrofluorometer.

lesser extent, to measure emission and excitation spectrums. This instrument was used to conduct both relative fluorescence and FRET experiments. Specifically, this instrument was used to acquire the data shown in Figures 3.1, 3.2, 3.3, 3.6, 4.2, 4.4, 4.5, and 5.3 Specific experimental procedures will be described in subsequent sections. This section serves as a practical guide towards understanding and operating a PTI-QM4 fluorometer.

The instrument consists of a reaction chamber as well as an excitation source and an emission detector (Figure 2.2). The light source used in this configuration is a high powered Xenon flash lamp with a repetition rate of up to 300 Hz with usable intensity between 185 nm and ~850 nm. Immediately after the lamp housing unit, along the direction of the emitted light path, is a light-side aperture with a manually adjustable diameter, ranging of 1 – 5 microns. Next, the light encounters an excitation diffraction grating with 1200 line/mm, blazed at 300 nm. The selected wavelength is then directed through a grating-side aperture, and then into the reaction chamber capable of housing a standard 3mL quartz cuvette. Included in the housing chamber is a temperature-stabilizing unit that can circulate fluid around the cuvette holder. A reaction-side aperture is located 90° offset from the incoming light path to direct light towards an emission grating with 1200 line/mm, blazed at 400nm. From there, the light is directed

through another grating-side aperture and is then detected by a single-shot transient digitizer (SSTD) detector.

This instrument is amenable to bulk fluorescence assays involving a standard sized cuvette. As a benchmark for designing fluorescence assays, a 5 nM dye solution of Cy3 is about the minimum that can be reliably detected with the current configuration. The general steps for operating the PTI-QM4 fluorometer are as follows:

STEP 1

Warm up the lamp. Turn on the Xenon lamp 30 minutes prior to the experiment. Failure to do this may result in a slow drift in fluorescence, possibly due to

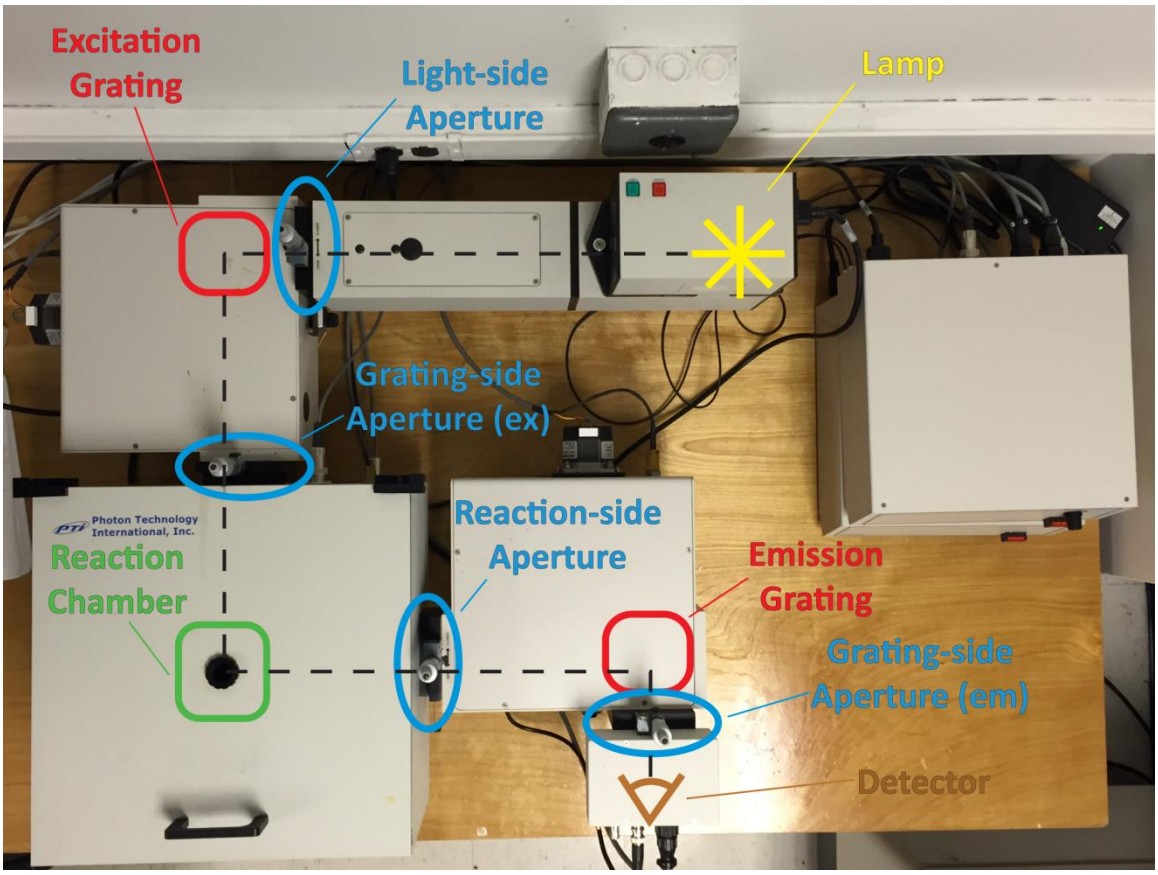

FIGURE 2.2 ***Light path of PTI-QM4 fluorometer.*** A pulsed xenon lamp emits light along the light path (*black dotted line*) through apertures (*blue*) and diffraction gratings (*red*) via a reaction chamber (*green*) to a K-171B red sensitive detector (*brown*).

temperature fluctuations in the lamp.

STEP 2

Turn on hardware. When ready to begin the experiment, turn on remaining hardware as needed. In order to operate the fluorometer, turn on the controller power box, the stir bar power box (if needed), and the PC. In the controlling PC, open the PTI software 'FelixGX'.

STEP 3

Manually adjust apertures. The apertures should be set so that the amount of fluorescence being detected is within the range of 100,000 – 1,000,000 counts/second. Operating above or below this range will yield irreproducible results and may damage the detector. Since diffraction gratings are used to select for both excitation and emission wavelengths, the grating-side apertures should be set to the smallest value amenable so as to reduce the likelihood that neighboring wavelengths of light will also be

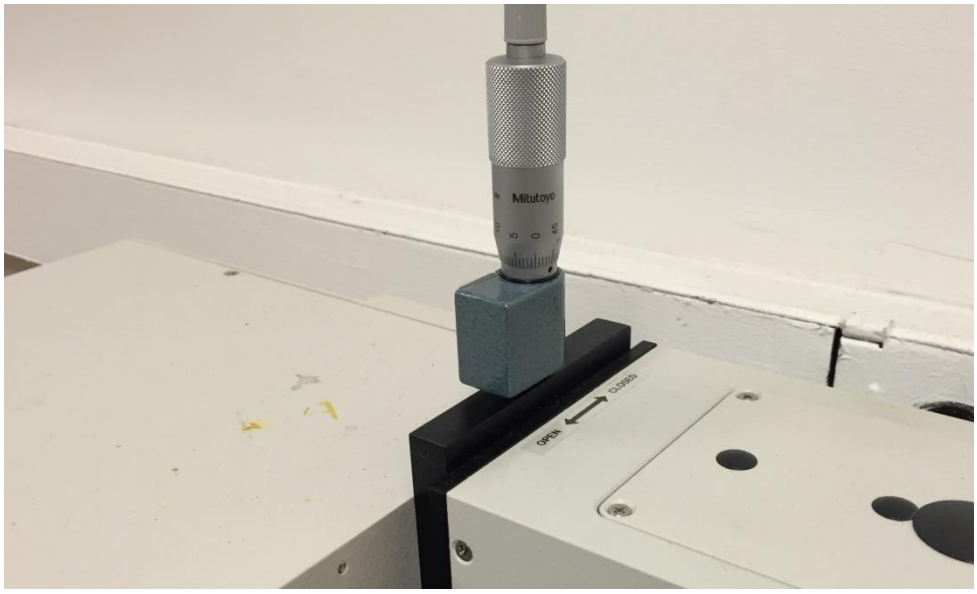

FIGURE 2.3 ***Manual aperture knob*****.** This is the manual knob that is used to open and close the light apertures.

selected. If more signal is needed to raise the counts/second into the usable range, first open the reaction-side aperture. If more signal is still needed, open the light-side aperture. Note that this will illuminate the sample with greater intensity so be weary of photobleaching. If there is still not enough signal reaching the detector, increase the grating-side apertures, or increase the concentration of fluorophore in the reaction.

STEP 4

Set up reaction. Place the cuvette in the reaction chamber. Afterwards, make sure the lid is securely in place, the sliding apertures are open, and that the side ports are properly closed. If needed, make sure that the stir bar is set appropriately (stir speed can be modulated on the stir bar power box).

STEP 5

Excitation correction. If excitation correction is desired, select *Digital Excor* (default is Digital) located on the top right-hand side of the computer screen in the FelixGX software. This will generate a warning titled 'FelixGX Hardware Configuration Changed'. Click *OK*.

STEP 6

Timebased Data Acquisition

i. In the FelixGX software, select *Setup*.

ii. Under the tab *Acquisition Type*, Select *Timebased*.

iii. Navigate to the *Acquisition Settings* tab and enter excitation and emission wavelengths.

iv. Enter data points per second (10 is a good starting point).

v. Enter the duration of the experiment in seconds.

vi. Navigate to the *Real-time Corrections* tab and enable Excitation Correction.

vii. A dialog box will open titled 'Open Ex Corr Lookup Table'. Select *excorr* and click *OK*.

viii. Input the excitation wavelength that will be used in the experiment and click the *Go to* button.

ix. Adjust the gain so that the Signal(V) reading is approximately 1.0. This must be done while illuminating the fluorescent reaction.

x. Click *Accept* to close dialog box.

xi. In the main screen select *Start* to begin data acquisition.

xii. To save an acquisition, right click on the data set in the text dialog box, and select export. This can be exported in a FelixGX format or a text file format (text is usually preferred).

xiii. To save the session, navigate to the *File* menu and select *Save*.

Timebased Data Acquisition – Steady State Titration Experiments

i. – iv. Proceed as indicated in the Timebased Data Acquisition procedure.

v. Enter the duration of acquiring each data point (10 seconds is a good starting point).

vi. Navigate to the *Real-time Corrections* tab and enable Excitation Correction.

i. A dialog box will open titled 'Open Ex Corr Lookup Table'. Select *excorr* and click *OK*.

ii. Input the excitation wavelength that will be used in the experiment and click the *Go to* button.

iii. Adjust the gain so that the Signal(V) reading is approximately 1.0. This must be done while illuminating the fluorescent reaction.

vii. Navigate to the *Preferences* tab.

viii. Uncheck *Always create a new Session*. This will allow multiple acquisitions to be made within one session.

ix. Click *Accept* to close dialog box.

x. In the main screen select *Start* to begin data acquisition.

xi. After acquisition, the cuvette can be accessed if needed. Wait a sufficient amount of time for the reaction to reach equilibrium (5 minutes is a good starting point). Proceed back to *step x* as needed.

xii. To save an acquisition, right click on the Session title of the data set in the text dialog box, and select export. This can be exported in a FelixGX format or a text file format.

xiii. To save the session, navigate to the *File* menu and select *Save*.

Spectral Data Acquisition

i. – iii. Proceed as indicated in the Timebased Data Acquisition procedure

iv. In the FelixGX software, select *Setup*.

v. Under the tab *Acquisition Type*, select *Emission* (or *Excitation*) *Scan*.

vi. Navigate to the *Acquisition Settings* tab and enter excitation and emission range.

vii. Enter *Step Size* (1 nm is a good starting point).

viii. Enter the *Integration* time of each data point in seconds (1 second is a good starting point)

ix. Enter the number of repeats (default is 0). This is the number of additional scans that will be executed. The final output will be an average of all of the scans.

x. Navigate to the *Real-time Corrections* tab and enable Excitation Correction.

xi. A dialog box will open titled 'Open Ex Corr Lookup Table'. Select *excorr* and click *OK*.

xii. Input the excitation wavelength that will be used in the experiment and click the *Go to* button.

xiii. Adjust the gain so that the Signal(V) reading is approximately 1.0.

xiv. Click *Accept* to close dialog box.

xv. In the main screen select *Start* to begin data acquisition.

xvi. To save an acquisition, right click on the data set in the text dialog box, and select export. This can be exported in a FelixGX format or a text file format.

xvii. To save the session, navigate to the *File* menu and select *Save*.

STEP 7

Data analysis can be done with any number of data analysis software. This discussion will focus on using Origin8, distributed by OriginLab.

i. Open Origin8 and create a new excel spreadsheet.

ii. Navigate to the *Data* tab, and select *Import Text Data*, making sure to delineate appropriately.

iii. Copy the data into an Origin workbook; omit any header and footer information. Note: data can be imported directly into a workbook,

though this is not recommended. Large datasets can lead to stability issues with the software.

a. Represent data by fold change.

i. In a new column, divide each raw data column by the average of the baseline.

ii. Highlight normalized data columns.

iii. Navigate to the *Statistics* menu and select *Descriptive Statistics* followed by *Statistics on Rows*.

iv. Plot data.

b. Represent data by percent change.

i. Right-click on a new column and select *Set Column Values*.

ii. In the dialog box, input (col(data) - AvgMin) / (AvgMax – AvgMin), where AvgMax and AvgMin are the average maximum and minimum values of the data respectively (Figure2.1.1.4).

iii. Highlight normalized data columns.

iv. Navigate to the *Statistics* menu and select *Descriptive Statistics* followed by *Statistics on Rows*.

v. Plot data.

iv. To fit the data, select the *Analysis* tab and then select *fitting* followed by the desired method.

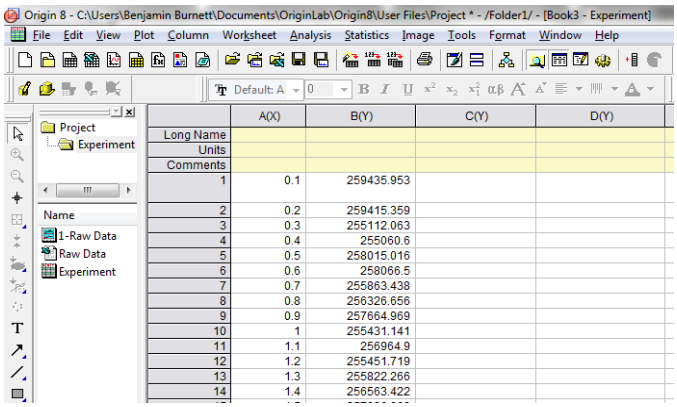

FIGURE 2.4 ***Importing data into OriginLab.*** The raw data is imported into an excel workbook within Origin. The relevant data is then copied into an origin workbook for analysis (shown). Column A(X) contains time data and Column B(Y) contains the raw fluorescence data.

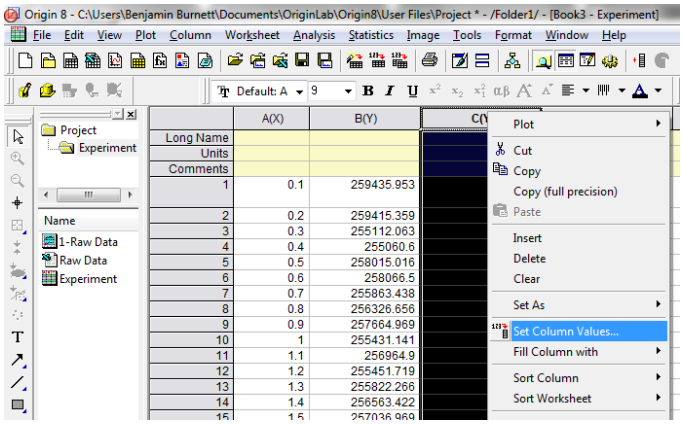

FIGURE 2.5 ***Data processing.*** Data analysis can be done by right-clicking on a new column (Column C(Y) shown here), and navigating to *Set Column Values...*

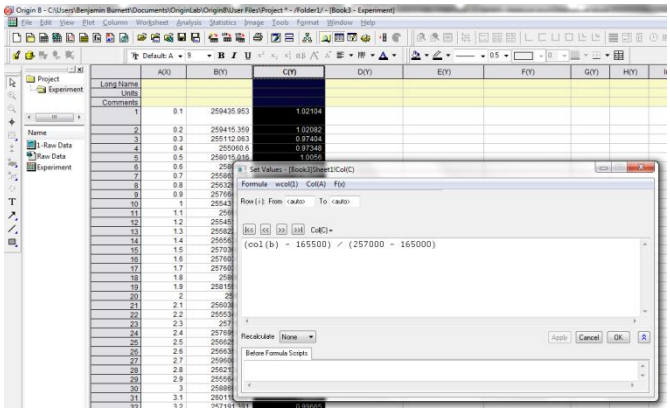

FIGURE 2.6 ***Normalize data by percent change.*** The *Set Values* dialogue box opens when selecting *Set Column Values...*. The normalization procedure to achieve percent change is shown.

2.1.2 SX20 Stopped-flow Spectrometer

A Stopped-flow spectrometer is a rapid mixing device used to measure changes in fluorescence intensity at fast time resolution. The experiments discussed in this document use an Applied Photophysics Single-Push SX20 Stopped-Flow spectrometer. This instrument was used to conduct both fluorescence and FRET experiments presented in Figures 3.4, 4.3, 4.6, 4.7, 5.3, 5.4, 5.5, 5.6, 5.7, 2.10, and 5.11. Specific experimental procedures will be described in subsequent sections. This section serves as a practical guide towards understanding and operating a SX20 Stopped-flow spectrometer.

At a basic level, this instrument consists of a T-mixer flow cell which resembles the shape of a tuning fork (Figure 2.7). The two arms of the fork contain separate reagents that are then mixed by direct flow into the central mixing chamber. The instrument is configured to complete the mixing process and begin data acquisition within approximately 1 ms. This instrument can be setup using either a monochromatic light source connected in line with an excitation side diffraction grating, or a light emitting diode (LED). The benefit of the monochromator is the inherent flexibility of selecting excitation wavelengths, though generally speaking this tends to be much dimmer than an LED. As a rule of thumb, use the monochromatic light source to pilot a new assay. Once established, purchasing a LED at the appropriate wavelength will likely increase the signal to noise substantially (user experience has been LEDs increase S/N by two to three fold over monochromators).

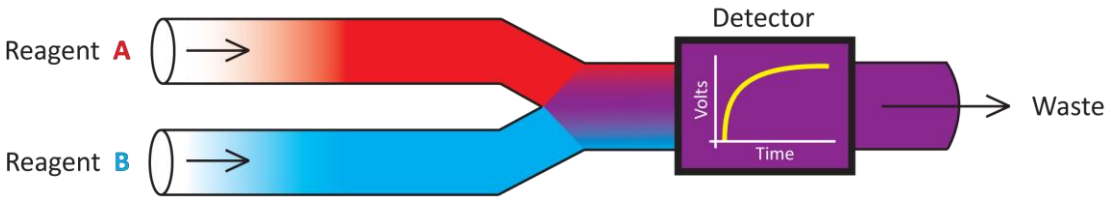

FIGURE 2.7 ***Schematic of T-mixer flow cell.*** Two reagents are mixed by a converging flow path. The rate of mixing is tightly controlled by the rate of fluid flow through the T-mixer. Once mixed, the solution flow is directed to the reaction chamber where fluorescence measurements can be made.

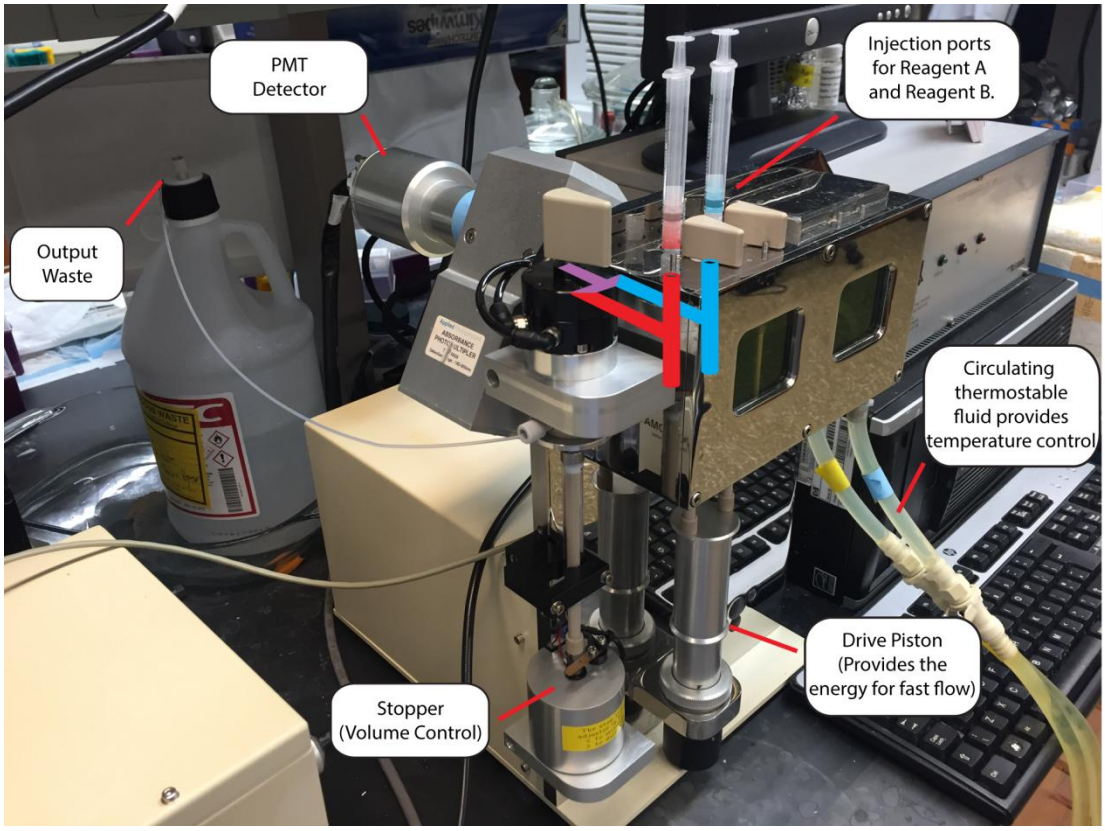

FIGURE 2.8 ***Applied Photophysics SX20 Stopped-flow spectrometer***. Each reagent is added using a 3 mL syringe connected to injection ports (*top right*). The Drive piston (*bottom right*) provides the mechanical energy to direct each reagent through the T-mixer (*schematized, center*) and into a reaction chamber monitored by a PMT Detector (*top left*). The sample is then dispensed as output waste (*left*). The volume driven through the T-mixer is regulated by the stopper (*bottom*) and temperature controlled by circulating thermostable fluid around the reaction chamber (*right*).

To use the SX20, reagents are first loaded into the injection ports (Figure 2.8). The sample is then driven through the T-mixer by an air-pressurized drive piston (Figures 2.8, 2.9). The volume of reagent that is driven through the T-mixer is controlled by a stopper and can be manually adjusted *via* a wheel located on the underneath side of the stopper. The reaction chamber is temperature stabilized by continuous flow of a thermostable fluid whose temperature is maintained by a water bath (Figure 2.9).

FIGURE 2.9 ***Air tank and water bath for the SX20*****.** Pressurized air tanks and regulator service the SX20 drive mechanism (*left*). A temperature controlled water bath regulates the temperature of the reaction chamber by circulating fluid (*right*).

Practical applications of this instrument include kinetic investigations of biomolecular interactions. When more complicated reactions are the subject of investigation, it is preferable to design the experiment in such a way as to interrogate a single kinetic step. This instrument is designed to probe kinetic processes that have a fluorescent readout at time scales of ~1 ms to ~1 minute. As a benchmark, 10 nM Cy3B is scarcely resolvable with the 532 nm LED. To reliable measure kinetic processes at fast time resolution, it is recommended to not use less than 60 nM Cy3B or equivalent fluorescence. The general steps for operating the SX20 are:

STEP 1

Configure the system and warm up the lamps. Assemble the appropriate PMT detector and emission filter (Figure 2.10). If using the monochromator, turn on the lamp at least 30 minutes prior to taking data. Failure to do this may result in a slow drift in fluorescence, possibly due to temperature fluctuations in the lamp. If using an

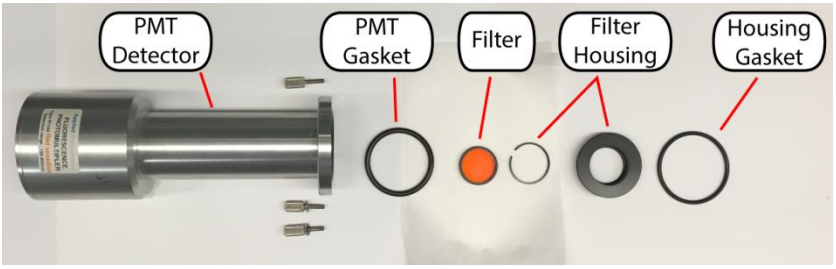

FIGURE 2.10 ***Filter assembly*****.** The filter is fitted into a filter house and assembled onto the SX20 with a housing gasket. The PMT is then screwed into the SX20, sandwiching the filter housing unit.

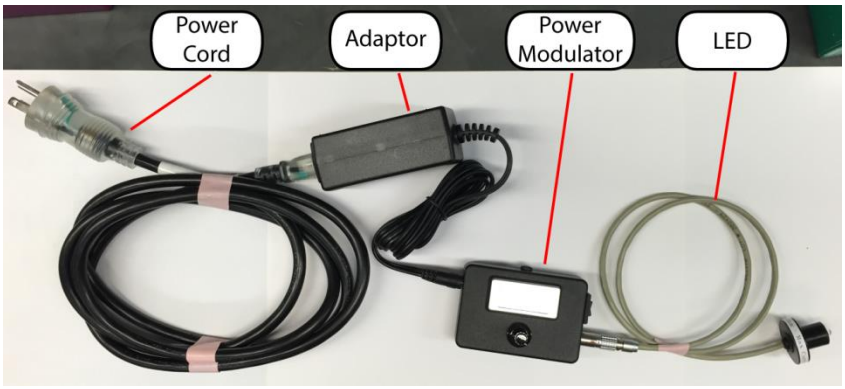

FIGURE 2.11 ***LED assembly*****.** The LED light source is connected to a power modulator and is subsequently connected to a power cord *via* an adaptor.

LED light source, assemble the appropriate LED to a power source and connect it to the SX20 (Figure 2.11).

STEP 2

Wash the system. To reduce the likelihood that a prior experiment will cause contamination, wash the system with water followed by methanol, then water a second time, and finally buffer. Specifically:

i. Water

   a. Manually push 4.5 mL of ddH_2O.

   b. Drive 120 µL of ddH_2O 10 times.

c. Manually push 1 mL of ddH_2O.

ii. Methanol

a. Manually push 4.5 mL of $30\%_V$ methanol.

b. Drive 120 µL of $30\%_V$ methanol.

c. Manually push 1 mL of$30\%_V$ methanol.

iii. Water

a. Manually push 4.5 mL of ddH_2O.

b. Drive 120 µL of ddH_2O 10 times.

c. Manually push 1 mL of ddH_2O.

iv. Buffer

a. Manually push 3 mL of buffer.

STEP 3

Prepare samples. Load samples into 3 mL Leur-Lok Syringes (Becton, Dickinson and Company). Pay careful attention to remove any air that may have been introduced

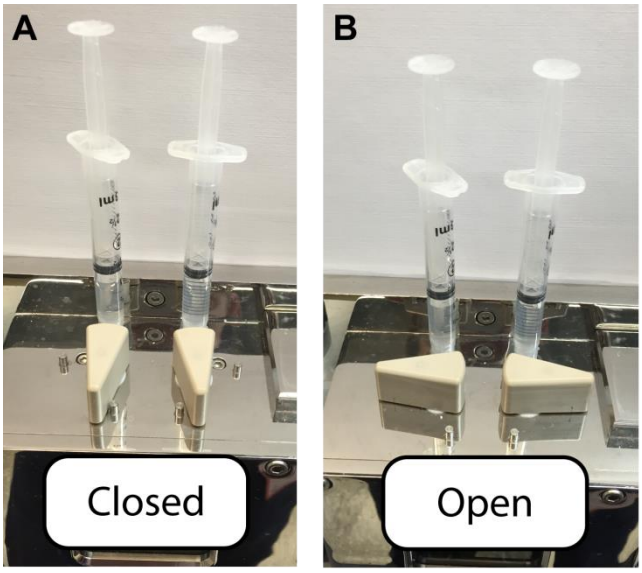

FIGURE 2.12 ***Sample chamber valves*****.** The sample chamber valves can be toggled to allow for sample injection. The chamber valve must be open to inject sample and during air extraction process. When operating the SX20 with the drive piston, the sample chamber valves must be in their closed position.

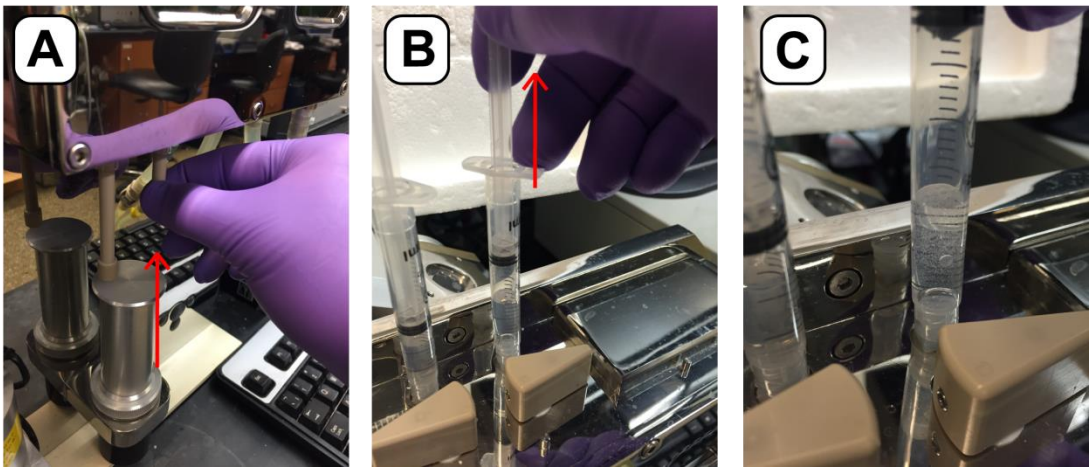

FIGURE 2.13 ***Extracting contaminating gas*****.** If not appropriately degassed, air bubbles in the system can propagate into the reaction chamber and distort the signal. It is therefore imperative that all gas is removed from the system. **A**, after injecting the sample into the sample chamber, flow the sample back into the syringe in rapid succession by push up on the piston leg. This should be repeated 4 to 5 times. **B**, pull upwards on the syringe plunger to purge they sample chamber of any remaining gas. **C**, a close-up of gas being purged in B.

during this process. Using the Luer-Lok tip, screw the syringes into the injector ports (Figure 2.8). Open the injector valves (Figure 2.12) and inject the sample into the sample chamber. With the valves open, manually push the sample back into the syringe using the piston leg (Figure 2.13*A*). Repeat this forward and backwards process 4 to 5 times to flush out air bubbles that may have been introduced into the sample chamber. As an extra precaution, when the sample is manually driven back into the syringe for the last time, gently pull upwards on the syringe plunger (Figure 2.13*B*,*C*). This will help to withdraw any remain gas from the sample chamber.

STEP 4

Set software parameters. In the Pro-Data SX software, navigate to the Signal section at the top left-hand side and select *Fluorescence* from the drop-down menu (Figure 2.14). Next, navigate to the Detector High Voltages section at the top right-hand side and input the appropriate gain setting in the *Abs. / Flu.* field. For best results, keep the voltage between 1.0 and 10 volts. Next, navigate to the KSHU

(Single Mixing) section at the right-hand side and select the *Setup* button. Adjust the shot counts appropriately and select *Okay*. If using a monochromator, navigate to the Monochromator section on the left-hand side and input the excitation wavelength and click *Set*. Proceed to the Trigger section of the menu, just below the Monochromator section and select *External* in the drop-down menu. Select *Pressure hold* if conducting experiments at time spans of one second or less. Otherwise, leave this unchecked. Move to the Timebase section and enter the total timeframe of the experiment and the desired number of data points. For a 250 ms experiment, 5,000 data points is ideal.

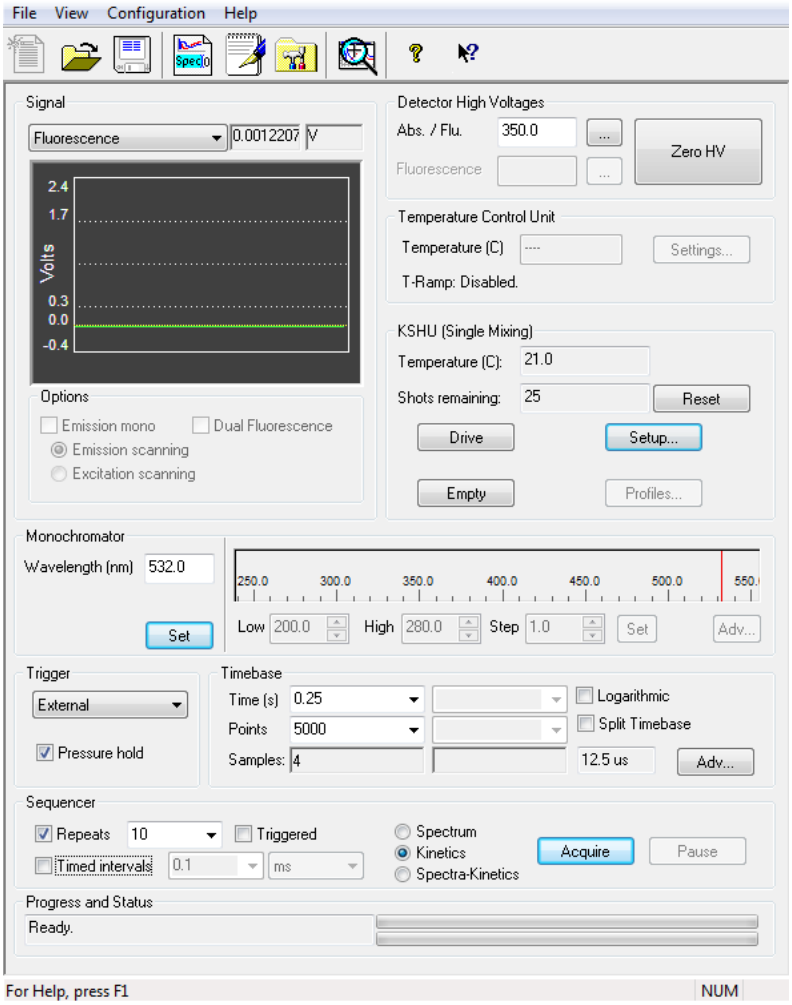

FIGURE 2.14 ***Pro-Data SX20 software interface.*** Screen shot of the Pro-Data SX20 software interface with typical parameters for a 250 ms timebased experiment. For fluorescence experiments using an LED, the monochromator settings can be ignored.

Finally, navigate to the Sequencer section and enable *Repeats* if desired. Unless specifically necessary, leave the *Triggered* box unchecked and the *Kinetics* selected. To begin data acquisition, select *Acquire*.

2.1.4 Single Molecule TIRF Microscopy

The single-molecule fluorescence imaging platform described here is a custom built instrument that is continually evolving to accommodate technological innovations in optics, data acquisition, and throughput. Thus, the particular components and methods described here are specifically applicable to its current setup as described by Juette et al.[63].

Single-molecule fluorescence resonance energy transfer (smFRET) experiments were conducted on a total internal reflection (TIR) setup achieved with a prism. Wide-field, fast-detection sCMOS cameras were used for data acquisition. Fluorescently labeled molecules were immobilized on chemically treated quartz surfaces and excited with an evanescent wave as detailed in Michael Wasserman's PhD dissertation.

All fluorescence data is analyzed with the SPARTAN program suite to generate fluorescence traces that contain FRET[63]. These traces are then idealized in QuB[64] and analyzed in Matlab (2014b) and Origin8.

2.2 REAGENT EXPRESSION AND PURIFICATION

This section describes the methods used to generate the reagents used in the assays discussed in later sections and chapters.

2.2.1 Bacterial Elongation Factor Tu Purification

The primary aim of this research is to understand the precise role of Elongation Factor Tu (EF-Tu) in bacterial protein synthesis. As such, this reagent was used extensively in various forms. In *Escherichia coli*, there are two isoforms of EF-Tu encoded by the genes *tufA* and *tufB*. The product of *tufB* is the primary form of EF-Tu expressed in the K12 strain of *E. coli* and is therefore the gene used in our investigations. Through previous efforts, the open reading frame of *tufB* was cloned into the high copy number expression vector pProEX HT-b which introduces a cleavable N-terminal six Histidine (His_6) affinity tag (Figure 2.15)[40]. The cleavability of the His_6 tag is achieved by the insertion of a Tobacco Etch Virus (TEV) protease recognition sequence: 5′-ENLYFQ˅G-3′. This amino acid sequence is recognized by the TEV protease and subsequently cleaved between the glutamine and glycine amino acids. This plasmid has been transformed into the bacterial cell strain DH5α and is cataloged as SCB41.

Expression of pProEX HT-b follows standard procedures. A small culture is grown over night and used to inoculate a large preparative culture. In the preparative culture, the expression of the plasmid is induced and the cultures are grown to a sufficient cell density. These cells are then harvested and prepared following standard

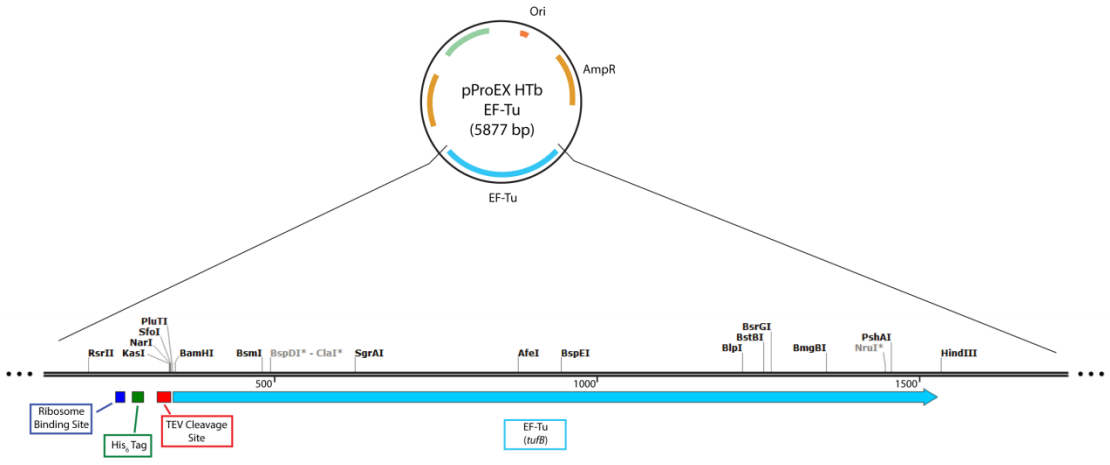

FIGURE 2.15 ***Map of His6-EF-Tu expression vector.*** *tufB* has been cloned into the expression vector pProEX HT-b. The construct contains an N-terminal His_6 tag that is cleavable with TEV protease.

Ni-NTA purification procedures. A detailed method for the expression of pProEX HT-b N-His_6 EF-Tu is as follows:

Overnight culture. Following sterile procedures, 10 mL of autoclaved LB media is measured into a glass 28 mL culture tube. Filtered ampicillin antibiotic is added to a final concentration of 100 µg/mL and inoculated with SCB41. The tube is placed in the rotating incubator at 37°C and left overnight. The ideal growth time is between 12 – 16 hrs.

Preparative cultures. Large 2.8L baffled culture flasks are filled with 1.5 L autoclaved LB media. Filtered ampicillin antibiotic is added to the flasks at a final concentration of 100 µg/mL and brought to 37°C. Although this may vary by demand, a typical preparation of EF-Tu uses 6 L of media. 2 mL of the overnight culture is then added to each flask. The flasks are then shaken at 225 rpm at 37°C.

Expression of EF-Tu. The flasks are grown at 37°C until an optical density (OD) of 0.1 is reached. At this point, the temperature is dropped to 30°C, maintaining 225 rpm shaking. The culture is then grown for another doubling and induced with filtered IPTG to a final concentration of 300 µM. The target OD for induction is 0.2 – 0.25.

Harvest Cells. Continue growing cultures until an OD of 1.0 is reached. Cultures are pelleted using 1 L JLA canisters and the JLA 8.1 rotor at 6,000 rpm, for 6 minutes at 4°C. Decant the supernatant and dry the pellets by inverting the canisters for 5 minutes at 4°C. Add cold EF-Tu Lysis Buffer (20 mM Tris-HCl, pH 7.5, 200 mM KCl, 1 mM BME) and resuspend the pellets by swirling or light pipetting with a serological pipettor. If resuspending pellets from 6 L of culture, use 100 mL of buffer. Pellet the cell resuspension by transferring into pre-weighed 50 mL falcon conical tubes and pelleting for 10 minutes at 4,000 rpm, 4°C. Decant the supernatant and flash

freeze the pellet(s) in liquid nitrogen (LN2). Pellets are thawed and used immediately or stored long-term at -80°C.

Purification of His_6 tagged EF-Tu follows standard Ni-NTA purification procedures as outlined in the QIAexpressionist handbook[65]. Typically, 6-12 grams of cells are purified in a single preparation which yields roughly 200 nmols of fully purified EF-Tu. A detailed method for the purification His_6 EF-Tu is as follows:

Lyse cells. Resuspend cells in 25 mL EF-Tu Lysis Buffer. Cells are then lysed by sonication. This is achieved by sonicating the cell resuspension with the output control set to 6 and the duty cycle set to 60% for 45 seconds. The resuspension is then removed from the sonicator tip and incubated on ice for 5 minutes at 4°C. The sonication process is repeated 5 more times for a total of 6 sonication steps.

Remove insoluble debris. The cell lysate is transferred into a JA 20 tube and pelleted with the JA 20 rotor for 15 minutes at 15,000 rpm, 4°C. The supernatant is transferred into a Ti-70 tube and pelleted in the Ti-70 rotor for 2 hours at 45,000 rpm, 4°C.

Isolate His_6 tagged EF-Tu using affinity Ni-NTA chromatography. In a 4°C cold room or a sliding door refrigerator, 4 mL of QIAGEN Ni-NTA Agarose slurry (QIAGEN – material no. 1018240) is deposited into a disposable Poly-Prep Chromatography Column (BioRad – material no. 7311550). The resin is then washed with 10 volumes ddH_2O (twice dialyzed MilliQ water), followed by 5 volumes EF-Tu Lysis Buffer With 10 mM imidazole, pH 8.

When the cell lysate is finished spinning in the Ti-70 rotor, decant the supernatant into a 50 mL conical falcon tube and add imidazole, pH 8, to a final concentration of 10 mM. Using a serological pipettor, slowly transfer the clarified lysate onto the resin, taking care not to disturb the resin bed. Allow the clarified lysate to completely flow through the column. Once finished, add 5 volumes of EF-Tu Wash Buffer (20 mM

Tris-HCl, pH 7.5, 500 mM KCl, 10 mM Imidazole, pH8, 1 mM BME) and allow to completely flow through the column. In 500 µL increments, add EF-Tu Elution Buffer (20 mM Tris-HCl, pH 7.5, 200 mM KCl, 250 mM Imidazole, pH 8, 1 mM BME) to the resin and collect the flow through. To verify the presence of eluted protein, add 5 µL of the collected fraction to 250 µL of Bradford Reagent. A transformation of the reagent from brown to blue indicates the presence of protein in the eluted fraction. The elution process is continued until there is no indication of protein.

The fractions containing protein are then pooled together and transferred into a MWCO 3kD dialysis bag, previously washed in ddH_2O. The dialysis bag is then transferred into a 2 L beaker containing EF-Tu Dialysis Buffer (20 mM Tris-HCl, pH 7.5, 200 mM KCl, 1 mM BME, 0.05%$_V$ Triton X-100 Surfactant), previously chilled to 4°C, and a stir bar. At 4°C, stir the container such that the dialysis bag is partially submerged in the buffer.

Cleave the His_6 tag. After 2 hours, transfer the dialysis bag into a new 2 L beaker containing EF-Tu Dialysis Buffer, previously chilled to 4°C. Add TEV protease at a molar ratio of 1:100 moles EF-Tu as verified by Bradford Reagent. The cleavage reaction is allowed to persist overnight at 4°C.

Isolate cleaved EF-Tu. The following day, collect the contents of the dialysis bag into 2 (or more) 2 mL Eppendorf centrifuge tubes. Spin the samples for 10 minutes at 15,000 rpm in the table top centrifuge to pellet away aggregated protein. Pool the supernatants of each tube into a 15 mL conical falcon tube and add imidazole, pH 8, to a final concentration of 10 mM.

Add sample to 1 mL Ni-NTA Agarose slurry prepared in the same manner as indicated in STEP 3. Collect the flow-through. Add 1.5 volumes of EF-Tu Lysis Buffer With Imidazole to the resin and collect the flow-through. Pool collected fractions together.

Transfer the sample into a 4.5 mL 10 kDa Amicon Ultra Centrifugal Filter and spin at 4,000 rpm for 10 minutes, 4°C. Repeat until the volume of the sample is concentrated to within a range of 750 µL to 1 mL. Transfer sample to a 1.5 mL centrifugation tube and spin at 15,000 rpm for 10 minutes, 4°C. Transfer the supernatant to a new centrifugation tube.

FPLC purification. Bring the volume of the tube up to 1,050 µL with EF-Tu Lysis Buffer. Inject the sample over a Superdex 75 gel filtration column, previously equilibrated in EF-Tu Lysis Buffer by running the program "Sephadex75 prepgrade fractionation" on the Äkta Purifier FPLC or "Superdex75" on the Äkta Pure FPLC.

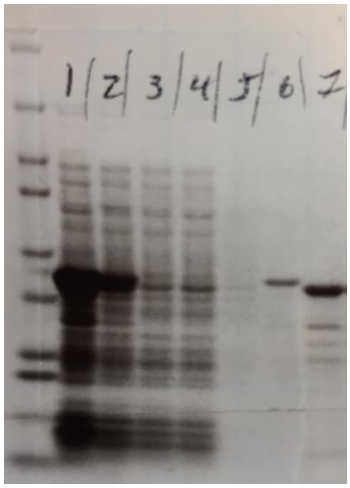

FIGURE 2.16 ***SDS-PAGE of EF-Tu purification*****.** Lane 1) Cell lysate, Lane 2) low speed spin supernatant, Lane 3) high speed spin supernatant, Lane 4) Ni-NTA column flow-through, Lane 5) Ni-NTA column wash, Lane 6) Ni-NTA column elution, Lane 7) TEV protease treated EF-Tu.

Natively folded EF-Tu will elute at around 58 mL. Collect this peak and buffer exchange into 2xFactor (20 mM Tris Acetate, pH 7, 100 mM KCl) Buffer using a 4.5 mL 10 kDa Amicon Ultra Centrifugal Filter, spinning at 4,000 rpm, 4°C.

Concentrate to around 150 µL and transfer to a 1.7 mL Eppendorf tube. Add DTT such that the final concentration is 1 mM. Finally, add 1 volume of 100% molecular biology grade glycerol and mix well. If bubbles appear, spin for 30 seconds at 15,000 rpm, 4°C. Store sample at -20°C.

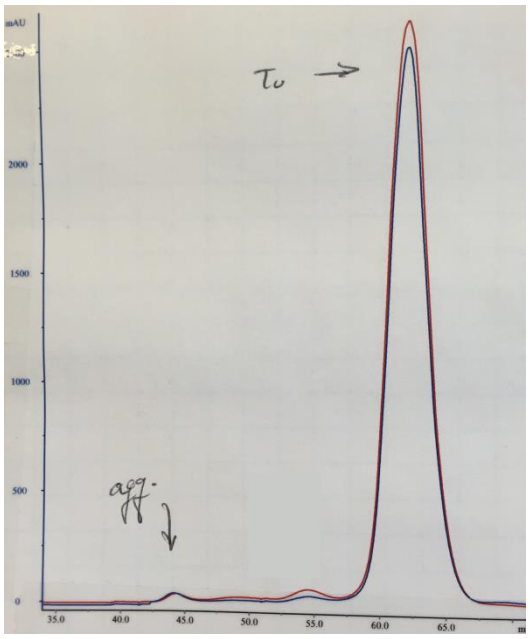

FIGURE 2.17 ***Chromatograph of EF-Tu purification.*** EF-Tu, purified using standard Ni-NTA strategies, is further purified on a Superdex75 gel filtration column using an ÄKTA purifier.

2.2.2 Bacterial Elongation Factor Tu-ACP Purification

In order to conduct experiments directly testing EF-Tu function, a fluorophore conjugated version of EF-Tu was made. Previous efforts to label EF-Tu *via* maleimide chemistry have failed to reproduce wild type activity[66]. As a result, an enzymatic labeling approach is used which leverages a 12 amino acid peptide tag on the carboxyl terminus of EF-Tu[67-69]. This peptide tag is a recognition sequence for the acyl carrier protein synthase (AcpS), a bacterial phosphopantetheinyl transferase. In *E. coli*, AcpS transfers 4′-phosphopantetheinyl (Ppant) groups from coenzyme A (CoA) to a conserved serine residue on acyl carrier protein (ACP) domains. Interestingly, AcpS exhibits promiscuity in transferring Ppant derivatives – including fluorescent small molecule probes. Here, we use AcpS to site specifically label our ACP-tagged EF-Tu.

The AcpS recognizes the consensus sequence 5′-GDSLDMLEWSLM-3′ and catalyzes Ppant addition onto the 5′ serine (denoted as S)[67]. The EF-Tu construct used here contains the AcpS consensus sequence on the carboxy terminus of the His_6-

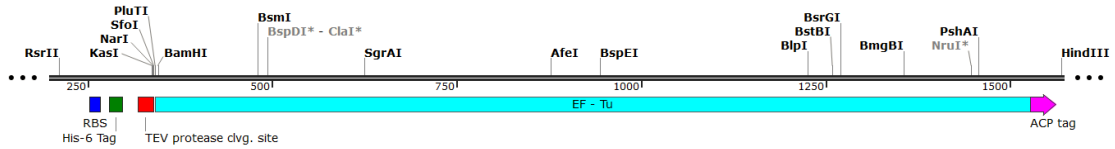

Figure 2.18 ***Map of His$_6$-EF-Tu$_{ACP}$ construct.*** The construct contains an N-terminal His$_6$ tag that is cleavable with TEV protease in addition to a C-terminal ACP tag.

tagged EF-Tu (Figure 2.18). Expression of this construct, His$_6$-EF-Tu$_{ACP}$, follows the procedures outlined in section 2.2.1. Specifically, a 10 mL overnight culture of LB media containing ampicillin at a concentration of 1 μg/mL is inoculated with a glycerol stock of DH5α cells containing a pProEx plasmid with His$_6$-EF-Tu$_{ACP}$ (Figure 2.18). This is grown for 14 hours with light agitation at 37°C.

Once this growth is complete, 2 mL of the overnight culture are used to inoculate 1.5 L of LB media containing ampicillin at a concentration of 1 μg/mL prepared in baffled 2.8 L flasks. Cultures are left to shake at 225 rmp at 37°C until an OD_{600} of 0.1 is reached. The temperature is then reduced to 20°C and the cultures are allowed to grow to an OD_{600} of 0.2 – 0.25. Once this cell density is reached, the cultures are induced with 300 μM IPTG and allowed to continue to grow until an OD_{600} of 1.0 is reached. Cells are harvested according to procedures outlined in section 2.2.1 using EF-Tu Lysis Buffer.

Purification of His$_6$-EF-Tu$_{ACP}$ is generally similar to the purification of His$_6$-EF-Tu outlined in section 2.2.1, with the exception that the His$_6$ tag is not proteolytically cleaved. Ultimately, the His$_6$ tag will be used to aid in the purification of fluorescently labeled EF-Tu and subsequently cleaved thereafter. Specifically, the cells are lysed using EF-Tu Lysis Buffer and His$_6$-EF-Tu$_{ACP}$ is isolated using standard Ni-NTA purification techniques. Here, both EF-Tu Wash Buffer and EF-Tu Elution Buffer are used to purify His$_6$-EF-Tu$_{ACP}$. Once purified, the sample is then dialyzed in 2 L of EF-Tu Dialysis Buffer for 2 hours at 4°C. After this process, the sample is then dialyzed in a fresh 2 L supply of EF-Tu Dialysis Buffer for a minimum of 2 hours or overnight

at 4°C. After dialysis, the sample is concentrated in a 10K MW Amicon filter concentrator to a volume of 900 μL. The sample is further purified using a Superdex74 gel filtration column with EF-Tu Lysis Buffer as the running buffer. The eluted sample is then buffer exchanged into 2xFactor Buffer using a 10K MWCO Amicon filter concentrator. Glycerol is then added to a final concentration of 50%$_V$. The sample is stored at -20°C.

2.2.5 Bacterial Elongation Factor Ts Purification

Elongation Factor Ts (EF-Ts) is an essential protein[58] and is the GEF for EF-Tu in bacteria[31]. In *E. coli*, EF-Ts is encoded by the gene *tsf* located downstream of the gene *rpsB* on the same operon[70]. The *tsf* gene has been previously cloned into the vector pProEX HT-b[40] (Figure 2.19). This construct includes an amino terminal His_6 tag that is cleavable by TEV protease. As such, expression and purification of EF-Ts mimics the protocol described in section 2.2.1.

2.2.6 Bacterial Elongation Factor Ts-A106C Purification

Fluorescently labeled EF-Ts was created to enable direct measurements of this protein in the context of other components of the translational machinery. This was achieved via cysteine labeling methods. EF-Ts has two native cysteines (C23 and C78) which do not participate in disulfide bonding. Using the pProEX His_6-EF-Ts construct (Figure 2.19), each cysteine was mutated to a serine following standard site directed mutagenesis procedures[71] to create a cysteine null EF-Ts (EF-Ts$^{\Delta C}$). The primers used to create the C23S mutation are:

Forward Primer: 5′-GGCGCAGGCATGATGGATTCGAAAAAAGCACTGAC-′3.

Reverse Primer: 5′-GTCAGTGCTTTTTTCGAATCCATCATGCCTGCGCC-′3.

The primers used to create the C78S mutation are:

Forward Primer: 5′-CATTCTGGAAGTTAACTCGCAGACTGACTTCG-′3.

Reverse Primer: 5′-CGAAGTCAGTCTGCGAGTTAACTTCCAGAATG-′3.

In each case, a 50 µL reaction was made containing 200 µM forward and reverse primer, 100 ng of the pProEx-His_6-EF-Ts plasmid, 200 µM dNTP, and 1 unite of PfuUltra Hotstart DNA polymerase in Agilent PfuUltra Hotstart buffer. An 18 cycle reaction was conducted on the thermocycler (Figure 2.2.6.2) and then digested with 1 unit of DpnI for one hour at 37°C. In this background, the alanine at position 160 was removed and replaced with a cysteine with site directed mutagenesis ($EF\text{-}Ts^{A160C}$). The primers used to create the A160C mutation are:

Forward Primer: 5′-GGTTGCTGCTAAAGGCTGCGACGAAGAGCTGG-′3.

Reverse Primer : 5′-CCAGCTCTTCGTCGCAGCCTTTAGCAGCAACC-′3.

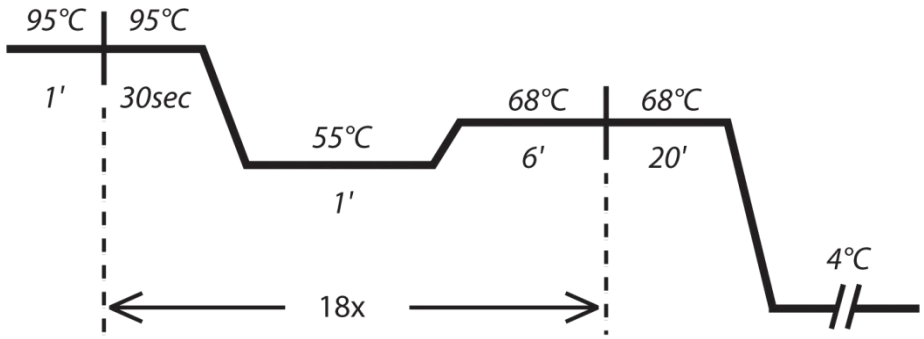

FIGURE 2.19 ***Site directed mutagenesis thermocycler protocol.*** Each mutation required the modification of two nucleotides. Standard procedures, as outlined in the QuikChange handbook, were followed.

All mutations were verified by Sanger sequencing. Purification of $His\text{-}EF\text{-}Ts^{A106C}$ is conducted following standard Ni-NTA purification techniques as described in section 2.2.1.

2.2.7 Phenylalanyl-tRNA Synthetase Purification

Phenylalanyl-tRNA synthetase (PheRS, also referred to as phenylalanyl-tRNA ligase) is used to aminoacylate phenylalanyl-tRNA for *in vitro* experiments. PheRS is a tetramer of two heterodimers composed of an alpha and beta subunit. The alpha and beta subunits are encoded by the genes pheS and pheT respectively. Both genes are cloned into a pET SUMO expression vector in a tandem fashion and is catalogued as the plasmid MRW1 (see Figure 2.20). The vector harbors a T7 RNA polymerase promoter, which controls expression of the PheRS open reading frame, and a kanamycin antibiotic resistance cassette. This plasmid is stored in TOP10 bacterial cells and therefore must be transformed into a cell strain that contains the T7 RNA polymerase machinery. The expression system used here is the BL21(DE3) cell strain. This strain is unique in that it contains a chromosomal copy of the phage T7 RNA polymerase gene under the control of a lac promoter. The procedure for the expression of PheRS is as follows:

Transform MRW1 plasmid into BL21(DE3) expression strain. 100 ngrams of MRW1 plasmid is added to a 50 µL BL21(DE3) competent cell aliquot. The mixture is incubated on ice for 30 minutes. The cells then are heat-shocked by incubating at 42°C for 45 seconds followed by a 2 minute incubation on ice. Next, 200 µL of SOC media is added and the culture is placed in a rotator (or agitator) at 37°C for 1 hour. After the out growth is completed, 10 mL of autoclaved LB in a glass culture tube containing 40 µg/mL of kanamycin is inoculated with 25 µL of the transformed cell culture. The 10 mL culture is then placed in a rotator at 37°C.

Inoculate preparative cultures. Add 5 mL of the overnight culture to 200 mL autoclaved LB with kanamycin (40 µg/mL). Cultures are grown until mid-log phase is reached (~2 hrs). When the OD of the log cultures are 0.5, inoculate 2 baffled culture

flasks containing 1.5 L autoclaved LB media and 40 µg/mL kanamycin with 95 of the log culture. The flasks are then shaken at 225 rpm, 37°C.

Induce expression of PheRS. The flasks are grown at 37°C until an optical density (OD) of 0.2 is reached. At this point, the temperature is dropped to 20°C, maintaining 225 rpm shaking. The culture is then grown to an OD of 0.4 and induced with filtered IPTG to a final concentration of 100 µM. Let cultures grow until an OD of 1.0 is reached.

Harvest cells. Cells are harvested as described in section 2.2.1 STEP 4, with the modification of using the low salt PheRS Lysis Buffer in place of EF-Tu Lysis Buffer. Typically, 6-12 grams of cells are purified in a single preparation which yields roughly 500 nmols of fully purified PheRS. Purification of His_6 tagged PheRS follows standard Ni-NTA purification procedures as outlined section 2.2.1. Cells are lysed in PheRS Lysis Buffer (50 mM NaH_2PO_4, 1 mM BME) by sonication. The lysate is clarified by centrifugation. Imidazole is added to a final concentration of 10 mM. The sample is then applied to a Ni-NTA column pre equilibrated in PheRS Lysis Buffer with 10 mM Imidazole, pH 8. The bound sample is washed with 5 column volumes of PheRS Wash Buffer (50 mM NaH_2PO_4, 200 mM NaCl, 10 mM Imidazole, pH 8, 1 mM BME) and eluted with PheRS Elution Buffer (50 mM NaH_2PO_4, 100 mM NaCl, 250 mM Imidazole, pH 8, 1 mM BME). The eluted sample is immediately dialyzed in cold PheRS Dialysis Buffer (10 mM Tris Acetate, pH 7.5, 100 mM KCl, 1 mM BME) at 4°C.

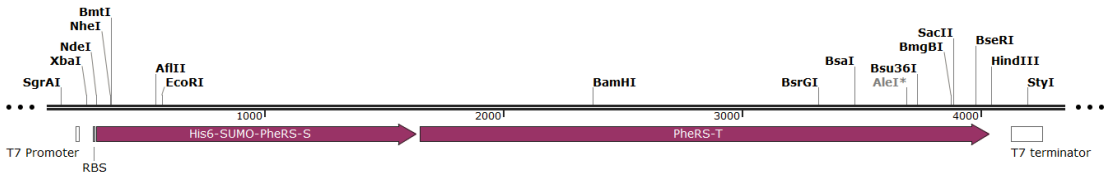

FIGURE 2.20 ***Map of His_6-PheRS construct.*** Both the α and the β subunit of PheRS have been cloned in to a pET-SUMO vector in tandem. The α subunit contains an N-terminal His_6 tag that is cleavable with SUMO protease.

After 2 hours, transfer the dialysis bag into a new 2 L beaker containing PheRS Dialysis Buffer, previously chilled to 4°C. Add SUMO protease at a molar ratio of 1:30 moles PheRS as verified by Bradford Reagent. The cleavage reaction was allowed to persist for 2.5 hr at 4°C. The cleaved PheRS is isolated as described in section 2.2.1 and buffer exchanged into Factor Storage Buffer. If bubbles appear, spin for 30 seconds at 15,000 rpm, 4°C. Store sample at -20°C.

2.2.8 Arginyl-tRNA Synthetase Purification

Arginyl-tRNA synthetase (ArgRS, also referred to as arginyl-tRNA ligase) is used to aminoacylate arginyl-tRNA ($tRNA^{Arg}$) for *in vitro* experiments. ArgRS is a class I synthetase that catalyzes the addition of arginyl-adenylate to the 2′ hydroxyl of the terminal adenosine of $tRNA^{Arg}$. ArgRS is encoded by the gene *argS* and has been previously cloned into a pET-SUMO vector. This plasmid is stored in TOP10 bacterial cells, cataloged as BJB15, and must be transformed into BL21(DE3) cells for expression. Once transformed, the purification of ArgRS is carried out as described in section 2.2.7.

2.2.9 TEV Protease Purification

Tobacco Etch Virus (TEV) protease is a cysteine protease that cleaves polypeptide bonds according to a highly specific amino acid sequence. The consensus recognition sequence is 5′-EXLYΦQˇφ-3′ where X is any amino acid, Φ is any large bulky hydrophobic amino acid and φ is any small hydrophobic or polar amino acid, typically serine or glycine[72,73]. TEV protease cleaves the polypeptide on the 3′ side of the glutamine, denoted by ˇ. In practice, this enzyme is used to remove a purification tag, such as the His_6 tag used to purify EF-Tu. Given the proximity of the cleavage site in

the consensus sequence, this strategy is ideally suited for removing tags located on the amino terminus of the protein being purified (Figure 2.15).

The active fragment of TEV protease used to here is 27 kDa and has been previously cloned into the pMAL expression vector. This construct contains a non-cleavable His_6 tag used to remove TEV during the purification of other His_6 tagged proteins. This plasmid has been previously transformed into DH5α cells and is cataloged as strain SCB51. A detailed procedure for the expression of TEV protease is as follows:

Overnight culture. Following sterile procedures, 10 mL of autoclaved TB media is measured into a glass 28 mL culture tube. This is repeated for a total of 2 culture tubes. Filtered ampicillin antibiotic is added to a final concentration of 100 µg/mL in each culture tube. One tube is inoculated with SCB51 and the other tube is brought into contact with the inoculation device, but is not inoculated – this will act as a contamination control. Both tubes are placed in the rotating incubator at 37°C and left overnight. The ideal growth time is between 12 – 16 hrs.

Preparative cultures. Large 2.8L baffled culture flasks are filled with 1.5 L autoclaved TB media. Filtered ampicillin antibiotic is added to the flasks at a final concentration of 100 µg/mL and brought to 37°C. Although this may vary by demand, a typical preparation of TEV protease uses 4.5 L of media. 2 mL of the overnight culture is then added to each flask. The flasks are then shaken at 225 rpm at 37°C.

Expression of TEV protease. The flasks are grown at 37°C until an optical density (OD) of 1.0 is reached. At this point, the temperature is dropped to 30°C, maintaining 225 rpm shaking. The culture is induced with filtered IPTG to a final concentration of 500 µM. The target OD for induction is 1.5. This is then left to grow overnight.

Harvest Cells. Typical OD at the time of harvest, the following morning, is about 8.5. The cells are harvested as described in section 2.2.1 using TEV Lysis Buffer

(20 mM Tris-HCl, pH 7.5, 200 mM NaCl, 1 mM BME, Protease inhibitor (1:10,000 by volume)).

Typically, 6-12 grams of cells are purified in a single preparation that yields roughly 2000 nmols of fully purified His_6-TEV. Purification of His_6 tagged TEV follows standard Ni-NTA purification procedures as outlined in section 2.2.2 using TEV Lysis Buffer, TEV Wash Buffer (20 mM Tris-HCl, pH 7.5, 500 mM NaCl, 10 mM Imidazole, pH 8, 1 mM BME), TEV Elution Buffer, and TEV Dialysis Buffer (20 mM Tris-HCl, pH 7.5, 200 mM NaCl, 1 mM BME). Once purified, TEV protease is stored at -20°C in Factor Storage Buffer until further use.

2.2.9 Bacterial Phosphate Binding Protein Purification

In order to measure GTP hydrolysis, we utilized an orthogonal inorganic phosphate (P_i) biosensor developed by Martin Webb[74-76]. Phosphate Binding Protein (PBP) from *E. coli* binds soluble P_i readily, having an on-rate of >100 $\mu M^{-1}s^{-1}$. The protein utilized here has an A197C mutation making it amenable to sulfhydryl labeling strategies. The PBP gene has been previously cloned into a pET22b which contains a C-terminal His_6 tag. However, during the cloning process the natural termination codon was inserted upstream of the C-terminal His_6 tag is therefore not transcribed. Thus, affinity purification strategies cannot be used. However, the native purification protocol has been well vetted and produces ample amounts of protein. This plasmid is stored in TOP10 cells cataloged as BJB26.

Expression of PBP. To express this protein, the pET22b-PBP plasmid is first transformed into BL21(DE3) cells as described in section 2.2.7. The transformance is then used to inoculate 10 mL of LB media containing 100 μg/mL ampicillin. The starter culture is incubated for 7 hours at 37°C in a rotating incubator. The starter

culture is added to 90 mL of LB media containing 100 µg/mL ampicillin in a baffled flask. The sample is then incubated overnight at 37°C, shaking at 225 rpm.

The next morning, 4 L of LB media containing 100 µg/mL ampicillin is inoculated with the overnight culture and incubated at 37°C, shaking at 225 rpm. Preparative cultures are grown to an OD of 1.0 and induced with 400 µg IPTG and left to grow fro 3 hours.

Harvest Cells. The cells are harvested as described in section 2.2.1 using PBP Lysis Buffer (20 mM Tris-HCl, pH 8, 1 mM EDTA, 5 mM BME).

Purification of PBP. Cell pellets are thawed with 20 mL PBP Lysis Buffer. Clarified lysate is then obtained as outlined in section 2.2.1. The clarified lysate is loaded onto a 120 mL Q-Sepharose FF column, equilibrated in PBP Buffer A (10 mM Tris-HCl, pH 7.6, 1 mM BME). This is then washed with two column volumes of PBP Buffer A followed by a shallow gradient into PBP Buffer B (10 mM Tris-HCl, pH 7.6, 200 mM NaCl, 1 mM BME). PBP is rather loosely bound and elutes around 50 mM NaCl. The eluted sample is then buffer exchanged into PBP Storage Buffer (20 mM Tris-HCl, pH 7.6, 2 mM DTT) and concentrated using an Amicon MWCO 10k filter concentrator. An equal volume of 100% molecular grade glycerol is added and the sample is stored at -20°C until further use.

2.2.10 Bacterial Phenylalanyl-tRNA Purification

Historically, the bacterial phenylalanyl-tRNA ($tRNA^{Phe}$) has been the workhorse of protein synthesis research. Expression of $tRNA^{Phe}$ is less straightforward than the

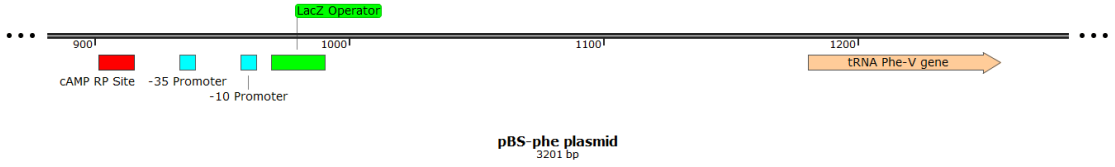

FIGURE 2.21 ***Map of tRNA^{Phe} construct.*** The *pheV* gene, along with ~175 nt of the native upstream elements, is cloned into a Lac operon in a pBS plasmid.

expression of single gene proteins. In bacteria, there are two genes that encode for $tRNA^{Phe}$, though the research described in this document exclusively uses the gene *PheV* for recombinant expression of this molecule. Through previous efforts[77], the *PheV* gene has been cloned into a pBS vector (Figure 2.21). This vector includes an IPTG inducible Lac operon and is engineered to express the open reading frame of genes. In this case however, the precise open reading frame of *PheV* is not known. Initially, *PheV* encodes for a precursor $tRNA^{Phe}$ which undergoes maturation by RNAases and base modifying enzymes. Ultimately, this maturation process leads to the removal of both 3′ and 5′ RNA elements yielding a 76 nucleotide tRNA product. Because the open reading frame is not precisely known, large DNA fragments, both upstream and downstream of the annotated *PheV*, were included in cloning into the pBS vector. As such, this construct houses a LacZ controllable transcription site as well as a native *PheV* promoter that is likely to be constitutively expressed. Additionally, this construct also contains an ampicillin resistance cassette.

Expression of $tRNA^{Phe}$ follows similar methods utilized in protein expression. An overnight culture is grown to saturation and used to induce a log-phase culture, so named because it is used to grow cells to mid log phase. This culture is then subsequently used to inoculate preparative cultures. Once expressed, purification of $tRNA^{Phe}$ relies upon methods that take advantage of both chemical and structural properties that are unique to this molecule. This protocol takes five days to complete and yields 50 – 80 nmoles of crude $tRNA^{Phe}$.

Overnight culture. Cell strain RA113 is used to inoculate 10 mL of LB media with 100 μg/mL ampicillin. Culture is grown overnight at 37°C in a rotating incubator.

Log culture. When the overnight culture is saturated, a baffled flask of 100 mL of LB media containing 100 μg/mL ampicillin is inoculated with 10 mL of the saturated

overnight culture. This culture is grown at 37°C with shaking at 225 rpm to an OD_{600} of 0.6.

Preparative culture. 9 L of LB media with 100 μg/mL ampicillin is prepared in 6 large 2.8 L baffled flask (1.5 L pre flask). Each large flask is inoculated with 15 mL of the log culture. Cultures are incubated at 37°C, 225 rpm shaking, until an OD_{600} of 0.25 is reached. Cultures are then innoculated with 300 μM IPTG and grown until an OD_{600} of 0.85 is achieved.

Harvest cells. Cultures are pelleted at 6,000 rpm for 6 minutes at 4°C using the JLA 8.1 rotor. Pellets are dried for 5 minutes by inverting over a paper towel for 5 minutes. Following this, pellets are resuspended in $tRNA^{Phe}$ Lysis Buffer by swirling. The resuspended cells are then pelleted at 4,000 rpm for 20 minutes at 4°C. Typically, 9 L of culture is used to create two $tRNA^{Phe}$ pellets. As such, no more than 80 mL of $tRNA^{Phe}$ Lysis Buffer is used when resuspending pellets so that two 50 mL falcon tubes can be used to pellet cells. After pelleting, the supernatant is decanted and the cells are weighted. The pellets are then flash frozen in LN_2 and stored at -80°C.

Lyse cells. Cell pellet(s) are resuspended with 20 mL cold $tRNA^{Phe}$ Lysis Buffer. Cells are lysed by sonicating six times at an output of 60%, duty cycle of 6 at 45-second intervals. The sample is allowed to cool down, on ice, for 5 minutes between cycles. To ensure rapid cooling, the sonicated tip is removed from the sample in between sonication rounds.

tRNA extraction. After lysis is complete, the cells are pelleted in a JA20 rotor for 15 minutes at 15,000 rpm, 4°C. The supernatant is collected and pelleted a second time in a Ti70 rotor for 2 hours at 45,000 rpm, 4°C. Once pelleted, the supernatant is collected and dispensed into phenol:chloroform tubes (decommissioned JA20 tubes allocated for this purpose only). An equal volume of cold phenol:chloroform is added and shaken vigorously (vortexing is specifically avoided). Because of the difference in

density, the organic phenol will naturally sink below the aqueous sample. Furthermore, the polar nature of the aqueous solution requires energy to mix with the hydrophobic phenol so mixing must be done vigorously.

The purpose of this process is to denature all proteins present in the sample. Owing to the large negative charge of nucleic acids, most of the $tRNA^{Phe}$ will partition into the aqueous phase. When properly mixed, the solution appears completely white and opaque. The mixture is pelleted in a JA20 rotor for 15 minutes at 15,000 rpm, 4°C. The centrifugal force accelerates the natural separation of the organic and aqueous phases. The top aqueous layer is collected and set aside on ice. A middle solid layer that mostly contains aggregated proteins also fomrs. This layer is avoided when collecting the aqueous layer. Next, ½ volume $tRNA^{Phe}$ Lysis Buffer is added to the remaining organic phase. This is referred to as a back extraction and has the purpose of extracting any remaining $tRNA^{Phe}$ that did not partition into the aqueous phase. The sample is mixed vigorously and pelleted as previously done. The top aqueous layer is collected and combined with the previously collected aqueous layer.

A second extraction is performed by again adding one volume of cold phenol:chloroform. The sample is mixed vigorously and pelleted as done previously. The aqueous layer is collected and one volume of chloroform is added. The purpose of this is to remove any phenol that may have partitioned into the aqueous phase. The sample is mixed vigorously and pelleted in a JA20 rotor for 5 minutes at 15,000 rpm, 4°C. The aqueous phase is collected and $1/10^{th}$ volume of 3M NaOAc, pH 3.7, is added to the sample. The $tRNA^{Phe}$ is concentrated by ethanol precipitation. 3 volumes of cold ethanol is added and the sample is inverted a few times to induce mixing. The reaction is allowed to precipitate at 4°C for a minimum of 30 minutes or up to 24 hours.

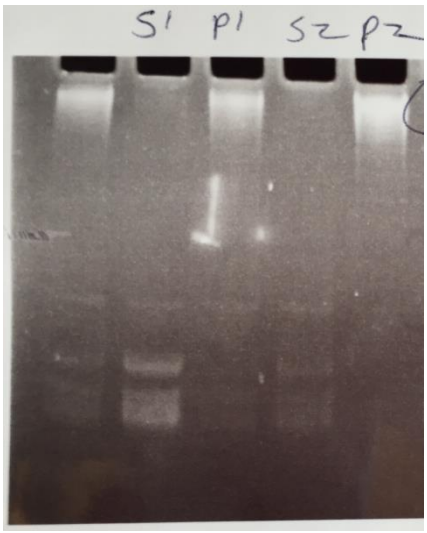

FIGURE 2.22 ***Isopropanol precipitation of tRNA^{Phe}.*** Components of the isopropanol precipitation reaction are analyzed on a 7 M Urea, 12% Bis-acrylamide gel made with Tris-Borate-EDTA buffer. Lane **1**) Bulk tRNA before isopropanol precipitation, lane **2**) Soluble fraction of the first isopropanol precipitation reaction, note that the majority of material is small, lane **3**) insoluble material from the first isopropanol precipitation reaction, note that the majority of the material is large, lane **4**) soluble fraction of the second isopropanol precipitation reaction, lane **5**) insoluble material from the second isopropanol precipitation reaction.

Isolating bulk tRNAs. The precipitation reaction yields a significant amount of particulate that is readily visible by eye. The solution is pelleted at 4,000 rpm for 10 minutes at 4°C. The supernatant is decanted and the pellets are dried by inverting over a paper towel at 4°C for 5 minutes. Pellets appear yellow in color. The pellets are then resuspend in cold 300 mM NaOAc, pH 7, in 50 mL conical tubes. The solution is diluted with this buffer to a concentration of 100 μM as calculated by assuming a molar extinction coefficient of 625,000 $M^{-1}cm^{-1}$ at an absorbance wavelength of 260 nm. Typically, this concentration is achieved by resuspending the pellets to a final volume of 30 – 40 mL. As a benchmark, there should be roughly 3,000 – 3,500 nmoles of material at this stage.

Once diluted appropriately, 0.54 volumes of cold isopropanol are added to the resuspension while mixing. This is done so that as the isopropanol is added to the solution, it is immediately mixed. The purpose of this is to bring up the percentage of isopropanol from 0% to 35% so that large molecules precipitate out of solution but

smaller, tRNA sized molecules remain soluble (Figure 2.2.10.2). If the isopropanol is added without mixing, there is a risk of temporarily having a very high concentration of alcohol near the surface of the solution which will have the undesired effect of precipitating some $tRNA^{Phe}$. Once mixed, the precipitation reaction is incubated at room temperature for 10 minutes. Following this, the precipitated material is pelleted in the clinical centrifuge by spinning at 4,000 rpm for 10 minutes at 4°C. The supernatant is collected and put aside on ice.

This process is repeated by resuspending the pellet (now much whiter in color) with cold 300 mM NaOAc, pH 7, to a concentration of 100 μM. Typically, this requires roughly 10 mL. 0.54 volumes of isopropanol is added while mixing. The precipitation reaction is incubated at room temperature for 10 minutes. As before, the sample is pelleted and the supernatant is combined with that of the previous precipitation.

The $tRNA^{Phe}$ is concentrated by ethanol precipitation. First, $1/100^{th}$ of the sample and set aside to be used subsequently as an analytical sample. Next, 3 volumes of cold ethanol is added to the remaining solution and mixed. Separately, 3 volumes of cold ethanol is added to the $1/100^{th}$ sample and mixed. Note that no additional salt is added. Samples are precipitated at -20°C for a minimum of 30 minutes or up to 24 hours.

Acylatyion of $tRNA^{Phe}$. Using the FPLC, the lines A1 and B1 are equilibrated in $tRNA^{Phe}$ Buffer A and $tRNA^{Phe}$ Buffer B respectively. Then, the analytical TSK Phenyl-5PW hydrophobic column is equilibrated with $tRNA^{Phe}$ Buffer A. The analytical precipitation reaction is pelleted by spinning for 10 minutes at the maximum force allowable for the tube being used for the reaction. If using a conical tube, the sample is spun in the clinical centrifuge at 4,000 rpm. If using an Eppendorf tube, the sample is spun in a table top centrifuge at 15,000 rpm. The supernatant is decanted and

the pellet is dried with a vacuum or by inversion on a paper towel at 4°C for 5 minutes.

The pellet is resuspended in $tRNA^{Phe}$ Buffer A and loaded into the FPLC injection loop. Next, the program *Cy3 tRNA purification analytical* is executed which implements a $tRNA^{Phe}$ Buffer A to $tRNA^{Phe}$ Buffer B gradient (Figure 2.2.10.3). Acylated $tRNA^{Phe}$ elutes at 19.75 mL.

In addition to acylated $tRNA^{Phe}$, there is also a significant amount of deacylated-$tRNA^{Phe}$. To isolate this, the bulk tRNA sample is charged with amino acid by incubating with a 10-fold excess of phenylalanine and a 1:100 dilution of PheRS in buffer (50 mM HEPES, pH 8, 20 mM KCl, 100 mM NH_4Cl, 1 mM DTT, 2.5 mM ATP, 0.5 mM EDTA, 10 mM $MgCl_2$) for 20 minutes in a 37°C water bath. The reaction is then quenched with $1/10^{th}$ volume of 3M NaOAc, pH 3.75. Following this, the sample is phenol:chloroform extracted and ethanol precipitated for a minimum of

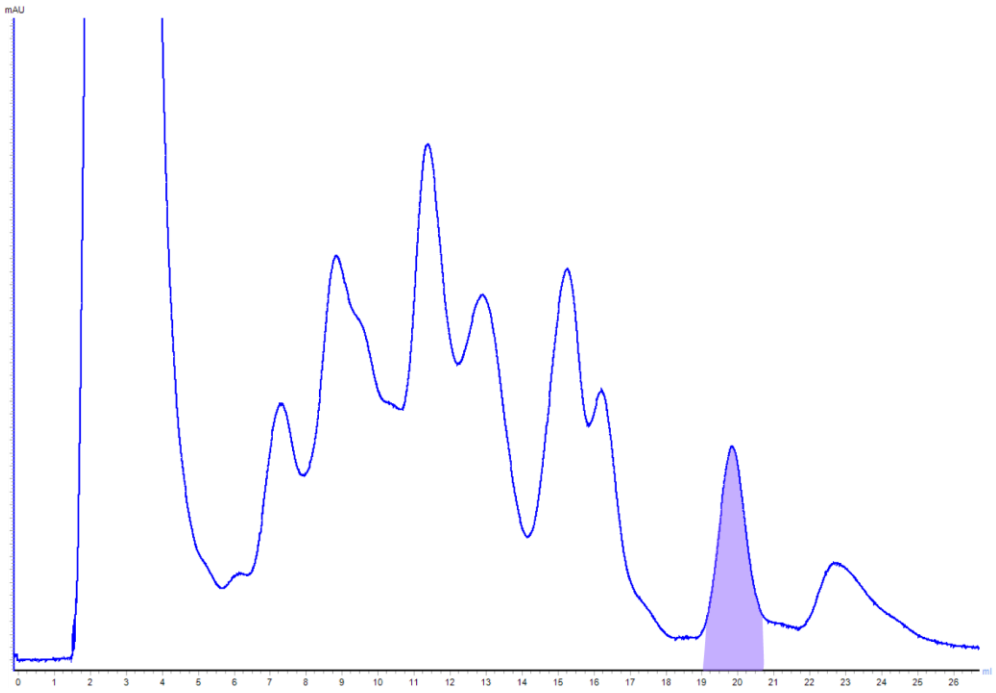

FIGURE 2.23 ***Hydrophobic separation of bulk tRNAs.*** The small RNA molecules that did not precipitate when mixed with isopropanol, collectively referred to as 'bulk tRNAs' is purified over a Phenyl-5PW TSK column. The shaded peak contains Phe-$tRNA^{Phe}$.

30 minutes or overnight. As done previously, 1/100th of the sample is set aside for analysis.

The analytical sample is pelleted as previously described and purified over a Phenyl-5PW TSL column. The charged Phe-tRNA^{Phe} peak is now much larger (Figure 2.2.10.4).

The precipitation reaction is pelleted as previously described and resuspended in tRNA Buffer A. The sample is then purified over a larger 40 mL Phenyl-5PW TSK column using tRNA^{Phe} Buffer A and B. The charged Phe-tRNA^{Phe} is isolated (Figure 2.2.10.4) and dialyzed into 2 L of tRNA Dialysis Buffer (10 mM KOAc, pH 6, 1 mM $MgCl_2$) for 2 hours. The sample is then transferred to a fresh 2 L supply of tRNA Dialysis Buffer and dialyzed overnight.

The following day, the sample is concentrated using a MCWO 10k Amicon centrifugation filter, previously blocked with a 0.5% triton solution. The sample is

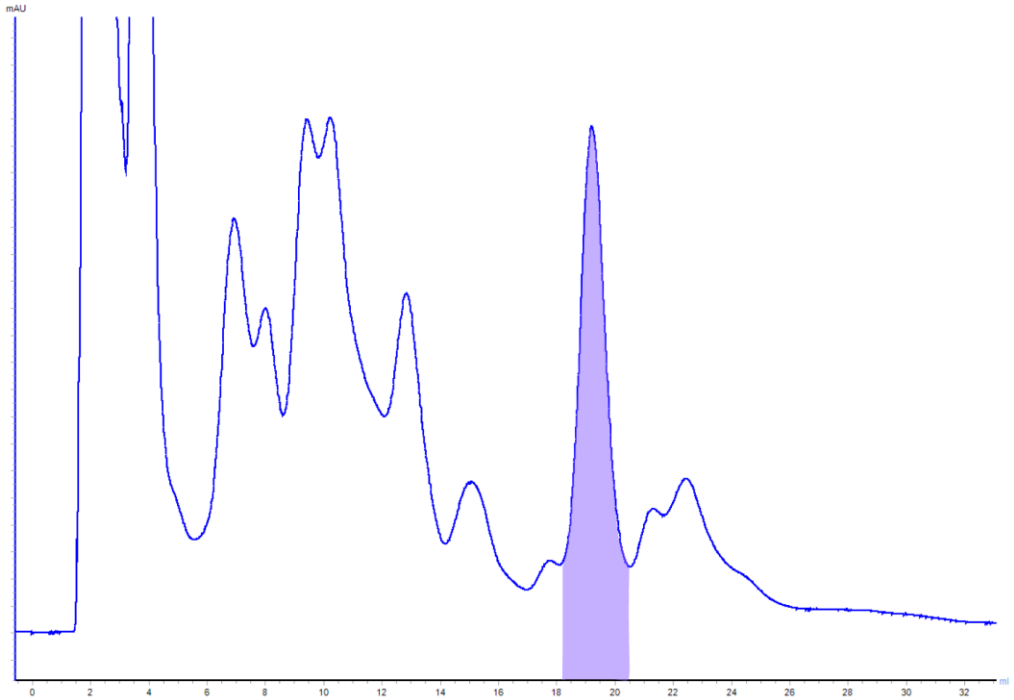

FIGURE 2.24 ***Hydrophobic separation of Phe-tRNA^{Phe}.*** An analytical sample of charged tRNA^{Phe} is purified over a 3 mL Phenyl-5PW TSK column. The dominant peak, eluting at 19.75 mL (shaded) represents Phe-tRNA^{Phe}.

then flash frozen in LN_2 and stored at -130°C to -196°C in a LN_2 storage tank.

2.1.11 Tight Coupled 70S Ribosome Purification

Prokaryotic ribosome particles consist of 3 large rRNA molecules, composed of a total of 4,560 nucleotides, and 52 proteins. Altogether, the fully formed ribosome is 2.5 MDa and is often referred to by its measured centrifugal sedimentation rate of 70S. Historically, the fraction of purified ribosomes that are active in translation are referred to as tight-coupled 70S (TC70) ribosomes. Here, a detailed description of the purification of TC70s from BL21 cells is described.

Overnight culture. A 10 mL culture of LB media is inoculated with BL21 cells from a glycerol stock. The culture is incubated overnight at 37°C in a rotating incubator.

Preparative growth. Overnight cultures are diluted 1:4000 into 4 L of LB media in

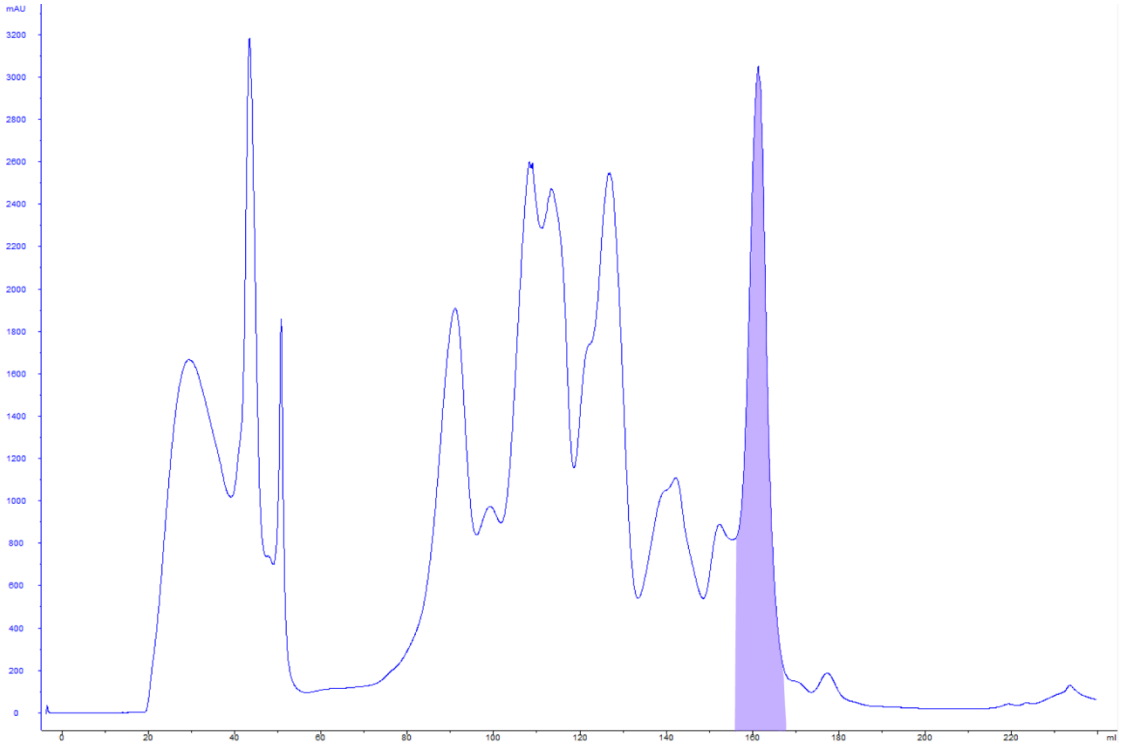

FIGURE 2.25 ***Hydrophobic separation of Phe-tRNA^{Phe}.*** Charged $tRNA^{Phe}$ is purified over a 40 mL Phenyl-5PW TSK column. The dominant peak, eluting at 165 mL (shaded) represents Phe-$tRNA^{Phe}$.

baffled flasks. Preparative cultures are incubated at 37°C and shaken at 225 rpm.

Harvest cells. Cells are harvested in early log phase at an OD of 0.3 to 0.5. Flasks are taken out of the incubator and subsequently incubated on ice for 30 minutes. The cultures are then pelleted in a Beckman JLA 8.1 rotor by centrifuging at 6,000 rpm for 6 minutes at 4°C. The supernatant is discarded and the pellets are dried on a paper towel for 5 minutes at 4°C. Pellets are resuspended in cold TC70 Buffer A (20 mM Tris-HCl, pH 7.5, 100 mM NH_4Cl, 10 mM $MgCl_2$, 0.5 mM EDTA, 6 mM BME) by swirling. The resuspension is pelleted a second time at 4,000 rpm for 20 minutes at 4°C. The supernatant is discarded and the pellets are flash frozen in LN_2 and stored at -80°C until further use.

Cell lysis. Pellets are lysed using a Retch MM400 Ball Mill. Pellets are removed from their container (50 mL falcon tube) by freezing in LN_2 and hammering the container. Pellet fragments are placed into a 50 mL metal canister previously cooled in LN_2. A 50 mm ball, previously cooled in LN_2, is added and the canister is tightly closed. The sample is crushed 5 times at 3 minute intervals at 15 Hz. In between milling cycles, the canister is incubated in LN_2 for 5 minutes. The milled pellet, referred to as crushate, is transferred into a JA-18 rotor tube and mixed with 20 mL TC70 Buffer A with 1:1000 DNAase added. The sample is incubated at room temperature for 10 minutes. Sample is then pelleted in a JA-18 rotor at 15,000 rpm for 15 minutes at 4°C.

Sucrose cushion 1. The supernatant is decanted into a Ti-45 rotor tube. Next, 35 mL of TC70 Buffer B (20 mM Tris-HCl, pH 7.5, 500 mM NH_4Cl, 10 mM $MgCl_2$, 0.5 mM EDTA, 6 mM EDTA) with 1.1 M sucrose is underlayed beneath the clarified lysate. The sucrose cushion is centrifuged in a Beckman Ti-45 rotor at 33,000 rpm for 22 hours at 4°C.

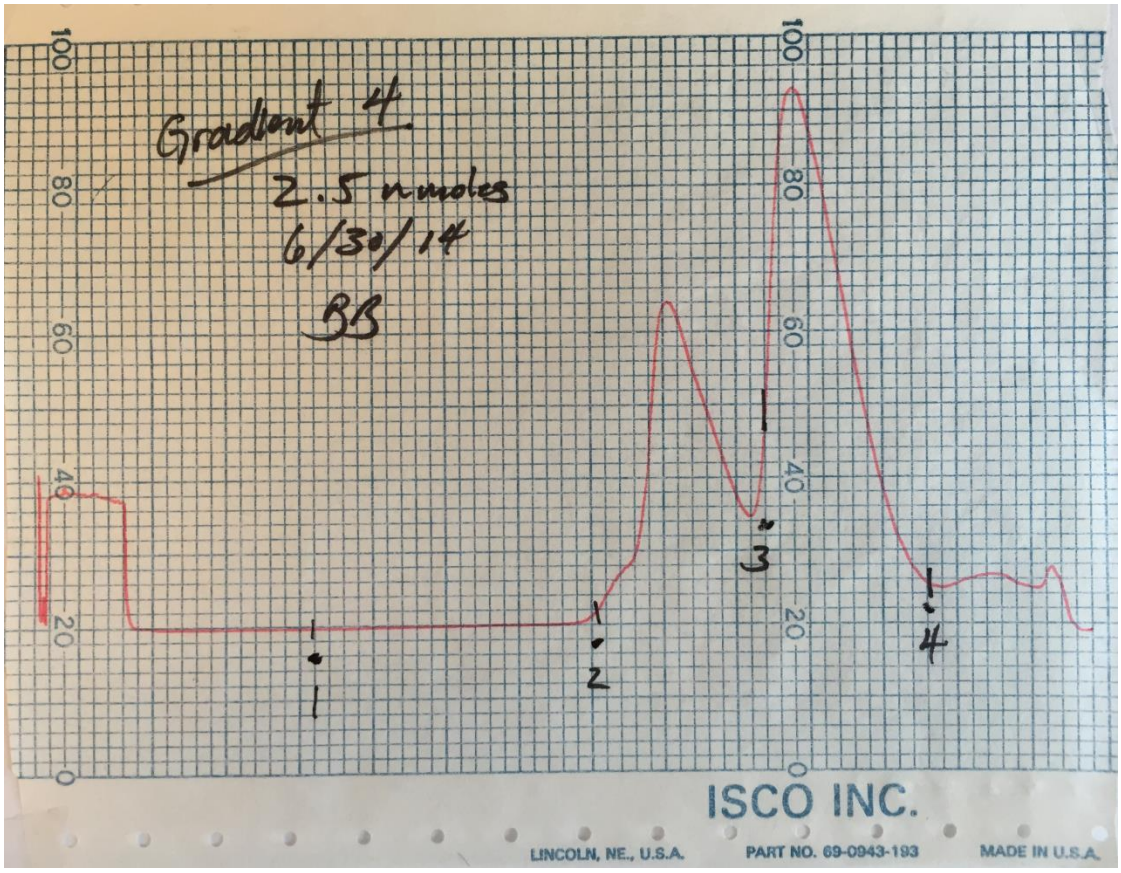

FIGURE 2.26 ***Fractionation of TC70 preparation*****.** TC70s are purified through a sucrose gradient and analyzed on a gradient fractionaor. Fraction **2**) 30S and 50S subunits. Fraction **3**) TC70S.

Sucrose cushion 2. The supernatant is decanted and the pellet is gently washed with 2 mL TC70 Buffer A. It is then gently resuspended with 2 mL TC70 Buffer A. A second sucrose cushion is made by adding 30 mL TC70 Buffer A to a clean Ti-45 rotor tube and underlaying with 35 mL TC70 Buffer B with 1.1 M sucrose. The resuspension is then gently applied to the top of the gradient. The sample is then centrifuged in a Beckman Ti-45 rotor at 33,000 rpm for 22 hours at 4°C.

Gradient purification. The supernatant is decanted and the pellet is resuspended in 2 mL TC70 Buffer A. Resuspension is gently laid onto a 10%-40%$_{w/v}$ sucrose gradient prepared using a Gradient Master 107 (BioComp) in a 25x89 polyallomer tubes (Beckman) with TC70 Buffer A and sucrose. Gradients are centrifuged in a Beckman SW-28 rotor at 22,000 rpm for 19 hours at 4°C.

Collect TC70s. Using a BR-186 gradient fractionator, the TC70 fraction is collected. Though settings vary depending on experimental conditions, typical settings are a chart speed of 30 cm/hr, sensitivity of 1.0, path length of 1 mm, and a push velocity of 1.5 mL/minute (Brandel syringe pump). One volume of TC70 Buffer A is added to the collected and pooled TC70 fractions and is transferred into a fresh Ti-70 rotor tube. Sample is centrifuged in a Beckman Ti-45 rotor for 22 hours at 45,000 rpm, 4°C. The supernatant is decanted and the pellets are resuspended in polymix buffer (50 mM Tris-OAc, pH 7.5, 100 mM KCl, 5 mM NH_4AOc, 0.5 mM $CaCl_2$, 0.1 mM EDTA, 5 mM putrecine, 1 mM spermidine, 5 mM $MgCl_2$, 5 mM BME). TC70s are aliquoted as necessary and flash frozen in LN_2. Samples are stored at -130°C to -196°C in a liquid nitrogen tank.

2.2.12 Nucleotide Purification

Guanosine triphosphate (GTP), guanosine diphosphate (GDP), GDPNP, and GTPγS were purchased from Sigma and further purified on a Tricorn Mono Q 5/50 GL ion exchange column. 2′-/3′-O-(*N*′-methylanthraniloyl)guanosine-5′-O-triphosphate (GTP_{mant}) was purchased from Jena Biosciences.

2.3 FLUORESCENT LABELING OF BIOMOLECULES

This section describes the methods used to conjugate fluorophores to the reagents used in the assays discussed in later sections and chapters.

2.3.1 Cy5Q EF-Tu_{ACP}

The AcpS enzyme is used to site-specifically label ACP-tagged proteins with CoA conjugated fluorophores. Cyanine 5 quencher (Cy5Q) with a maleimide side group is

conjugated to CoA by sulfhydryl chemistry. A 100-fold excess of CoA is added to Cy5Q-maleimide in 100 mM MES, pH 6.5, and incubated at room temperature for 2 hours in the dark. The reaction is then loaded onto a C18 HPLC column equilibrated in degassed C18 Buffer A (10 mM TEA acetate, pH 7). CoA linked Cy5Q is eluted by performing a shallow gradient into C18 Buffer B (10 mM TEA acetate, pH 7, 50%$_V$ acetonitrile). The eluted fraction is then desalted using a Sep-Pak SPE and stored at -80°C until further use.

His_6-EF-Tu_{ACP} is mixed with AcpS enzyme at a 1:1 ratio in ACP Labeling Buffer (50 mM HEPES, pH 7.5, 10 mM $MgCl_2$) along with a 10-fold excess of CoA-Cy5Q. The labeling reaction is incubated for 2 hours at 4°C in the dark. Afterwards, imidazole, pH8, is added to a final concentration of 10 mM. The sample is then applied to gravity column prepared with Ni-NTA resin previously equilibrated with EF-Tu Lysis Buffer with 10 mM Imidazole, pH 8. The resin is then washed with 5 volumes of EF-Tu Wash Buffer and eluted with EF-Tu Elution Buffer. The eluted fraction is transferred into a 3.5 kDa dialysis bag and placed in 2 L of EF-Tu Dialysis Buffer for 2 hours, at 4°C in the dark. Following this, the sample is transferred to a fresh 2 L supply of EF-Tu Dialysis Buffer. TEV protease is added at a molar ratio of 1:100 and left at 4°C in the dark overnight.

Following cleavage, imidazole, pH 8, is added to the sample at a final concentration of 10 mM. The sample is then applied to a gravity column prepared with Ni-NTA resin previously equilibrated with EF-Tu Lysis Buffer with 10 mM imidazole, pH 8. The flow-through is collected along with the flow-through of a one column volume wash with EF-Tu Lysis Buffer containing 10 mM imidazole, pH 8. The sample is buffer exchanged into 2xFactor Buffer using a MWCO 10k Amicon filter and concentrated. An equal volume of 100% molecular grade glycerol is added and the sample is stored at -20°C until further use.

2.3.2 Cyanine Dye Labeling Of EF-Ts^{A106C} (Cy3 and Cy5)

His_6-EF-Ts^{A106C} is engineered to have only one cystine such that site-specific labeling can be achieved through sulfhydryl labeling strategies. A 100-fold excess of either Cy3 or Cy5 containing a maleimide side group is added to EF-Ts in buffer (100 mM KP_i, pH 6.5, 100 μM TCEP, 100 mM NH_4Cl). The reaction is incubated at room temperature for 1.5 hours in the dark.

Purification of labeled EF-Ts(Cy3/5) is carried out as described in section 2.3.1.

2.3.4 MDCC Labeling Of PBP

PBP is engineered to have only one reactive cystine for the purpose of conjugating a maleimide linked fluorophore. Maleimide conjugated MDCC is used to label PBP as previously described[74,75].

2.3.6 NHS-Cyanine Dye Labeling of tRNA

E. coli tRNA expressed from the gene pheV has a single 3-(3-amino-3-carboxypropyl) modification on the Uridine at position 47 (acp^3U47). Importantly, this modification adds a unique primary amine to the tRNA (Figure 2.27). By taking advantage of *N*-hydroxysuccinimide (NHS) conjugated cyanine dyes, the $tRNA^{Phe}$ can be site specifically labeled at position U47.

Two nanomoles of crude $tRNA^{Phe}$ is buffer exchanged into 312 mM HEPES, pH 7.9. The sample concentrated to 40 μM using a MWCO 10k Amicon centrifugation filter (the final volume is 50 μL). NaCl is added to a final concentration of 1 M. Next, 25 nmoles of NHS conjugated Cy3, Cy3B, or Cy5 (previously resuspended in DMSO at a concentration of 10 mM) is added to 2 nmoles of $tRNA^{Phe}$ and incubated for 30 minutes at room temperature in the dark. This is repeated 4 times for a total

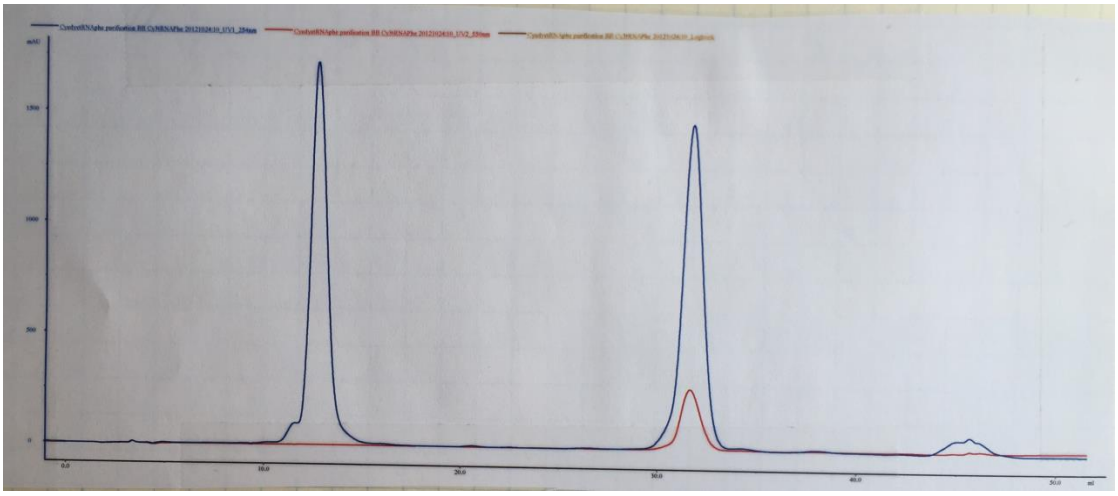

FIGURE 2.27 ***Purification of Cy3 labeled tRNA^{Phe}.*** Two nmols of tRNA^{Phe} is labeled with 100 nmols of Cy3-NHS and purified over a 3 mL Phenyl-5PW TSK column using an ÄKTA purifier. tRNA^{Phe} elution is tracked using 254 nm (blue) and 550 nm (red) absorbance.

addition of 100 nmoles of dye and a total incubation of 2 hours. Following this, the reaction volume is brought to 400 µL with ddH_2O and phenol:chloroform extracted and ethanol precipitated as described in section 2.2.10.

The precipitation reaction is centrifuged in a table-top centrifuge at 15,000 rpm for 10 minutes at 4°C. The sample is resuspended in 1 mL of tRNA Buffer A and purified using a Phenyl-5PW TSQ hydrophobic column. Gradienting into tRNA Buffer B, as described in section 2.2.10, tRNA^{Phe} is eluted at 12 mL and dye labeled tRNA^{Phe} is eluted at 32 mL for Cy3, Cy3B and Cy5 respectively. The tRNA is buffer exchanged into tRNA Storage Buffer using a MWCO 10k Amicon centrifugation filter and flash frozen in LN_2. Samples are stored at -135°C to -196°C in a LN_2 tank until further use.

2.4 EXPERIMENTAL PROCEDURES

This section describes the assays used to generate the data discussed in later sections and chapters.

2.4.1 Acylation of $tRNA^{Met}$, $tRNA^{Arg}$, and $tRNA^{Phe}$

tRNA is acylated by mixing 7.5 pmol purified tRNA in buffer (50 mM Tris-HCl, pH 8, 20 mM KCl, 100 mM NH_4Cl, 1 mM DTT, 2.5 mM ATP, 0.5 mM EDTA, 10 mM $MgCl_2$) with 6 pmol of tRNA synthetase and 1 mM amino acid (previously solubilized in ddH_2O). The reaction is then incubated at 37°C for 20 minutes and then placed at room temperature until further use.

2.4.2 Acylation and formylation of $tRNA^{fMet}$

Initiator tRNA ($tRNA^{fMet}$) is prepared by mixing the desired amount into a reaction containing 1 mM methionine amino acid, methionyl-tRNA synthetase (at a sub-saturating ratio of 1:2), transformylase (at a sub-saturating ration of 1:10), FTHF (prepared by incubating 5 µL of MTHF with 0.5 µL 1M Tris, pH 8, and 0.5 µL NaOH) in buffer (- am/fm buffer -). The sample is incubated for 20 minutes at 37°C and placed at room temperature until further use.

2.4.3 Formation of Ribosome Initiation Complex

The initiation complex (IC) described here consists of bacterial ribosomes subunits, purified from BL21 cells, programmed on an mRNA transcript start-site with an initiator fMet-$tRNA^{fMet}$ positioned in the P-site. The mRNA is purchased from Dharmacon and consists of first 6 codons of the *tufA* open reading frame inline with the gp120 viral promoter (mRNA sequence).

IC is generated by first incubating 10 nmoles of TC70 for 10 minutes at 37°C in polymix buffer with 10 µM GTP. Next, 15 nmoles of IF1, IF2, and IF3 are added along with 10 nmoles of S1. The reaction is incubated at 37°C for 5 minutes. 15 nmoles of mRNA is added and the reaction is incubated at 37°C for 5 minutes. Following this, 15 nmoles of fMet-$tRNA^{fMet}$ is added at the reaction is incubated for

another 5 minutes at 37°C. The sample is then incubated on ice for 10 minutes and loaded onto a sucrose cushion containing 1.5 mL of polymix buffer with containing 1.1 M sucrose in six 13x51 mm polycarbonate centrifuge tubes (Beckman Coulter). The tubes are spun for 4 hours at 95,000 rpm in a table-top ultra centrifuge. Once complete, the supernatant is discarded and the pellets are resuspended in polymix buffer and flash frozen in LN_2 and stored at -80°C until further use.

2.4.4. Ternary Complex Isolation by Gel Filtration Chromatography

Ternary complex was formed by adding EF-Tu, or previously formed EF-Tu/Ts complex, to Phe-$tRNA^{Phe}$ at a ratio of 4 to 1 in buffer (50 mM HEPES, pH 7, 20 mM KCL, 100 mM NH_4Cl, 1 mM DTT, 0.5 mM EDTA, 2.5 mM $MgCl_2$, 10 μM GTP) and incubating for 15 minutes at 37°C. Samples were purified using a Superdex75 gel filtration column on an ÄKTA Purifier pre-equilibrated with buffer in either the absence of presence of GTP or GDPNP (10 μM).

2.4.5 Relative Fluorescence Ternary Complex Assay

All fluorescence experiments were performed using a 532 nm high pass filter (LP03-532RS-25 RazorEdge by Semrock) on the emission side. All samples wree analyzed in a 3 mL quartz cuvette with constant mixing at 23C in buffer (50 mM HEPES, pH 7, 20 mM KCL, 100 mM NH_4Cl, 1 mM DTT, 0.5 mM EDTA, 2.5 mM $MgCl_2$) with either 10 μM GTP or 400 nM EF-Tu or EF-Tu/Ts. Steady state measurements were made by manually adding EF-Tu or EF-Tu/Ts to a solution of Phe-$tRNA^{Phe}$ labeled with Cy3 or Cy3B to the modified acp^3U47 as indicated. The dissociation constant, K_D, was determined by fitting the fluorescence data obtained to Equation 1[78].

$$F/F_{\circ}(Tu) = 1 + \frac{\left(F/F_{\circ}{}_{max} - 1\right)}{2C_t}\left(C_t + Tu + K_D - \sqrt{(C_t + Tu + K_D)^2 - 4C_tTu}\right)$$

EQUATION 2.1

where F is the total fluorescence intensity, F_o is the initial fluorescence intensity, C_t is the total aa-tRNA concentration, and Tu is the total EF-Tu concentration.

Pre-steady state measurements were made by manually adding saturating protein factor (400 nM EF-Tu or EF-Tu/Ts) to 5 nM Phe-tRNA^{Phe} (Cy3-acp^{3}U47) and 10 μM GTP and monitoring fluorescence change over time. Apparent rates, k_{app}, were determined by fitting data to a single exponential function[79].

2.4.6 Quench-fluorescence Ternary Complex Assay

All quench-based fluorescence measurements were obtained using a Photon Technology International fluorescence spectrometer with a 523 nm long pass emission filter (LP03-532RS-25 RazorEdge by Semrock). Reactions were analyzed in buffer (100 mM HEPES, pH 7, 20 mM KCL, 100 mM NH_4Cl, 1 mM DTT, 0.5 mM EDTA, 2.5 mM $MgCl_2$, 10 μM GTP) in a 3 mL quartz cuvette with constant mixing at room temperature. Measurements were made by manually adding EF-Tu (Cy5Q) or an EF-Tu(Cy5Q)/Ts complex (preincubated in buffer for 10 minutes at room temperature) to a reaction of 5 nM aa-tRNA fluorescently labeled with Cy3B while exciting at 532 nm and monitoring at 565 nm. The dissociation constant, K_D, was determined as described in section 2.3.2. Apparent rates, k_{app}, were determined from pre-steady state measurements where the time-dependent changes in fluorescence observed were fit to a single exponential function (ferscht 1985).

2.4.7 Ternary Complex Activity Assay

Ternary complex is formed by titrating EF-Tu or EF-Tu/Ts (0 nM to 1 μM) into a reaction containing 400 nM Cy3 labeled Phe-tRNA^{Phe} and 10 μM GTP as described in

section 2.4.5. The fluorescence values are monitored using a PTI QM4 fluorometer with excitation set to 532 nm and detecting at 565 nm with a emission side 550 nm long pass filter (LP03-532RS-25 RazorEdge by Semrock). Fluorescence values are processed by normalizing to the initial data point and evaluated the earliest high fluorescence data point. The corresponding concentration of EF-Tu or EF-Tu/Ts is compared to the total Phe-$tRNA^{Phe}$ in the reaction (Figure 3.2).

2.4.8 Rapid Stopped-flow Experiments Monitoring Relative Fluorescence

All experiments were performed at 23C in buffer (50 mM HEPES, pH 7, 20 mM KCL, 100 mM NH_4Cl, 1 mM DTT, 0.5 mM EDTA, 2.5 mM $MgCl_2$) using an SX20 stopped-flow spectrometer from Applied Photophysics with a 550 nm long pass filter (OG550 by Schott). One injector port was loaded with protein factor preincubated with 2 mM GTP, whereas the other injector port was loaded with 400 nM Phe-$tRNA^{Phe}$ (Cy3-acp^3U47). Concentrations reported in subsequent chapters are final concentrations after mixing.

2.4.9 Rapid Stopped-flow Experiments Monitoring FRET

Quench-fluorescence measurements were obtained in buffer (100 mM HEPES, pH 7, 20 mM KCL, 100 mM NH_4Cl, 1 mM DTT, 0.5 mM EDTA, 2.5 mM $MgCl_2$, 10 μM GTP) at room temperature using an SX20 stopped-flow spectrometer from Applied Photophysics equipped with either a 550 nm long pass emission filter (OG550 by Schott) or a 633 nm long pass emission filter (LP01-633RS-25 RazorEdge by Semrock) for monitoring Cy3 and Cy5 fluorescence respectively. All concentrations are stated as final concentrations after mixing. Error bars represent standard error of the mean of three separate experiments.

2.4.10 GTP Exchange Assay

EF-Tu (15 nmoles) is incubated with 10 μM GTP_{mant} or GDP_{mant} in buffer (50 mM HEPES, pH 7, 20 mM KCl, 100 mM NH_4Cl, 1 mM DTT, 0.5 mM EDTA, 2.5 mM $MgCl_2$) at a final volume of 1 mL for 10 minutes at room temperature in the dark. Samples are rapidly mixed with either 15 nmoles EF-Ts or buffer using an Applied Photophysics SX20 exciting 280 nm using the monochromator and detecting 440 nm fluorescence. Nucleotide exchange was monitored as a function of time. Apparent rates were estimated by fitting fluorescent decay processes to a single exponential function.

2.4.11 Ternary Complex GTP Exchange Assay

Experiments were performed at room temperature in buffer (50 mM HEPES, pH 7, 20 mM KCL, 100 mM NH_4Cl, 1 mM DTT, 0.5 mM EDTA, 2.5 mM $MgCl_2$, 10 μM GTP) under conditions > 10-fold above the KD for ternary complex formation to ensure that all EF-Tu present in the reaction is bound to aa-tRNA (400 nM Phe-$tRNA^{Phe}$, 5 nM Phe-$tRNA^{Phe}$ (Cy3-acp^3U47), 400 nM EF-Tu or EF-Tu/Ts, 10 μM GTP_{mant}). Complex formation was monitored by tracking the fluorescence of the Cy3 and mant fluorophore over time. Measurements of Cy3 and mant fluorescence were made by switching detection modes from 532 nm excitation and 565 nm emission to 280 nm excitation and 440 nm emission, respectively[31]. The mant fluorescence signal was processed using the Savitzky-Golay method in OriginLab8 with a window of nine points[80].

2.4.12 Initiation Complex Activity Assay

Quenched Phe-TC (Cy3B labeled Phe-$tRNA^{Phe}$ previously complex with Cy5Q labeled EF-Tu·GTP) is formed as previously described in section 2.4.6 and aliquoted

into 10 20 nM reactions containing varying concentrations of ribosomes (0 nM, 2.5 nM, 5 nM, 10 nM, 20 nM, 30 nM, 40 nM, 50 nM, 100 nM, 200 nM) in polymix buffer with 1 mM GTP. Reactions are transferred into a 384-well flat black-bottom microplate (128/85 mm, Greiner Bio-One) and imaged using a TECAN Infinite M1000 Pro plate reader with the following settings: 540 nm excitation, 20 nm excitation bandwidth, 585 nm emission, 20 nm emission bandwidth, top mode, 122 gain and using 3x3 square multiple reads per well. Fluorescence values are processed by normalizing to the first data point. Activity is determined by evaluating the earliest fully dequenced value and its corresponding IC concentration relative to the concentration of Phe-TC (Figure 5.9). For a fully active IC, the earliest fully dequenced data point occurs at a concentration equal to the concentration of Phe-TC, or 20 nM IC.

2.4.13 tRNA Selection Dequench Assay

Quenched TC (60 nM_F) is rapidly mixed with varying concentrations of IC using an SX20 in polymix buffer containing 1 mM_F GTP. Monitoring Cy3B fluorescence, the dequencing process is tracked real time. The apparent rate, k_{app}, of dequencing is determined by fitting the rise process with a single exponential function. The calculated rates are then plotted as a function of IC concentration. Error bars represent standard deviation.

2.4.14 tRNA Selection GTP Hydrolysis Assay

Phe-TC (500 pmol) is mixed with the P_i-MOP system (0.1 unit/mL of PNPase and 1.5 mM 7-methylguanosine (7MG), reagents purchased from Sigma) and 1 nmol of MDCC-PBP in 1 mL of polymix buffer with 10 μM GTP for 20 minutes at room temperature. Similarly, 800 pmol of IC is incubated with the P_i-MOP system and

1 nmol of MDCC-PBP in 1 mL polymix with 10 μM GTP for 20 minutes at room temperature. The samples are rapidly mixed using an SX20 stopped-flow spectrometer from Applied Photophysics using a 435 nm LED excitation and a 475 nm notch filter (FF01-475/35-25, Semrock) and monitoring fluorescence. MDCC fluorescence increase is normalized to percent change. The apparent rate of GTP hydrolysis is determined by fitting the rise process to a single exponential function.

2.4.15 smFRET tRNA Selection – tRNA Reaction Coordinate

The procedure followed here closely mimics the procedure described previously by Juette et al[63]. Using the custom built TIRF microscope, Phe-TC (Cy5 labeled tRNA) is rapidly mixed with either surface immobilized ICs containing Cy3 on the initiator tRNA in the P-site, or with surface immobilized ICs containing Cy3B at the C-terminus of protein S12 on the small subunit in polymix buffer containing 1 mM GTP and photostabilizers (TROLOX, COT, NBA)[81,82]. FRET is measured as the percentage of Cy5 intensity detected when illuminating with a 532 nm laser. Raw data is first analyzed with the SPARTAN package to generate a set of traces that include FRET[63]. These traces are then idealized in QuB[64] to generate survival histograms of each FRET state identified. Survival plots are then analyzed in OriginLab8 to determine characteristic time constants (τ) for each FRET state. All time constants are reported as rates ($1/\tau$).

2.4.16 smFRET tRNA Selection – EF-Tu Reaction Coordinate

Experiments are conducted as outlined in section 2.4.15 with the exception that Phe-TC containing either Cy5 or Cy7 labeled EF-Tu^{SCO} is delivered to surface immobilized ICs containing Cy3B labeled S12 illuminated with a 532 nm laser. Raw data is processed as described above in section 2.4.15.

2.4.17 smFRET tRNA Selection – EF-Tu & tRNA Reaction Coordinate

Experiments are conducted as outlined in section 2.4.15 with the exception that Phe-TC containing both Cy5 labeled Phe-tRNA^{Phe} and Cy7 labeled EF-Tu^{SCO} is delivered to surface immobilized ICs containing Cy3B labeled S12 illuminated with a 532 nm laser. Raw data is processed as described above in section 2.4.15.

2.4.18 Simulation Of Ternary Complex Formation

Ternary complex formation was simulated using MATLAB (R2010b) built on the following six reactions:

$$\text{EF-Tu/Ts} + \text{GTP} \underset{85\ s^{-1}}{\overset{6 \cdot 10^{6} M^{-1} s^{-1}}{\leftrightarrow}} \text{EF-Tu/Ts·GTP}$$

REACTION 2.1

$$\text{EF-Tu·GTP} + \text{EF-Ts} \underset{60\ s^{-1}}{\overset{3 \cdot 10^{7} M^{-1} s^{-1}}{\leftrightarrow}} \text{EF-Tu/Ts·GTP}$$

REACTION 2.2

$$\text{EF-Tu/Ts·GTP} + \text{aa-tRNA} \underset{0.05\ s^{-1}}{\overset{80\ s^{-1}}{\leftrightarrow}} \text{EF-Tu/Ts·GTP·aa-tRNA}$$

REACTION 2.3

$$\text{EF-Tu·GTP} + \text{aa-tRNA} \underset{0.01\ s^{-1}}{\overset{10\ s^{-1}}{\leftrightarrow}} \text{EF-Tu·GTP·aa-tRNA}$$

REACTION 2.4

$$\text{EF-Tu·GTP·aa-tRNA} + \text{EF-Ts} \underset{100\ s^{-1}}{\overset{20\ s^{-1}}{\leftrightarrow}} \text{EF-Tu/Ts·GTP·aa-tRNA}$$

REACTION 2.5

$$\text{EF-Tu} + \text{EF-Ts} \underset{0.03\ s^{-1}}{\overset{1 \cdot 10^{7} M^{-1} s^{-1}}{\leftrightarrow}} \text{EF-Tu/Ts}$$

REACTION 2.6

Rate constants used in reactions 1-3 and reaction 6 were determined previously by Gromadski et al{Gromadski, 2002 #532} while the remaining rate constants were estimated from Figures 3.3 and 3.4. The simulation was conducted with the ode45 (Dormand-Prince) solver with an absolute tolerance setting of 1.10×10^{-6} using the starting condition of 2 μM EF-Tu/Ts, 1 mM GTP, and 250 nM aa-tRNA.

CHAPTER 3

DYNAMIC PROPERTIES OF EF-TU·GTP·AMINOACYL-tRNA TERNARY COMPLEX

3.1 OVERVIEW

The data and figures presented in this chapter have been previously published in modified form:

Burnett BJ[a], Altman RB[b], Ferrao R[b], Alejo JL[b], Kaur N[b], Kanji J[b], Blanchard SC[c]. "Elongation Factor Ts Directly Facilitates the Formation and Disassembly of the Escherichia coli Elongation Factor Tu·GTP·Aminoacyl-tRNA Ternary Complex" *Journal of Biological Chemistry*. 2013 **288**:13917-13928[83].

[a]Burnett BJ designed and conducted all experiments solely, or in conjunction with other authors.

[b]Authors conducted experiments in conjunction with Burnett BJ.

[c]Corresponding author, designed experiments in conjunction with Burnett BJ.

3.2 SUMMARY

Aminoacyl-tRNA enters the translating ribosome in a ternary complex with elongation factor Tu (EF-Tu) and GTP. Here, we describe bulk steady state and pre-steady state fluorescence methods that enabled us to quantitatively explore the kinetic features of *Escherichia coli* ternary complex formation and decay. The data obtained suggest that both processes are controlled by a nucleotide-dependent, rate-determining conformational change in EF-Tu. Unexpectedly, we found that this conformational change is accelerated by elongation factor Ts (EF-Ts), the guanosine nucleotide exchange factor for EF-Tu. Notably, EF-Ts attenuates the affinity of EF-Tu for GTP and destabilizes ternary complex in the presence of non-hydrolyzable GTP analogs. These results suggest that EF-Ts serves an unanticipated role in the cell of actively regulating the abundance and stability of ternary complex in a manner that contributes to rapid and faithful protein synthesis.

3.3 INTRODUCTION

GTP-hydrolyzing proteins (GTPases) play a central role in a vast array of biological systems[7,9,13,22]. In bacteria, the three-domain GTPase elongation factor (EF) Tu, a member of the TRAFAC (translation factors) class of G-proteins[9,15], chaperones the entry of aa-tRNA into the messenger RNA (mRNA)-programmed ribosome during the process of protein synthesis[14,84-86]. This multistep and highly conserved process is a critical determinant of the mechanism of translational fidelity[1] and is exquisitely regulated by EF-Tu-catalyzed GTP hydrolysis while bound to the ribosome. Efforts to understand how EF-Tu facilitates the process of aa-tRNA selection have depended critically on high resolution structural information of active (EF-Tu·GTP) and inactive

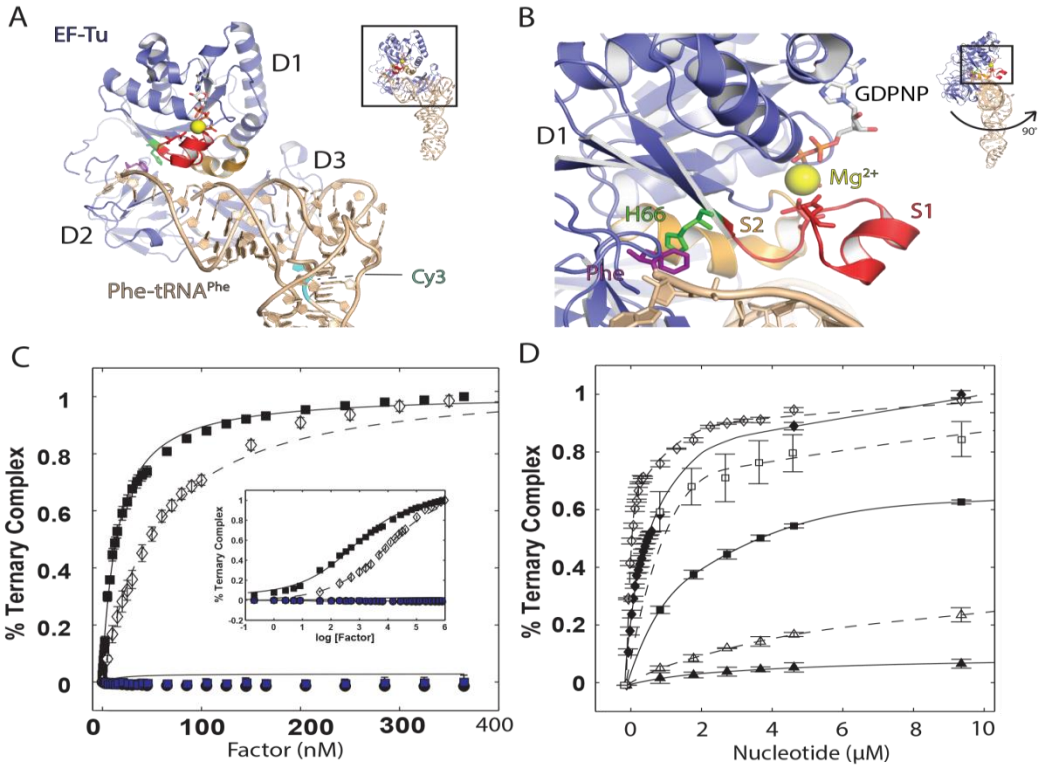

FIGURE 3.1 ***Ternary complex structure and steady state measurements of ternary complex formation.*** **A**, structure of ternary complex stabilized by the antibiotic kirromycin (Protein Data Bank code 1OB2). *E. coli* EF-Tu (*blue*) bound to GDPNP (carbon atoms in *grey*, nitrogen in *blue*, oxygen in *red*, and phosphorous atoms in *orange*) is complexed with *Saccharomyces cerevisiae* Phe-tRNA^{Phe} (*wheat*). Domains of EF-Tu are represented as *D1*, *D2*, and *D3*. For simplicity, kirromycin is not shown. **B**, specific functional elements are highlighted: switch 1 (*S1*) is in red, switch 2 (*S2*) is in orange, His-66 is in green, and the phenylalanine amino acid is in *purple*. **C**, the affinity of EF-Tu for aminoacyl-tRNA was determined by titrating EF-Tu (*open diamonds*) or EF-Tu/Ts (*closed squares*) into a solution of Cy3-labeled Phe-tRNA^{Phe} and 10 μM GTP. An identical titration of EF-Tu was performed either with deacylated tRNA^{Phe} (*circles*) or in the absence of GTP (*blue squares*). **D**, the apparent nucleotide affinity was measured by titrating GTP into a cuvette containing Phe-tRNA^{Phe} (Cy3-acp^{3}U47) and EF-Tu (open diamonds) or EF-Tu/Ts (*closed diamonds*). Identical titration experiments of GDPNP with EF-Tu (*open triangles*) and EF-Tu/Ts (*closed triangles*) and GTPγS with EF-Tu (*open squares*) or EF-Tu/Ts (*closed squares*) are shown. *Error bars* represent the S.E. of three separate experiments. Estimates of the apparent K_D were obtained by fitting the titration data as described in Chapter 2. Data points are splined for clarity.

(EF-Tu·GDP) forms of EF-Tu. Toward this goal, atomic resolution structures of EF-Tu bound within its "ternary complex" with GTP and aa-tRNA and bound to GDP have been solved[28,87-91]. This work revealed that EF-Tu·GTP and EF-Tu·GDP exhibit markedly distinct conformations characterized by "compact" and "extended" configurations, respectively. Related investigations showing that only EF-Tu·GTP binds aa-tRNA with high affinity (approximately nanomolar) suggested that the capacity of EF-Tu to achieve its activated, compact form is a critical determinant of high affinity aa-tRNA binding[78,92-95]. In its compact configuration, the three domains of EF-Tu (D1, D2, and D3) closely interact with each other and with the tRNA acceptor stem (see Figures 3.1, *A* and *B*)[29,88]. The high affinity nature of the EF-Tu·GTP·aa-tRNA interaction is further buttressed by the formation of an amino acid binding pocket at the interface of domains 1 (also referred to as the G domain) and 2 of the protein[57,95]. There, histidine 66 (His-66) within domain 1 stacks on the aminoacyl side chain linked to the 3′-hydroxyl group of the terminal adenosine residue (A76) of tRNA[95]. In EF-Tu·GDP, domain 1 is distal to domains 2 and 3[88], rationalizing why this form of the protein does not bind aa-tRNA[78,92,94]. These findings suggest that compact and extended conformations of EF-Tu define active and inactive states of the G-protein, respectively, and that the active EF-Tu fold is somehow dependent on the terminal phosphate of GTP. High resolution structures of ternary complex bound to the ribosome have revealed that GTP hydrolysis leads directly to conformational changes within the GTP binding pocket[28]. This region includes the so-called switch-1 (S1), switch-2 (S2), and P loop motifs that are conserved in all G-proteins[9]. The S1 element is structurally linked to the amino acid binding pocket and engages the triphosphate moiety of the GTP nucleotide via a bridging magnesium ion (Mg^{2+}) (see Figure 3.1*B*). The S1 element becomes disordered following GTP hydrolysis on the ribosome[28] and adopts an alternative β-hairpin conformation in the

EF-Tu·GDP structure[91]. Collectively, these findings suggest that structural transitions within S1 likely contribute to the transition between GTP and GDP-bound conformations of the protein and the aa-tRNA selection mechanism.

Ensemble, steady state measurements of ternary complex[25,78,92,94,96-99] together with estimated intracellular concentrations of EF-Tu, aa-tRNA (approximately tens of micromolar), and GTP (approximately millimolar) suggest that most (~90%) aa-tRNA is complexed with EF-Tu in actively growing bacteria[31,96]. However, the steady state concentration of ternary complex is strongly dependent on numerous biochemical processes, including the rates of ribosome-catalyzed protein synthesis, amino acid availability, and the relative intracellular concentrations of GTP and GDP. The concentration of ternary complex is also dependent on the activity of EF-Ts, the guanosine nucleotide exchange factor (GEF) for EF-Tu that is required to convert EF-Tu·GDP released from the ribosome into an EF-Tu·GTP form that is again competent for aa-tRNA binding. Notably, EF-Ts is also present at micromolar concentrations in the cell[37,58,100]. EF-Tu has a ~60-fold higher affinity for GDP over GTP and a slow rate of spontaneous nucleotide exchange[31]. Correspondingly, EF-Ts activity is essential for cellular growth[101,102] (32, 33) as it regulates ternary complex abundance in the cell and consequently the rates of protein synthesis.

The importance of normal EF-Tu functions to cellular growth is highlighted by the prevalence of chemically distinct antibiotics that alter EF-Tu activities[35,103-105]. Thiostrepton class peptide antibiotics bind to the large ribosomal subunit GTPase-activating center to disrupt ternary complex binding to the A site[106]. GE2270A class thiazolyl peptide antibiotics bind directly to EF-Tu at the domain 1/2 interface to prevent its interaction with aa-tRNA[104]. Kirromycin binds at the domain 1/3 interface of EF-Tu to stall ternary complex on actively translating ribosomes[1,3,26,107,108] immediately after GTP hydrolysis by preventing conformational changes in EF-Tu

required for its release from aa-tRNA. Thus, the dynamics of ternary complex formation and stability are critical for cellular viability. However, pre-steady state kinetic information regarding the rates of ternary complex formation and decay is currently lacking.

To assess dynamic aspects of the *Escherichia coli* EF-Tu·GTP·aa-tRNA ternary complex, here we describe a presteady state, fluorescence-based approach that reports on binding between EF-Tu and aa-tRNA. We used this signal to investigate rate-determining conformational changes that control the high affinity interactions of EF-Tu with aa-tRNA. Remarkably, these investigations revealed that the dynamics of ternary complex formation and decay are markedly increased in the presence of EF-Ts. We conclude that EF-Ts directly interacts with EF-Tu while bound to aa-tRNA to regulate its affinity for GTP and aa-tRNA ligands. We speculate that EF-Ts regulates the stability and turnover of ternary complex by catalyzing rate-limiting conformational processes in the nucleotide binding pocket of EF-Tu that are responsible for aa-tRNA binding and release.

3.4 RESULTS

3.4.1. Kinetics of Ternary Complex Formation

The process of ternary complex formation minimally proceeds through the following sequence of biochemical steps[109,110].

$$\text{EF-Tu·GDP} + \text{EF-Ts} \underset{k_{1-}}{\overset{k_{1+}}{\leftrightarrow}} \text{EF-Tu·EF-Ts} + \text{GDP}$$

REACTION 1

$$\text{EF-Tu·EF-Ts} + \text{GTP} \underset{k_{2-}}{\overset{k_{2+}}{\leftrightarrow}} \text{EF-Tu·GTP} + \text{EF-Ts}$$

REACTION 2

$$\text{EF-Tu·GTP} + \text{aa-tRNA}^{aa} \underset{k_{3-}}{\overset{k_{3+}}{\leftrightarrow}} \text{EF-Tu·GTP·aa-tRNA}^{aa}$$

REACTION 3

Here, Reactions 1 and 2 define the GEF activities of EF-Ts where EF-Ts functions to displace GDP from EF-Tu and facilitate the association of EF-Tu with GTP[31,93,111,112]. In this minimal reaction scheme, the EF-Tu·GDP·EF-Ts complex implicit in Reaction 1 exists only transiently (k_- = 125 s^{-1})[31]. Likewise, the EF-Tu·GTP·EF-Ts species implicit in Reaction 2 is also transient in nature (k_- = 60 s^{-1})[31]. The rates of ternary complex formation and dissociation (Reaction 3 in this reaction scheme) have been largely inferred from an array of steady state investigations[25,78,92,94,97,98]. Direct presteady state information, however, is currently lacking. In particular, little is presently known about how this reaction proceeds in the presence of EF-Ts as it natively occurs in the cell.

3.4.2 Steady State Measurements of Ternary Complex Formation

Following procedures analogous to those previously described using Phe-$tRNA^{Phe}$ fluorescently labeled at the 4-thiouridine residue at position 8 (s^4U8)[78], we first attempted to determine the apparent affinity of EF-Tu for Cy3-acp^3U47-labeled Phe-$tRNA^{Phe}$ using a steady state approach. Here, the fluorescence intensity of the Cy3 fluorophore linked to tRNA was tracked as a function of EF-Tu concentration.

Titrations were performed by addition of either EF-Tu·GTP where EF-Tu was preincubated with 10 µM GTP or an EF-Tu·EF-Ts complex (EF-Tu/Ts) to a reaction mixture containing 5 nM Phe-tRNA^{Phe} (Cy3-acp^{3}U47) and 10 µM GTP at room temperature (23°C).

Under these experimental conditions, both measurements resulted in an EF-Tu-dependent increase in Cy3 fluorescence intensity that plateaued at ~30% above base line (Figure 3.1*C*). Such changes are speculated to arise from an environment-specific increase in Cy3 quantum yield upon ternary complex formation, stemming from reductions in solvent-mediated, non-radiative relaxation pathways and/or cis-trans isomerization rates[113,114]. Consistent with previous studies[78] and the determinants of ternary complex formation as outlined in Reaction 3, the observed increase in Cy3 fluorescence intensity was strictly dependent upon the presence of GTP as well as the

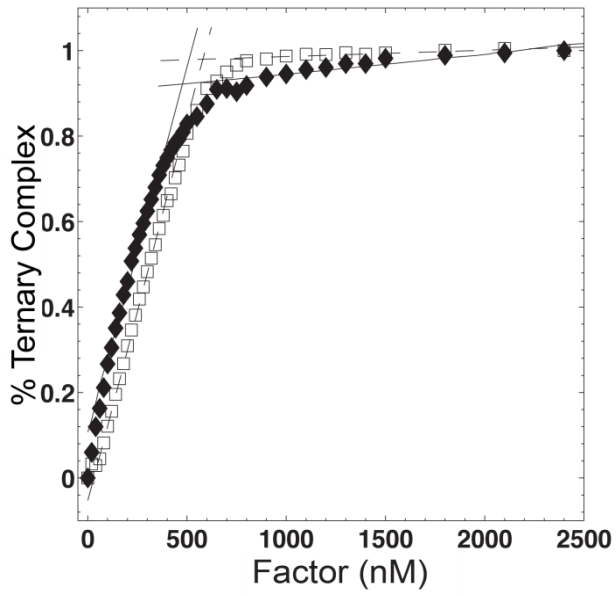

FIGURE 3.2 ***EF-Tu is highly active in both the absence and presence of EF-Ts.*** The fraction of active EF-Tu molecules present in our protein preparation was determined by titrating EF-Tu (*open squares*) or EF-Tu/Ts (*closed diamonds*) into a solution of 400 nM Phe-tRNA^{Phe} (Cy3-acp^{3}U47) in the presence of 10 µM GTP. Linear fits of the initial and final 10 data points of these two experiments intercept at 517 and 496 nM for EF-Tu and EF-Tu/Ts, respectively, indicating that EF-Tu is ~80% active in the absence and presence of EF-Ts.

acylation of $tRNA^{Phe}$ with the phenylalanine amino acid (Figure 3.1*C*). The apparent dissociation constant for the ternary complex interaction was estimated by fitting the raw data to the reaction scheme derived for relative fluorescence measurements (see Chapter 2). In agreement with previously described steady state measurements of this type, a high affinity interaction was observed both in the absence (K_D = 47 ± 3.1 nM) and presence of EF-Ts (K_D = 12.6 ± 1.1 nM) (Table 3.1)[25,78,92,94,95,115,116]. These findings suggest that the observed changes in Cy3 fluorophore intensity specifically report on a GTP-dependent interaction of EF-Tu with the acylated acceptor stem of Phe-tRNAPhe. They also suggest that EF-Ts substantially increases the apparent affinity of this interaction. The observed disparity between EF-Tu and EF-Tu/Ts affinities for aa-tRNA could not be explained by differences in EF-Tu activities (Figure 3.2). Activity was determined by titrating either EF-Tu or EF-Tu/Ts into a solution of 400 nM $Phe\text{-}tRNA^{Phe}$ (Cy3-acp^3U47) and 10 µM GTP. For 100% active reagents, a linear increase in signal is expected followed by a sharp inflection at a protein concentration equal to the concentration of $Phe\text{-}tRNA^{Phe}$ present in the reaction[117]. In our experiments, such an inflection was observed at ~500 nM factor, indicating that EF-Tu is ~80% active both in the absence and presence of EF-Ts.

Analogous steady state measurements were next conducted to assess the nucleotide dependence of ternary complex formation. To do so, experiments were performed by titrating GTP into a solution of 5 nM $Phe\text{-}tRNA^{Phe}$ (Cy3-acp^3U47) in the presence of saturating concentrations of either nucleotide-free EF-Tu or EF- Tu/Ts complex both at 500 nM (~10-fold above their apparent K_D). For both systems, an ~30% increase in Cy3 fluorescence intensity was observed at elevated GTP concentrations (Figure 3.1*D*). For the experiments with EF-Tu alone, fitting procedures (see Chapter 2) revealed an apparent affinity of K_D = 195 ± 12 nM, whereas experiments performed with EF-Tu/Ts revealed that the apparent affinity was

TABLE 3.1 *Dissociation constant of ternary complex*. The ternary complex was formed by titrating either factor or nucleotide in the absence or presence of EF-Ts.

	Dissociation constant K_D	
	EF-Ts(-)	EF-Ts(+)
	nm	
Factor	47 ± 3.1	12.6 ± 1.1
GTP	195 ± 25	685 ± 35
GDPNP	7000 ± 100	9270 ± 105
GDPγS	240 ± 18	490 ± 41

~3.5-fold weaker (K_D = 685 ± 35 nM) (Figure 3.1*D*). These data suggest that additional complexities exist in the ternary complex formation reaction beyond those delineated by Reaction 3. Such findings could be explained if ternary complex is in a dynamic equilibrium and EF-Ts alters this exchange process by specifically modulating the affinity of the nucleotide for EF-Tu.

This model predicts that the ternary complex formation and thus the observed fluorescence intensity change will be sensitive to the precise nature of the EF-Tu·GTP interaction. To examine this hypothesis, identical experiments were repeated with non-hydrolyzable GTP analogs GDPNP and GTPγS. As anticipated by the model, the extent of ternary complex formation was significantly lower in the presence of non-hydrolyzable GTP analogs (Figure 3.1*D* and Table 3.1). For each analog, this trend was exacerbated in the presence of EF-Ts. These findings suggest that the observed fluorescence change reports on conformational events in the system that are sensitive to chemical and/or structural features of the γ-phosphate constituent of the nucleotide. Inspection of the ternary complex structure (Figure 3.1, *A* and *B*) suggests that such conformational changes likely entail the formation of contacts between the S1 helix and the γ-phosphate of GTP.

3.4.3 Pre-Steady State Measurements of Ternary Complex Formation

To obtain a deeper understanding of the kinetic parameters underpinning Reaction 3, we performed pre-steady state measurements to monitor ternary complex formation in real time. Data were obtained by rapidly adding saturating (400 nM final) concentrations of EF-Tu or EF-Tu/Ts complex to a solution of 5 nM Phe-tRNA^{Phe} (Cy3-acp^{3}U47) and 10 µM GTP. Consistent with our steady state measurements, the addition of EF-Tu resulted in a ~30% increase in Cy3 fluorescence intensity that reached steady state within seconds (Figure 3.3*A*) and remained stable over several hours (data not shown). Fitting the time course of the fluorescence intensity change to an equation for pre-steady state reactions of this kind (see Chapter 2) revealed an apparent association rate, $k_{app,1}$, of 0.38 s^{-1} for EF-Tu and 0.5 s^{-1} for the EF-Tu/Ts complex (Figure 3.3*B*). The factor concentration-dependence of $k_{app,1}$ revealed that the maximum rates of ternary complex formation for both systems at 10 µM GTP saturated at approximately similar levels: ~0.5 s^{-1} for EF-Tu and 0.55 s^{-1} for the EF-Tu/Ts complex.

Further insights into the on- and off-rate kinetics underpinning ternary complex formation and dissociation reactions were obtained by inspecting how $k_{app,1}$ changed at low factor concentrations where the concentration-dependence is linear. The on-rate of the ternary complex formation, determined by setting the slope of $k_{app,1}$ to $k_{on}/(1 + k_{off}/k_{app,\infty})$[79], revealed that the on-rate in the presence of 10 µM GTP is ~1.2 ± 0.07 and 1.7 ± 0.1 $\mu M^{-1}s^{-1}$ for EF-Tu and the EF-Tu/Ts complex, respectively (Figure 3.3*B*, *inset*, and Table 3.2), in close agreement with published values[92]. A preliminary estimate of the factor off-rates, defined by the *y* intercept, revealed that EF-Tu dissociates slowly from aa-tRNA (on the order of 0.05 s^{-1}). These values are in good agreement with both our own (Table1) and previous affinity measurements[95].

To directly examine the dissociation kinetics of ternary complex, pre-steady state measurements were performed in which a 10-fold molar excess of GDP (100 µM) was

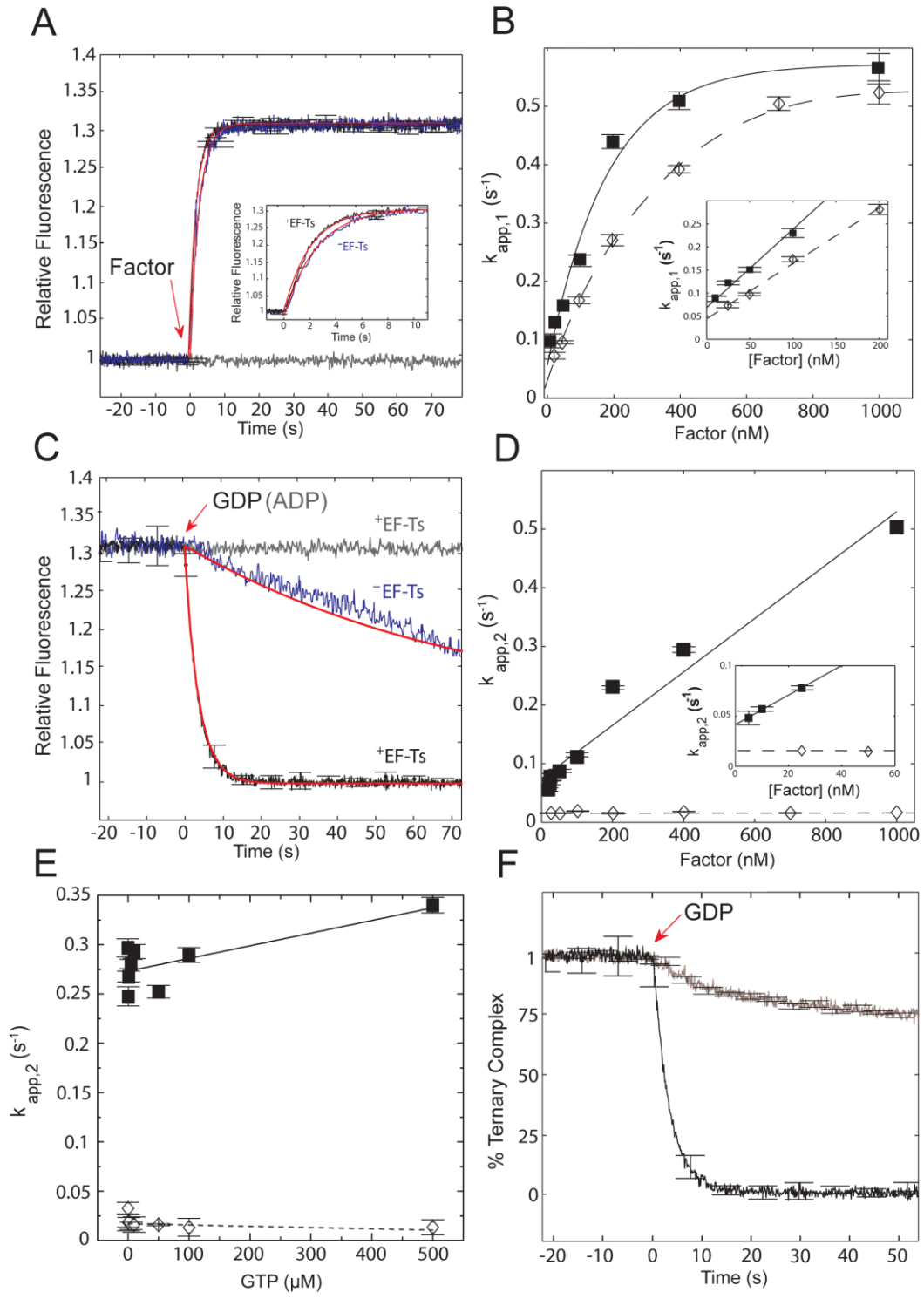

FIGURE 3.3 ***Pre-steady state measurements of ternary complex formation and dissociation: dependence on factor concentration.*** **A**, the time-dependent response in fluorescence intensity observed upon addition of saturating amounts (400 nM) of either EF-Tu (*blue*) or EF-Tu/Ts (*black*) to Cy3-labeled Phe-tRNA^{Phe} (5 nM) and GTP (10 μM) or EF-Tu/Ts in the absence of GTP (*gray*).

added to ternary complex preformed with 10 μM GTP and a 400 nM concentration of either EF-Tu or EF-Tu/Ts. In line with the notion that EF-Tu binds tightly to aa-tRNA, the addition of GDP to the preformed ternary complex caused a slow decrease in Cy3 fluorescence, returning the system to base-line intensity at a rate, $k_{app,2}$, of ~0.015 s^{-1} (Figure 3.3*C*). This rate was independent of factor (Figure 3.3*D*) and GTP concentrations (Figure 3.3*E*) and consistent with our off-rate estimates (Figure 3.3*B*).

Identical experiments performed with 400 nM EF-Tu/Ts showed a similar overall reduction in fluorescence intensity upon GDP addition but at an ~20-fold faster decay rate ($k_{app,2}$ ~ 0.3 s^{-1}) (Figure 3.3*C*). Notably, the apparent rate of GDP-induced ternary complex dissociation, k_{app2}, increased linearly as a function of EF-Tu/Ts concentration from ~0.03 s^{-1}, extrapolated to 0 nM EF-Ts, up to ~0.5 s^{-1} at the highest concentration tested (1 μM) (Figure 3.3*D*). The accelerated rate of GDP-induced ternary complex dissociation in the presence of EF-Ts was observed to be independent of GTP concentration (Figure 3.3*E*). Although the concentration of free EF-Ts (not bound to EF-Tu) in these experiments is difficult to estimate, it is anticipated to be substantially

Fitting the data (see Chapter 2) provided a quantitative measure of the apparent rate of ternary complex formation, $k_{app,1}$. A focused plot of the formation process is also shown (*inset*). **B**, measurements of $k_{app,1}$ as a function of either EF-Tu (*open diamonds*) or EF-Tu/Ts (*closed squares*). The inset shows the linear fits of early factor titration data points. **C**, the time-dependent response in fluorescence intensity observed upon addition of saturating amounts of GDP (100 μM) to ternary complex preformed as described in A with either EF-Tu (*blue*) or EF-Tu/Ts (*black*). Identical experiments were performed using ADP (100 μM) (*grey*). **D**, fitting to a single exponential function provided a quantitative measure of the off-rate of ternary complex formation, $k_{app,2}$, as a function of either EF-Tu (*open diamonds*) or EF-Tu/Ts (*closed squares*) as described in C. **E**, similar disassociation experiments were performed at varying GTP concentrations. Addition of saturating GDP to ternary complex preformed with an excess of EF-Tu (*open diamonds*) or EF-Tu/Ts (*closed squares*) and 5 nM Phe-$tRNA^{Phe}$ in the presence of GTP (50 nM – 500 μM). Apparent decay rates, $k_{app,2}$, were estimated by fitting to a single exponential function. **F**, GDP (100 μM) was delivered to ternary complex preformed with EF-Tu/Ts in the absence (*black*) or presence (*tan*) kirromycin. The rate of GDP mediated dissociation in the absence of kirromycin ($k_{app,2}$ = 0.28 s^{-1}) was found to be 14 times faster than in the presence of kirromycin ($k_{app,2}$ = 0.002 s^{-1}). *Error bars* represent the S.E. from three independent experiments.

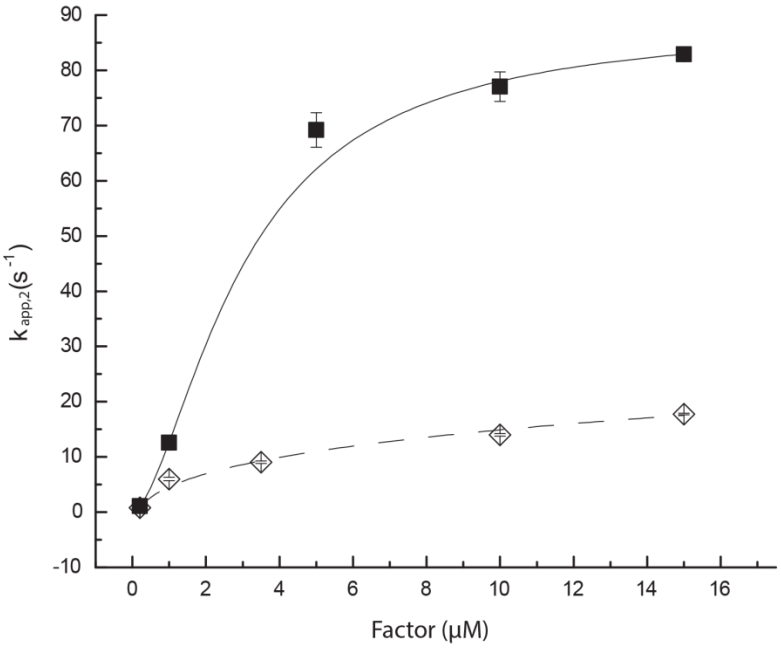

FIGURE 3.4 ***EF-Ts accelerates the rate-determining step in EF-Tu binding to aa-tRNA.*** Ternary complex was formed by rapid mixing of 200 nM Phe-tRNA^{Phe} (Cy3-acp^{3}U47) with EF-Tu or EF-Tu/Ts preincubated in the presence of 1 mM GTP. Time courses of complex formation were fit to a single exponential function, and apparent rates were plotted as a function of EF-Tu (*open diamonds*) or EF-Tu/Ts (*closed squares*) concentration. Under these conditions, the apparent rate of complex formation observed asymptotically approached ~20 s^{-1} for EF-Tu and ~80 s^{-1} for EF-Tu/Ts. *Error bars* represent the S.E.

lower than EF-Tu/Ts concentration given the known K_D of the EF-Tu/Ts interaction (3 nM)[31]. We conclude that EF-Ts plays a direct role in ternary complex dissociation in the presence of GDP and that the recognition process occurs at a rate that is likely to significantly exceed 1.5 $\mu M^{-1}s^{-1}$ (determined from the slope of the line shown in Figure 3.3*D*, *inset*).

To examine the physical basis of the observed dissociation reaction coordinate, identical experiments were performed in the presence of kirromycin, an antibiotic that directly binds EF-Tu at the interface between domains 1 and 3[29]. As anticipated from its known propensity to prevent EF-Tu dissociation from aa-tRNA[3,107,108], in the presence of kirromycin, ternary complex was observed to be strongly resistant to GDP-induced dissociation even in the presence of EF-Ts (Figure 3.3*F*). This finding is

consistent with a model in which the dissociation of EF-Tu from aa-tRNA proceeds via rearrangements at the interface between domains 1 and 3 of EF-Tu.

To address the physiological relevance of these findings, we performed pre-steady state measurements of ternary complex formation at near cellular concentrations of protein factors (0.2–15 µM), aa-tRNA (0.2 µM), and GTP (1 mM) using stopped-flow instrumentation. Here, EF-Tu and EF-Tu/Ts were pre-incubated with GTP. As shown previously (Figure 3.3), the signal obtained was strictly dependent on the aminoacyl moiety of Phe-tRNA^{Phe} and GTP (data not shown). At these concentrations, the apparent rate of ternary complex formation for EF-Tu alone plateaued at a rate of

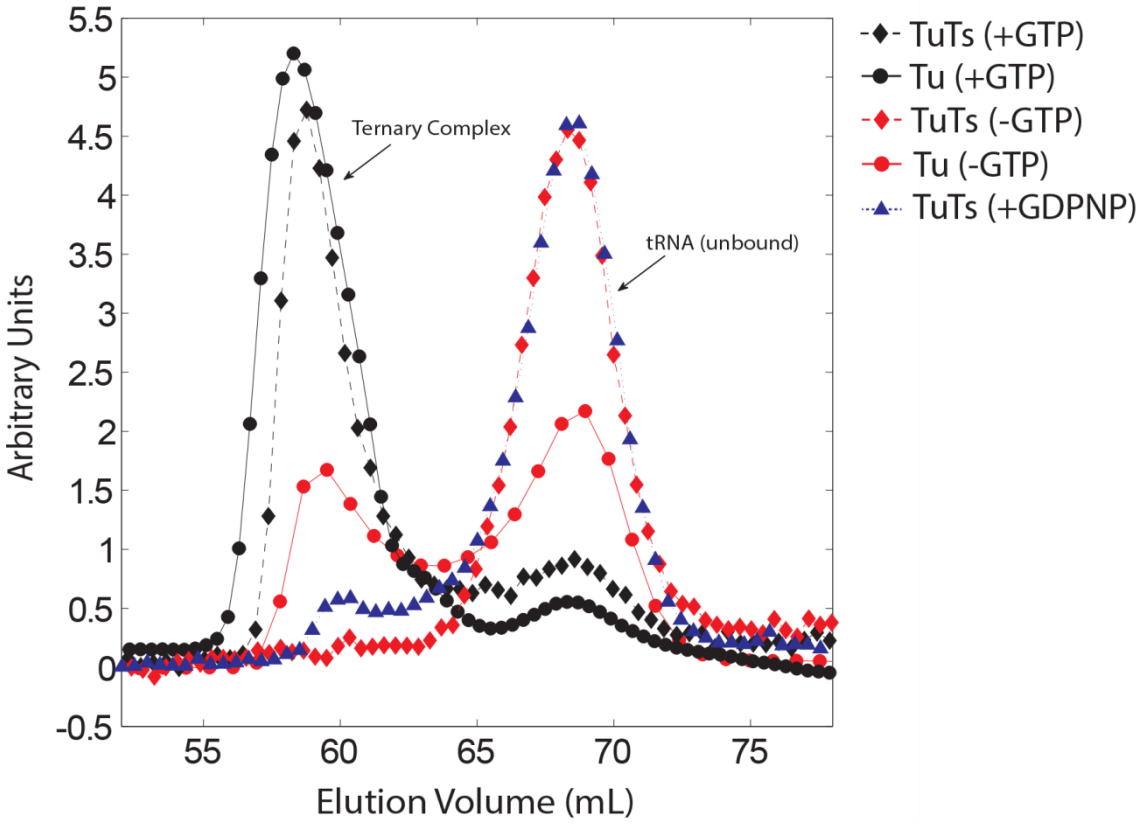

FIGURE 3.5 ***Physical isolation of ternary complex.*** Ternary complex formed in the presence of saturating concentrations of EF-Tu (*circles*) or EF-Tu/Ts (*diamonds*), Cy3-labeled Phe-tRNA^{Phe}, and GTP (see Chapter 2) was fractionated over a Superdex75 gel filtration column in the presence (*black*) or absence (*red*) of GTP (10 µM) in the running buffer. Absorbance was recorded at 260 and 550 nm to specifically track the elution times of "unbound" and ternary complex-bound Cy3-labeled Phe-tRNA^{Phe} as indicated. This was repeated with GDPNP in the reaction and running buffer (*blue triangles*).

TABLE 3.2 ***Summary of kinetic parameters of ternary complex.*** Kinetic descriptors of ternary complex were determined from the apparent rates of ternary complex formation at 10 μM GTP.

	Kinetic parameters		
	k_{on} [a]	k_{off} [a]	$k_{turnover}$ [b]
	$\mu M^{-1} s^{-1}$	s^{-1}	s^{-1}
EF-Tu	1.2 ± 0.07	0.05 ± 0.004	$0.005 \pm 4 \times 10^{-5}$
EF-Tu·EF-Ts	1.7 ± 0.07	0.07 ± 0.06	0.6 ± 0.03

~20 s^{-1} (Figure 3.4), whereas in the presence of EF-Ts, the rate of ternary complex formation increased to ~85 s^{-1}. These distinct asymptotic values suggest that EF-Ts accelerates the rate-determining step of ternary complex formation by directly facilitating the process of EF-Tu·GTP loading onto Phe-$tRNA^{Phe}$. Under these conditions, ternary complex dissociation was also observed to be accelerated by the presence of EF-Ts (Figure 3.3*D*). These findings suggest that our findings are relevant to ternary complex dynamics as they occur in the cell.

3.4.4. Physical Isolation of the Dynamic Ternary Complex

To directly test the hypothesis that ternary complex formation and decay are in dynamic equilibrium, we set out to examine its stability by gel filtration chromatography. Here, a strong prediction of the dynamic equilibrium model is that ternary complex will dissociate when efficiently separated from GTP. For these experiments, a single solution of ternary complex was prepared using saturating concentrations of GTP, EF-Tu (or EF-Tu/Ts), and Phe-$tRNA^{Phe}$ (Cy3-acp^3U47) (10, 12, and 3 μM, respectively). Portions of this reaction were subjected to gel filtration experiments first in the absence and then in the presence of GTP in the running buffer while monitoring the elution time of Cy3-labeled Phe-$tRNA^{Phe}$ by UV absorbance at 550 nm (see "Chapter 2").

Both in the absence and presence of EF-Ts, detection of the Cy3-labeled Phe-tRNAPhe ternary complex, eluting at the predicted molecular mass of ~75,000 Da, was maximized when GTP was included in the running buffer (Figure 3.5). Consistent with the highly active nature of the components used in our investigations, ~90% of Cy3-labeled Phe-tRNA^{Phe} was found in a ternary complex under these conditions. When GTP was not included in the mobile phase, the amount of tRNA detected in ternary complex was significantly reduced in the absence of EF-Ts and completely

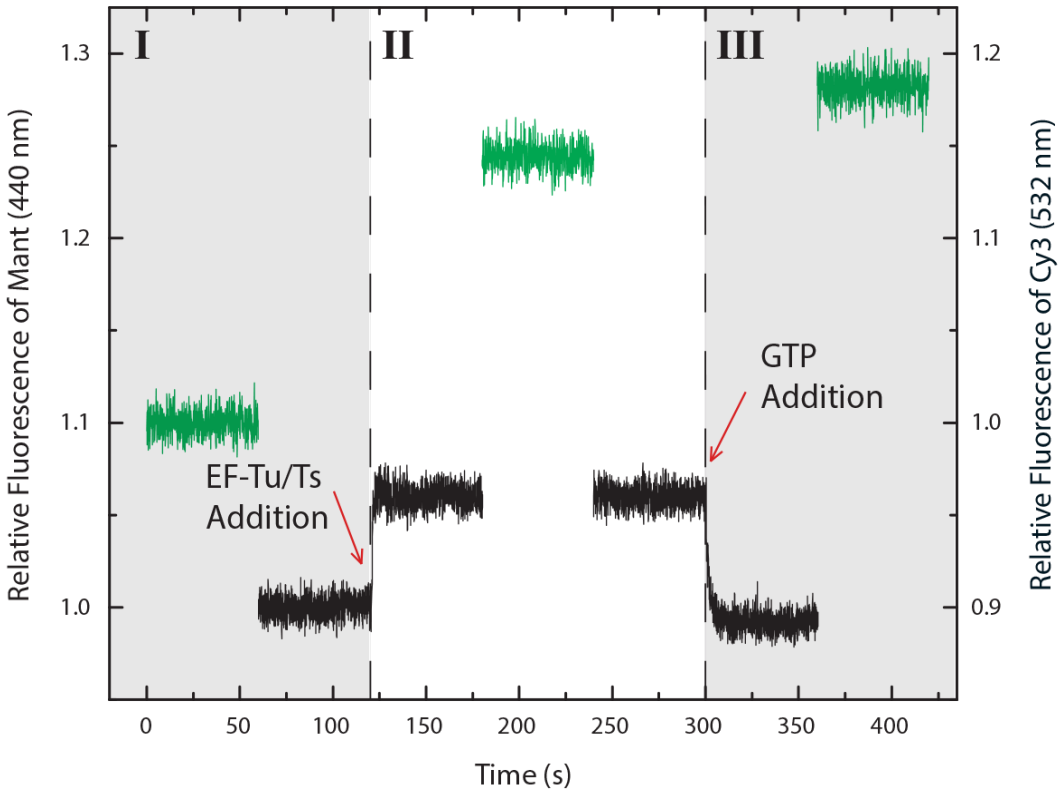

FIGURE 3.6 ***EF-Ts directly facilitates ternary complex turnover.*** Region I, the relative fluorescence intensities of Cy3 (*green; right axis*) and mant (*black; left axis*) obtained from a solution containing 400 nM Phe-tRNA^{Phe} (*unlabeled*), 5 nM Phe-tRNA^{Phe} (Cy3-acp^{3}U47), and 10 µM GTP$_{mant}$ in the absence of factor. Region II, the increase in mant fluorescence intensity (*black; left axis*) and Cy3 fluorescence intensity (*green; right axis*) resulting from addition of 400 nM EF-Tu/Ts to the mixture. Region III, addition of saturating amounts of unlabeled GTP (100 µM) resulted in a rapid decrease ($k_{turnover}$ = 0.6 ± 0.03 s^{-1}) in the mant signal (*black; left axis*), whereas the Cy3 signal (*green; right axis*) exhibited a small increase in intensity.

abolished in the presence of EF-Ts. Analogous experiments conducted with 10 μM GDPNP in the mobile phase showed only ~5% of the total tRNA in ternary complex (Figure 3.5). These findings provide compelling evidence in support of the dynamic nature of ternary complex. They also support a model in which ternary complex dissociation proceeds through sequential conformational events in EF-Tu that first enable GTP dissociation and then aa-tRNA release.

3.4.5. Direct Evidence That EF-Ts Facilitates Ternary Complex Dynamics

Our previous data indicate that EF-Ts accelerates the disassembly of ternary complex upon GDP addition. To differentiate between a model where EF-Ts only breaks down ternary complex in response to GDP addition or where EF-Ts is continually facilitating ternary complex formation and decay, we set out to directly monitor the nucleotide exchange process on EF-Tu using the fluorescent GTP analog (10 μM) GTP_{mant} under conditions where ternary complex appears to be stable for extended periods (as seen in Fig. 3*A*). To ensure that the majority of EF-Tu is bound to aa-tRNA at steady state, ternary complex was formed at component concentrations ~10-fold the apparent K_D (400 nM EF-Tu or EF-Tu/Ts, 400 nM Phe-$tRNA^{Phe}$, 5 nM Phe-$tRNA^{Phe}$ (Cy3-acp^3U47) (Figure 3.2 and see "Chapter 2"). This experimental setup allowed us to monitor ternary complex formation by two distinct spectroscopic means in the same experiment: a change in Cy3 fluorescence intensity (Figure 3.1, 3.3, and 3.4) and FRET between tryptophan 184 in EF-Tu and the mant moiety of the GTP_{mant} nucleotide[31]. As expected for a reaction in which the GTP_{mant} nucleotide binds to EF-Tu, addition of the EF-Tu/Ts complex to Phe-$tRNA^{Phe}$ and GTP_{mant} resulted in a rapid increase in GTP_{mant} fluorescence intensity (Figure 3.6, *region II*). Consistent with ternary complex formation, Cy3 fluorescence intensity also increased during this reaction.

To directly monitor the process of nucleotide exchange, a 10-fold molar excess of unlabeled GTP was added to the same reaction while monitoring GTP_{mant} fluorescence (Figure 3.6, *region III*). Here, the GTP_{mant} signal rapidly returned to base line ($k_{turnover}$ ~0.6 ± 0.03 s^{-1}; Tale 2), whereas examination of the Cy3 fluorescence intensity showed that ternary complex remained intact (Figure 3.6, *region III*). A slight increase in Cy3 fluorescence was also observed, likely reflecting a subtle change in ternary complex stability in the presence of unlabeled GTP. In similar experiments using only EF-Tu, the rate of the GTP_{mant} exchange was greatly reduced ($k_{turnover}$ = ~$0.005 \pm 4 \cdot 10^{-5}$ s^{-1}). These experiments demonstrate that the EF-Ts activities observed are not in response to an insult (such as GDP) but are instead actively occurring in the presence of GTP where ternary complex appears stable. Inclusion of kirromycin in the experiment effectively blocked the GTP_{mant} nucleotide exchange process. This finding suggests that rearrangements at the interface of domains 1 and 3 of EF-Tu are required for the exchange process.

3.5 DISCUSSION

In the present investigation, we developed a means to explore the kinetic and thermodynamic properties of the *E. coli* ternary complex EF-Tu·GTP·Phe-$tRNA^{Phe}$ using bulk fluorescence methods. Akin to earlier steady state measurements of ternary complex formation[78], the fluorescence-based assays described here are based on changes in relative fluorescence intensity. However, unlike earlier work, the approach we describe is based on the environmentally sensitive Cy3 fluorophore[40,82] at a distinct site of tRNA attachment, the naturally occurring modified nucleotide acp^3U present at position 47 in *E. coli* $tRNA^{Phe}$. Although this modification is not as ubiquitous as the s^4U residue utilized previously, tRNA molecules modified at this site have been shown

to be fully functional in all aspects of the translation process, including aminoacylation, tRNA selection, and translocation[40,53,118]. The data presented show that the functionality of acp^{3}U-labeled tRNA^{Phe} also extends to ternary complex formation. In agreement with prior fluorescence investigations of ternary complex formation obtained under steady state conditions[78], we show that the formation of ternary complex strictly depends on the GTP nucleotide and the aminoacyl moiety of aa-tRNA. We also show that the EF-Tu·GTP·Phe-tRNA^{Phe} complex forms a high affinity (nM K_D) interaction (Figure 3.1*C*)[25,92,94,95,97,98].

Unexpectedly, however, we observed that the apparent affinity of ternary complex formation is significantly enhanced in the presence of EF-Ts, the GEF for EF-Tu (K_D ~12 *versus* ~47 nM; Table 3.1). These findings could not be rationalized based on trivial differences in EF-Tu activities in the absence and presence of EF-Ts (*e.g.* that 80% of the EF-Tu preparation was bound to GDP; Figure 3.2). Moreover, the propensity of EF-Ts to decrease the efficiency with which ternary complex was formed in the presence of non-hydrolyzable GTP analogs also suggested an unanticipated function of EF-Ts as a fidelity determinant of ternary complex formation and stability (Figure 3.1*D*). In striking contrast to contemporary models in which EF-Ts serves only as the GEF for EF-Tu[109,119], these findings collectively led us to examine whether EF-Ts functions to regulate ternary complex stability in a direct manner through modulation of the nucleotide binding site.

In line with previous investigations using yeast components[120], pre-steady state measurements obtained under conditions designed to approximate the cellular concentrations of aa-tRNA, GTP, and EF-Tu suggested that the bacterial ternary complex forms via a rate-limiting conformational event in EF-Tu that occurs at a rate of ~20 s^{-1}. However, in the presence of cellular concentrations of EF-Ts, ternary complex formation was observed to proceed at a rate 4 times faster (~85 s^{-1}) (Figure

3.4). As the fluorescence signal detected here depends exquisitely on the presence of the aminoacyl moiety and the nature of the γ-phosphate of the GTP nucleotide, this conformational change likely reports on the ordering of S1, S2, and P loop elements in the G domain of EF-Tu, the structural scaffold of the nucleotide binding pocket (Figure 3.1, *A* and *B*).

A trivial explanation for the observed disparity in rates would be that EF-Ts drives ternary complex formation by accelerating nucleotide loading (Reactions 1 and 2). However, in this case, the apparent rates of ternary complex formation would

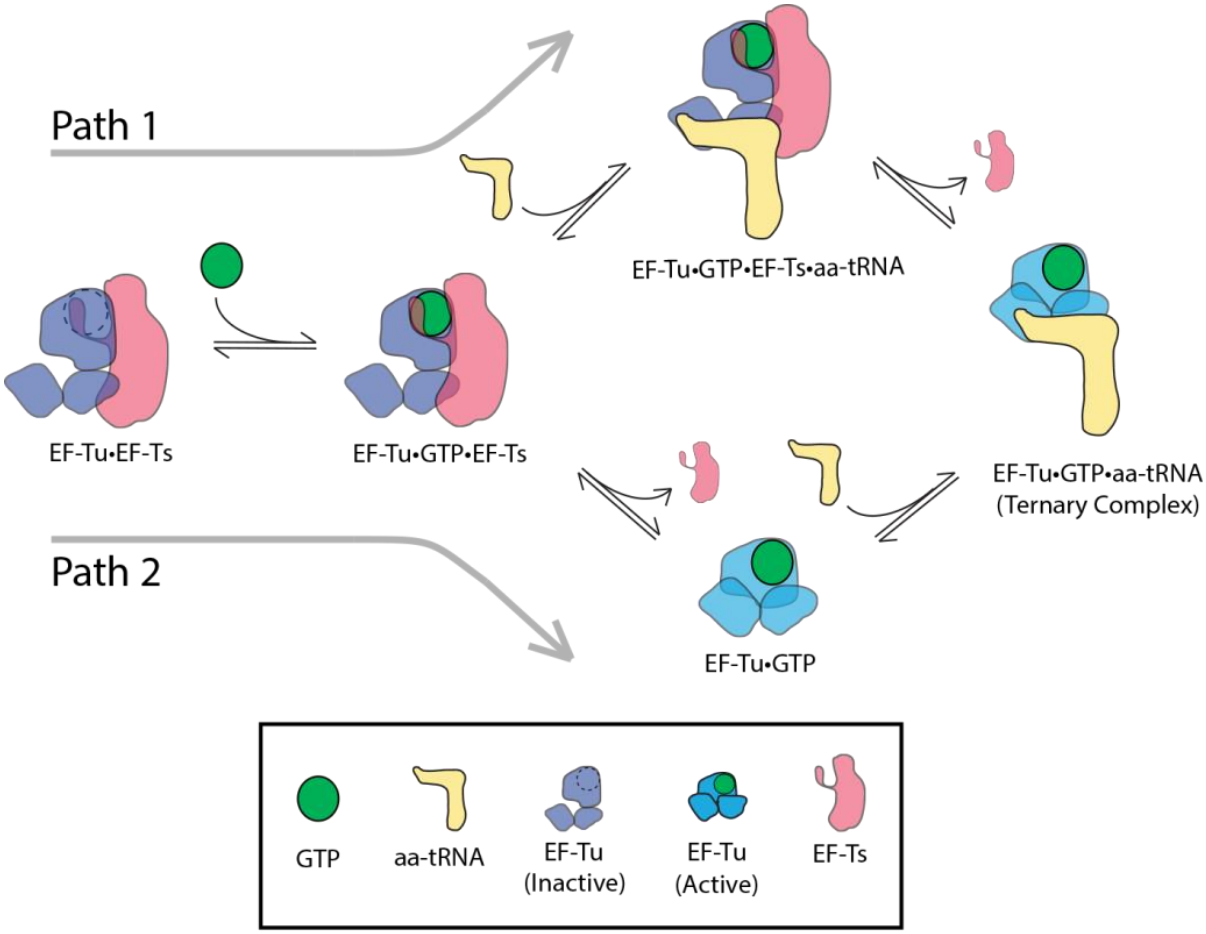

FIGURE 3.7 ***Ternary complex formation and disassembly can occur via two distinct pathways.*** In both pathways, the binary complex EF-Tu/Ts binds GTP, forming an EF-Tu·GTP·EF-Ts complex. In *Path 1*, this species directly binds aa-tRNA, forming a quaternary complex of EF-Tu·GTP·EF-Ts·aa-tRNA, which decays to the EF-Tu·GTP·aa-tRNA ternary complex following EF-Ts dissociation. In *Path 2*, EF-Ts dissociates from the EF-Tu·GTP·EF-Ts complex, allowing EF-Tu·GTP to bind aa-tRNA directly to form ternary complex.

eventually plateau at the same maximum value (~85 s^{-1}). Instead, two distinct maximum rates were observed. Moreover, these experiments were performed following preincubation of EF-Tu and the EF-Tu/Ts complex with saturating concentrations of GTP (1 mM). We conclude that EF-Ts directly facilitates ternary complex formation by accelerating EF-Tu·GTP loading onto aa-tRNA. Indeed, direct interactions between EF-Ts and ternary complex have been suggested previously[93,121,122]. Such insights suggest that the established model of ternary complex formation (Reactions 1–3 above) needs revision. Thus, although the direct binding of EF-Tu·GTP to aa-tRNA is feasible (Reaction 3)[4,24,57,92,94,95,119], our findings suggest that the kinetically favored pathway for ternary complex formation proceeds via the direct binding of an EFTu·GTP·EF-Ts complex to aa-tRNA (Figure 3.7).

Although previous investigations have shown that the EF-Tu·GTP·EF-Ts complex is labile, dissociating at a rate of 60 s^{-1} [31], at cellular concentrations of EF-Ts (~10 μM)[37,58,100], the rate of EF-Ts rebinding to EF-Tu·GTP is estimated to be on the order of 300 s^{-1} [31]. These considerations predict that the EF-Tu·GTP·EF-Ts complex may be relatively abundant in the cell. Based on these insights, we conclude that EF-Ts directly facilitates ternary complex formation and disassembly by lowering the effective activation barrier for a rate-determining conformational change in EF-Tu that is required for the protein to fully engage aa-tRNA and GTP ligands (Figure 3.7). Our nucleotide binding studies suggest that ordering of the switch-1 helix in EF-Tu plays a critical role in this process (Figure 3.1*D*). We speculate that EF-Ts influences the folding of the switch-1 helix in a manner that modulates this commitment step. Further experiments will be required to delineate precisely how EF-Ts impacts the reaction coordinate for ternary complex formation and disassembly.

These previously unanticipated functions of EF-Ts may provide several advantages to the cell. First, the observed capacity to increase the rate of ternary

complex formation may increase the maximum rate of translation that can be achieved in the cell. Second, under steady state conditions, the capacity of EF-Ts to facilitate nucleotide turnover may allow a means of translational control under changing cellular conditions. For instance, under conditions of rapid growth where the concentration of

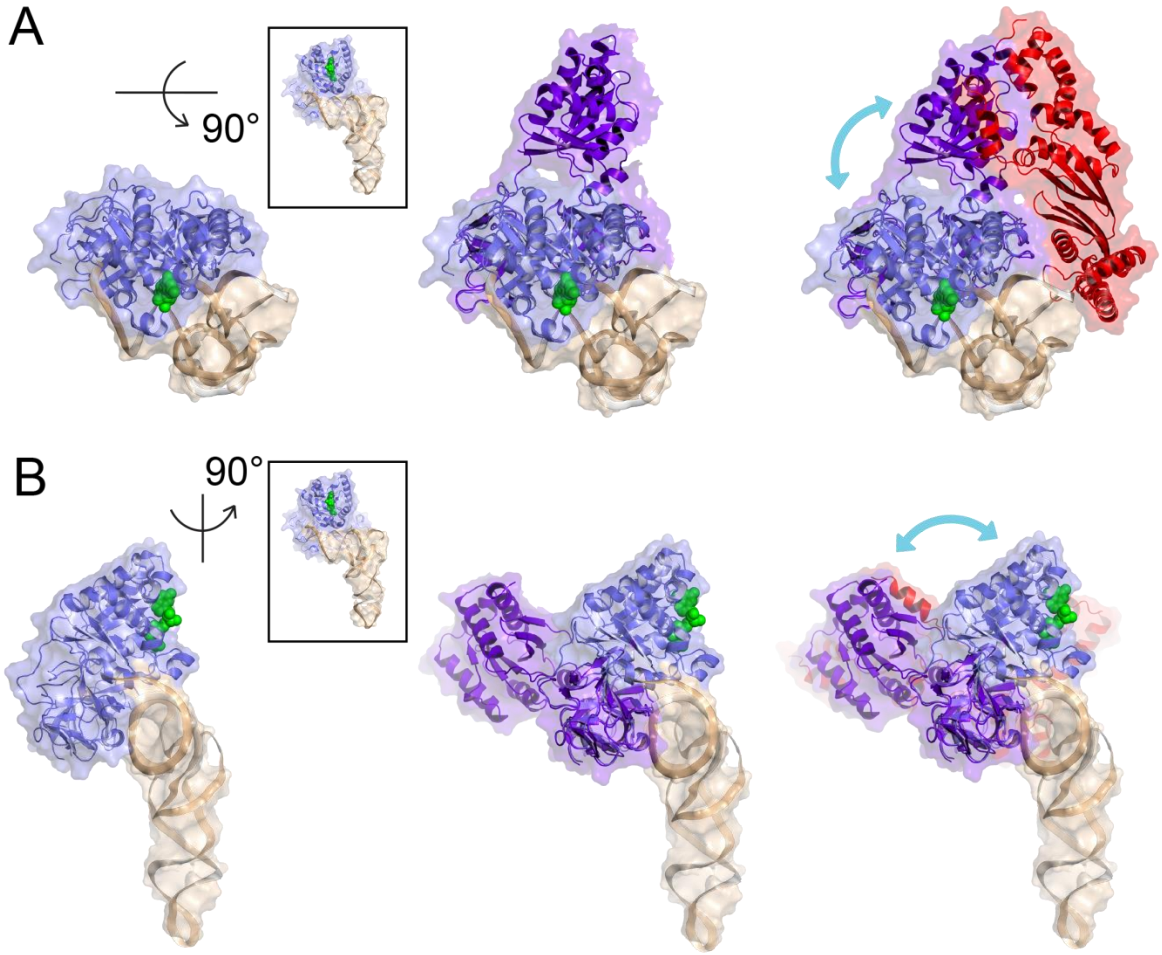

FIGURE 3.8 ***Hypothetical EF-Tu·GTP·EF-Ts·Phe-tRNA^{Phe} quaternary complex*****.** **A**, a top-down perspective of the EF-Tu·GTP·Phe-tRNA^{Phe} ternary complex (Protein Data Bank code 1OB2) showing EF-Tu (*blue*) bound to Phe-tRNA^{Phe} (*wheat*) and GDPNP (*green spheres*). Here, the center panel shows an extended conformation (*purple*) of EF-Tu as it is observed in *E. coli* EF-Tu/Ts crystal structure (Protein Data Bank code 1EFU) where domains 2 and 3 of both EF-Tu structures are superimposed (N, Cα, CO, O root mean square deviation is 0.886Å). The right panel highlights the position of EF-Ts (*red*) in a quaternary complex if its interactions with EF-Tu are identical to those observed in *E. coli* EF-Tu/Ts crystal structure. This model reveals only minor steric clashes between EF-Ts and the D-stem of the aa-tRNA. The *blue arrow* indicates the hypothesized motions of the G domain of EF-Tu during ternary complex formation and decay. **B**, identical structures as in A from the perspective of looking down the axis of the tRNA acceptor stem. Structures were analyzed and rendered in PyMOL.

GTP (900 μM) is in great excess over GDP (100 μM), EF-Ts ensures that ternary complex is abundant. However, during stress where the GTP/GDP ratio drops, EF-Ts may enable an energy-neutral means of lowering the cellular concentrations of ternary complex and thus the rate of translation. The inferred capacity of EF-Ts to directly act on the EF-Tu·GDP·aa-tRNA complex also has potentially important implications for the mechanism of translation. Indeed, an EF-Tu·GDP·aa-tRNA complex is formed on the ribosome during every step of the elongation cycle of protein synthesis. Therefore, during active growth, the concentration of EF-Tu·GDP·aa-tRNA approaches the concentration of ribosomes in the cell (~10 μM). Notably, the concentrations of EF-Ts and ribosomes have been shown to exhibit a 1:1 stoichiometry over a range of cellular conditions[37,58,100]. To our knowledge, the kinetic impact of EF-Ts on the rates and fidelities of aa-tRNA selection have yet to be explored. However, experiments performed in the absence of EF-Ts suggest that the departure of EF-Tu·GDP from the ribosome is rate-determining for the process (~2–4 s^{-1})[4,24].

The structure of the EF-Tu·GTP·EF-Ts complex is not presently known but has is speculated to adopt a conformation that is distinct from EF-Tu·GTP, EF-Tu·GDP, and the EF-Tu/Ts complex[31]. Structural modeling suggests that an EF-Tu·GTP·EF-Ts complex would be sterically permitted to bind the acceptor stem of aa-tRNA if it adopts a conformation that is globally similar to that of the EF-Tu·EF-Ts complex (Figure 3.8). Functional investigations of the Qβ replicase, an RNA-dependent RNA polymerase that contains an EF-Tu/Ts complex, are consistent with this model as the template recognition in this system has been attributed to the direct binding of the EF-Tu/Ts component of Qβ replicase to a primer region that contains a single-stranded 3′-CCA overhang[123]. We therefore speculate that initial interactions between the EF-Tu·GTP·EF-Ts and aa-tRNA may occur in a manner akin to what is observed for Qβ replicase and more recently for archaeal translation initiation factor-2[124] wherein

domains 1 and 2 of EF-Tu bind the 3′-CCA end of aa-tRNA. Alternatively, initial interactions could occur via the direct binding of domains 2 and 3 of EF-Tu in complex with EF-Ts to the acceptor stem helix (Figure 3.8). Irrespective of these considerations, we propose that the rate-determining conformational change in EF-Tu that gives rise to the high affinity ternary complex interaction is initiated with the compaction of the G domain onto domains 2 and 3 and the aa-tRNA acceptor stem. This conformational change would terminate with the formation of the interaction network linking the amino acid to the switch domains of EF-Tu and the γ-phosphate of GTP followed by the release of EF-Ts (Figures 3.1 and 3.8).

In direct support of a model in which EF-Ts can physically associate with EF-Tu while it is bound to aa-tRNA, we found that EF-Ts actively dissociates ternary complex in the presence of GDP (Figure 3.3, *C* and *D*). Ternary complex dissociation was inhibited by kirromycin (Figure 3.3*F*), suggesting that the dissociation pathway likely entails reorganization of the interface of domains 1, 2, and 3 in EF-Tu prior to EF-Tu release in a manner that mirrors the association pathway.

Importantly, precedence for direct interactions between GEFs and activated G-proteins exists in signal transduction cascades involving other small G-proteins that are regulatory in nature. In yeast, the GEF Scd1 chaperones its activated G-protein, Cdc42, to its effector Shk1 via interactions with Scd2[125]. GEFs for the monomeric G-protein Ral, RalGDS and Rlf, interact with the GTP-bound state of upstream G-proteins Ras and Rap through Ras association domains[13,126]. Effector-bound conformational changes of G-proteins have also been described previously. For instance, the monomeric G-protein Ras has been shown to bind to its effector protein Raf in a two-step process termed “dynamic triggering”[127]. NMR studies have revealed that switch-1 of Ras-GDPNP is dynamic, exhibiting at least two conformations in the Raf-bound state[127,128]. Thus, the findings presented here likely reflect a more general

capacity of GEFs to facilitate G-protein loading onto their effector substrates. In addition to accelerating signaling processes, such interactions may also serve to influence the choice of downstream effectors. Future experiments testing these hypotheses are warranted and will need to be explored using approaches that are amenable to probing the complexity and range of dynamics that are likely to be found.

CHAPTER 4

4.1 OVERVIEW

The data and figures presented in this chapter have been previously published in modified form:

Burnett BJ[a], Altman RB[b], Ferguson A[b], Wasserman MR[b], Zhou Z[b], Blanchard SC[c]. "Direct Evidence of Elongation Factor-Tu/Ts·GTP·Aminoacyl-tRNA Quaternary Complex" *Journal of Biological Chemistry*. 2014 **289**:23917-23927[129].

[a]Burnett BJ designed and conducted all experiments solely, or in conjunction with other authors.

[b]Authors conducted experiments in conjunction with Burnett BJ.

[c]Corresponding author, designed experiments in conjunction with Burnett BJ.

4.2 SUMMARY

During protein synthesis, elongation factor-Tu (EF-Tu) bound to GTP chaperones the entry of aminoacyl-tRNA (aa-tRNA) into actively translating ribosomes. In so doing, EF-Tu increases the rate and fidelity of the translation mechanism. Recent evidence suggests that EF-Ts, the guanosine nucleotide exchange factor for EF-Tu, directly accelerates both the formation and dissociation of the EF-Tu·GTP·Phe-tRNA^{Phe} ternary complex[83]. A central feature of this model is the existence of a quaternary complex of EF-Tu/Ts·GTP·aa-tRNA^{aa}. Here, through comparative investigations of phenylalanyl, methionyl, and arginyl ternary complexes, and the development of a strategy to monitor their formation and decay using fluorescence resonance energy transfer, we reveal the generality of this newly described EF-Ts function and the first direct evidence of the transient quaternary complex species. These findings suggest that EF-Ts may regulate ternary complex abundance in the cell through mechanisms that are distinct from its guanosine nucleotide exchange factor functions.

4.3 INTRODUCTION

Guanosine nucleotide-binding proteins (G-proteins) regulate a diverse range of essential cellular processes in all three kingdoms of life, including the universally conserved and energy- intensive process of protein synthesis. Elongation factor Tu (EF-Tu) in bacteria and elongation factor 1A (eEF1A) in eukaryotes are conserved members of the TRAFAC (translation factor) class of G-proteins comprising three globular domains (I–III). Both proteins play a critical role in translation by chaperoning messenger RNA (mRNA) codon-dependent incorporation of aminoacyl-

tRNA (aa-tRNA) into the aminoacyl (A) site of the two-subunit ribosome during the substrate selection step of the elongation cycle[9,14,15,84,86].

EF-Tu, through its capacity to form a ternary complex with aa-tRNA in the presence of guanosine triphosphate (GTP) (EFTu·GTP·aa-tRNA), increases both the rate and fidelity of aa-tRNA selection on the ribosome[53,78,92,130] (see Figure 4.1*A*). EF-Tu simultaneously promotes ribosome binding and couples the aa-tRNA selection mechanism to irreversible GTP hydrolysis[1]. Following the release of inorganic phosphate[3], aa-tRNA dissociates from EF-Tu·guanosine diphosphate (GDP) to enter the ribosome where it undergoes irreversible peptide bond formation[4,24].

The rates of protein synthesis and cellular growth critically depend on and are highly correlated with the availability of the complete complement of ternary complex species needed to translate the mRNA open reading frame[35,50,58,131,132]. In *Escherichia coli*, there are ~86 genes encoding for elongator tRNAs that exhibit a range of expression levels[132-134]. Depending on the species, organism, and cellular growth rate, the total tRNA concentration in the cell ranges from 100 μM to 1 mM[135]. Although a component of these fluctuations likely relates to the proximity of each gene to the origin of replication as postulated for ribosomal RNA[133,136], changes in tRNA gene expression also reflect regulatory cues[134].

Ternary complex levels also depend on the extent to which tRNAs are aminoacylated, which is a prerequisite for EF-Tu·GTP binding[78,137]. Direct measurements suggest that ~80% of expressed tRNAs are charged during logarithmic growth in nutrient-rich conditions[138,139]. Under nutrient poor conditions, however, where amino acid reserves become limiting, this level drops substantially[139,140]. Such

conditions may ultimately trigger the stringent response leading to the down-regulation of the translational machinery[139].

The abundance of distinct ternary complex species is also dictated by the affinity of EF-Tu for each aa-tRNA. EF-Tu exhibits tRNA-specific dissociation constants ranging from a few nanomolar to a few hundred nanomolar[92,141,142]. A substantial proportion of the overall binding energy between EF-Tu·GTP and aa-tRNA arises from contacts between the aminoacyl moiety of tRNA and the amino acid binding pocket formed at the interface of domains I and II of EF-Tu[57,88,95] (see Figure 4.1*B*). In the case of the phenylalanyl-tRNA^{Phe} ternary complex (Phe-TC), the aromatic ring of the 2′-linked phenylalanyl moiety has been shown to directly interact with the conserved histidine 66 (His-66) residue of EF-Tu. The switch regions of EF-Tu (S1 and S2), which are present in all G-proteins and facilitate nucleotide interactions, help position His-66, thereby enabling EF-Tu to read out the aminoacyl state of the tRNA molecule in a manner that depends on the phosphorylation state of the guanosine nucleotide[89,95] (see Figure 4.1*B*).

The distinct chemical and physical properties of each amino acid predict significant differences in EF-Tu binding affinity to distinct tRNA species[57,95]. These disparities are thought to be dampened by a thermodynamic compensation mechanism based on unique EF-Tu interactions with sequence determinants in the tRNA acceptor stem and T-loop (Figure 4.1*C*) that result in a relatively uniform EF-Tu·GTP affinity for each aa-tRNA species[141,143,144]. In this model, the tRNA species bearing an aminoacyl moiety that contributes strongly to the free energy of ternary complex affinity have tRNA bodies that bind weakly to EF-Tu. Conversely, tRNAs bearing

aminoacyl moieties that contribute relatively little to the free energy of ternary complex formation bind strongly to EF-Tu[57,144]. Taken together with structural and kinetic evidence that EF-Tu undergoes large scale conformational changes during aa-tRNA binding and release[89-91], this model posits a degree of coupling between these two distinct determinants of EF-Tu affinity. Under steady-state, logarithmic growth conditions where aa-tRNA, EF-Tu, and GTP are at high concentrations, the vast majority of aa-tRNAs are bound to EF-Tu·GTP in ternary complex[96]. At growth saturation or under nutrient-limited conditions, however, where the effective aa-tRNA concentrations are reduced, lower affinity species shift away from the EF-Tu·GTP-bound state, reducing their cellular concentrations.

Finally, the total ternary complex concentration in the cell is proportional to the concentration of GTP and the activated EF-Tu·GTP pool. The concentration of this latter complex in turn depends on the function of elongation factor Ts (EF-Ts), the guanosine nucleotide exchange factor for EF-Tu. The guanosine nucleotide exchange factor functions of EF-Ts facilitate the conversion of EF-Tu·GDP to EF-Tu·GTP following each round of tRNA selection. Given that the amount of EF-Tu·GDP is proportional to the concentration of ribosomes in the cell (10–100 μM) and the rate of protein synthesis (approximately 2–20 amino acids polymerized per second), high concentrations of EF-Ts promote a rapid rate of cell growth[36]. In *E. coli*, the concentration of EF-Ts is tightly coupled with ribosome biogenesis and thus the ribosome concentration[36,58,100,145-148]. Hence, a stoichiometry of EF-Tu/Ts·GDP in the cell that approaches 1:1 with ribosomes would facilitate prompt nucleotide exchange on EF-Tu and the maintenance of the highest concentration of EF-Tu·GTP possible.

Our recent efforts, which established a kinetic framework for examining ternary complex stability using fluorescence-based methods[83], provided evidence that EF-Ts directly regulates conformational changes in EF-Tu that facilitate the formation and disassembly of the Phe-TC. These observations suggested that EF-Ts has a capacity to directly regulate ternary complex concentration via the formation of an EF-Tu/Ts·GTP·aa-tRNA quaternary complex[83]. Here, we directly examined whether such findings are general in nature by measuring the impact of EF-Ts on the kinetic properties of distinct ternary complex species that exhibit distinct apparent *KD* values[141]. These investigations, combined with fluorescence resonance energy transfer (FRET) methods that facilitated the direct monitoring of EF-Tu/Ts interactions, yielded a general kinetic framework that explains how EF-Ts may influence the thermodynamic compensation model underpinning ternary complex stability, why quaternary complex has escaped detection previously, and how cellular interactions between EF-Ts and ternary complex can influence the regulation of protein synthesis in the cell.

4.4 RESULTS

4.4.1 EF-Tu Binds Distinct aa-tRNAs with High Affinity

To monitor ternary complex formation, we used a steady-state, fluorescence-based approach that yields an increase in relative intensity of Cy3 fluorescence when EF-Tu binds to site-specifically labeled aa-tRNA[83]. We measured the apparent affinity of highly purified, nucleotide-free EF-Tu or an EF-Tu/Ts complex for three distinct elongator tRNA species, each containing the same acp3U post-transcriptional modification at position 47 used for Cy3 labeling: Phe-tRNA^{Phe}, Met-tRNA^{Met}, and Arg-tRNA^{Arg}. For these experiments, EF-Tu and EF-Tu/Ts were preincubated with an excess of GTP (10 µM) to ensure complex formation (see Chapter 2). In each case, EF-Tu·GTP or EF-Tu/Ts·GTP was titrated into a 1.5-ml reaction containing 5 nM aa-tRNA (Cy3-acp^{3}U) and 10 µM GTP (Chapter 2). As anticipated from previous studies on Phe-tRNA^{Phe} (Cy3-acp^{3}U47) (1), each aa-tRNA species exhibited a marked

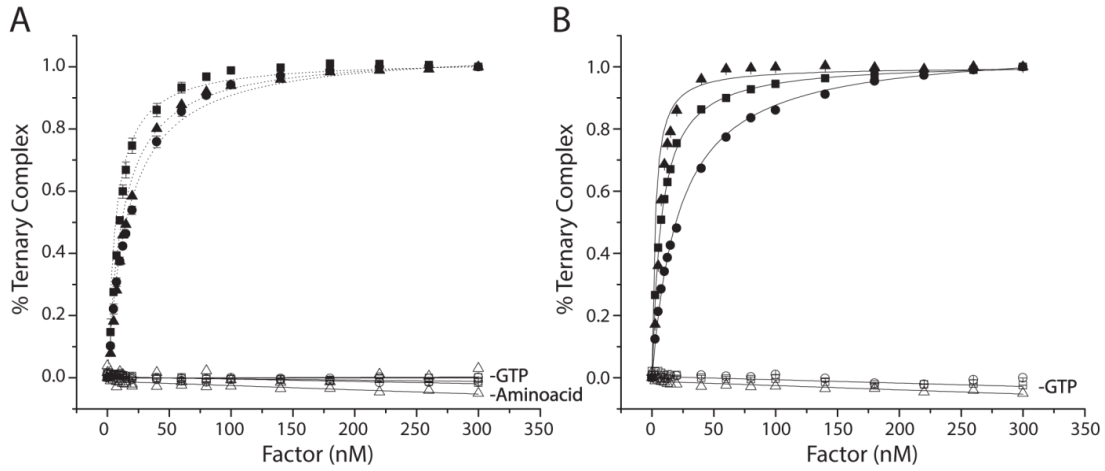

FIGURE 4.1. ***EF-Tu binds ternary complex with nanomolar affinity.*** Titration of EF-Tu·GTP (**A**) or EF-Tu/Ts·GTP (**B**) into a solution of Cy3-labeled Phe-tRNA^{Phe} (*solid triangles*), Met-tRNA^{Met} (*solid squares*), or Arg-tRNA^{Arg} (*solid circles*) in the presence of 10 µM GTP. The apparent dissociation constant (K_D) for each tRNA species was estimated by fitting (see Methods). Identical experiments performed in the absence of GTP or the tRNA synthetase (*open symbols*). Error bars represent the S. D. of three separate experiments.

increase in Cy3 relative fluorescence as a function of increasing factor concentration (Figure 4.2). Under the current experimental conditions (Chapter 2), Cy3 fluorescence increased 32, 45, and 30% for Phe-tRNA^{Phe}, Met-tRNA^{Met}, and Arg-tRNA^{Arg}, respectively. As expected, no change in fluorescence intensity was observed when identical experiments were performed either in the absence of GTP or when the tRNA was not aminoacylated. To provide an estimate of the affinity of each factor for aa-tRNA from these experiments, each titration was fit to an equation for a bimolecular interaction[83]. As expected from prior investigations[78,141], all three aa-tRNA species exhibited an apparent K_D in the nanomolar range both in the presence and absence of EF-Ts (Figure 4.2 and Table 4.1). The lowest apparent K_D was for Phe-tRNA^{Phe} (6 nM), whereas Arg-tRNA^{Arg} was the highest (22 nM) (Table 4.1). Compared with

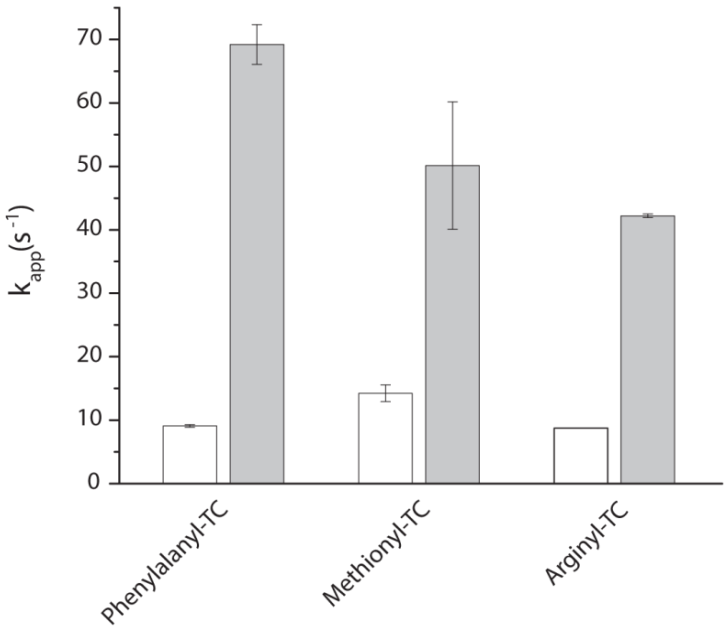

FIGURE 4.2 ***EF-Ts directly facilitates ternary complex formation*****.** The estimated rate of ternary complex formation ($k_{app,1}$) measured by a change in fluorescence intensity upon stopped-flow delivery of 5 µM EF-Tu·GTP (*open bars*) or 5 µM EF-Tu/Ts (*solid bars*) to 100 nM Cy3-labeled Phe-tRNA^{Phe}, Arg-tRNA^{Arg}, or Met-tRNA^{Met}. Error bars represent the S.D. of three separate experiments.

the relatively large impact on Phe-TC affinity (a 3-fold increase) in the presence of EF-Ts[83], the apparent K_D values of Met-tRNA^{Met} and Arg-tRNA^{Arg} were only modestly affected (approximately ~20–30%; Table 4.1).

4.4.2 EF-Ts Accelerates the Rate of Ternary Complex Formation

To delineate the kinetic features governing ternary complex formation, pre-steady-state, rapid mixing experiments were performed using the same Cy3-labeled Phe-tRNA^{Phe}, Met-tRNA^{Met}, and Arg-tRNA^{Arg} reagents under conditions estimating the physiological concentrations of each component (5 µM factor, 1 mM GTP, and 100 nM aa-tRNA). Purified EF-Tu and EF-Tu/Ts complex were pre-incubated with saturating concentrations of GTP (1 mM) to ensure complete nucleotide binding. For all three aa-tRNAs, the apparent rate of ternary complex formation using EF-Tu was between ~8 and ~14 s^{-1} (Fig. 4.3, *open bars*). Identical experiments conducted using

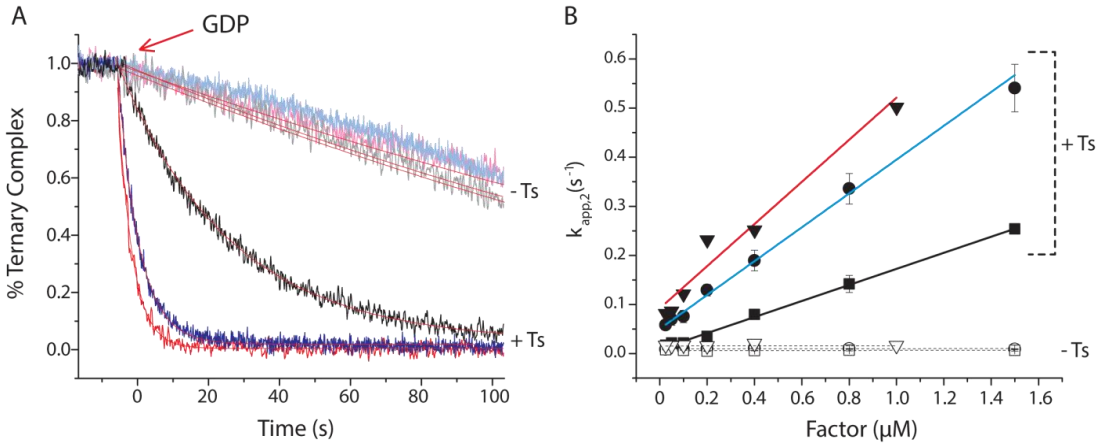

FIGURE 4.3 ***EF-Ts accelerates ternary complex decay in response to GDP*****. A**, addition of a 10-fold molar excess of GDP to Arg-TC (*blue*) or Met-TC (*black*) preformed with EF-Tu (*light colored curves*) or EF-Tu/Ts (*dark colored curves*) in the presence of 10 µM GTP. **B**, the apparent rate of ternary complex dissociation ($k_{app,2}$) was estimated by fitting each decay process to a single exponential function. The relationship between $k_{app,2}$ and the concentration of EF-Tu (*open symbols*) or EF-Tu/Ts (*solid symbols*) is shown for both Met-TC (*squares*) and Arg-TC (circles). Error bars represent the S.D. of three separate experiments. For comparison, $k_{app,2}$ (*acquired previously*) is shown for Phe-TC (*red triangles*)).

the EF-Tu/Ts complex resulted in an increase in the apparent rate of ternary complex formation for each tRNA species to ~40 to ~70 s^{-1} (Figure 4.3, *solid bars*). As suggested for Phe-TC formation, these data argue that EF-Ts also facilitates rate-determining conformational events in EF-Tu that are required for nucleotide-dependent binding to both Met-tRNA^{Met} and Arg-tRNA^{Arg}.

4.4.3 EF-Ts Facilitates Ternary Complex Dissociation in the Presence of GDP

To examine whether EF-Ts influences the dissociation pathways of these two distinct ternary complex species as has been demonstrated for the Phe-TC, we performed GDP chase experiments on Met-TC and Arg-TC preformed with either EF-Tu or EF-Tu/Ts. As noted previously, a hallmark kinetic signature of the EF-Tu/Ts·GTP·aa-tRNA quaternary complex is the factor concentration dependence of the ternary complex dissociation rate in the presence of GDP. In such experiments, ternary complex is formed by adding 0.4 µM factor (preincubated with 10 µM GTP) to 5 nM Cy3-labeled Phe-tRNAPhe, Met-tRNAMet, or Arg-tRNA^{Arg}. A 10-fold excess of GDP (100 µM) is then added, and the rate of fluorescence decay is then tracked over time.

In the absence of EF-Ts, all three ternary complexes were observed to decay at a slow rate of ~0.01 s^{-1}, consistent with ternary complex being a stable, high affinity species (Figure 4.4*A*). As shown previously for Phe-TC, the measured decay rate was independent of EF-Tu concentration as expected for a spontaneous dissociation process followed by GDP binding, an event that prevents ternary complex from re-

TABLE 4.1 ***Kinetic parameters measured in the presence and absence of EF-Ts.***

	Kinetic parameters					
	K_D (Fig. 4.1)		$k_{app,1}$ (Fig. 4.2)		$k_{app,2}$ (Fig. 4.3)	
	-EF-Ts	+EF-Ts	-EF-Ts	+EF-Ts	-EF-Ts	+EF-Ts
	nm		s^{-1}		s^{-1}	
Phe-TC	18.2 ± 1.2	6.1 ± 0.8	9.01 ± 0.2	69.2 ± 3.1	0.015 ± 1x10^{-3}[a]	0.25 ± 0.04[a]
Met-TC	10.8 ± 1.5	7.5 ± 1.2	14.2 ± 1.3	50.1 ± 10.0	0.01 ± 1.7x10^{-3}	0.08 ± 0.01
Arg-TC	19.6 ± 0.8	22 ± 0.3	8.73 ± 0.04	42.19 ± 0.3	0.01 ± 1.6x10^{-4}	0.19 ± 0.02

forming (Figure 4.4*B*). When the same experiment was performed with EF-Tu/Ts, however, the rate of fluorescence intensity decay was ~25-, ~13-, and ~20-fold faster for Phe-TC, Met-TC, and Arg-TC, respectively (Figure 4.4*A*). The observed rate of decay was also linearly dependent on the concentration of EF-Tu/Ts (Figure 4.4*B*). This trend is inconsistent with a simple unimolecular dissociation pathway, suggesting that EF-Ts facilitates ternary complex dissociation through a bimolecular interaction that influences the nucleotide binding pocket of EF-Tu. Here, the apparent EF-Ts on-rate estimated from the slope of the concentration dependent process ranged from ~0.3 to 1.0 $\mu M^{-1}s^{-1}$ depending on the tRNA species and taking into account that the

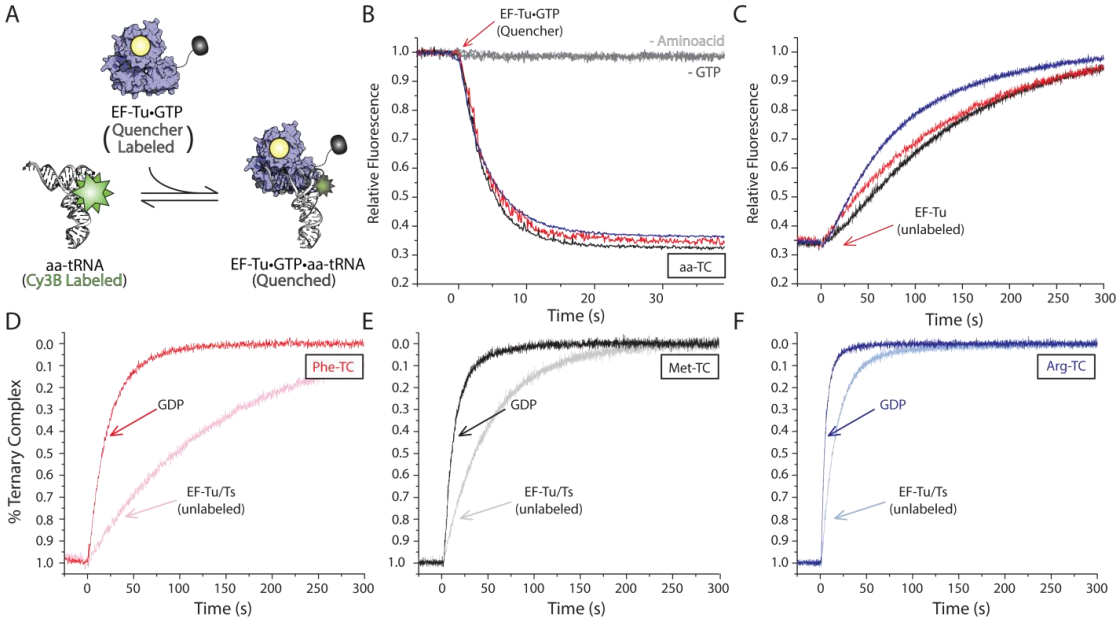

FIGURE 4.4 ***Measuring ternary complex formation and dissociation via FRET*****. A**, schematic illustration of TC quenching assay showing Cy5Q-labeled EF-Tu (*blue*) bound to GTP (*yellow*) quenches the fluorescence of Cy3B-labeled aa-tRNA (*white*) upon ternary complex formation. **B**, addition of 0.4 µM EF-Tu·GTP (Cy5Q) to 5 nM Cy3B-labeled Phe-$tRNA^{Phe}$ (*red*), Met-$tRNA^{Met}$ (*black*), or Arg-$tRNA^{Arg}$ (*blue*) in the presence of 10 µM GTP. Omission of the tRNA synthetase (*-Amino acid*) or GTP (*-GTP*) from the ternary complex formation assay resulted in no change in Cy3B fluorescence intensity. **C**, addition of excess unlabeled EF-Tu to the ternary complexes formed in B. Addition of excess GDP (*bold colors*) or unlabeled EF-Tu/Ts (*light colors*) to Phe-TC (**D**), Met-TC (**E**), and Arg-TC (**F**) preformed with EF-Tu/Ts (Cy5Q). Apparent rates of ternary complex decay were estimated by fitting to a single exponential function (see Chapter 2, Methods).

concentration of free EF-Ts is roughly 50% of the total factor concentration. As this rate is more than 2 orders of magnitude slower than a diffusion-limited process as well as the established rate of nucleotide binding to EF-Tu[31], we conclude that one or more rate-determining events in EF-Tu, likely related to GTP release, precede the EF-Ts-facilitated ternary complex dissociation process leading to the loss of fluorescence.

4.4.4 EF-Ts Increases the Rate of Ternary Complex Turnover under Steady State Conditions

To probe whether EF-Ts influences rate-determining step that precede the dissociation process observed in the presence of GDP, we next sought to ascertain whether the rate of ternary complex turnover was influenced by EF-Ts under steady-state conditions. To do so, we developed a FRET-based approach to directly examine the rate of ternary complex turnover by site-specifically labeling EF-Tu with a quencher fluorophore at its C terminus (see Chapter 2). The C terminus of EF-Tu and the acp^{3}U47 residue in tRNA are in close proximity (approximately 30 Å) (Figure 4.1). To dampen the environment-dependent increase in Cy3 fluorescence that accompanies ternary complex formation (Figure 4.2), Phe-tRNA^{Phe}, Met-tRNA^{Met}, and Arg-tRNA^{Arg} were labeled at their acp^{3}U47 residues using Cy3B, a fluorophore less prone to cis-trans isomerization and environment-dependent changes in quantum yield[149-151]. Hence, the formation of ternary complex is anticipated to result in a substantial decrease in Cy3B fluorescence intensity as a result of energy transfer to the nearby quencher (Figure 4.5*A*).

TABLE 4.3 ***Apparent rates of EF-Tu and EF-Ts interactions.***

k (Fig. 4.5)			
Rxn 1	**Rxn 2**	**Rxn 3a**	**Rxn 4**
		s^{-1}	
18.5 ± 0.5	148 ± 5	177 ± 0.08 (decay) 5.8 ± 0.04 (rise)	242 ± 7

Using this approach, ternary complex formation resulted in an ~65% decrease in Cy3B fluorescence intensity for all three aa-tRNAs examined (Figure 4.5*B*). As expected, this change in signal was strictly dependent on GTP and the aminoacyl moiety of aa-tRNA (Figure 4.5*B*). Consistent with the findings presented for unlabeled EF-Tu (Figure 4.4), this reduction in Cy3B fluorescence intensity could be fully recovered by the addition of a 10-fold molar excess of GDP. These data convincingly revealed that quencher-labeled EF-Tu is fully competent to form ternary complex.

To directly examine ternary complex turnover under steady state conditions, a competition experiment was performed in which a 10-fold molar excess of unlabeled EF-Tu or EF-Tu/Ts was added to a preformed, quencher-labeled EF-Tu·GTP·PhetRNA^{Phe} (Cy3B-acp^{3}U47) ternary complex. As the vast majority of ternary complex re-formed after dissociation will not be quenched, the intrinsic rate of ternary complex turnover in this assay is revealed by the rate of increase in Cy3B fluorescence intensity.

In both the absence and presence of EF-Ts, Cy3B fluorescence recovered at a rate that was tRNA-specific (Figure 4.5, *C–F*). For the unlabeled EF-Tu chase experiment, the rates of steady state ternary complex turnover approximated those observed upon quenching with GDP in the absence of EF-Ts (Figure 4.5*C* and compare Table 4.2 k_{off} with Table 4.1 $k_{app,2}$). However, distinct responses were evidenced in each EF-Tu/Ts chase experiment (Figure 4.5, *D–F*). Here, the steady-state turnover rates were

approximately an order of magnitude slower than those observed in the presence of GDP (compare Table 4.1 $k_{app,2}$ with Table 4.2 k_{off}).

These findings suggest that EF-Ts has the propensity to destabilize each ternary complex and to specifically promote ternary complex dissociation in the presence of GDP. Such trends are consistent with the notion that nucleotide exchange occurs at a slow rate within ternary complex and that EF-Ts increases the rate of such processes via direct interactions with EF-Tu while it remains bound to aa-tRNA. We speculate that, when only GTP is present in the reaction, nucleotide can reload onto EF-Tu prior to its dissociation from aa-tRNA. When GDP is present in excess of GTP, however, GDP binding to EF-Tu leads to ternary complex dissociation. We therefore infer that

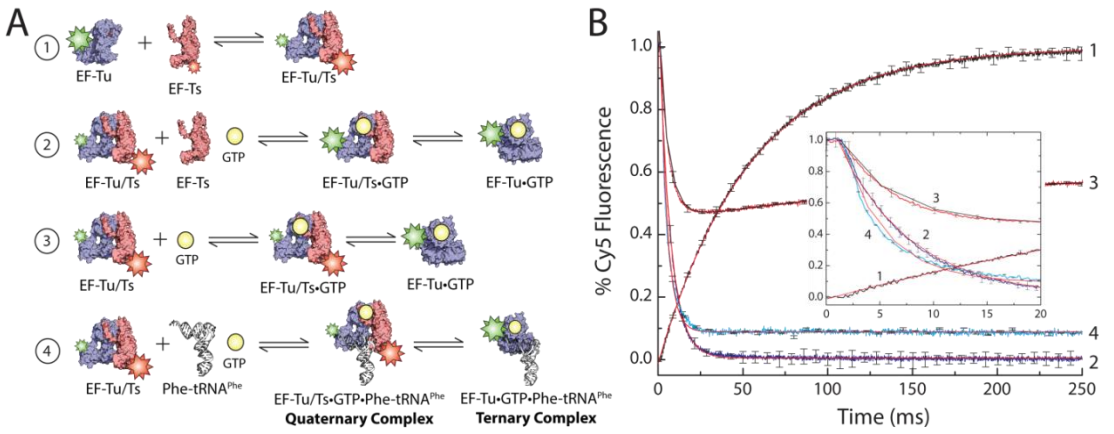

FIGURE 4.5 ***Significant amounts of EF-Tu/Ts remain bound to GTP under physiological nucleotide concentrations.*** **A**, schematic illustrating the EF-Tu/Ts FRET assay. 1, Cy3-labeled EF-Tu (*blue*) is added to Cy5-labeled EF-Ts (*red*). 2, EF-Tu(Cy3)/Ts(Cy5) mixed with unlabeled EF-Ts and GTP (*yellow*). 3, EF-Tu(Cy3)/Ts(Cy5) added to GTP. 4, EF-Tu(Cy3)/Ts(Cy5) mixed with unlabeled Phe-tRNA^{Phe} (*white*) and GTP. **B**, 2 µM EF-Tu(Cy3) mixed with 2 µM EF-Ts(Cy5) while monitoring Cy5 fluorescence (*curve 1*), 2 µM EF-Tu(Cy3)/Ts(Cy5) added to 20 µM unlabeled EF-Ts and 1 mM GTP (*curve 2*), 2 µM EF-Tu(Cy3)/Ts(Cy5) mixed with 1 mM GTP (*curve 3*), and 2 µM EF-Tu(Cy3)/Ts(Cy5) mixed with 0.5 µM Phe-tRNA^{Phe} and 1 mM GTP (*curve 4*). A plot focusing on the early time points in the reactions is shown for clarity (*inset*). Apparent rates were estimated by fitting to either a single exponential function (*curves 1, 2, and 4*) or a double exponential function (*curve 3*). Error bars represent the S.D. of three separate experiments.

EF-Ts can act as a guanosine nucleotide exchange factor for EF-Tu while it is bound to aa-tRNA via a quaternary complex where the formation of an EF-Tu·GDP·aa-tRNA ternary complex stimulates EF-Tu release from aa-tRNA, which is accelerated by EF-Ts.

4.4.5 EF-Tu/Ts·GTP Is an Abundant Species under Cellular Conditions

The notion that EF-Ts can interact with EF-Tu while it is bound to aa-tRNA provides a plausible model for the observation that EF-Ts accelerates the process of ternary complex formation (Figure 4.3). As speculated previously, EF-Ts may increase the rate of ternary complex formation via a transient EF-Tu/Ts·GTP·aa-tRNA quaternary complex. A key issue with this model is that the EF-Tu/Ts·GTP species is expected to dissociate at a rate of ~60 s^{-1} at physiological GTP concentrations (approximately 1 mM)[31]. Meaningful concentrations of the EF-Tu/Ts·GTP complex, however, are expected at EF-Ts concentrations above 1 µM as the bimolecular rate constant between EF-Ts and EF-Tu·GTP is $3 \cdot 10^7$ $M^{-1}s^{-1}$ [31]. Indeed, such considerations predict that ~50% of EF-Tu will be in an EF-Tu/Ts·GTP complex under the conditions where EF-Ts is observed to accelerate ternary complex formation (Figure 4.3). At cellular EF-Ts concentrations, which under nutrient-rich conditions are estimated to be ~10 µM [36,145], the proportion of EF-Tu/Ts·GTP complex is expected to be even higher as the apparent rate of EF-Tu/Ts·GTP reformation will be as much as ~5-fold faster than the rate of EF-Ts dissociation from EF-Tu·GTP.

To directly test these predictions, we set out to measure the interactions between EF-Tu and EF-Ts through a FRET-based approach (Figure 4.6*A*). To do so, we used enzymatic tagging procedures to site-specifically label EF-Tu with a Cy3 fluorophore

TABLE 4.4 ***Apparent rates of quaternary complex formation and decay.***

k (Fig. 4.6)	
Rise	Decay
s^{-1}	
870 ± 23	143 ± 7

at its C terminus and EF-Ts with a Cy5 fluorophore through maleimide chemistry at a position engineered to yield high FRET (A160C)[91] (Chapter 2). When 2 μM Cy3-labeled EF-Tu was rapidly mixed with 2 μM Cy5-labeled EF-Ts under stopped flow (Chapter 2), a rapid increase in Cy5 emission was observed (k_{app} = 18.5 s^{-1}), which as expected from the kinetics and high affinity nature of the EF-Tu/Ts interaction[31] remained stable over time (Figure 4.6, *A* and *B*, *black* curve, and Table 4.3).

To determine the dissociation rate of the EF-Tu/Ts complex in the presence of saturating concentrations of GTP, a preformed EF-Tu(Cy3)/Ts(Cy5) complex was rapidly mixed with 1 mM GTP in the presence of a 10-fold molar excess of unlabeled EF-Ts to prevent the complex from re-forming (Figure 4.6, *A* and *B*, *blue* curve). As expected[31], a rapid loss of fluorescence was observed (~148 s^{-1}) (Table 4.3). This value is ~2-fold faster that the EF-Tu/Ts·GTP dissociation rate estimated using native components[31], suggesting that the modifications to EF-Tu and EF-Ts may modestly destabilize the EF-Tu/Ts complex.

We next investigated the extent to which GTP disrupts the EF-Tu/Ts complex under steady state conditions in the absence of unlabeled EF-Ts where a dynamic equilibrium between dissociation and association is expected. In line with known kinetic parameters of this system[31], mixing the preformed EF-Tu(Cy3)/Ts(Cy5) complex (2 μM) with GTP (1 mM) led to a rapid loss of FRET, which stabilized at approximately ~55% of the starting intensity (Figure 4.6, *A* and *B*, *red* curve, and Table 4.3). These data argue that the EF-Tu/Ts·GTP complex is an abundant species both in our experiments and the cellular milieu.

To test the hypothesis that EF-Ts accelerates the binding of aa-tRNA to EF-Tu·GTP, a preformed EF-Tu(Cy3)/Ts(Cy5) complex was rapidly mixed with

1 mM GTP and 500 nM Phe-tRNA^{Phe} (Figure 4.6, *A* and *B*, *cyan* curve). Here, Cy5 fluorescence was observed to decay at a rate of ~242 s^{-1} (Table 4.3), a rate significantly faster than when only GTP or unlabeled EF-Ts was added (Figure 4.6*B*, *inset*). This finding suggests that aa-tRNA contributes to the apparent rate of EF-Tu(Cy3)/Ts(Cy5) dissociation as would be expected if ternary complex is formed rapidly (approximately ~140 s^{-1}).

4.4.6 Quaternary Complex Is Transient by Nature

To directly observe the EF-Tu/Ts·GTP·aa-tRNA quaternary complex, we designed an experiment to detect FRET between EF-Ts and aa-tRNA during ternary complex formation where the hypothesized architecture of quaternary complex predicts a physical proximity between the Cy3B fluorophore at position U47 of aa-tRNA and Cy5 at position 160 of EF-Ts (Figure 4.7*A*). The conditions of this experiment were derived by simulating the expected rate of quaternary complex formation and decay that should accompany ternary complex formation based on a framework that included the known kinetic features of the interactions among EF-Tu, EF-Ts, guanosine nucleotide, and Phe-tRNA^{Phe31,83} (Figure 4.7*B*, *red* curve). Using this approach, the optimal conditions for detecting quaternary complex were determined to be a concentration of 2 µM EF-Tu/Ts, 250 nM Phe-tRNA^{Phe}, and 1 mM GTP.

As anticipated by these simulations, when 2 µM EF-Tu/Ts(Cy5) was rapidly mixed with 250 nM Phe-tRNA^{Phe} (Cy3B-acp^{3}U47) and 1 mM GTP, FRET was observed between the excited Cy3B fluorophore and the Cy5-labeled EF-Ts (Figure 4.7*C*, *black*). No evidence of FRET was observed when the exact same experiment was performed using deacylated tRNA^{Phe} (Figure 4.7*C*, *gray*).

The biphasic nature of the transient FRET signal observed was fit to a double exponential process to estimate the apparent rates of quaternary complex formation

and decay, respectively. Here, the rise and decay portions were estimated to occur at rates of ~870 ± 23 and 143 ± 7 s^{-1}, respectively (Table 4.4). These apparent rates suggest that the appearance of FRET is diffusion-limited and that the rate of quaternary complex decay and thus ternary complex formation may be as fast as 140 s^{-1}. Notably, this rate is strikingly consistent with our stopped-flow measurements based on changes in Cy3 relative fluorescence intensity where ternary complex formation occurs at a rate of ~70 s^{-1} (Figure 4.3) under conditions in which ~50% of

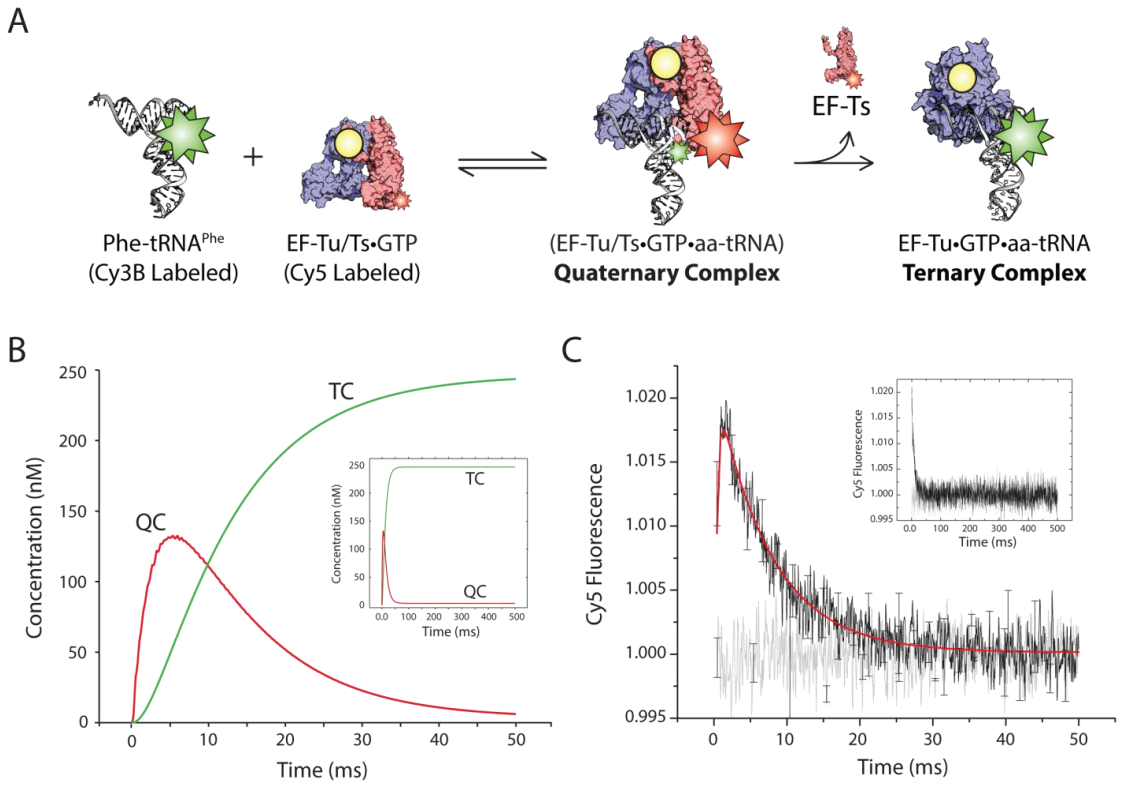

FIGURE 4.6 ***Direct evidence of the transient intermediate, quaternary complex*****. A**, schematic illustrating the FRET assay used to detect quaternary complex. Cy3B-labeled Phe-tRNA^{Phe} (*white*) is mixed with EF-Tu/Ts·GTP (*blue/red*) harboring a Cy5 fluorophore linked to EF-Ts. **B**, simulation of the time-dependent formation of quaternary complex (*red curve*, *QC*) and ternary complex (*green curve*, *TC*) based on the schematic presented in A. **C**, transient FRET observed upon mixing 2 µM EF-Tu/Ts(Cy5) and 250 nM Phe-tRNA^{Phe} (Cy3B) in the presence of 1 mM GTP (*black*). These data were fit to a double exponential function (*red*). This experiment was repeated with deacylated tRNA^{Phe} (Cy3B) (*grey*). Error bars represent the S.D. of three separate experiments.

EF-Tu is expected to be in an EF-Tu/Ts·GTP complex (Figure 4.6). Such findings provide compelling, direct evidence that ternary complex formation occurs via a highly transient quaternary complex species under cellular conditions.

4.5 DISCUSSION

Contemporary models posit that the EF-Tu life cycle parallels the quintessential model of G-protein function[7,109,119]. After aa-tRNA is delivered to the actively translating ribosome, EF-Tu·GDP is released as an inactive species whereupon the guanosine nucleotide exchange factor, EF-Ts, operates on it to exchange GDP for GTP. Thereafter, EF-Tu·GTP is released as an activated species that is again competent to bind free aa-tRNA with uniformly high affinity[4,17,24,31,109,119,144,152].

The data presented here and elsewhere[83,93] argue that refinements to this model are needed. At cellular EF-Ts concentrations (approximately >1 μM), our findings suggest that ternary complex preferentially forms via a transient EF-Tu/Ts·GTP·aa-tRNA quaternary complex (Figure 4.8). This pathway is kinetically preferred because EF-Ts

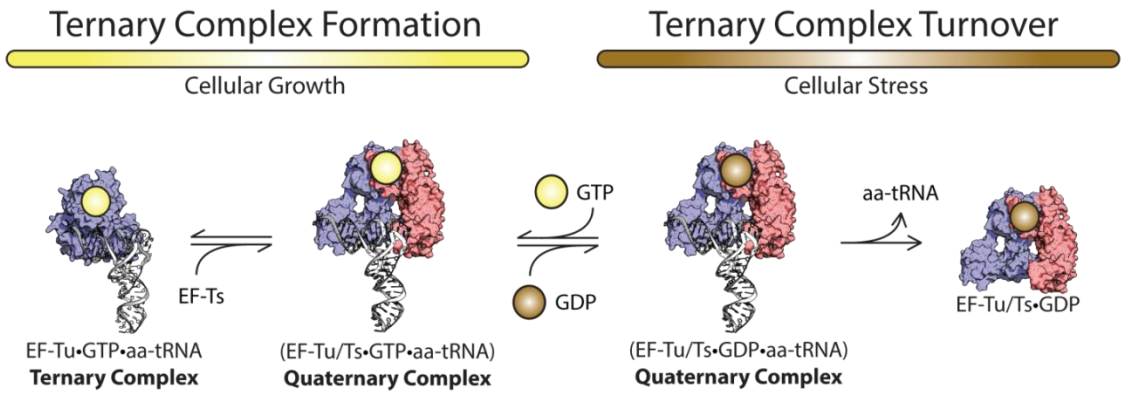

FIGURE 4.7 ***EF-Ts regulates ternary complex abundance*****.** During growth-promoting conditions, EF-Ts (*red*) facilitates the formation of GTP (*yellow*)-bound EF-Tu (*blue*) to aa-tRNA (*white*) by accelerating rate-determining conformational processes in EF-Tu. The guanosine nucleotide exchange function of EF-Ts also serves to preferentially load GDP during conditions of cellular stress.

lowers the activation barrier for rate-determining conformational processes in EF-Tu that accompany the formation of a high affinity complex with aa-tRNA. Given what is presently known, the nature of these conformational processes likely surrounds the allosteric linkage between the aminoacyl moiety linked to the terminus of aa-tRNA and the switch regions surrounding the GTP nucleotide that coordinate magnesium and the γ-phosphate group (Figure 4.1).

Our direct measurements suggest that the lifetime quaternary complex is on the order of ~10 ms (Figure 4.7). As the predominant means for investigating ternary complex formation have entailed size exclusion chromatography, filter binding, and gel mobility shift assays[25,92,153] where rapid kinetic studies have been specifically lacking, its inherent instability is likely the key reason why quaternary complex has escaped detection previously. Although the existence of a quaternary encounter complex species is an expected result based on purely physical considerations, the capacity of EF-Ts to increase the rate of ternary complex formation substantially above that of protein synthesis (approximately 100 *versus* 10–20 s^{-1}; Figure 4.3 and 4.7) argues that it serves a critical biological role related to replenishing the supply of ternary complexes as they are consumed by the process of protein synthesis.

The data presented also suggest that EF-Ts destabilizes ternary complex species to make their abundance sensitive to the nucleotide status of the cell (Figure 4.5). Such tendencies are consistent with EF-Ts remodeling the switch regions in EF-Tu while it is bound to aa-tRNA (as it does when EF-Tu is not bound to aa-tRNA)[60] to influence the rate of nucleotide exchange. Two notable corollaries to this observation are that 1) the nucleotide exchange rate may not be the same for all tRNA species, and 2) the activated EF-Tu molecule in ternary complex may be deactivated by energy-neutral processes. Evidence supporting the first corollary is shown for the three tRNA species investigated in this study (Phe-$tRNA^{Phe}$, Met-$tRNA^{Met}$, and Arg-$tRNA^{Arg}$) where the

effects of EF-Ts on ternary complex differ by as much as an order of magnitude (Figure 4.3, 4.4, and 4.5).

As the effective concentration of quaternary complex will be strongly dependent on EF-Ts concentration, such effects are also expected to be highly responsive to the active EF-Ts pool. Although the second corollary is likely irrelevant under nutrient-rich conditions where the intracellular concentration of GTP is much higher than GDP, it may play a significant role in regulating ternary complex abundance upon a change in the GTP/GDP ratio. EF-Ts rapidly dissociates ternary complex when GDP loads onto EF-Tu while it is bound to TC (Figure 4.4, 4.5, and 4.8). Correspondingly, changes in EF-Ts concentration as well as the GDP/GTP ratio are likely to contribute differentially to the relative stabilities and effective concentrations of specific ternary complex species in interdependent ways. Although it is not presently clear whether EF-Ts contributes evenly or differentially to the stabilities of distinct ternary complex species, the data obtained for the three ternary complex species assessed here suggest that ternary complex affinities become somewhat more dispersed in the presence of EF-Ts (Table 4.1). Such differences likely arise from a balance of the distinct contributions to ternary complex affinity, including contacts between aa-tRNA and EF-Tu as well as the nucleotide exchange rate. A key prediction of these considerations is that the abundance and lifetime of each ternary complex type will be sensitive to the metabolic state of the cell where EF-Ts can serve to rapidly dissipate the ternary complex pool through an energy-neutral mechanism in the event of cellular stress. Such a capacity would provide a means for the cell to immediately cease the energy-expensive process of translation without waiting for ternary complex to be consumed and allow for the repurposing of GTP.

The demonstration that EF-Ts actively resolves quaternary complex species that contain GDP (Figure 4.5) also has potentially important implications for the

mechanism of tRNA selection as an EF-Tu·GDP·aa-tRNA ternary complex is formed each time an actively translating ribosome decodes mRNA[17]. A key open question that must be resolved through future investigations is whether EF-Ts is able to gain access to the EF-Tu·GDP·aa-tRNA ternary complex while engaged at the A site of the ribosome. If so, EF-Ts may accelerate the rate of EF-Tu·GDP release from the ribosome following aa-tRNA entry into the peptidyl transferase center, a step reported to be rate-limiting to the process[4,24]. To our knowledge such questions have yet to be explored.

CHAPTER 5

THE REACTION COORDINATE OF EF-Tu

5. OVERVIEW

Chapter 5 presents data aimed at measuring the lifetime of EF-Tu on the ribosome during tRNA selection. A summary is given in section 5.1, followed by an introduction in section 5.2 that contains relevant background and motivating themes for pursing the proposed hypothesis. Section 5.3 describes the results, the impact of which is then discussed in section 5.4.

5.1 SUMMARY

tRNA selection has been studied extensively from the perspective of the ribosome and the aa-tRNA. However, direct measurements of EF-Tu are conflicting with these studies in that its dissociation from the ribosome is predicted to be an order of magnitude slower than the rate of tRNA accommodation. Using both bulk and single molecule fluorescence assays, we are investigating the EF-Tu residence time on the ribosome during tRNA selection. We test the model that EF-Ts impacts this reaction coordinate by accelerating the removal of EF-Tu·GDP from the ribosome, rendering this step compatible with the reported rate of protein synthesis *in vivo*. These data will

describe the role that EF-Ts plays in the context of EF-Tu's inactivation and provide further understanding of how GEFs and GAPs regulate G-proteins.

5.2 INTRODUCTION

The final phase of gene expression involves the faithful translation of messenger RNA (mRNA) transcripts into amino acid polymers that ultimately gives rise to the cells diverse repertoire of proteins. Translation requires the orchestrated effort of a myriad of biomolecules, collectively referred to as the translational machinery. Among the most important member of this group is the ribosome, a 2.5 MDa complex consisting of 52 proteins and 4,660 nucleotides in *E. coli*. Once the translational machinery is assembled on an mRNA start site, the ribosome decodes the open reading frame by testing each triplet codon against the anticodon of adaptor transfer-RNA (tRNA) molecules each carrying an amino acid. Successful matching of mRNA codons with tRNA anticodons leads to the subsequent addition of the newly incorporated amino acid to the nascent polypeptide chain.

Crucial to the tRNA selection process, the three domain GTPase protein Elongation Factor Tu (EF-Tu) chaperones aminoacylated tRNA (aa-tRNA) to the ribosome as a ternary complex (TC) with GTP. EF-Tu is not only important for fast and efficient delivery of aa-tRNA to the ribosome, but it actively contributes to the decoding process *via* its catalytic GTPase functionality[154,155]. Drugs that serve to decouple GTP hydrolysis from EF-Tu function, such as kirromycin, are inhibitory to tRNA selection and are accordingly bactericidal in nature. Crystallographic data have revealed that EF-Tu simultaneously engages aa-tRNA and the leading edge of the large ribosomal subunit. Concurrently, the anticodon loop of aa-tRNA is also bound to

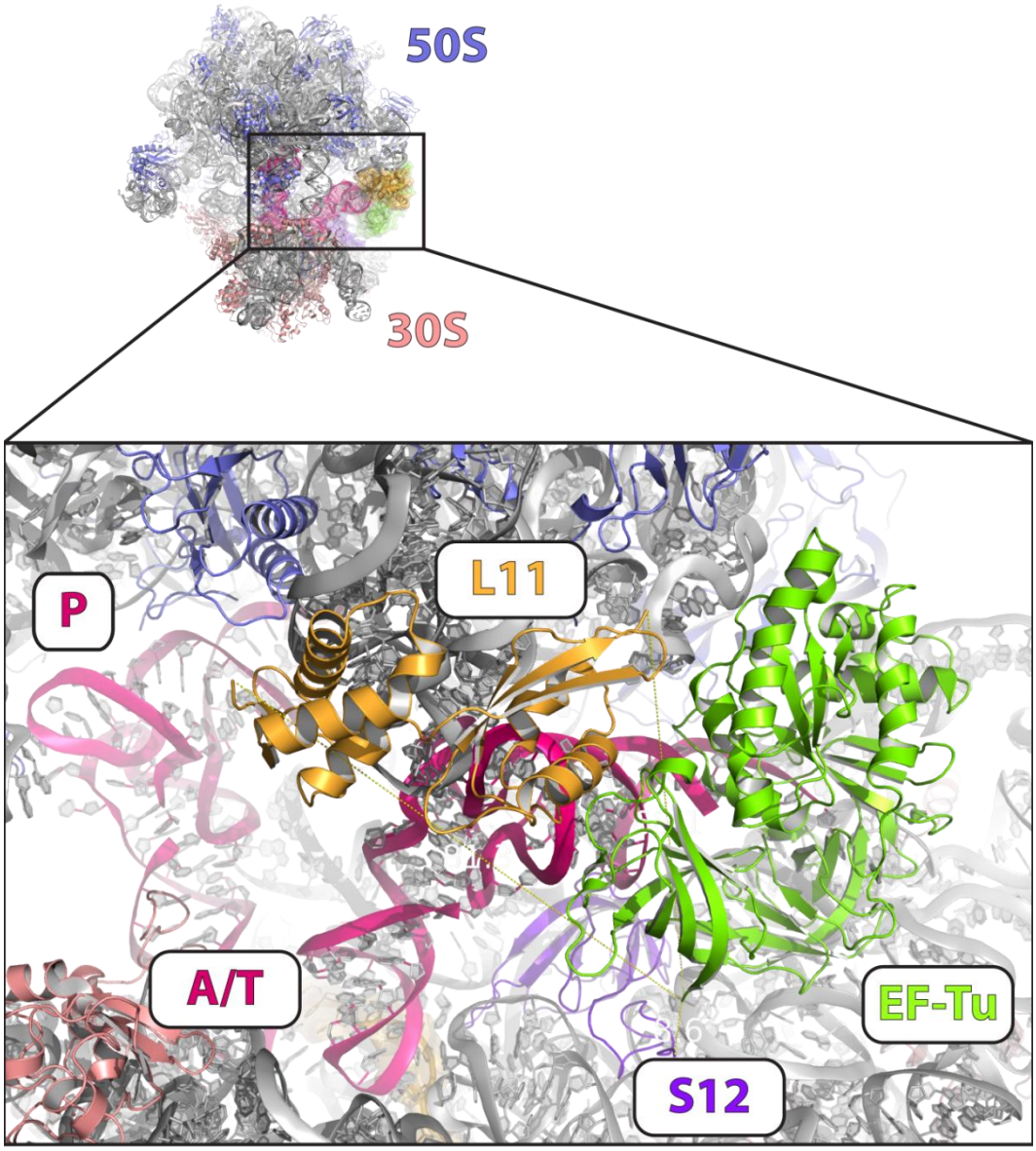

FIGURE 5.1 ***EF-Tu delivers aa-tRNA to the leading edge of the ribosome*****.** Aa-tRNA (*A/T*, *magenta*, *foreground*) is delivered to the A-site of the small subunit of the ribosome by EF-Tu (*green*). In doing so, EF-Tu comes into close proximity to the small subunit protein S12 (*purple*) and the large subunit protein L11 (*orange*). Following *initial selection*, the CCA- end of the aa-tRNA samples the A-site of the large subunit during *proofreading*. tRNA selection culminates in the formation of a peptide bond resulting from the transfer of the nascent polypeptide from the P-site tRNA (*P*, *magenta*, *background*) to the accommodated A-site tRNA.

the A-site of the small ribosomal subunit in a bent-like conformation, referred to as the A/T-state (Figure 5.1).

The precise order and timing of EF-Tu interactions in the translation of mRNA has been largely inferred from investigations of aa-tRNA and the ribosome[1,4,40,53,86,156-159]. Our kinetic understanding of EF-Tu's role in tRNA selection has been predominantly constructed from GTP hydrolysis measurements resulting from interactions between EF-Tu and the GTPase Activating Center (GAC) of the large ribosomal subunit[3,14]. The only direct measurement of EF-Tu ever made during the decoding process[4,24] has contrasted starkly with the rates of tRNA selection as measured from the tRNA reaction coordinate[1,42], and as measured *in vivo* [35]. This experiment argues that the rate-determining step in translation elongation is the release of EF-Tu·GDP during the decoding process. Paradoxically, the predicted rate of EF-Tu·GDP release is 5 to 10 fold slower than the measured aa-tRNA accommodation rate. Moreover, it is an order of magnitude too slow to be compatible with protein synthesis rates measured *in vivo*, ca. 15-20 amino acids polymerized per ribosome per second[35,61,62].

Current models of protein synthesis (Figure 5.2) predict rapid testing of TCs with

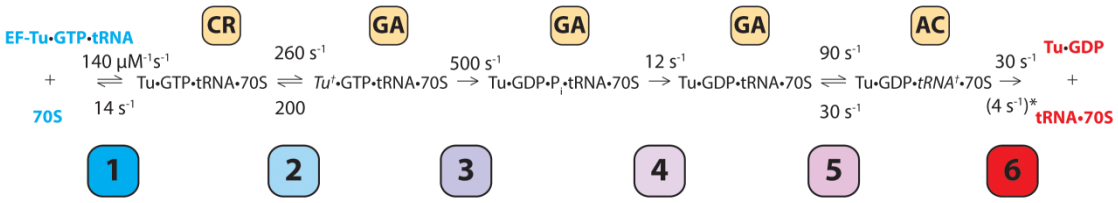

FIGURE 5.2 ***Kinetic model of tRNA selection.*** Reaction **1**, ternary complex binds to the ribosome with a fast bimolecular rate leading to the codon recognition (CR) state. Reaction **2**, reversible tRNA motions either lead to the rejection of ternary complex (not shown) or to the achievement of a second stable intermediate, termed the GTPase activated (GA) state. Reaction **3**, GTP is irreversibly hydrolyzed. Reaction **4**, P_i is released. Reaction **5**, reversible tRNA motions ultimately lead to the fully accommodated (AC) state. Reaction **6**, although EF-Tu has not been directly tracked during this process, it is inferred from off-rate studies that EF-Tu·GDP releases slowly, and is therefore present throughout the decoding process. In contrast, some models posit that EF-Tu·GDP dissociation is prerequisite for achieving the AC state. Rates presented in reactions 1, 2, 5, and 6 were determined from investigating the tRNA reaction coordinate[1]. Rates presented in reactions 3 and 5 were made using an orthogonal Pi sensor and global fitting[3], while the * rate shown in reaction 6 is inferred from $EF\text{-}Tu_{mant}$ dissociation studies[4].

ribosomes at a bimolecular rate that is approaching a diffusion-limited process, ca. 140 $\mu M^{-1}s^{-1}$. Upon successful interaction, the aa-tRNA anticodon is tested against the mRNA codon programmed in the A-site of the small subunit. Pre-steady state data tracking the tRNA throughout this process have revealed a stable intermediate at this first interaction step, termed codon recognition (CR). Here, the TC is either rejected, and thus dissociated from the ribosome, or the tRNA proceeds to a second stable intermediate, termed the GTPase activating (GA) state. All of the interactions that serve to bring the aa-tRNA to the GA state are collectively referred to as *Initial Selection* and together constitute a single testing of the codon-anticodon pair. As kirromycin inhibits progress beyond the GA state, it is largely thought that the kirromycin stalled crystal structure resembles the GA state (Figure 5.1). *Initial Selection* concludes with the hydrolysis of GTP, a process that is facilitated by ribosomal elements in the GTPase activating center (GAC) known as the sarcin-ricin loop.

The second phase of tRNA selection involves another testing of the codon-anticodon pair through a series of kinetic steps referred to as *Proofreading*. It is here that the canonical models of the decoding process begin to diverge substantially. Some models posit that EF-Tu·GDP quickly dissociates from the aa-tRNA and the large ribosomal subunit and that this step is prerequisite for the continuation of the aa-tRNA accommodation process[17]. However, direct measurements of EF-Tu dissociation from ribosomes contradict this notion. Instead, an EF-Tu residence time greatly outlasting tRNA accommodation has been observed[4]. These data argue in favor of a model wherein EF-Tu·GDP remains bound to the ribosome throughout the tRNA selection process and disembarks after a peptide bond has been formed.

Although the order and timing of aa-tRNA accommodating into the ribosome has been described in detail, direct measurements of EF-Tu are lacking. To sufficiently

delineate between the different models of *Proofreading*, and to better reconcile biophysical measurements with *in vivo* observations, further understanding of the EF-Tu reaction coordinate during tRNA selection is needed. Here, we employ several new assays to directly monitor EF-Tu during the tRNA selection process and propose new refinements to the canonical model.

5.3 RESULTS

5.3.1 EF-Tu Hydrolyzes GTP In A Timeframe Consistent With aa-tRNA Accommodation

During aa-tRNA selection, EF-Tu converts GTP to GDP after the codon-anticodon pair is successfully tested. Investigations of the tRNA reaction coordinate during tRNA selection have led to a model where the GTPase activated state is reached within an average of 30 ms after TC begins interacting with the ribosome. In order to investigate this more directly, we monitored tRNA selection using an orthogonal

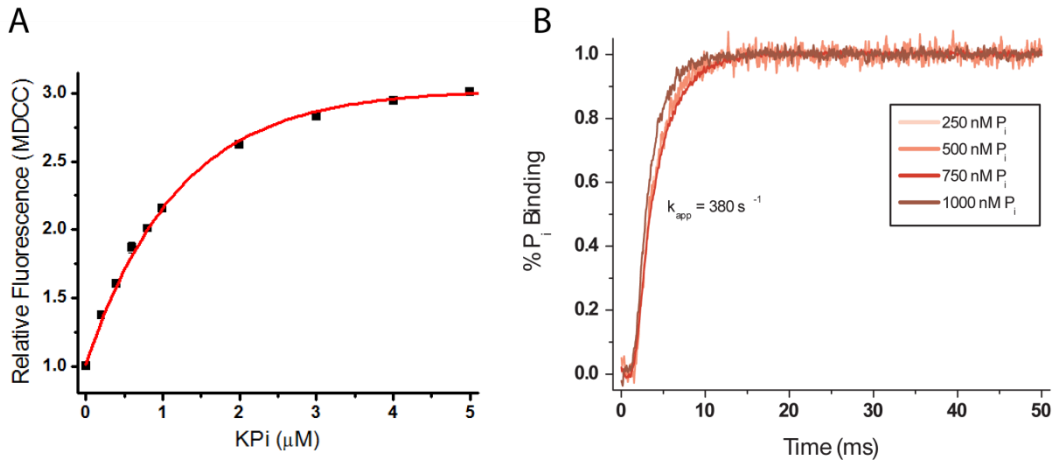

FIGURE 5.3 ***PBP binds P_i with a fast on-rate.*** **A**, Titration of P_i into a reaction containing MDCC-PBP reveal a large increase in relative fluorescence and a dissociation constant of ~1 μM. **B**, the rate of Pi binding is fast relative to the published rates of GTP hydrolysis during tRNA selection (ca. 30 s^{-1}). Instruments used to acquire data for A, and B were a QM4 PTI fluorometer and a SX20 stopped-flow spectrometer, respectively.

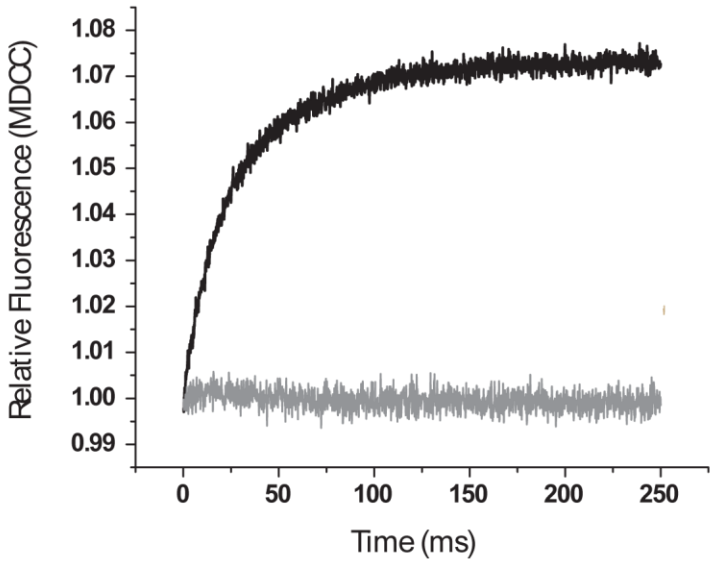

FIGURE 5.4 ***GTP Hydrolysis during tRNA selection*****.** GTP hydrolysis resulting from mixing Phe-TC and IC in the presence of MDCC-PBP reveals a relative fluorescence increase (*black*). An apparent rate of 38 s^{-1} was estimated by fitting to a single exponential function. An identical experiment lacking Phe-$tRNA^{Phe}$ results in no fluorescence change (*grey*).

inorganic phosphate (P_i) biosensor[76]. *E. coli* Phosphate Binding Protein (PBP) labeled with the environmentally sensitive MDCC fluorophore was used to detect free P_i as it is produced from the hydrolysis of GTP (see Chapter 2)[3]. Upon PBP binding to P_i, the relative fluorescence of MDCC increases irreversibly at timescales of less than one second (Figure 5.3).

The rate of GTP hydrolysis during tRNA selection was measured by rapidly mixing 800 nM of cognate Phe-TC and 400 nM ribosomal initiation complexes (IC) in the presence of 2 μM MDCC-PBP. This resulted in a fast increase in MDCC fluorescence that was dependent on the complete repertoire of translational machinery (Figure 5.4). The rate of GTP hydrolysis, k_{GTP}, was estimated to be 38 s^{-1} by fitting the process to a single exponential. Our measurements indicate that EF-Tu hydrolyzes GTP on times scales that are consistent with the rate of the decoding process as measured from the perspective of the tRNA reaction coordinate[1].

5.3.2 EF-Tu·GDP_{mant} release is slow in the absence of EF-Ts

To directly monitor the rate of aa-tRNA selection along the EF-Tu reaction coordinate, the GTP fluorescent analog GTP_{mant} was used. Here, the fluorescent mant moiety is conjugated to either the 2′ or 3′ of the ribose of GTP. EF-Tu binds to both GTP_{mant} and to GDP_{mant} with high affinity and, importantly, the mant moiety does not significantly perturb the interaction between EF-Tu and EF-Ts (Figures 5.5, 5.6). Phe-TC_{mant} was formed with 2.5 μM EF-Tu, 0.1 μM EF-Ts, 0.3 μM GTP_{mant}, and 0.3 μM Phe-$tRNA^{Phe}$ and rapidly mixed with ICs using an SX20 stopped-flow spectrometer. Consistent with previous studies[4,24], ternary complex binding to ribosomes resulted in an increase in the mant relative fluorescence (Figure 5.7, *dark blue curve*). This is likely due to alterations in the environment (water exposure) and diffusional freedom (steric hindrance) that occur upon EF-Tu·GTP_{mant} binding to the ribosome. This process is quickly followed by a return to baseline fluorescence, consistent with EF-Tu·GDP_{mant} releasing from the ribosome. Each component of the biphasic process was fit to a single exponential to estimate the rate of ternary complex association and the rate of EF-Tu·GDP_{mant} release.

The rate of association, k_{on}, was estimated to be ~55 s^{-1}. This is consistent with previous measurements of tRNA selection using EF-Tu·GTP_{mant} [4,24], as well as initial binding measurements tracking the accommodating aa-tRNA into the ribosome[1]. The observed fluorescence decay process, k_{off}, is observed to be ~7 s^{-1}, in line with what has been previously reported with this assay[4,24].

Although this signal does not distinguish between productive and non-productive interactions, the lifetime of non-productive interactions as measured from the aa-tRNA reaction coordinate are much shorter than the off rate measured here, ca. 30 s^{-1} versus 7 s^{-1} [1]. It therefore seems plausible that this signal is dominated by

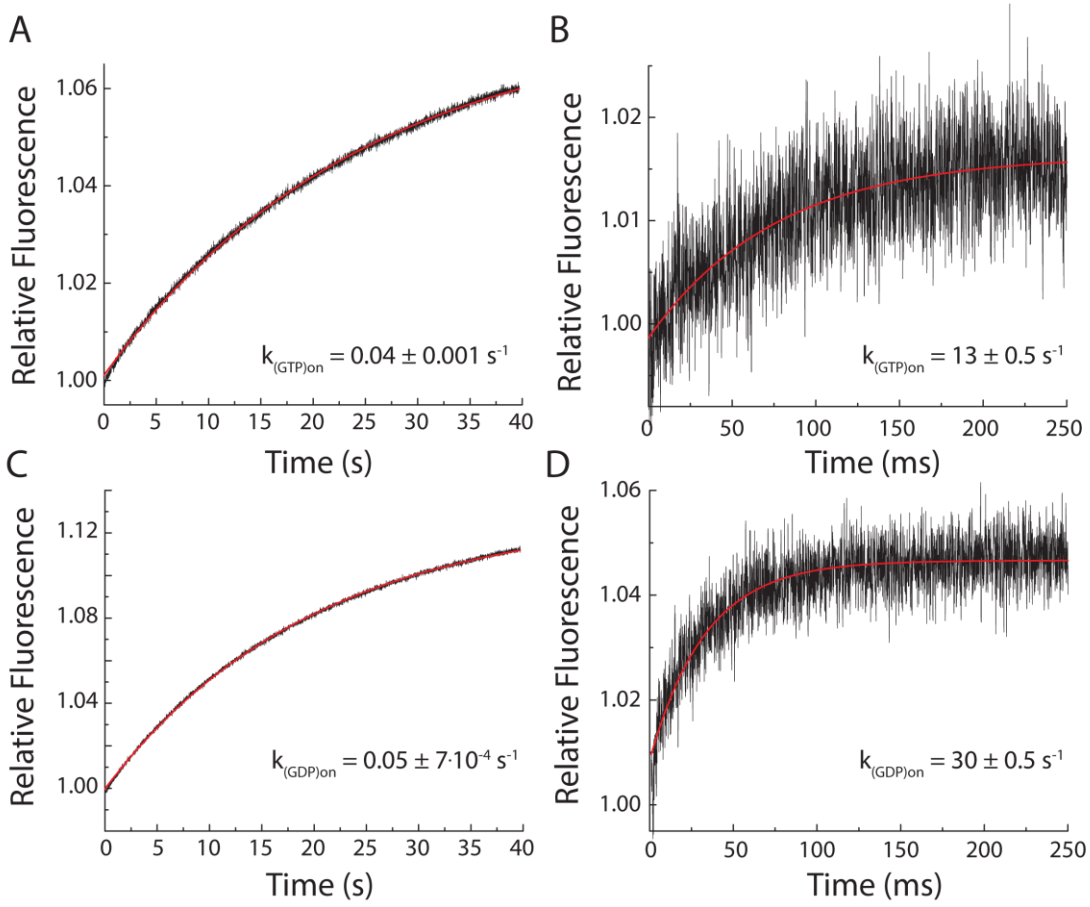

FIGURE 5.5 ***EF-Tu binds mant nucleotides with high affinity*****.** 1 µM EF-Tu, **A**, or 1 µM EF-Tu/Ts, **B**, is rapidly mixed with 10 µM GTP_{mant} using an SX20. The relative fluorescence of mant was monitored by illuminating at 280 nm with a monochromator and measuring emission intensity using a 440 nm long pass filter. These experiments were repeated with GDP_{mant} without, C, and with, D, EF-Ts. Apparent rates are estimated by fitting to a single exponential function.

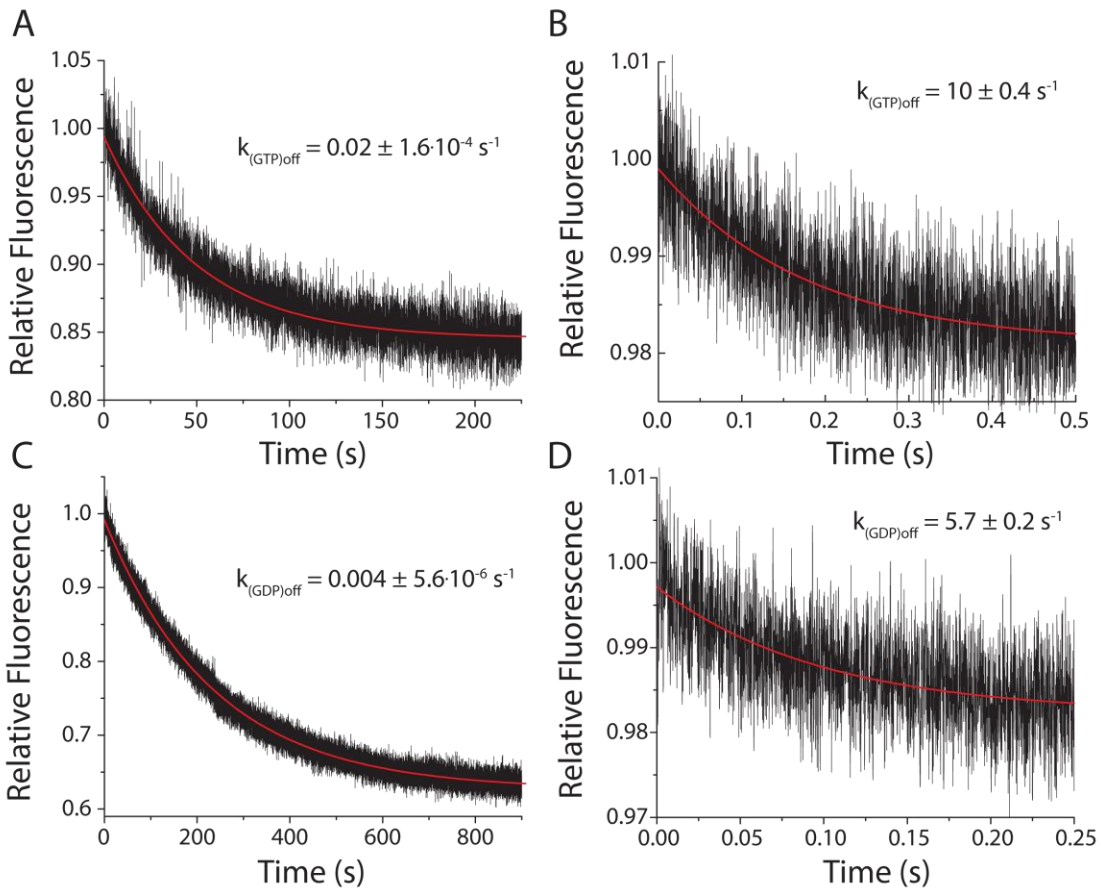

FIGURE 5.6 ***EF-Ts accelerates nucleotide release from EF-Tu.*** 1 µM EF-Tu·GTP$_{mant}$ was rapidly mixed with nucleotide free buffer, **A**, or 1 µM EF-Ts, **B**, using a SX20. The relative fluorescence of mant was monitored by illuminating at 280 nm with a monochromator and measuring emission intensity using a 440 nm long pass filter. These experiments were repeated with EF-Tu·GDP$_{mant}$ without, **C**, and with, **D**, EF-Ts. Apparent rates are estimated by fitting to a single exponential function.

productive EF-Tu interactions and that the fluorescence decay is product of EF-Tu·GDP_{mant} dissociation. As this rate is vastly slower than the anticipated rate of tRNA accommodation[1], we further investigated this process using cellular concentrations of EF-Ts (1 μM and 2.5 μM). However, the Phe-$tRNA^{Phe}$ concentration is unchanged and therefore it is assumed that the concentration of Phe-TC also remains the same. Increasing EF-Ts to 1 μM had little impact on the observed rates of fluorescence increase and decay (Figure 5.7, *medium blue curve*). However, the effect of increasing EF-Ts to 2.5 μM, now equimolar with EF-Tu, resulted in a drastically faster process. Here, the increase of fluorescence was not quantifiable, and the decrease is estimated to be approximately two orders of magnitude faster than what was observed at the lower EF-Ts concentrations (Figure 5.7, *light blue curve*).

The release of EF-Tu·GDP from the ribosome is prerequisite for EF-G binding and thus translocation[32]. Therefore, the slow release of EF-Tu·GDP_{mant} measured here at sub-micromolar amounts of EF-Ts argues in favor of a model where this is the rate-

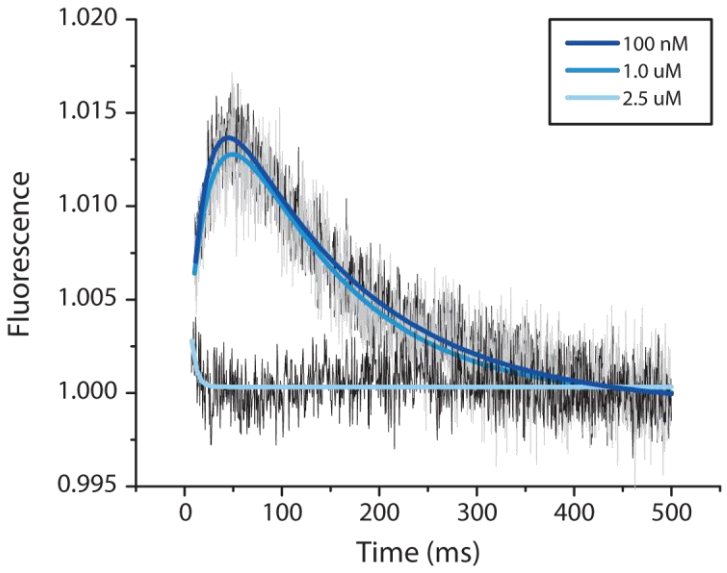

FIGURE 5.7 ***tRNA selection monitored using mant labeled EF-Tu.*** EF-Tu_{mant}·GTP·Phe-$tRNA^{Phe}$ ternary complex is rapidly mixed with initiation complexes at increasing concentrations of protein factor. The fluorescence process is fit to a double exponential model for 100 nM and 1 μM data point. The 2.5 μM protein factor data was fit to a single exponential model.

limiting step for not only the decoding process, but also for the broader elongation cycle. Based on current models of tRNA selection[1,17,24,53], it is unclear how increasing the concentration of a GEF, and not ternary complex, could account for the faster process observed.

In a previous study, EF-Tu dissociation from aa-tRNA was observed to be accelerated in the presence of GDP and EF-Ts (Figures 3.3*C*,*D*, Figures 4.5*D*,*E*,*F*). Furthermore, the rate-determining step of ternary complex formation was previously identified to be catalyzed by EF-Ts through a direct EF-Tu/Ts·GTP·aa-tRNA quaternary complex interaction (Figure 4.7). Importantly, this interaction is postulated to occur at high concentrations of protein factor, with an estimated K_D of ~2 μM between EF-Ts and Phe-TC. Based on these previous observations, and the faster mant fluorescence decay observed here (Figure 5.6, *light blue curve*), we hypothesize that EF-Ts accelerates the dissociation of EF-Tu·GDP during tRNA accommodation. Specifically, we speculate that, at near cellular concentrations of EF-Ts, EF-Tu·GDP dissociation is accelerated by directly binding to EF-Ts while it is still bound to the ribosome.

5.3.3 EF-Tu Releases aa-tRNA In A Timeframe Consistent With aa-tRNA Accommodation

To test the impact that EF-Ts has on the EF-Tu reaction coordinate, we performed tRNA selection experiments using a quenched ternary complex. This reagent enables us to track the proximity of EF-Tu to the accommodating aa-tRNA during the decoding process. Quenched TC is formed with a quencher labeled EF-Tu (Cy5Q) bound to a fluorescently labeled aa-tRNA (Cy3B-acp^{3}U47) (Figure 5.8*A*). Upon

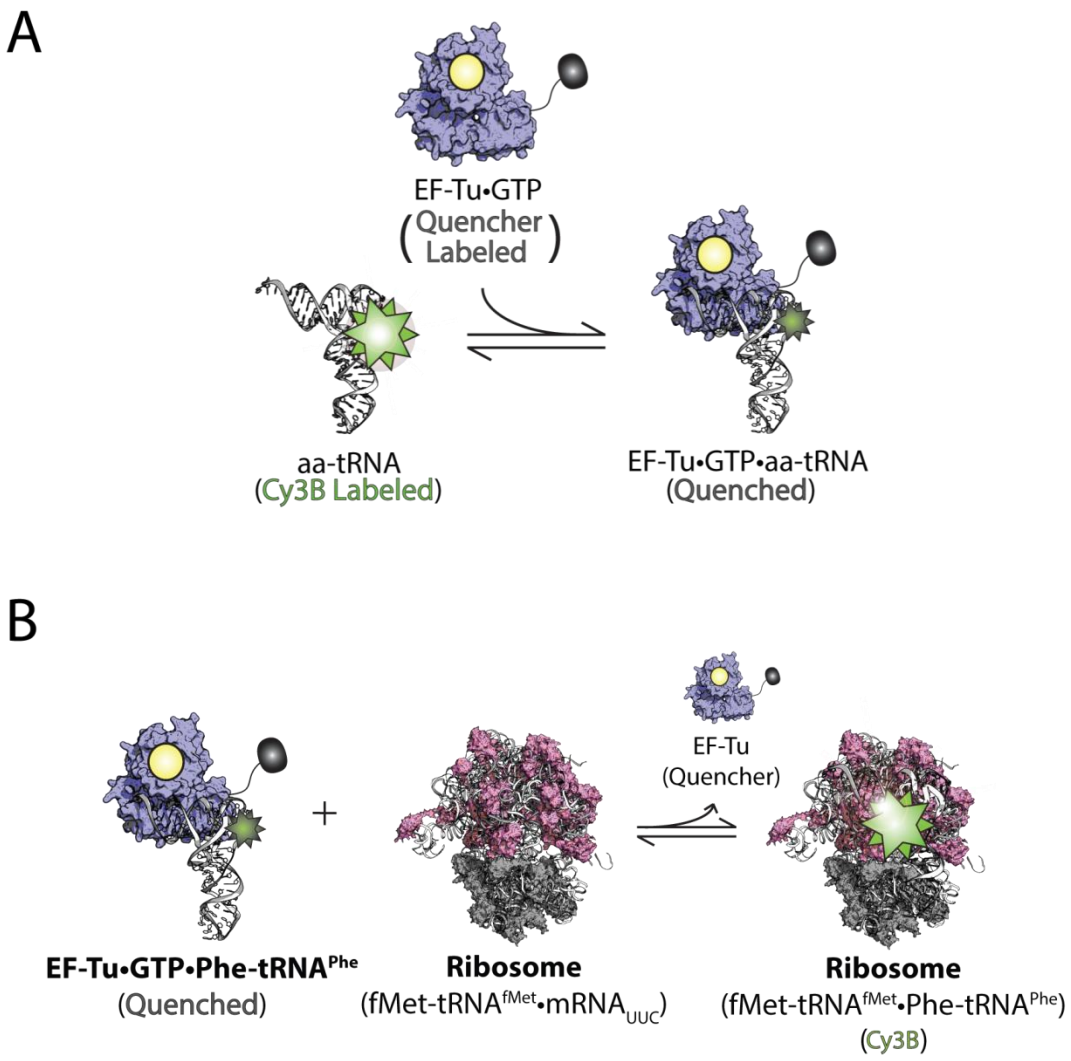

FIGURE 5.8 ***Schematic of quenched TC formation and tRNA selection*****. A**, Quenched Phe-TC is formed by the addition of EF-Tu (C-Term Cy5Q) and Phe-tRNA^{Phe} (Cy3B-acp^{3}U47) in the presence of GTP. Excitation of Cy3B fluorescence reveals a diminished value upon formation of ternary complex as a result of the proximal Cy5Q. **B**, Quenched Phe-TC is mixed with ribosomes formed with an initiator tRNA in the P-site and an empty A-site cognate for tRNA^{Phe} (referred to as an initiation complex (IC) in the text). Upon successful delivery of Cy3B Phe-tRNA^{Phe}, the quencher labeled EF-Tu dissociates thus removing the quenching effect of Cy5Q. This results in a measureable increase in Cy3B fluorescence.

successful delivery of the fluorescently labeled aa-tRNA, the EF-Tu separates from the aa-tRNA, thus eliminating the quenching effect (Figure 5.8*B*).

The activity of quenched Phe-TC is demonstrated using ICs programmed with an initiator tRNA in the P-site and an empty A-site cognate for $tRNA^{Phe}$. Varying concentrations of ICs are mixed with 20 nM quenched Phe-TC in the presence of 1 mM GTP and incubated at room temperature for 10 minutes. Measurement of Cy3B fluorescence reveals that quenched Phe-TC is fully active in translation (Figure 5.9, *black squares*). This experiment was repeated with 1 mM GDPNP in replace of GTP (Figure 5.9, *open squares*) and with ICs lacking an mRNA (Figure 5.9, *open triangles*) demonstrating that the dequenched effect requires productive interactions between Phe-TC and ICs.

To track the interaction between EF-Tu and aa-tRNA in real time, pre-steady state experiments were conducted with quenched Phe-TC and ICs using a SX20 stopped-flow spectrometer. Quenched Phe-TC, previously formed with 1 μM Cy5Q labeled

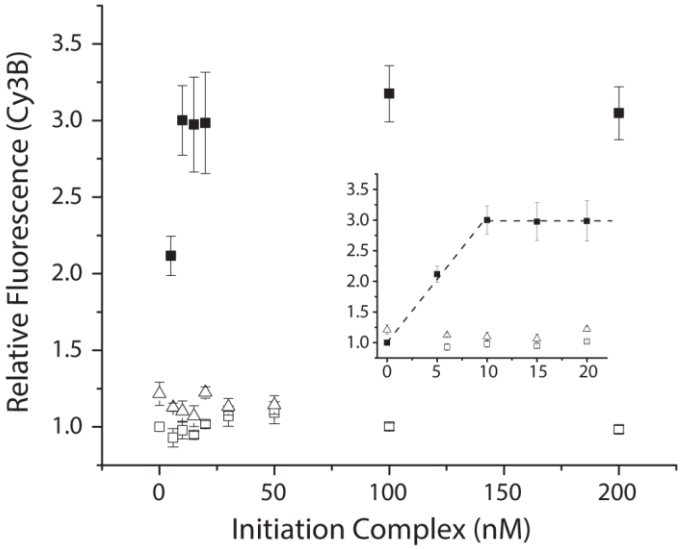

FIGURE 5.9 ***Initiation complexes are active in translation*****.** Quenched Phe-TC (20 nM) is mixed with increasing amounts of ICs in the presence of 1 mM GTP and incubated for 10 minutes (*black squares*). Upon Phe-$tRNA^{Phe}$ accommodation, Cy3B fluorescence increases. Experiments are repeated with either GDPNP (*open squares*) or using ICs lacking mRNA (*open triangles*). *Inset*, fitting the linear portions of the data reveal an intersection at the earliest maximum value of 10 nM IC.

EF-Tu, 120 nM Cy3B labeled Phe-tRNA^{Phe}, and 1 mM GTP, is rapidly mixed with varying concentrations of IC (0 to 2 μM) while monitoring Cy3B fluorescence. Rapid mixing of quenched Phe-TC with IC resulted in a two-step process. First, an initial delay of 17 ms is observed to precede the predicted increase in Cy3B fluorescence (Figure 5.10*A*, *inset*). This initial delay was also observed to be invariable to IC concentration, consistent with the notion that at least one rate-determining intermediate step precedes the separation of EF-Tu from the aa-tRNA during the decoding process. Significantly, the delay in Cy3B fluorescence is also consistent with the previously reported rate of aa-tRNA achieving the GTPase activating (GA) state, ca. 67 s^{-1}, an on-path intermediate described for the tRNA reaction coordinate[1].

After the initial delay, Cy3B fluorescence was observed to increase at a rate that is dependent on the concentration of IC (Figure 5.10*B*). Expectantly, the dequencing process is dependent on a cognate interaction (Figure 5.10*A*, *light grey curve*) and on GTP (Figure 5.10*A*, *dark grey curve*). The rate at which dequencing occurs, after the delay period, approaches an asymptotic value of 30 s^{-1}, at which the rate no longer bears any concentration dependence. This rate is consistent with the rate previously

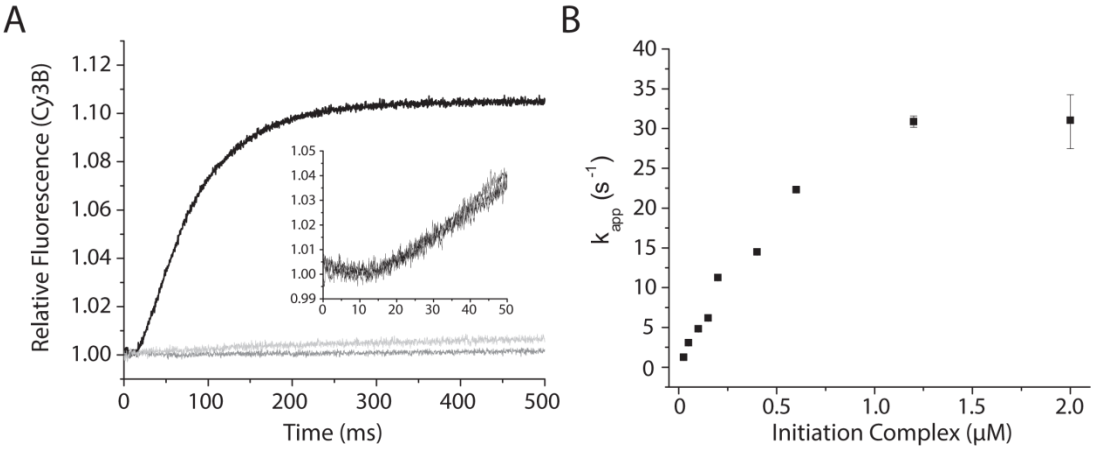

FIGURE 5.10 ***tRNA selection occurs in multiple steps*****. A**, quenched Phe-TC (60 nM) is rapidly mixed with 400 nM ICs in the presence of 1 mM GTP (*black curve*). A delay of ~17 ms is observed (*inset*) before dequencing. The apparent rate of the fluorescence increase was estimated to be 15 s^{-1} by fitting to a single exponential function. **B**, concentration dependence of Cy3B dequenching. An asymptotic rate of ~32 s^{-1} is observed to occur at micromolar IC concentrations.

described for aa-tRNA traversing from the GA state into the fully accommodated (AC) state[1]. Both the intermediate delay period, and the maximal rate of dequenching agree with current models of the decoding process and indicate that the slow mant fluorescent decay signal is capturing a component of the reaction coordinate that follows after the separation of EF-Tu from the aa-tRNA.

After evaluating the concentration dependence of our signal, we set out to test the impact that EF-Ts has on the dequencing signal. Specifically, we predicted that this would manifest by accelerating the rate of Cy3B dequenching, but have no bearing on the initial delay process. This experiment was performed by rapidly mixing 2 μM IC along with 60 nM quenched Phe-TC in the presence of 10 μM EF-Tu(Cy5Q)/Ts. As expected, the initial delay phase was identical to experiments conducted in the absence of EF-Ts (Figure 5.11). However, under these conditions, no change was observed in the maximum rate of dequencing. Here, at micromolar concentrations of EF-Ts, we still observed EF-Tu separating from aa-tRNA at a rate of ca. 30 s^{-1}.

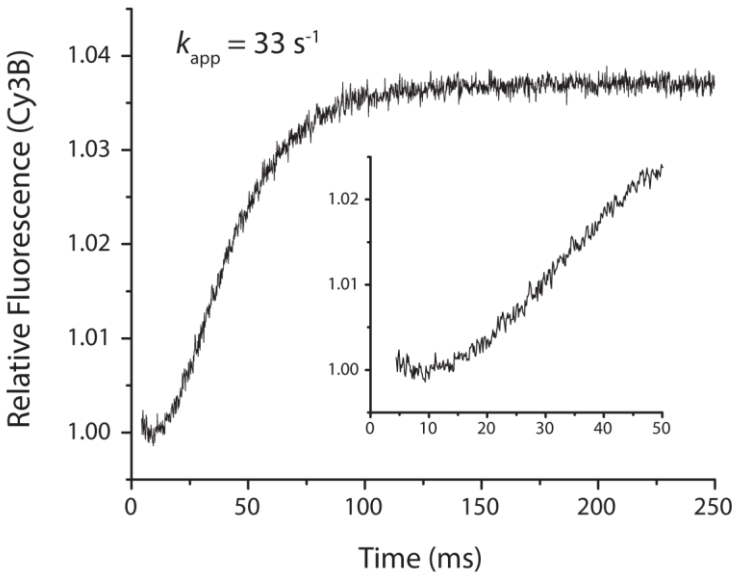

FIGURE 5.11 ***EF-Ts does not accelerate EF-Tu dissociation for Phe-tRNA^{Phe}.*** Quenched Phe-TC, formed in the presence of 10 μM EF-Tu(Cy5Q)/Ts and 1 mM GTP, is rapidly mixed with 2 μM IC. A delay period of ~15 ms is observed (*inset*) followed by an increase in Cy3B fluorescence at an apparent rate of 33 s-1.

5.3.4 Direct Measurements of EF-Tu Reveal A Short Residence Time With The Small Subunit

Although we observed no direct impact on EF-Tu release from the aa-tRNA, we were not able to directly ascertain when EF-Tu·GDP is released from the ribosome. In order to do so, we developed a single molecule FRET (smFRET) assay to measure the residence time of EF-Tu on the ribosome (Figure 5.12). This was done by labeling the C-terminus of the small subunit protein S12 with Cy3B·3S and labeling a non-natural amino acid incorporated into position 305 of EF-Tu with Cy5·4S·COT (see Chapter 2). By utilizing FRET between the donor fluorophore on the ribosome and the acceptor fluorophore on EF-Tu, the residence time of EF-Tu can be directly measured.

To determine the FRET efficiency between the donor and acceptor fluorophore upon EF-Tu binding, Phe-TC (EF-Tu-Cy5) was incubated with surface immobilized ICs (S12-Cy3B) in a TIRF-based microscope (see Chapter 2) in the presence of 2 μM kirromycin. This revealed a high FRET signal, indicating that EF-Tu and S12 are in close proximity in the kirromycin stabilized state (Figure 5.13). This is consistent with

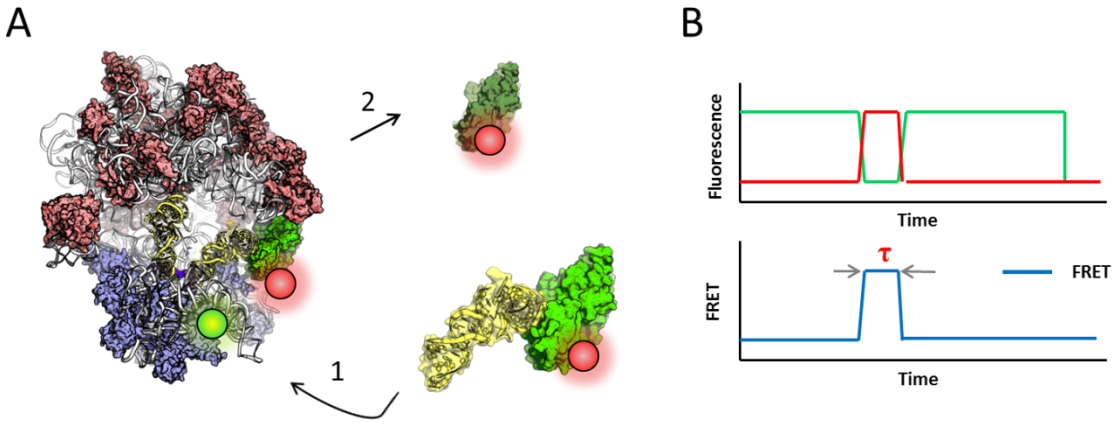

FIGURE 5.12 ***Schematic for smFRET tRNA selection assay*****. A**, Phe-TC, formed with Cy5 labeled EF-Tu, GTP, and Phe-tRNA^{Phe} is rapidly mixed with ICs containing a Cy3B fluorophore on the C-terminus of S12 which is positioned near the A-site of the small subunit. **B**, using a TIRF based microscope, Cy3B will be directly excited while monitoring the fluorescence intensity of both Cy3B (*donor*) and Cy5 (*acceptor*). Based on the canonical model of tRNA selection, we predict that the residence time of EF-Tu will manifest as a transient, high FRET signal A, B.

crystallographic data of the kirromycin-stalled A/T-state which predicts that the fluorophore labeling sites used here are within 20 Å of one another.

Having established the EF-Tu bound FRET value, this experiment was repeated without kirromycin and the tRNA selection process was tracked in real time (Figure 5.14). Ternary complex was formed by incubating 100 nM Phe-tRNA^{Phe} and 20 nM EF-Tu(Cy5) in the presence of 1 mM GTP. This was delivered to surface immobilized ICs (S12-Cy3B), while illuminating Cy3B fluorescence. At a population level, we

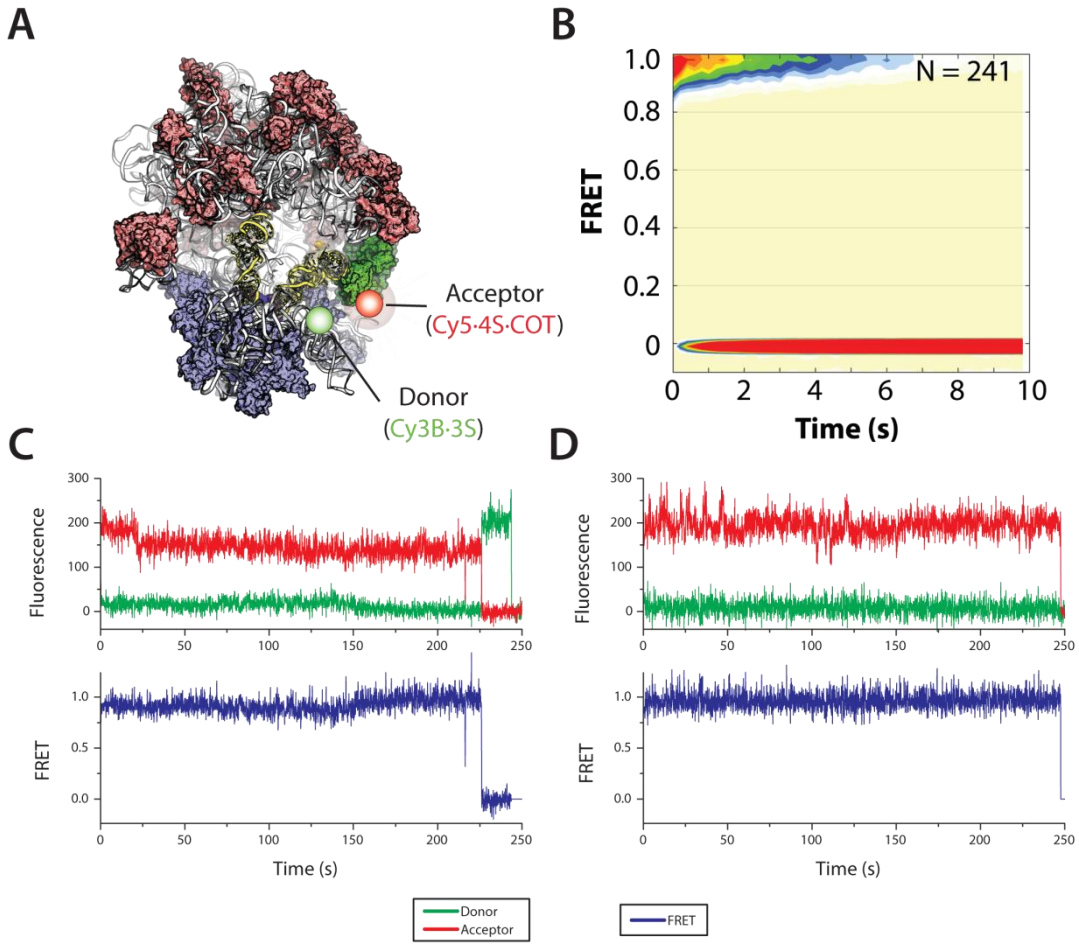

FIGURE 5.13 ***EF-Tu engages the ribosome in close proximity to protein S12.*** Phe-TC, formed with Cy5 labeled EF-Tu in the presence of 2 μM kirromycin, is incubated with ICs (S12-Cy3B) for 2 minutes forming a stabilized EF-Tu bound intermediate, **A**. At a population level, the resulting interaction results in high FRET, **B**. Individual molecules reveal long lived, stable interactions , **C**, **D**.

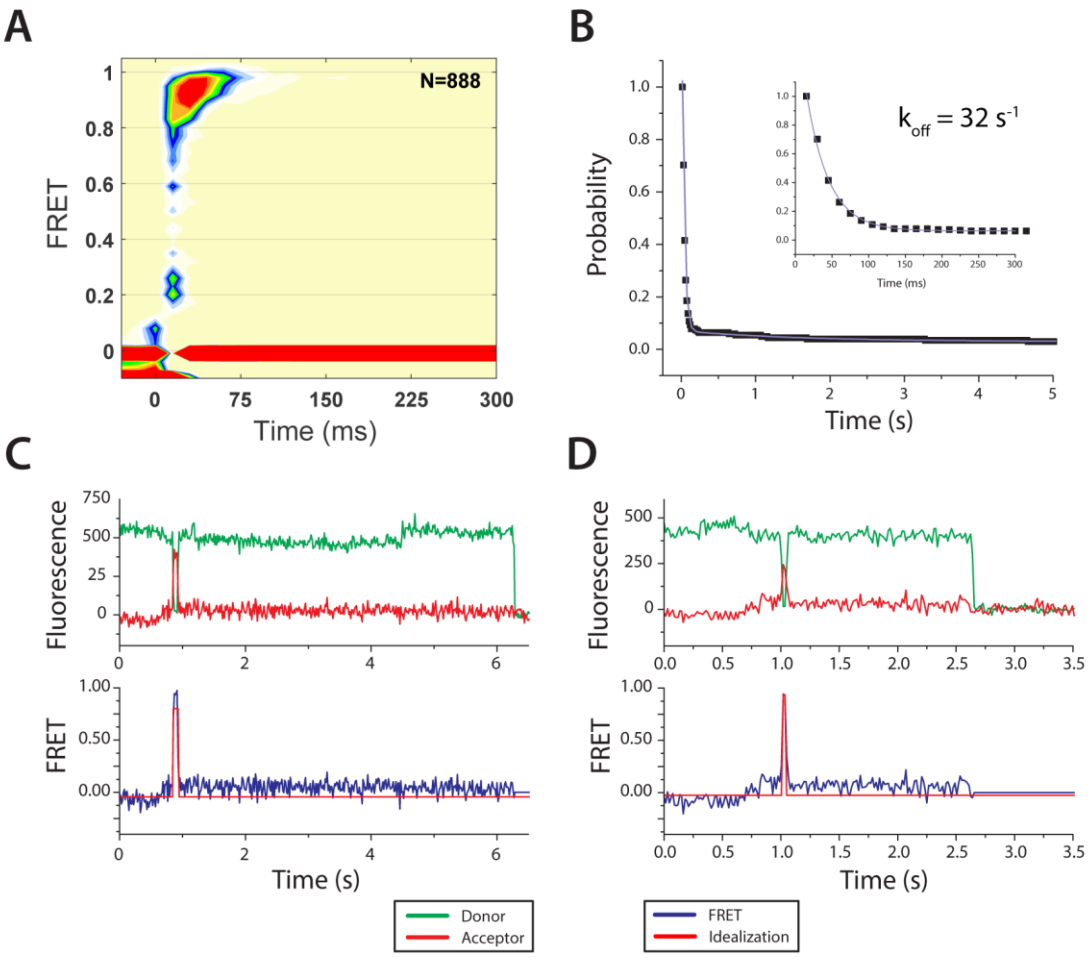

FIGURE 5.14 ***EF-Tu interacts transiently with the ribosome*****. A**, Rapid mixing of Phe-TC (EF-Tu-Cy5) with IC (S12-Cy3B) resulted in a transient interaction with a FRET value that is consistent with the kirromycin stabilized intermediate. **B**, fitting the high FRET interaction lifetimes with a single exponential model revealed an EF-Tu off rate, k_{off}, of 32 s^{-1}. C**, D**, individual molecules show fast, high FRET interactions.

observed a transient interaction at a FRET value consistent with the kirromycin stalled intermediate state. Individual molecules reveal EF-Tu·Ribosome interactions that are transient in nature. The residence time of EF-Tu, estimated by fitting the distribution of high FRET lifetimes to a single exponential, is measured to be 33 s^{-1} under the conditions used here.

5.3.5 EF-Tu, aa-tRNA, and the ribosome are tracked simultaneously

The smFRET assay used to track EF-Tu binding to the ribosome reports on all interactions, both productive and non-productive. Based on prior investigations of tRNA selection[1], we anticipate that roughly 30-50% of cognate TC interactions result in the successful delivery of aa-tRNA. To delineate between productive and non-productive interactions, a three-color smFRET experiment was implemented. Here, the donor fluorophore Cy3B is conjugated to protein S12 as before, but now the acceptors Cy5·4S·COT and Cy7·4S·COT are conjugated to Phe-$tRNA^{Phe}$ and to EF-Tu respectively (Figure 5.15*A*). This enables the simultaneous measurements of Phe-$tRNA^{Phe}$ and EF-Tu with respect to each other, and with respect to the ribosome.

To establish the FRET efficiency to each of the acceptors when TC is bound in the A/T-state, tRNA selection experiments were conducted using 2 μM kirromycin (Figure 5.15). Consistent with Phe-$tRNA^{Phe}$, EF-Tu and the C-terminus of S12 being in close proximity to one another, high FRET efficiencies were observed for both acceptor fluorophores. Individual molecules reveal long-lived, stable interactions. However, poor labeling efficiencies, and possibly diminished functionality greatly diminished the number of molecules observed (compare Figures 5.14 and 5.15). As a result, pre-steady state measurements in the absence of kirromycin is not possible with these reagents.

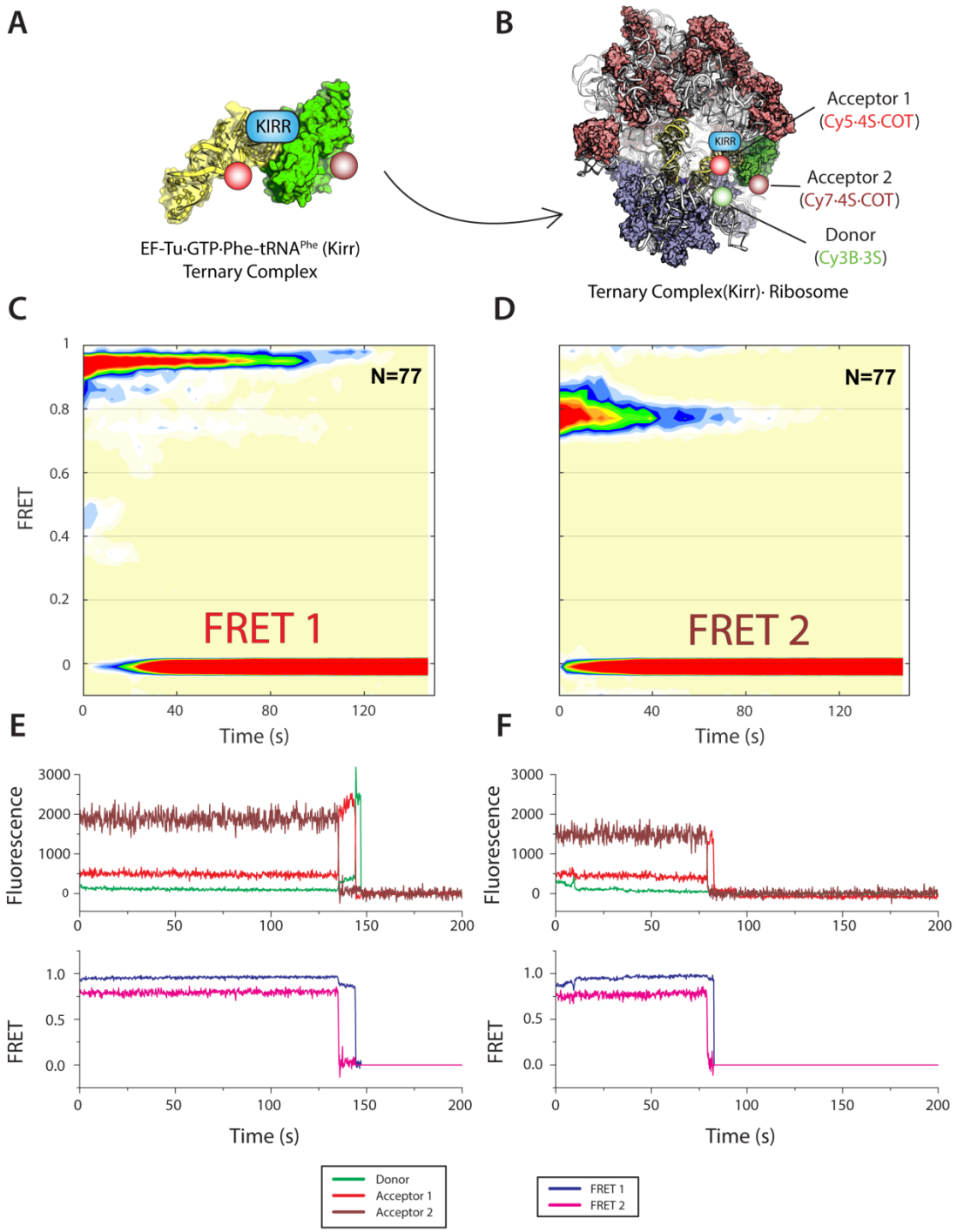

FIGURE 5.15 ***EF-Tu and Phe-tRNAPhe can be tracked simultaneously.*** **A**, schematic of three-color FRET assay. Phe-TC is formed with Phe-tRNA^{Phe} (Cy5-acp^{3}U47) and EF-Tu(Cy7) in the presence of 1mM GTP and 2 μM kirromycin is mixed with surface immobilized ICs (S12-Cy3B). A 2 minute incubation reveals stable FRET to both Cy5, **B**, and Cy7, **C**, at a population level. **D**, **E**, individual molecules show long-lived, stable interactions between the ribosome, the tRNA, and the protein factor EF-Tu.

5.4 DISCUSSION

Measurements tracking the accommodating aa-tRNA into the ribosome have revealed that decoding occurs in multiple steps with long-lived intermediates that correlate with *Initial Selection* and *Proofreading* (Figure 5.2). EF-Tu has long been recognized as playing a critical role in the fidelity of tRNA selection[130,160,161]. However, the knowledge of the precise order and timing of EF-Tu function during decoding has lagged far behind investigations of other coordinates of this process. As such, a complete framework for tRNA selection has not been realized. In this study, we present direct measurements of EF-Tu with respect to both the accommodating aa-tRNA and the ribosome.

Our measurements of EF-Tu fit within the known paradigm of tRNA selection and serve to augment current models with the EF-Tu reaction coordinate (Figure 5.16). EF-Tu delivers aa-tRNA to the ribosome where, at least one rate-determining step lasting ~17 ms delays EF-Tu's release of the aa-tRNA (Figure 5.10, *inset*). This delay period coincides with the time it takes for aa-tRNAs to successfully traverse through the CR state and to begin sampling the GA state[1]. Bulk measurements of GTP hydrolysis indicate that EF-Tu hydrolyzes GTP at a rate that coincides with the time it takes for aa-tRNAs to traverse through the GA state and begin sampling the AC state, 31 ms. The rapid mixing experiments tracking the dequenching of TC reveal that EF-Tu separates from aa-tRNA at a rate of 30 s^{-1}. This corroborates smFRET experiments tracking EF-Tu's proximity to the small subunit protein S12, which also reveal a rate of separation of 30 s^{-1}. It should be noted, however, that these experiments do not distinguish between productive and non-productive interactions. Finally, experiments using GTP_{mant} betray a dissociation rate, τ_{off} that coincides with published rates of peptide bond formation, ~145 ms (7 s^{-1})[2].

The prediction of our model is that inclusion of EF-Ts in the reaction will specifically manifest in the τ_{off} value. Direct experiments tracking EF-Tu's residence time with respect to the accommodating aa-tRNA and to the ribosome are needed. Based on the τ_{off} measured using mant nucleotides (Figure 5.7), we predict that EF-Ts will have a significant impact at concentrations > 2 μM.

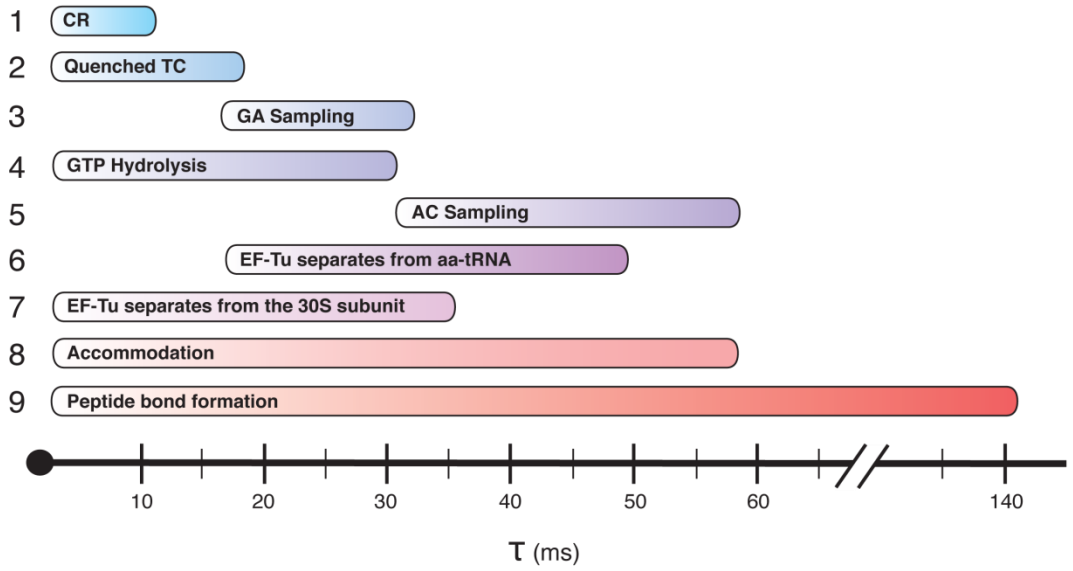

FIGURE 5.16 ***Measurements of tRNA selection*****. 1**, TC samples the CR state at fast timescales. Experiments of near cognate tRNA selection reveal that τ_1 is on the order of ~10 ms. **2**, EF-Tu remains bound to the aa-tRNA in a TC-like conformation for ~17 ms (Figure 5.10, *inset*). **3**, the aa-tRNA begins sampling the second intermediate sate, GA, with a τ_3 of ~15-20 ms[1]. **4**, GTP is hydrolyzed with a τ_4 of 26 ms (Figure 5.4). **5**, the aa-tRNA begins sampling the AC state with a τ_5 of ~30 ms during *Proofreading*[1]. **6**, EF-Tu separates from aa-tRNA with a τ_6 of 31 ms (Figures 5.9, 5.10). **7**, EF-Tu separates from the 30S subunit with a τ_7 of 31 ms (Figure 5.14). **8**, aa-tRNAs fully accommodate into the AC state and stop sampling the GA state[1], **9**, a peptide bond is formed with the A-site tRNA with a τ_9 of ~145 ms[2]. Finally, EF-Tu·GDP putatively dissociates from the large subunit with a τ_{off} of ~145 ms. This will be verified with pre-steady state experiments designed to directly resolve this step (see Figure 5.15).

CHAPTER 6

IMPACT AND FUTURE IMPLICATIONS

6. IMPACT AND FUTURE IMPLICATIONS

This chapter focuses on broad implications of the themes discussed in earlier chapters, as summarized in section 6.1. Section 6.2 outlines important concepts from Chapters 3, 4, and 5. The general implications of our discovery of quaternary complex are discussed in Section 6.3 followed by the impact of measuring the deactivation of EF-Tu in Section 6.4. Future directions and conclusions are discussed in sections 6.5 and 6.6 respectively.

6.1 SUMMARY

The data presented in prior chapters argue for an update to the canonical G-protein model. EF-Ts was shown to catalyze the formation of TC through the production of a previously unidentified intermediate, QC. In doing so, the rate of TC formation is accelerated above the rate of protein synthesis. Thus, TC formation is not rate-limiting in the presence of EF-Ts. Beyond protein synthesis, the observation that GEFs may catalyze the formation of the G-protein·effector complex has implications for other systems. Small G-proteins have been observed to participate in multiple signal transduction cascades through the interaction of distinct effectors. We propose a

model wherein GEFs chaperone activated small G-proteins to specific effectors thereby imparting specificity to the signal being transduced. Additionally, we have also predicted EF-Ts to impact the disassembly of EF-Tu·GDP from the ribosome. These studies are ongoing but will reveal a more complete framework for G-protein activation and deactivation.

6.2 INTRODUCTION

Our general understanding of G-protein activation and inactivation is largely a product of investigations of select model systems. These include studies of Ras, a member of the small GTPase family[10,162,163], G_α, a member of the heterotrimeric class[164-166], and EF-Tu[167,168]. Together, these investigations led to a model wherein G-proteins are able to sample between two distinct functional conformations, and that nucleotide binding stabilizes these states. In all observed cases, GDP binding stabilizes the G-protein in an inert state while GTP binding favors a conformation that induces active participation with downstream effector molecules (Figure 1.2). Further investigations uncovered a direct relationship between the γ-phosphate of GTP and structural elements within the active conformation, namely switch 1 and switch 2 (Figure 1.1, 1.7, 3.1)[7,88].

Biochemical data has revealed that a significant number of G-proteins have higher affinities for GDP than for GTP. Even when considering the excess of GTP over GDP in the cell, Guanosine Nucleotide Exchange Factors (GEFs) are often required to catalyze the removal of GDP and the subsequent binding of GTP. The resulting GEF•G-protein interaction leads to a lower the nucleotide binding transition state on, thus accelerating the rates of nucleotide exchange. Much of what is known about the kinetics underpinning GEFs and G-proteins have been determined from steady state experiments, or from isolated G-protein-GEF systems that did not include target

effectors[31,169-172]. Furthermore, many of these studies were designed to measure high affinity, long-lived interactions. Given this, it is perhaps not surprising that the transient observations made here between EF-Ts and ternary complex (Chapter 3, Chapter 4) have not been described elsewhere. As such, the prevailing model of G-protein activation and inactivation predicts that GEFs serve only to activate G-proteins. The data presented here (Chapters 3, 4) argue for a more active role for GEFs. Considering that EF-Tu and EF-Ts have been studied as a basis for the canonical model (Figure 1.2), we speculate that the expanded role of EF-Ts may represent GEFs more generally.

6.3 QUATERNARY COMPLEX

6.3.1 EF-Ts catalyzed Ternary complex formation is not rate-limiting

At cellular concentrations, EF-Ts was shown to catalyze the formation of ternary complex by chaperoning EF-Tu to the aa-tRNA. Given that the *in vivo* elongation rate is ~20 amino acids per second per ribosome in log-phase growth[35], the rate of TC formation, $k_{on(TC)}$ would be rate limiting to protein synthesis in the absence of EF-Ts for all tRNA species tested. A major impact of the EF-Ts catalyzed reaction coordinate is that the rate determining step of TC formation was accelerated 7.5-, 3.5-, and 4.8-fold in the case of Phe-, Met-, and Arg-TC (Figure 4.4, Table 4.1). Thus, the involvement of EF-Ts pushes the rate of TC formation to well above the rate of protein synthesis.

The rate of TC formation appears to be finely tuned with the amount of EF-Ts in the reaction (Figure 3.4*B*,*D*). The expression of EF-Ts is believed to occur in tandem with the critical ribosomal protein S2[70] as they are on the same operon. In cells, ribosome concentrations have been measured to be in the range of 20μM – 100 μM

depending on growth conditions[36]. Since S2 is critical for ribosome maturation, the concentration of EF-Ts likely corresponds to the concentration of ribosomes (ca. >10 μM). At low concentrations of EF-Ts, TC presumably forms without the involvement of quaternary complex (Figure 3.7, *Path 2*). If the concentration of EF-Ts increases above 2 μM, the predicted on rate of EF-Ts binding to EF-Tu·GTP of 30 $\mu M^{-1}s^{-1}$ begins to outweigh the fast off rate of 60 s^{-1}. Thus, although this is a transient, low-affinity interaction (K_D = 2 μM)[31], the fraction of EF-Tu·GTP bound to EF-Ts increases to >80% at cellular concentrations of EF-Ts as predicted by:

$$Tu/TsGTP_{\%} = \frac{1}{2 \cdot TuGTP}\left(TuGTP + Ts + K_D - \sqrt{(TuGTP + Ts + K_D)^2 - 4 \cdot TuGTP \cdot Ts}\right)$$

EQUATION 6.1

Here, $Tu/TsGTP_{\%}$ denotes the fraction of EF-Tu·GTP bound to EF-Ts, and *TuGTP* and *Ts* represent the total amount of EF-Tu·GTP and EF-Ts in the reaction (bound + unbound). At high concentrations of EF-Ts, the species EF-Tu/Ts·GTP exists at high enough proportions for TC to form via the quaternary complex intermediate (Figure 3.7, *Path 1*). By simply altering the concentration of EF-Ts in the cell, the rate of TC formation can be modulated. This opens up the possibility that, by adjusting the expression of EF-Ts, the cell may be able to tune the steady state concentration of TC, and thus globally affect the rate of protein synthesis.

6.3.2 EF-Ts may couple global protein synthesis rates to GTP abundance

In the presence of GTP, EF-Ts has no impact on the steady state concentrations of TC (Figure 3.5, Figure 4.2*A*, *B*). Intriguingly, when either GTP was removed from the reaction (Figure 3.5) or when saturating amounts of GDP was added (Figures 3.3*C*,

4.4), EF-Ts was shown to have a major impact on the stability of TC. Further investigation revealed that EF-Ts constantly exchanges nucleotide with EF-Tu, even when it is bound to aa-tRNA (Figure 3.6). These observations led to a model wherein EF-Ts continually interacts with TC and facilitates guanine nucleotide exchange with EF-Tu bound to aa-tRNA much the same way as it does with unbound EF-Tu. When EF-Ts engages EF-Tu·GTP bound to aa-tRNA in the presence of saturating GTP, the bound GTP molecule is exchanged for another GTP molecule in the milieu, having no net effect (Figure 6.1, p*ath 1*). However, when GTP is removed from the system (Figure 3.5), EF-Ts removes the bound GTP and remains bound to EF-Tu, which subsequently dissociates from the aa-tRNA (Figure 6.1, *path 2*). Similarly, when GDP

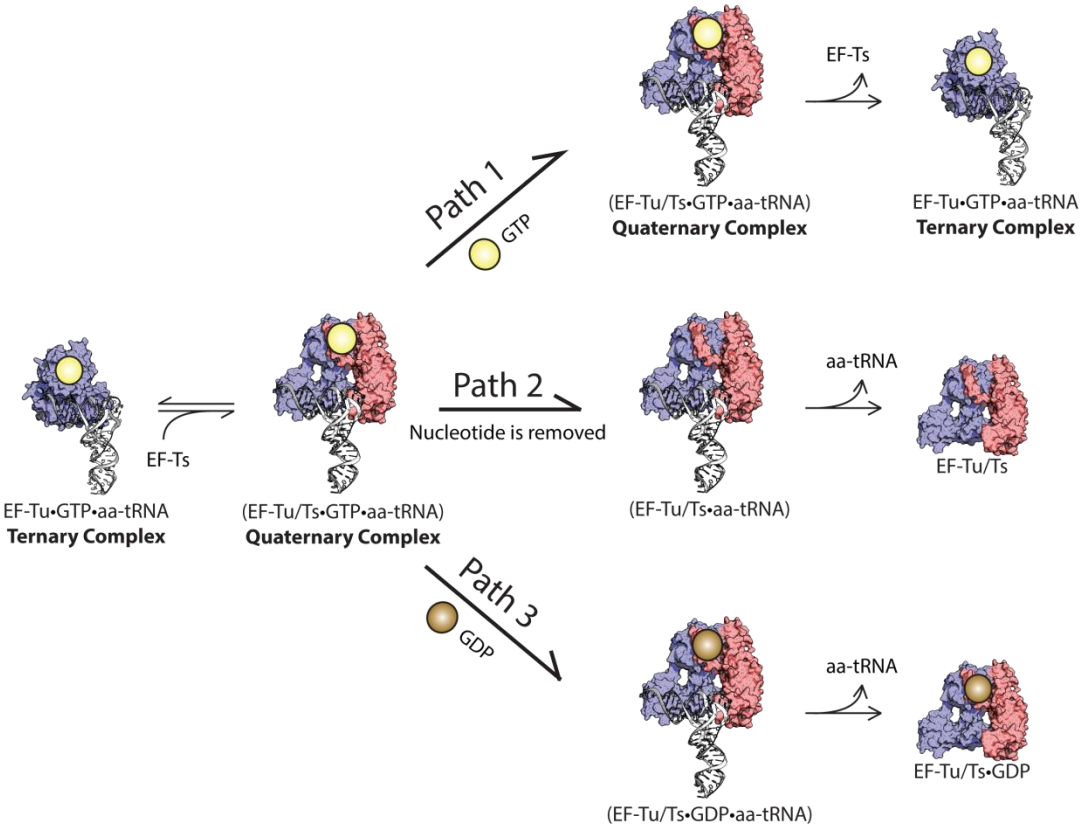

FIGURE 6.1 ***EF-Ts couples TC stability with local nucleotide abundance.*** The formation of TC occurs via the intermediate QC. Likewise, EF-Ts can bind to TC in the reverse pathway to form QC. Under conditions of saturating GTP, the equilibrium of TC and QC is unperturbed (Path 1). However, if GTP is removed from the local environment (Path 2), or if GDP is present at high concentrations relative to GTP (Path 3), the formation of QC will lead to the disassembly of TC.

is abruptly added in excess (Figures 3.3*C*, 4.4), EF-Ts exchanges the bound GTP with GDP, causing EF-Tu to adopt an inactive conformation and rapidly dissociate from the aa-tRNA (Figure 6.1, *path 3*).

The model that EF-Ts can perform its GEF function on EF-Tu while it is bound to its effector may have important implications for coupling protein production to cellular GTP concentrations. Should the cellular environment change rapidly from a nutrient rich condition to a nutrient poor condition, it may be important for the cell to quickly down regulate the energy intensive process of protein synthesis. Furthermore, it may also be important to quickly repurpose the >100 μM GTP that is bound in TC under fast growing conditions. The observation that EF-Ts can rapidly dissociate TC leads to a model wherein EF-Ts serves to couple the steady state concentration of TC with the abundance of free GTP (Figure 4.8).

6.3.3. Quaternary complex may represent a general mechanism of G-protein activation

The observation that, at cellular concentrations, EF-Ts physically chaperones the activated G-protein EF-Tu·GTP to its effector aa-tRNA has stark implications for other G-protein systems. As a class, small G-proteins function in a variety of signaling pathways. Paradoxically, some small G-proteins function in multiple signaling pathways involving multiple effectors expressed in the same cell simultaneously[173]. For example, activated Rho has been shown to stimulate a number of different targets such as: the kinases PIP5 kinase, PKN, PRK2, and ROK; the proteins REM-1 and REM-2; as well as MBS to name a few. Precisely how binding specificity is achieved for each of the effectors is not entirely understood[174]. In addition to having multiple effectors as potential targets, Rho also has multiple GEFs that can facilitate GTP binding[173].

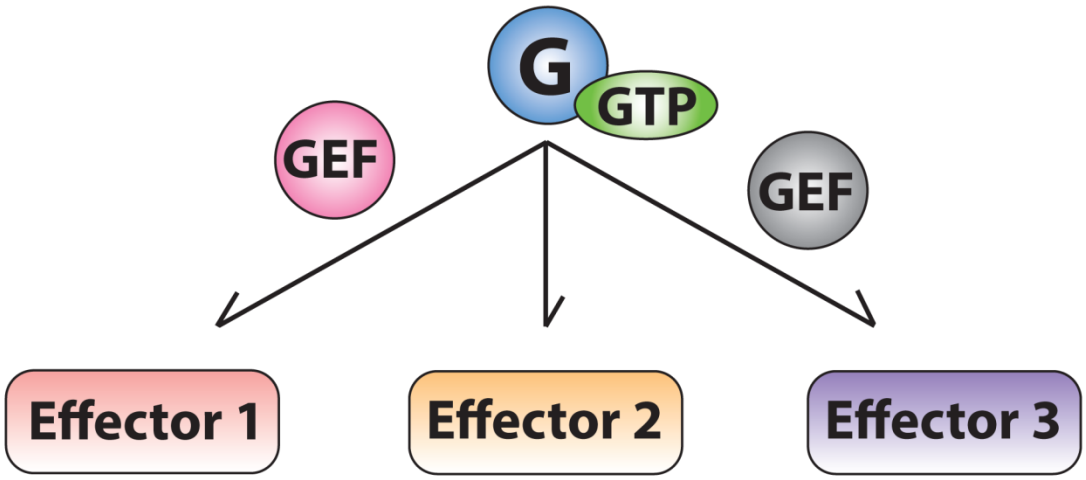

FIGURE 6.2 ***General mechanism for GEF mediated signal transduction.*** The observation of a GEF impacting G-protein·effector binding may have broad implications for other G-protein systems. Some small GTPases, such as Rho, have a large number of effector targets giving rise to the predicament of signal specificity. Furthermore, GEFs that activate small GTPases outnumber them by roughly 3 to 1. We propose a general mechanism whereby GEFs shunt activated G-proteins towards one effector or another thereby maintaining signal specificity and minimizing cross talk.

Based on the observations of EF-Ts presented here, one model that would explain how target specificity is achieved would be that the GEFs physically catalyze the binding of activated Rho to its effector (Figure 6.2). Furthermore, the larger repertoire of GEFs may provide specificity to the equally large repertoire of effectors such that signaling pathways are determined by the particular GEF·G-protein complex formed. Investigations focused on measuring GEF·G-protein·effector interactions are needed to evaluate this validity of this model.

6.4 DEACTIVATION OF G-PROTEINS

6.4.1 Do GEFs facilitate the removal of inactive G-proteins from their effectors?

The data presented in Chapters 3 and 4 have led to the corollary that, in addition to interacting with an effector-bound G-protein, GEFs may also play a role in their deactivation. This model is intriguing in the context of protein synthesis because it would resolve a long-standing dilemma with the kinetic framework of tRNA selection.

This model would also be appealing to the broader G-protein field because it would assert GEFs as important for both activation and deactivation. Such a finding would require a complete redrafting of the generally accepted model of G-proteins (Figure 1.2).

6.5 FUTURE DIRECTIONS

6.5.1 Measuring the residence time of EF-Tu

The GTP_{mant} assay used to estimate k_{off} has two significant drawbacks. The first is that the mant fluorophore group could alter the binding interface between EF-Tu and the GAC of the large subunit. Without controlling for this, the possibility that the measured off rate is an artifact of the nucleotide analog cannot be sufficiently ruled out. Secondly, the biphasic signal that is observed is the result of a multistep process. Global fitting can be used to estimate the rates of each of these steps, though k_{off} cannot be directly isolated. It is for these reasons that new methods are needed.

Here, we are developing a smFRET assay to resolve the residence time of EF-Tu with respect to the accommodating aa-tRNA and the ribosome (Figure 5.15). This will allow us to distinguish between productive and nonproductive interactions, a necessary procedure to properly identify the characteristic k_{off} for each. It may also be crucial to distinguish the residence time of EF-Tu with respect to the individual subunits of the ribosome. Our efforts to measure this with respect to the small subunit have thus far revealed a fast interaction. Furthermore, a histogram of dwell times appear to be modeled well by a single exponential process, suggesting that one rate is dominating. This was interpreted as a failure to distinguish between productive and non-productive events, though an alternative hypothesis would be that the dwell time

with respect to the small subunit is short for all interactions. Therefore, it may be necessary to track EF-Tu with respect to a large subunit protein, such as L11.

6.6 CONCLUSION

The endeavor to develop a comprehensive framework of tRNA selection is important and should continue to be pursued with conviction. As an exercise, the construction of a model that explains all the data provides some consolation that our understanding of the underlying mechanism is complete – or as complete as the data will allow. More practically, a kinetic framework aids in our ability to predict perturbations. In the case of tRNA selection, a complete model will guide our understanding of antibiotics and small molecules that target the protein synthesis machinery. Perhaps more importantly, it will also be critical to future *in silico* models of cellular processes. Although beyond our capabilities today, *in silico* modeling of molecular networks, and even larger scale cell, and tissue modeling will rely on a complete understanding of fundamental processes. As our understanding and our capabilities advance, detailed kinetic frameworks will only become more important. These models will be the foundation for modern medicine and will ultimately enable the next generation of biotechnology.

APPENDIX: BUFFERS AND SOLUTIONS

EF-Tu Lysis Buffer

20 mM Tris-HCl, pH 7.5

200 mM KCl

1 mM BME

EF-Tu Lysis Buffer With Imidazole

20 mM Tris-HCl, pH 7.5

200 mM KCl

10 mM Imidazole, pH 8

1 mM BME

EF-Tu Wash Buffer

20 mM Tris-HCl, pH 7.5

500 mM KCl

10 mM Imidazole, pH 8

1 mM BME

EF-Tu Elution Buffer

20 mM Tris-HCl, pH 7.5

200 mM KCl

250 mM Imidazole, pH 8

1 mM BME

EF-Tu Dialysis Buffer (Cleavage Buffer)

20 mM Tris-HCl, pH 7.5

200 mM KCl

1 mM BME

0.05% Triton X-100 Surfactant

2xFactor Buffer

20 mM Tris Acetate, pH 7

100 mM KCl

Factor Storage Buffer

10 mM Tris Acetate, pH 7

50 mM KCl

1 mM DTT

50%$_V$ Glycerol

PheRS Lysis Buffer

50 mM NaH_2PO_4

1 mM BME

PheRS Lysis Buffer With Imidazole

50 mM NaH_2PO_4

10 mM Imidazole, pH 8

1 mM BME

PheRS Wash Buffer

50 mM NaH_2PO_4

200 mM NaCl

10 mM Imidazole, pH 8

1 mM BME

PheRS Elution Buffer

50 mM NaH_2PO_4

100 mM NaCl

250 mM Imidazole, pH 8

1 mM BME

PheRS Dialysis Buffer

10 mM Tris Acetate, pH 7.5

100 mM KCl

1 mM BME

TEV Lysis Buffer

20 mM Tris-HCl, pH 7.5

200 mM NaCl

1 mM BME

Protease inhibitor (1:10,000).

TEV Lysis Buffer With Imidazole

20 mM Tris-HCl, pH 7.5

200 mM NaCl

1 mM BME

10 mM Imidazole, pH 8

Protease inhibitor (1:10,000).

TEV Wash Buffer

20 mM Tris-HCl, pH 7.5

500 mM NaCl

10 mM Imidazole, pH 8

1 mM BME

TEV Elution Buffer

20 mM Tris-HCl, pH 7.5

200 mM NaCl

250 mM Imidazole, pH 8

1 mM BME

Polymix

50 mM Tris Acetate, pH 7.5

100 mM KCl

5 mM NH_4AOc

0.5 mM CaCl2

0.1 mM EDTA

5 mM Putrecine

1 mM Spermidine

5 mM $MgCl_2$

5 mM BME

TC70S Buffer A

20 mM Tris HCl, pH 7.5

100 mM NH_4Cl

10 mM $MgCl_2$

0.5 mM EDTA

6 mM BME

TC70S Buffer B

20 mM Tris HCl, pH 7.5

500 mM NH_4Cl

10 mM $MgCl_2$

0.5 mM EDTA

6 mM BME

PBP Lysis Buffer

20 mM Tris-HCl, pH 8

1 mM EDTA

5 mM BME

$tRNA^{Phe}$ Lysis Buffer

20 mM Tris HCl, pH 7.5

50 mM $MgCl_2$

20 mM BME

$tRNA^{Phe}$ Buffer A

10 mM NH_4OAc, pH 5.85

1.7 M $(NH_4)_2SO_4$

$tRNA^{Phe}$ Buffer B

10 mM NH_4OAc, pH 5.85

10%$_V$ Methanol

tRNA^{Phe} Deacyl Buffer

0.5 M Tris HCl, pH 8.8

1 mM EDTA

tRNA^{Phe} Storage Buffer

50 mM K_4OAc, pH 6

1 mM $MgCl_2$

GTP Buffer A

20 mM KOAc, pH 6

GTP Buffer B

20 mM KOAc, pH 6

2 M KCl

TC Buffer (Chapter 3)

50 mM HEPES, pH 7

20 mM KCl

100 mM NH_4Cl

1 mM DTT

0.5 mM EDTA

2.5 mM $MgCl_2$

TC Buffer (Chapter 4)

100 mM HEPES, pH 7

20 mM KCl

100 mM NH_4Cl

1 mM DTT

0.5 mM EDTA

2.5 mM $MgCl_2$

tRNA Charge Buffer

50 mM Tris HCl, pH 8

20 mM KCl

100 mM NH_4Cl

1 mM DTT

0.5 mM EDTA

2.5 mM ATP

10 mM $MgCl_2$

SOB Media

2% Bactotryptone

0.5% Bactoyeast extract

10 mM NaCl

10 mM KCl

1 mL of 2M (1M $MgCl_2$, 1M $MgSO_4$)

RF 1

100 mM $RbCl_2$

50 mM $MnCl_2$·4H2O

30 mM KOAc

10 mM $CaCl_2·2H_2O$

15%$_{(w/v)}$ glycerol

RF 2

10 MOPS, 6.8

10 mM $RbCl_2$

75 mM $CaCl_2·2H_2O$

15%$_{(w/v)}$ glycerol

EF-Tu/Ts Buffer

50 mM Tris HCl, pH 7.5

100 mM NH_4Cl

10 mM $MgCl_2$

50 mM KCl

0.5 mM EDTA

BIBLIOGRAPHY

1 Geggier, P. *et al.* Conformational sampling of aminoacyl-tRNA during selection on the bacterial ribosome. *Journal of molecular biology* **399**, 576-595, doi:10.1016/j.jmb.2010.04.038 (2010).

2 Gromadski, K. B. & Rodnina, M. V. Kinetic determinants of high-fidelity tRNA discrimination on the ribosome. *Molecular cell* **13**, 191-200 (2004).

3 Kothe, U. & Rodnina, M. V. Delayed Release of Inorganic Phosphate from Elongation Factor Tu Following GTP Hydrolysis on the Ribosome. *Biochemistry* **45**, 12767-12774 (2006).

4 Pape, T., Wintermeyer, W. & Rodnina, M. V. Induced fit in initial selection and proofreading of aminoacyl-tRNA on the ribosome. *The EMBO journal* **18**, 3800-3807 (1999).

5 Sorensen, H. P., Hedegaard, J. & Sperling-Petersen, H. U. Remarkable conservation of translation initiation factors: IF1/eIF1A and IF2/eIF5B are universally distributed phylogenetic markers. *IUBMB Life* **51**, 321-327 (2001).

6 Lopez, P., Forterre, P. & Philippe, H. The Root of the Tree of Life in the Light of the Covarion Model. *Journal of molecular evolution* **49**, 496-508 (1999).

7 Wittinghofer, A. & Vetter, I. R. Structure-function relationships of the G domain, a canonical switch motif. *Annu Rev Biochem* **80**, 943-971, doi:10.1146/annurev-biochem-062708-134043 (2011).

8 Dorsam, R. T. & Gutkind, J. S. G-protein-coupled receptors and cancer. *Nature reviews. Cancer* **7**, 79-94, doi:10.1038/nrc2069 (2007).

9 Vetter, I. R. & Wittinghofer, A. The guanine nucleotide-binding switch in three dimensions. *Science* **294**, 1299-1304, doi:10.1126/science.1062023 (2001).

10 Milburn, M. V. *et al.* Molecular switch for signal transduction: structural differences between active and inactive forms of protooncogenic ras proteins. *Science* **247**, 939-945 (1990).

11 Carvalho, A. T., Szeler, K., Vavitsas, K., Aqvist, J. & Kamerlin, S. C. Modeling the mechanisms of biological GTP hydrolysis. *Arch Biochem Biophys* **582**, 80-90, doi:10.1016/j.abb.2015.02.027 (2015).

12 Siderovski, D. P. & Willard, F. S. The GAPs, GEFs, and GDIs of heterotrimeric G-protein alpha subunits. *Int J Biol Sci* **1**, 51-66 (2005).

13 Bos, J. L., Rehmann, H. & Wittinghofer, A. GEFs and GAPs: critical elements in the control of small G proteins. *Cell* **129**, 865-877, doi:10.1016/j.cell.2007.05.018 (2007).

14 Rodnina, M. V., Pape, T., Fricke, R. & Wintermeyer, W. Elongation factor Tu, a GTPase triggered by codon recognition on the ribosome: mechanism and GTP consumption. *Biochem. Cell Biol.* **73**, 1221-1227 (1995).

15 Leipe, D. D., Wolf, Y. I., Koonin, E. V. & Aravind, L. Classification and Evolution of P-loop GTPases and Related ATPases. *J. Mol. Biol.* **317**, 41-72 (2002).

16 Villa, E. *et al.* Ribosome-induced changes in elongation factor Tu conformation control GTP hydrolysis. *Proceedings of the National Academy of Sciences of the United States of America* **106**, 1063-1068, doi:10.1073/pnas.0811370106 (2009).

17 Voorhees, R. M. & Ramakrishnan, V. Structural basis of the translational elongation cycle. *Annu Rev Biochem* **82**, 203-236, doi:10.1146/annurev-biochem-113009-092313 (2013).

18 Aitken, C. E. & Lorsch, J. R. A mechanistic overview of translation initiation in eukaryotes. *Nature structural & molecular biology* **19**, 568-576, doi:10.1038/nsmb.2303 (2012).

19 Myasnikov, A. G., Simonetti, A., Marzi, S. & Klaholz, B. P. Structure-function insights into prokaryotic and eukaryotic translation initiation. *Current opinion in structural biology* **19**, 300-309, doi:10.1016/j.sbi.2009.04.010 (2009).

20 Munro, J. B., Sanbonmatsu, K. Y., Spahn, C. M. & Blanchard, S. C. Navigating the ribosome's metastable energy landscape. *Trends in biochemical sciences* **34**, 390-400, doi:10.1016/j.tibs.2009.04.004 (2009).

21 Korostelev, A. A. Structural aspects of translation termination on the ribosome. *Rna* **17**, 1409-1421, doi:10.1261/rna.2733411 (2011).

22 Bourne, H. R., Sanders, D. A. & McCormick, F. The GTPase superfamily conserved structure and molecular mechanism. *Nature* **349**, 117-127 (1991).

23 Hauryliuk, V. *et al.* Thermodynamics of GTP and GDP binding to bacterial initiation factor 2 suggests two types of structural transitions. *Journal of molecular biology* **394**, 621-626, doi:10.1016/j.jmb.2009.10.015 (2009).

24 Pape, T., Wintermeyer, W. & Rodnina, M. V. Complete kinetic mechanism of elongation factor Tu-dependent binding of aminoacyl-tRNA to the A site of the E.coli ribosome. *The EMBO journal* **17**, 7490-7497 (1998).

25 Pingoud, A., Urbanke, C., Krauss, G., Peters, F. & Maass, G. Ternary Complex Formation between Elongation Factor Tu, GTP and Aminoacyl-tRNA: an Equilibrium Study. *Eur J Biochem* **78**, 403-409 (1977).

26 Rodnina, M. V., Gromadski, K. B., Kothe, U. & Wieden, H. J. Recognition and selection of tRNA in translation. *FEBS letters* **579**, 938-942, doi:10.1016/j.febslet.2004.11.048 (2005).

27 Aleksandrov, A. & Field, M. Mechanism of activation of elongation factor Tu by ribosome: Catalytic histidine activates GTP by protonation. *Rna*, doi:10.1261/rna.040097.113 (2013).

28 Voorhees, R. M., Schmeing, T. M., Kelley, A. C. & Ramakrishnan, V. The mechanism for activation of GTP hydrolysis on the ribosome. *Science* **330**, 835-838, doi:10.1126/science.1194460 (2010).

29 Kristensen, O. *et al.* Isolation, crystallization and X-ray analysis of the quaternary complex of Phe-tRNAPhe, EF-Tu, a GTP analog and kirromycin. *The FEBS journal* **399**, 59-62 (1996).

30 Parmeggiani, A. *et al.* Enacyloxin IIa pinpoints a binding pocket of elongation factor Tu for development of novel antibiotics. *The Journal of biological chemistry* **281**, 2893-2900, doi:10.1074/jbc.M505951200 (2006).

31 Gromadski, K. B., Wieden, H. J. & Rodnina, M. V. Kinetic Mechanism of Elongation Factor Ts-Catalyzed Nucleotide Exchange in Elongation Factor Tu. *Biochemistry* **41**, 162-169 (2002).

32 Wasserman, M. R., Alejo, J. L., Altman, R. B. & Blanchard, S. C. Multiperspective smFRET reveals rate-determining late intermediates of ribosomal translocation. *Nature structural & molecular biology*, doi:10.1038/nsmb.3177 (2016).

33 Wilden, B., Savelsbergh, A., Rodnina, M. V. & Wintermeyer, W. Role and timing of GTP binding and hydrolysis during EF-G-dependent tRNA translocation on the ribosome. *Proceedings of the National Academy of Sciences of the United States of America* **103**, 13670-13675, doi:10.1073/pnas.0606099103 (2006).

34 Koutmou, K. S., McDonald, M. E., Brunelle, J. L. & Green, R. RF3:GTP promotes rapid dissociation of the class 1 termination factor. *Rna* **20**, 609-620, doi:10.1261/rna.042523.113 (2014).

35 Young, R. Y. & Bremer, H. Polypeptide-Chain-Elongation Rate in Escherichia coli B/r as a Function of Growth Rate. *Biochem. J.* **160**, 185-194 (1976).

36 Bremer, H. & Dennis, P. P. in *Escherichia coli and Salmonella typhimurium: Cellular and Molecular Biology* Ch. 97, (1996).

37 Bremer, H. & Dennis, P. P. *Escherichia coli and Salmonella typhimurium*. 1527-1542 (American society for microbiology, 1987).

38 Neijssel, O. M. *Escherichia coli and Salmonella cellular and molecular biology*. 1683-1693 (1996).

39 Noeske, J. *et al.* High-resolution structure of the Escherichia coli ribosome. *Nature structural & molecular biology* **22**, 336-341, doi:10.1038/nsmb.2994 (2015).

40 Blanchard, S. C., Kim, H. D., Gonzalez, R. L., Jr., Puglisi, J. D. & Chu, S. tRNA dynamics on the ribosome during translation. *Proceedings of the National Academy of Sciences of the United States of America* **101**, 12893-12898, doi:10.1073/pnas.0403884101 (2004).

41 Konevega, A. L. Purine bases at position 37 of tRNA stabilize codon-anticodon interaction in the ribosomal A site by stacking and Mg2+-dependent interactions. *Rna* **10**, 90-101, doi:10.1261/rna.5142404 (2004).

42 Wohlgemuth, I., Pohl, C., Mittelstaet, J., Konevega, A. L. & Rodnina, M. V. Evolutionary optimization of speed and accuracy of decoding on the ribosome. *Philosophical transactions of the Royal Society of London. Series B, Biological sciences* **366**, 2979-2986, doi:10.1098/rstb.2011.0138 (2011).

43 Parker, J. Errors and Alternatives in Reading the Universal Genetic Code. *Microbiological Revies* **53**, 273-298 (1989).

44 Kurland, C. G. & Ehrenberg, M. Growth-Optimizing Accuracy of Gene Expression. *Ann. Rev. Biophys. Chem.* **16**, 291-317 (1987).

45 Ruusala, T., Andersson, D., Ehrenberg, M. & Kurland, C. G. Hyper-accurate ribosomes inhibit growth. *The EMBO journal* **3**, 2575-2580 (1984).

46 Bilgin, N., Claesens, F., Pahverk, H. & Ehrenberg, M. Kinetic properties of Escherichia coli ribosomes with altered forms of S12. *J. Mol. Biol.* **224**, 1011-1027 (1992).

47 Ninio, J. A semi-quantitative treatment of missense and nonsense suppression in the strA and ram ribosomal mutans of Escherichia coli Evaluation of some molecular parameters of translation in vivo. *Journal of molecular biology* **84**, 297-313 (1974).

48 Ehrenberg, M. & Kurland, C. G. Costs of accuracy determined by a maximal growth rate constraint. *Quarterly reviews of biophysics* **17**, 45-82 (1984).

49 Lovmar, M. & Ehrenberg, M. Rate, accuracy and cost of ribosomes in bacterial cells. *Biochimie* **88**, 951-961, doi:10.1016/j.biochi.2006.04.019 (2006).

50 Johansson, M., Lovmar, M. & Ehrenberg, M. Rate and accuracy of bacterial protein synthesis revisited. *Current opinion in microbiology* **11**, 141-147, doi:10.1016/j.mib.2008.02.015 (2008).

51 Rodnina, M. V. & Wintermeyer, W. Ribosome fidelity: tRNA discrimination, proofreading and induced fit. *Trends in biochemical sciences* **26**, 124-130 (2001).

52 Kaur, J., Raj, M. & Cooperman, B. S. Fluorescent labeling of tRNA dihydrouridine residues: Mechanism and distribution. *Rna* **17**, 1393-1400, doi:10.1261/rna.2670811 (2011).

53 Blanchard, S. C., Gonzalez, R. L., Kim, H. D., Chu, S. & Puglisi, J. D. tRNA selection and kinetic proofreading in translation. *Nature structural & molecular biology* **11**, 1008-1014 (2004).

54 Lee, T. H., Blanchard, S. C., Kim, H. D., Puglisi, J. D. & Chu, S. The role of fluctuations in tRNA selection by the ribosome. *Proceedings of the National Academy of Sciences of the United States of America* **104**, 13661-13665, doi:10.1073/pnas.0705988104 (2007).

55 Polikanov, Y. S. *et al.* Distinct tRNA Accommodation Intermediates Observed on the Ribosome with the Antibiotics Hygromycin A and A201A. *Molecular cell*, doi:10.1016/j.molcel.2015.04.014 (2015).

56 Sanderson, L. E. & Uhlenbeck, O. C. The 51-63 base pair of tRNA confers specificity for binding by EF-Tu. *Rna* **13**, 835-840, doi:10.1261/rna.485307 (2007).

57 Dale, T., Sanderson, L. E. & Uhlenbeck, O. C. The Affinity of Elongation Factor Tu for an Aminoacyl-tRNA Is Modulated by the Esterified Amino Acid. *Biochemistry* **43**, 6159-6166 (2004).

58 Pedersen, S., Bloch, P. L., Reeh, S. & Neidhardt, F. C. Patterns of protein synthesis in E. coli: a catalog of the amount of 140 individual proteins at different growth rates. *Cell* **14**, 179-190 (1978).

59 Shimizu, Y. *et al.* Cell-free translation reconstituted with purified components. *Nature New Biology* **19**, 751-755 (2001).

60 Schummer, T., Gromadski, K. B. & Rodnina, M. V. Mechanism of EF-Ts-Catalyzed Guanine Nucleotide Exchange in EF-Tu: Contribution of Interactions Mediated by Helix B of EF-Tu. *Biochemistry* **46**, 4977-4984 (2007).

61 Morris, D. R. & Hansen, M. T. Influence of polyamine limitation on the chain growth rates of beta-galactosidase and of its messenger ribonucleic acid. *Journal of bacteriology* **116**, 588-592 (1973).

62 Forchhammer, J. & Lindahl, L. Growth rate of polypeptide chains as a function of the cell growth rate in a mutant of Escherichia coli 15. *Journal of molecular biology* **55**, 563-568 (1971).

63 Juette, M. F. *et al.* Single-molecule imaging of non-equilibrium molecular ensembles on the millisecond timescale. *Nature methods*, doi:10.1038/nmeth.3769 (2016).

64 Nicolai, C. & Sachs, F. Solving ion channel kinetics with the QuB software. *Biophysical Reviews and Letters* **8**, 1-21 (2013).

65 Qiagen. *The QIAexpressionist*. 5 edn, (QIAGEN, 2003).

66 Perla-Kajan, J. *et al.* Properties of Escherichia coli EF-Tu mutants designed for fluorescence resonance energy transfer from tRNA molecules. *Protein Eng Des Sel* **23**, 129-136, doi:10.1093/protein/gzp079 (2010).

67 Zhou, Z. *et al.* Genetically encoded short peptide tags for orthogonal protein labeling by Sfp and AcpS phosphopantetheinyl transferase. *ACS Chemical Biology* **2**, 337-346 (2007).

68 Zhou, Z., A., K., Wang, Y., McMahon, A. P. & Walsh, C. T. An eight residue fragment of an acyl carrier protein suffices for post-translational introduction of fluorescent pantetheinyl arms in protein modification in vitro and in vivo. *J. Am. Chem. Soc.* **130**, 9925-9930 (2008).

69 Yin, J., Lin, A. J., Golan, D. E. & Walsh, C. T. Site-specific protein labeling by Sfp phosphopantetheinyl transferase. *Nature protocols* **1**, 280-285, doi:10.1038/nprot.2006.43 (2006).

70 Aseev, L. V., Levandovskaya, A. A., Tchufistova, L. S., Scaptsova, N. V. & Boni, I. V. A new regulatory circuit in ribosomal protein operons: S2-mediated control of the rpsB-tsf expression in vivo. *Rna* **14**, 1882-1894, doi:10.1261/rna.1099108 (2008).

71 Technologies, A. *QuikChange II site-directed mutagenesis kit*. (Agilent Technologies).

72 Boulware, K. T., Jabaiah, A. & Daugherty, P. S. Evolutionary optimization of peptide substrates for proteases that exhibit rapid hydrolysis kinetics. *Biotechnol Bioeng* **106**, 339-346, doi:10.1002/bit.22693 (2010).

73 Kostallas, G., Lofdahl, P. A. & Samuelson, P. Substrate profiling of tobacco etch virus protease using a novel fluorescence-assisted whole-cell assay. *PloS one* **6**, e16136, doi:10.1371/journal.pone.0016136 (2011).

74 Brune, M., Hunter, J. L., Corrie, J. E. T. & Webb, M. R. Direct, real-time measurement of rapid inorganic phosphate release using a novel fluorescent probe and its application to actomyosin subfragment 1 ATPase. *Biochemistry* **33** (1994).

75 Brune, M. *et al.* Mechanism of inorganic phosphate interaction with phosphate binding protein from Escherichia coli. *Biochemistry* **37**, 10370-10380 (1998).

76 Okoh, M. P., Hunter, J. L. C., J. E. T. & Webb, M. R. A biosensor for inorganic phosphate using a Rhodamine-labeled phosphate binding protein. *Biochemistry* **45** (2006).

77 Cayama, E. *et al.* New chromatographic and biochemical strategies for quick preparative isolation of tRNA. *Nucleic acids research* **28**, e64 (2000).

78 Abrahamson, J. K., Laue, T. M., Miller, D. L. & Johnson, A. E. Abrahamson et al. - 1985 - Direct determination of the association constant between

elongation factor Tu and GTP and aminoacyl-tRNA using fluorescence. *Biochemistry* **24**, 692-700 (1985).

79 Fersht, A. *Enzyme structure and mechanism*. 2 edn, (W. H. Freeman and Company, 1985).

80 Savitzky, A. & Golay, M. J. E. Smoothing and Differentiation of Data by Simplified Least Squares Procedures. *Analytical Chemistry* **36**, 1627-1639 (1964).

81 Zheng, Q. *et al.* Intra-molecular triplet energy transfer is a general approach to improve organic fluorophore photostability. *Photochem Photobiol Sci* **15**, 196-203, doi:10.1039/c5pp00400d (2016).

82 Altman, R. B. *et al.* Cyanine fluorophore derivatives with enhanced photostability. *Nature methods* **9**, 68-71, doi:10.1038/nmeth.1774 (2012).

83 Burnett, B. J. *et al.* Elongation Factor Ts Directly Facilitates the Formation and Disassembly of the Escherichia coli Elongation Factor Tu-GTP-Aminoacyl-tRNA Ternary Complex. *The Journal of biological chemistry* **288**, 13917-13928, doi:10.1074/jbc.M113.460014 (2013).

84 Thomposon, R. C. & Dix, D. B. Accuracy of Protein Biosynthesis. A kinetic study of the reaction of poly(U)-programmed ribosomes ith a leucyl-tRNA2-elongation factor Tu-GTP complex. *The Journal of biological chemistry* **257**, 6677-6682 (1982).

85 Hopfield, J. J., Yamane, T., Yue, V. & Coutts, S. M. Direct experimental evidence for kinetic proofreading in amino acylation of tRNAIle. *Proceedings of the National Academy of Sciences of the United States of America* **73**, 1164-1168 (1976).

86 Rodnina, M. V., Savelsbergh, A. & Wintermeyer, W. Dynamics of translation on the ribosome: molecular mechanics of translocation. *FEMS Microbiology Reviews* **23**, 317-333 (1999).

87 Nissen, P., Kjeldgaard, M., Thirup, S., Clark, B. F. C. & Nyborg, J. The ternary complex of aminoacylated tRNA and EF-Tu-GTP. Recognition of a bond and a fold. *Biochemie* **78**, 921-933 (1996).

88 Nissen, P. *et al.* Crystal structure of the Ternary Complex of Phe-tRNAPhe, EF-Tu, and a GTP Analog. *Science* **270**, 1464-1472 (1995).

89 Abel, K., Yoder, M., Hilgenfeld, R. & Jurnak, F. An alpha to beta conformational switch in EF-Tu. *Structure* **4**, 1153-1159 (1996).

90 Polekhina, G. *et al.* Helix unwinding in the effector region of elongation factor EF-Tu-GDP. *Structure* **4**, 1141-1151 (1996).

91 Kawashima, T., Berthet-Colominas, C., Wulff, M., Cusack, S. & Leberman, R. The structure of the Escherichia coli EF-TuEF-Ts complex at 2.5 Ang resolution. *Nature* **379**, 511-518 (1996).

92 Louie, A. & Jurnak, F. Kinetic Studies of Escherichia coli Elongation Factor Tu-Guanosine 5-Triphophate-Aminoacyl-tRNA Complexes. *Biochemistry* **24**, 6433-6439 (1985).

93 Romero, G., Chau, V. & Biltonen, R. L. Kinetics and thermodynamics of the interaction of elongation factor Tu with Ts. *The Journal of biological chemistry* **280**, 6167-6174 (1985).

94 Delaria, K., Guillen, M., Louie, A. & Jurnak, F. Stabilization of the Escherichia coli elongation factor Tu-GTP-Aminoacyl-tRNA Complex. *Archives Of Biochemistry And Biophysics* **286**, 207-211 (1991).

95 Chapman, S. J., Schrader, J. M. & Uhlenbeck, O. C. Histidine 66 in Escherichia coli elongation factor tu selectively stabilizes aminoacyl-tRNAs.

The Journal of biological chemistry **287**, 1229-1234, doi:10.1074/jbc.M111.294850 (2012).

96 Cai, Y. C., Bullard, J. M., Thompson, N. L. & Spremulli, L. L. Interaction of mitochondrial elongation factor Tu with aminoacyl-tRNA and elongation factor Ts. *The Journal of biological chemistry* **275**, 20308-20314, doi:10.1074/jbc.M001899200 (2000).

97 Watson, B. S. *et al.* Macromolecular arrangement in the Aminoacyl-tRNAElongation Factor TuGTP Ternary Complex. A Fluorescence Energy Transfer Study. *Biochemistry* **34**, 7904-7912 (1995).

98 Janiak, F. *et al.* Fluorescence characterization of the interaction of various transfer RNA species with elongation factor Tu.GTP: evidence for a new functional role for elongation factor Tu in protein biosynthesis. *Biochemistry* **29**, 4268-4277 (1990).

99 Hazlett, T. L., Johnson, A. E. & Jameson, D. M. Time-Resolved Fluorescent Studies on the Ternary Complex Formed between Bacterial Elongation Factor Tu, Guanosine 5'-Triphosphate and Phenylalanyl-tRNA(Phe). *Biochemistry* **28** (1989).

100 Miyajima, A. & Kaziro, Y. Coordination of Levels of Elongation Factors Tu, Ts, and G, and Ribosomal Protein S1 in Escherichia coli. *J Biochem* **83**, 453-462 (1978).

101 Ji, Y. *et al.* Identification of critical staphylococcal genes using conditional phenotypes generated by antisence RNA. *Science* **293**, 2266-2269 (2001).

102 Forsyth, R. A. *et al.* A genome-wide strategy for the identification of essential genes in Staphylococcus aureus. *Molecular microbiology* **43**, 1387-1400 (2002).

103 Parmeggiani, A. & Nissen, P. Elongation factor Tu-targeted antibiotics: four different structures, two mechanisms of action. *FEBS letters* **580**, 4576-4581, doi:10.1016/j.febslet.2006.07.039 (2006).

104 Parmeggiani, A. *et al.* Structural Basis of the Action of Pulvomycin and GE2270 A on Elongation Factor Tu. *Biochemistry* **45**, 6846-6857 (2006).

105 Spahn, C. M. & Prescott, C. D. Throwing a spanner in the works: antibiotics and the translation apparatus. *J Mol Med* **74**, 423-439 (1996).

106 Gonzalez, R. L., Jr., Chu, S. & Puglisi, J. D. Thiostrepton inhibition of tRNA delivery to the ribosome. *Rna* **13**, 2091-2097, doi:10.1261/rna.499407 (2007).

107 Rodnina, M. V., Fricke, R., Kuhn, L. & Wintermeyer, W. Codon-dependent conformational change of elongation factor Tu preceding GTP hydrolysis on the ribosome. *The EMBO journal* **14**, 2613-2619 (1995).

108 Vogeley, L., Palm, G. J., Mesters, J. R. & Hilgenfeld, R. Conformational change of elongation factor Tu (EF-Tu) induced by antibiotic binding. Crystal structure of the complex between EF-Tu.GDP and aurodox. *The Journal of biological chemistry* **276**, 17149-17155, doi:10.1074/jbc.M100017200 (2001).

109 Miller, D. L. & Weissbach, H. Interactions Between the Elongation Factors: The Displacement of GDP from the Tu-GDP Complex by Factor Ts. *Biochemical and biophysical research communications* **38**, 1016-1022 (1970).

110 Weaver, R. F. *Molecular Biology*. 4 edn, (2007).

111 Dahl, L. D., Wieden, H. J., Rodnina, M. V. & Knudsen, C. R. The importance of P-loop and domain movements in EF-Tu for guanine nucleotide exchange. *The Journal of biological chemistry* **281**, 21139-21146, doi:10.1074/jbc.M602068200 (2006).

112 Wieden, H. J., Mercier, E., Gray, J., Steed, B. & Yawney, D. A combined molecular dynamics and rapid kinetics approach to identify conserved three-

dimensional communication networks in elongation factor Tu. *Biophysical journal* **99**, 3735-3743, doi:10.1016/j.bpj.2010.10.013 (2010).

113 Levitus, M. & Ranjit, S. Cyanine dyes in biophysical research: the photophysics of polymethine fluorescent dyes in biomolecular environments. *Quarterly reviews of biophysics* **44**, 123-151, doi:10.1017/S0033583510000247 (2011).

114 Munro, J. B., Wasserman, M. R., Altman, R. B., Wang, L. & Blanchard, S. C. Correlated conformational events in EF-G and the ribosome regulate translocation. *Nature structural & molecular biology* **17**, 1470-1477, doi:10.1038/nsmb.1925 (2010).

115 Ott, G., Faulhammer, H. G. & Sprinzl, M. Interaction of elongation factor Tu from Escherichia coli with aminoacyl-tRNA carrying a fluorescent reporter group on the 3' terminus. *Eur J Biochem* **184**, 345-352 (1989).

116 Sanderson, L. E. & Uhlenbeck, O. C. Directed mutagenesis identifies amino acid residues involved in elongation factor Tu binding to yeast Phe-tRNAPhe. *Journal of molecular biology* **368**, 119-130, doi:10.1016/j.jmb.2007.01.075 (2007).

117 Goodrich, J. A. & Kugel, J. F. *Binding and Kinetics for Molecular Biologists*. (Cold Spring Harbor Laboratory Press, 2007).

118 Podkowinski, J., Dymarek-Babs, T. & Gornicki, P. Modified tRNAs for probing tRNA binding sites on the ribosome. *Acta Biochim Pol* **36**, 235-244 (1989).

119 Weissbach, H., Miller, D. L. & Hachmann, J. Studies on the role of factor Ts in polypeptide synthesis. *Archives Of Biochemistry And Biophysics* **137**, 262-269 (1970).

120 Gromadski, K. B. *et al.* Kinetics of the interactions between yeast elongation factors 1A and 1Balpha, guanine nucleotides, and aminoacyl-tRNA. *The Journal of biological chemistry* **282**, 35629-35637, doi:10.1074/jbc.M707245200 (2007).

121 Schwartzback, C. J. & Spremulli, L. L. Interaction of Animal Mitochondrial EF-TuEF-Ts with Aminoacyl-tRNA, Guanine Nucleotides, and Ribosomes. *The Journal of biological chemistry* **266**, 16324-16330 (1991).

122 Bubunenko, M. G., Kireeva, M. L. & Gudkov, A. T. Novel data on interactions of elongation factor Ts. *Biochimie* **74**, 419-425 (1992).

123 Takeshita, D. & Tomita, K. Molecular basis for RNA polymerization by Qbeta replicase. *Nature structural & molecular biology* **19**, 229-237, doi:10.1038/nsmb.2204 (2012).

124 Schmitt, E. *et al.* Structure of the ternary initiation complex aIF2-GDPNP-methionylated initiator tRNA. *Nature structural & molecular biology* **19**, 450-454, doi:10.1038/nsmb.2259 (2012).

125 Endo, M., Shirouzu, M. & Yokoyama, S. The Cdc42 binding and scaffolding activities of the fission yeast adaptor protein Scd2. *The Journal of biological chemistry* **278**, 843-852, doi:10.1074/jbc.M209714200 (2003).

126 Urano, T., Emkey, R. & Feig, L. A. Ral-GTPases mediate a distinct downstream signaling pathway from Ras that facilitates cellular transformation. *The EMBO journal* **15**, 810-816 (1996).

127 Stumber, M. *et al.* Observation of Slow Dynamic Exchange Processes in Ras Protein Crystals by 31P Solid State NMR Spectroscopy. *Journal of molecular biology* **323**, 899-907, doi:10.1016/s0022-2836(02)01010-0 (2002).

128 Spoerner, M., Herrmann, C., Vetter, I. R., Kalbitzer, H. R. & Wittinghofer, A. Dynamic properties of the Ras switch I region and its importance for binding

to effectors. *Proceedings of the National Academy of Sciences of the United States of America* **98**, 4944-4949, doi:10.1073/pnas.081441398 (2001).

129 Burnett, B. J. *et al.* Direct Evidence of an Elongation Factor-Tu/Ts.GTP.Aminoacyl-tRNA Quaternary Complex. *The Journal of biological chemistry* **289**, 23917-23927, doi:10.1074/jbc.M114.583385 (2014).

130 Rodnina, M. V., Fricke, R. & Wintermeyer, W. Transient conformational states of aminoacyl-tRNA during ribosome binding catalyzed by elongation factor Tu. *Biochemistry* **33**, 12267-12275 (1994).

131 Varenne, S., Buc, J., Lloubes, R. & Lazdunski, C. Translation is a non-uniform process Effect of tRNA availability on the rate of elongation of nascent polypeptide chains. *Journal of molecular biology* **180**, 549-576 (1984).

132 Wohlgemuth, S. E., Gorochowski, T. E. & Roubos, J. A. Translational sensitivity of the Escherichia coli genome to fluctuating tRNA availability. *Nucleic acids research* **41**, 8021-8033, doi:10.1093/nar/gkt602 (2013).

133 Blattner, F. R. The Complete Genome Sequence of Escherichia coli K-12. *Science* **277**, 1453-1462, doi:10.1126/science.277.5331.1453 (1997).

134 Jinks-Robertson, S., Gourse, R. L. & Nomura, M. Expression of rRNA and tRNA genes in Escherichia coli: Evidence for feedback regulation by products of rRNA operons. *Cell* **33**, 865-876 (1983).

135 Dong, H., Nilsson, L. & Kurland, C. G. Co-variation of tRNA abundance and codon usage in escherichia coli at different growth rates. *Journal of molecular biology* **260**, 649-663 (1996).

136 Condon, C., Philips, J., Fu, Z.-Y., Squires, C. & Squires, C. L. Comparison of the expression of the seven ribosomal RNA operons in Escherichia coli. *The EMBO journal* **11**, 4175-4185 (1992).

137 Ehrenberg, M., Bremer, H. & Dennis, P. P. Medium-dependent control of the bacterial growth rate. *Biochimie* **95**, 643-658, doi:10.1016/j.biochi.2012.11.012 (2013).

138 Yegian, C. D., Stent, G. S. & Martin, E. M. Intracellular condition of Escherichia coli transfer RNA. *Proceedings of the National Academy of Sciences of the United States of America* **55**, 839-846 (1966).

139 Sorensen, M. A. Charging levels of four tRNA species in Escherichia coli Rel+ and Rel- strains during amino acid starvation: A simple model for the effect of ppGpp on translational accuracy. *Journal of molecular biology* **307**, 785-798 (2001).

140 Dittmar, K. A., Sorensen, M. A., Elf, J., Ehrenberg, M. & Pan, T. Selective charging of tRNA isoacceptors induced by amino-acid starvation. *EMBO reports* **6**, 151-157, doi:10.1038/sj.embor.7400341 (2005).

141 Louie, A., Ribeiro, S., Reid, B. R. & Jurnak, F. Relative Affinities of All Escherichia coli Aminoacyl-tRNAs for Elongation Factor Tu-GTP. *The Journal of biological chemistry* **259**, 5010-5016 (1984).

142 Sanderson, L. E. & Uhlenbeck, O. C. Exploring the Specificity of Bacterial Elongation Factor Tu for Different tRNAs. *Biochemistry* **46**, 6194-6200 (2007).

143 Ott, G. *et al.* Ternary complexes of Escherichia coli aminoacyl-tRNAs with the elongation factor Tu and GTP: thermodynamic and structural studies. *Biochemica et Biophysica Acta* **1050**, 222-225 (1990).

144 LaRiviere, F. J., Wolfson, A. D. & Uhlenbeck, O. C. Uniform binding of aminoacyl-tRNAs to elongation factor Tu by thermodynamic compensation. *Science* **294**, 165-168, doi:10.1126/science.1064242 (2001).

145 Furano, A. V. Content of elongation factor Tu in escherichia coli. *Proceedings of the National Academy of Sciences of the United States of America* **72**, 4780-4784 (1975).

146 Gordon, J. Regulation of the in Vivo Synthesis of the Polypeptide Chain Elongation Factors in Escherichia coli. *Biochemistry* **9**, 912-917 (1970).

147 Gordon, J. & Weissbach, H. Immunochemical Distinction between the Escherichia coli Polypeptide Chain Elongation Factors Tu and Ts. *Biochemistry* **9**, 4233-4236 (1970).

148 Yamamoto, M., Strycharz, W. A. & Nomura, M. Identification of genes for elongation factor Ts and ribosomal protein S2 in E. coli. *Cell* **8**, 129-138 (1976).

149 Luo, G., Wang, M., Konigsberg, W. H. & Xie, X. S. Single-molecule and ensemble fluorescence assays for a functionally important conformational change in T7 DNA polymerase. *Proceedings of the National Academy of Sciences of the United States of America* **104**, 12610-12615, doi:10.1073/pnas.0700920104 (2007).

150 Zechmeister, L. & Pinckard, J. H. On stereoisomerism in the cyanine dye series. *Experientia* **9**, 16-17 (1953).

151 Hwang, H., Kim, H. & Myong, S. Protein induced fluorescence enhancement as a single molecule assay with short distance sensitivity. *Proceedings of the National Academy of Sciences of the United States of America* **108**, 7414-7418, doi:10.1073/pnas.1017672108/-/DCSupplemental (2011).

152 Schuette, J.-C. *et al.* GTPase activation of elongation factor EF-Tu by the ribosome during decoding. *The EMBO journal* **28**, 755-765, doi:10.1038/ (2009).

153 Ribeiro, S., Nock, S. & Sprinzl, M. Purification of aminoacyl-tRNA by affinity chromatography on immobilized Thermus thermophilus EF-TuGTP. *Analytical Biochemistry* **228**, 330-335 (1995).

154 Rodnina, M. V. & Wintermeyer, W. GTP consumption of elongation factor Tu during translation of heteropolymeric mRNAs. *Proceedings of the National Academy of Sciences of the United States of America* **92**, 1945-1949 (1995).

155 Daviter, T., Wieden, H.-J. & Rodnina, M. V. Essential Role of Histidine 84 in Elongation Factor Tu for the Chemical Step of GTP Hydrolysis on the Ribosome. *Journal of molecular biology* **332**, 689-699, doi:10.1016/s0022-2836(03)00947-1 (2003).

156 Pan, D., Zhang, C. M., Kirillov, S., Hou, Y. M. & Cooperman, B. S. Perturbation of the tRNA tertiary core differentially affects specific steps of the elongation cycle. *The Journal of biological chemistry* **283**, 18431-18440, doi:10.1074/jbc.M801560200 (2008).

157 Pan, D., Qin, H. & Cooperman, B. S. Synthesis and functional activity of tRNAs labeled with fluorescent hydrazides in the D-loop. *Rna* **15**, 346-354, doi:10.1261/rna.1257509 (2009).

158 Llano-Sotelo, B., Hickerson, R. P., Lancaster, L., Noller, H. F. & Mankin, A. S. Fluorescently labeled ribosomes as a tool for analyzing antibiotic binding. *Rna* **15**, 1597-1604, doi:10.1261/rna.1681609 (2009).

159 Dorywalska, M. *et al.* Site-specific labeling of the ribosome for single-molecule spectroscopy. *Nucleic acids research* **33**, 182-189, doi:10.1093/nar/gki151 (2005).

160 Rodnina, M. V. & Wintermeyer, W. Fidelity of Aminoacyl-tRNA Selection on the Ribosome. *Annu Rev Biochem* **70**, 415-435 (2001).

161 Ehrenberg, M. & Blomberg, C. Thermodynamic constraints on kinetic proofreading in biosynthetic pathways. *Biophysical journal* **31**, 333-358 (1980).

162 Scolnick, E. M., Papageorge, A. G. & Shih, T. Guanine nucleotide-binding activity as an assay for src protein of rat-derived murine sarcoma viruses. *Proceedings of the National Academy of Sciences of the United States of America* **76**, 5355-5359 (1979).

163 Hall, A. The cellular functions of small GTP-binding proteins. *Science* **249** (1990).

164 Gilman, A. G. G proteins: Transducers of receptor-generated signals. *Ann. Rev. Biophys. Chem.* **56**, 615-649 (1987).

165 Tesmer, J. J. G., Sunahara, R. K., Gilman, A. G. & Sprang, S. R. Crystal structure of the catalytic domains of adenylyl cyclase in a complex with Gsalpha-GTPgS. *Science* **278**, 1907-1916 (1997).

166 Hepler, J. R. & Gilman, A. G. G proteins. *TIBS* **17**, 383-387 (1992).

167 Sprang, S. R. G protein mechanisms Insights from structural analysis. *Analytical and bioanalytical chemistry* **66**, 639-678 (1997).

168 Wolf, H., Chinali, G. & Parmeggiani, A. Mechanisms of the Inhibition of Protein Synthesis by Kirromycin. *Eur J Biochem* **75**, 67-75 (1977).

169 Zhang, B., Zhang, Y., Wang, Z. & Zheng, Y. The role of Mg2+ cofactor in the guanine nucleotide exchange and GTP hydrolysis reactions of Rho family GTP-binding proteins. *The Journal of biological chemistry* **275**, 25299-25307, doi:10.1074/jbc.M001027200 (2000).

170. Lenzen C., Cool, R. H., Prinz, H., Kuhlmann, J. & Wittinghofer, A. Kinetic Analysis by Fluorescence of the Interaction between Ras and the Catalytic Domain of the Guanine Nucleotide Exchange Factor Cdc25. *Biochemistry **37**,*

7420-7430 (1998).

171 Kintscher, C. & Groemping, Y. Characterisation of the nucleotide exchange factor ITSN1L: evidence for a kinetic discrimination of GEF-stimulated nucleotide release from Cdc42. *Journal of molecular biology* **387**, 270-283, doi:10.1016/j.jmb.2009.01.056 (2009).

172 Klebe, C., Bischoff, F. R., Ponstingl, H. & Wittinghofer, A. Interaction of the Nuclear GTP-Binding Protein Ran with Its Regulatory Proteins RCCl and RanGAPl *Biochemistry* **34**, 639-647 (1995).

173 Garcia-Mata, R. & Burridge, K. Catching a GEF by its tail. *Trends Cell Biol* **17**, 36-43, doi:10.1016/j.tcb.2006.11.004 (2007).

174 Aelst, L. V. & D'Souza-Schorey, C. Rho GTPases and signaling networks. *Genes & development* **11**, 2295-2322 (1997).